

# **Development of a Heat-Transfer Correlation for Supercritical Water in Supercritical Water-cooled Reactor Applications**

**by**

**Sarah Mokry**

**A Thesis Submitted in Partial Fulfillment  
of the Requirements for the Degree of**

**Master of Applied Science**

**in**

**The Faculty of Energy Systems and Nuclear Science**

**Nuclear Engineering**

**University of Ontario Institute of Technology**

**December, 2009**

**© Sarah Mokry, 2009**

## ABSTRACT

A large set of experimental data, obtained in Russia, was analyzed and a new heat-transfer correlation for supercritical water was developed. This experimental dataset was obtained within conditions similar to those for proposed SuperCritical Water-cooled nuclear Reactor (SCWR) concepts. Thus, this new correlation, for forced convective heat transfer in the normal heat-transfer regime, can be used for preliminary heat-transfer calculations in SCWR fuel channels. It has demonstrated a good fit for Heat Transfer Coefficient (HTC) values ( $\pm 25\%$ ) and for wall temperature calculations ( $\pm 15$ ) for the analyzed dataset. This correlation can be used for supercritical water heat exchangers linked to indirect-cycle concepts and the co-generation of hydrogen, for future comparisons with other independent datasets, with bundle data, as the reference case, for the verification of computer codes for SCWR core thermalhydraulics and for the verification of scaling parameters between water and modeling fluids.

**Keywords:** Supercritical Water-cooled Reactors, Supercritical Water, Nuclear, Heat-Transfer, Correlations, Generation IV

## **ACKNOWLEDGEMENTS**

Financial support from the NSERC Discovery Grant, NSERC/NRCan/AECL Generation IV Energy Technologies Program and the Ontario Research Excellence Fund are gratefully acknowledged.

I would like to thank and acknowledge the work and contribution of the following peers: Maria Nadin, Yevgeniy Gospodinov, Amjad Farah, Krysten King, Sahil Gupta, Wargha Peiman and Karan Chophla.

Finally, I would like to acknowledge my supervisor, Dr. Igor Pioro, for all his encouragement, help and support with this thesis project. I was able to exceed my own expectations with his guidance and expertise. I would like to sincerely thank Dr. Pioro and offer my deepest appreciation for everything he has done for me along the way.

## SUMMARY

The concept of the SuperCritical Water-cooled nuclear Reactor (SCWR) dates back to the late 1950s. Research for the SCWR conducted in the United States and former USSR provided significant contribution to the preliminary conceptual design phase (late 1950s – 1960s). Currently, two main SCWR conceptual designs are in consideration. The first design involves a reactor pressure-vessel concept, while the second design is a pressure-channel concept.

In support of developing SCWRs, studies are being conducted on heat transfer at supercritical conditions. This thesis presents an analysis of heat transfer to supercritical water flowing in bare vertical tubes as a first step towards thermohydraulic calculations in a fuel channel. A large set of experimental data, obtained in Russia, was analyzed and an updated heat-transfer correlation for supercritical water was developed.

The experimental dataset was obtained for supercritical water flowing upward in a 4-m-long vertical bare tube. The data was collected at pressures of about 24 MPa for several combinations of wall and bulk-fluid temperatures that were below, at, or above the pseudocritical temperature. The values for mass flux ranged from 200 – 1500 kg/m<sup>2</sup>s, for heat flux up to 1250 kW/m<sup>2</sup> and inlet temperatures from 320 to 350°C.

This experimental dataset was obtained within conditions similar to those for proposed SCWR concepts. The HTC data were compared to those values calculated with the Dittus-Boelter, Bishop et al., Swenson et al. and Jackson correlations. The comparison showed that the Dittus-Boelter correlation deviates significantly from experimental data within the pseudocritical range. However, outside the pseudocritical region, the Dittus-Boelter correlation can closely predict experimental HTCs. The Bishop et al. and Jackson correlations represented more closely HTC profiles along the heated length of the tube than

the Dittus-Boelter correlation. However, they still deviate substantially from the experimental data within the pseudocritical range. The Swenson et al. correlation provided a better fit for the experimental data than the previous three correlations within some flow conditions, but does not closely follow the experimental data within others. It should be noted that neither of these correlations can be used for prediction of HTCs within the deteriorated heat-transfer regime.

Thus, an updated heat-transfer correlation is presented in this paper, for forced convective heat transfer in the normal heat-transfer regime, to supercritical water in a bare vertical tube. It has demonstrated a good fit for HTC values ( $\pm 25\%$ ) and for wall temperatures ( $\pm 15$ ) for the analyzed dataset. Thus, the new correlation presented in this thesis can be used (1) for preliminary heat-transfer calculations in SCWR fuel bundles, as a conservative approach; (2) for calculations of supercritical water heat-transfer in heat exchangers in SCWR indirect-cycle concepts; (3) for calculations of heat-transfer in heat exchangers for the co-generation of hydrogen at supercritical water NPPs; (4) for calculations of supercritical water heat-transfer in heat exchangers for other Generation IV reactor concepts with an indirect cycle; (5) for future comparisons with other independent datasets; (6) for comparisons with bundle data, as the reference case; (7) for the verification of computer codes for SCWR core thermalhydraulics; and (8) for the verification of scaling parameters between water and modeling fluids ( $\text{CO}_2$ , refrigerants, etc).

# Table of Contents

<b>1 INTRODUCTION</b>	<b>1</b>
1.1 First Concepts	1
1.2 Objectives	3
<b>2 GENERATION IV NUCLEAR-ENERGY SYSTEMS</b>	<b>5</b>
2.1 Generation IV Reactor Systems	5
2.2 Description of the Generation IV Systems	6
2.3 Supercritical Water-Cooled Reactor Concepts	8
<b>3 GENERAL FEATURES OF SUPERCRITICAL FLUIDS</b>	<b>12</b>
3.1 General Definition of Selected Terms and Expressions Related to Fluids at Critical and Supercritical Pressures	12
3.2 Physical Properties of Fluids in Critical and Pseudocritical Regions	16
3.2.1. Thermophysical Properties	16
3.2.2. Parametric Trends	19
<b>4 GENERAL CONSIDERATIONS FOR SUPERCRITICAL WATER     NPP CYCLES</b>	<b>25</b>
4.1 Review of Supercritical Turbines	25
4.2 Direct-, Indirect- and Dual-Cycle Options	26
4.3 Reheating Options	27
4.4 Regenerative Cycle	28
4.5 Turbine Options	28
4.6 Supercritical Water NPP Cycles Description	29
4.6.1. Single-Reheat Cycles System Description	29
4.6.2. No-Reheat Cycles System Description	32

4.7 Supercritical Water NPP Cycles Analysis and Results	34
4.8 Single-Reheat Option with Two Heat Exchangers	36
4.9 Co-Generation of Hydrogen	37
<b>5 HEAT TRANSFER CALCULATIONS FOR AN SCWR FUEL-CHANNEL</b>	<b>41</b>
5.1 SCWR Fuel-Channel Design	41
5.2 Axial Heat Flux Profiles	44
5.3 Parametric Trends	47
5.4 Bulk-Fluid Temperature Profile	50
5.5 Thermal Conductivity of the Cladding	51
5.6 Thermal Conductivity of the Fuel	52
5.7 Heat Transfer and Surface Temperature of Fuel Elements	53
5.8 Fuel Centerline Temperature	56
<b>6 HEAT TRANSFER CORRELATIONS AT SUPERCRITICAL PRESSURES</b>	<b>61</b>
6.1 Existing Heat Transfer Correlations	62
6.2 Comparison of Heat Transfer Correlations	64
6.3 Final Objective	66
<b>7 EXPERIMENTAL DATASET</b>	<b>68</b>
7.1 Test Facility	68
7.2 Test-Section Design	70
7.3 Instrumentation and Test Matrix	71
7.4 Experimental Procedure	72
7.5 Data Reduction	73
<b>8 EXPERIMENTAL RESULTS</b>	<b>77</b>
<b>9 DEVELOPING THE CORRELATION</b>	<b>95</b>

9.1 Dimensional Analysis	<b>95</b>
9.2 Manual Iterations	<b>99</b>
9.3 Second Iterations	<b>103</b>
9.4 Finalizing the Correlation	<b>105</b>
9.5 Verifying the Correlation	<b>107</b>
9.6 Comparison Graphs	<b>111</b>
<b>10 CONCLUSIONS</b>	<b>119</b>
<b>11 FUTURE WORK</b>	<b>120</b>
<b>REFERENCES</b>	<b>121</b>
<b>APPENDICES</b>	<b>131</b>

## LIST OF FIGURES

<b>Figure 2.1:</b> Nuclear Reactor Technology Progression Timeframe	<b>5</b>
<b>Figure 2.2:</b> Pressure Vessel SCWR Concept	<b>9</b>
<b>Figure 2.3:</b> Pressure-Tube Supercritical Water CANDU Nuclear Reactor Concept	<b>9</b>
<b>Figure 2.4:</b> Supercritical Water CANDU Fuel-Channel Design	<b>10</b>
<b>Figure 3.1:</b> Pressure-Temperature Diagram for Water in the Critical Region	<b>14</b>
<b>Figure 3.2:</b> Pressure-Temperature Diagram of Water for Typical Operating Conditions of SCWRs, PWRs, CANDU-6 Reactors and BWRs	<b>15</b>
<b>Figure 3.3:</b> Temperature-Entropy Diagram Comparison of Current Generation Nuclear Reactors and SCWRs	<b>15</b>
<b>Figure 3.4:</b> General Pressure-Temperature Phase Diagram	<b>16</b>
<b>Figure 3.5:</b> Specific Heat Peak vs. Temperature and Pressure	<b>17</b>
<b>Figure 3.6:</b> Effect of Pressure on Specific Heat Peaks for Water	<b>18</b>
<b>Figure 3.7:</b> Basic Thermophysical Properties of Water Near the Critical and Pseudocritical Points	<b>21</b>
<b>Figure 3.8:</b> Selected Properties for Supercritical Water within the Pseudocritical Region	<b>22</b>
<b>Figure 4.1:</b> Single-Reheat Cycle A for Supercritical Water NPP	<b>30</b>
<b>Figure 4.2:</b> Single-Reheat Cycle B for Supercritical Water NPP	<b>32</b>
<b>Figure 4.3:</b> No-Reheat Cycle C for Supercritical Water NPP	<b>33</b>
<b>Figure 4.4:</b> Single-Reheat Cycle with Two Heat Exchangers	<b>36</b>
<b>Figure 4.5:</b> Layout for $H_2$ Co-Generation Associated with Proposed Single-Reheat Supercritical Water NPPs	<b>39</b>
<b>Figure 5.1:</b> Axial Heat Flux Distribution Along a Heated Channel	<b>46</b>

<b>Figure 5.2:</b> Bulk-Fluid and Temperature and Thermophysical Properties Profiles for Water along Heated Length of Fuel-Channel	<b>48</b>
<b>Figure 5.3:</b> Prandtl Number and Specific Heat Profiles for Water along Heated Length of Fuel-channel	<b>48</b>
<b>Figure 5.4:</b> Bulk-Fluid Temperature and Enthalpy Profiles along Heated Fuel-Channel	<b>51</b>
<b>Figure 5.5:</b> Thermal Conductivity of Inconel-718	<b>52</b>
<b>Figure 5.6:</b> Thermal Conductivity of Uranium Oxide ( $UO_2$ )	<b>53</b>
<b>Figure 5.7:</b> Fuel Element Temperature and Heat Transfer Coefficient Profiles	<b>54</b>
<b>Figure 5.8:</b> Bulk-Fluid Temperature, Sheath Temperature and HTC Profiles	<b>55</b>
<b>Figure 5.9:</b> Profiles for Fuel Centerline Temperature	<b>59</b>
<b>Figure 6.1:</b> Temperature and HTC (Experimental and Calculated Values) Profiles along Heated Length of Bare Vertical Tube	<b>65</b>
<b>Figure 7.1:</b> Schematic of the SKD-1 Loop	<b>69</b>
<b>Figure 7.2:</b> SKD-1 Loop Test Section Schematic	<b>70</b>
<b>Figure 7.3:</b> Sample Experimental Run with Removed Outliers	<b>76</b>
<b>Figure 7.4:</b> Sample Experimental Run with Removed Points in the Deteriorated Heat Transfer and Improved Heat Transfer Regimes	<b>76</b>
<b>Figure 8.1:</b> Temperature and Heat Transfer Coefficient Variations along a 4-m Circular Tube at Various Heat Fluxes: Nominal Operating Conditions – $P_{in}=24.0 \text{ MPa}$ and $G=1500 \text{ kg/m}^2\text{s}$	<b>80</b>
<b>Figure 8.2:</b> Temperature and Heat Transfer Coefficient Variations along a 4-m Circular Tube at Various Heat Fluxes: Nominal Operating Conditions – $P_{in}=24.0 \text{ MPa}$ and $G=1000 \text{ kg/m}^2\text{s}$	<b>83</b>

<b>Figure 8.3:</b> Temperature and Heat Transfer Coefficient Variations along a 4-m Circular Tube at Various Heat Fluxes: Normal Operating Conditions – $P_{in}=24.0 \text{ MPa}$ and $G=500 \text{ kg/m}^2\text{s}$	<b>85</b>
<b>Figure 8.4:</b> Temperature and Heat Transfer Coefficient Variations along a 4-m Circular Tube at Various Heat Fluxes: Normal Operating Conditions – $P_{in}=24.0 \text{ MPa}$ and $G=200 \text{ kg/m}^2\text{s}$	<b>87</b>
<b>Figure 8.5:</b> Comparison of Experimental Heat Transfer Coefficient Values with Those Calculated Through Bishop et al. Correlation	<b>88</b>
<b>Figure 8.6:</b> Temperature and Heat Transfer Coefficient Variations along a 4-m Circular Tube at Various Heat Fluxes: Normal Operating Conditions – $P_{in}=24.0 \text{ MPa}$ , $G=1500 \text{ kg/m}^2\text{s}$	<b>90</b>
<b>Figure 8.7:</b> Temperature and Heat Transfer Coefficient Variations along a 4-m Circular Tube at Various Heat Fluxes: Normal Operating Conditions – $P_{in}=24.0 \text{ MPa}$ , $G=1000 \text{ kg/m}^2\text{s}$	<b>91</b>
<b>Figure 8.8:</b> Temperature and Heat Transfer Coefficient Variations along a 4-m Circular Tube at Various Heat Fluxes: Normal Operating Conditions – $P_{in}=24.0 \text{ MPa}$ , $G=500 \text{ kg/m}^2\text{s}$	<b>93</b>
<b>Figure 8.9:</b> Temperature and Heat Transfer Coefficient Variations along a 4-m Circular Tube at Various Heat Fluxes: Normal Operating Conditions – $P_{in}=24.0 \text{ MPa}$ , $G=200 \text{ kg/m}^2\text{s}$	<b>94</b>
<b>Figure 9.1:</b> Regular and Averaged Specific Heat and Prandtl Number Values	<b>98</b>
<b>Figure 9.2:</b> Scatter Plot for $\text{Re}_b$ versus $\text{Nu}_b$	<b>99</b>
<b>Figure 9.3:</b> Determination of the Exponent of the Average Prandtl Number	<b>100</b>
<b>Figure 9.4:</b> Determination of the Exponent of the Ratio of Densities	<b>101</b>
<b>Figure 9.5:</b> Determination of the Exponent of the Ratio of Viscosities	<b>102</b>
<b>Figure 9.6:</b> Determination of Refined Reynolds Number Exponent	<b>103</b>

<b>Figure 9.7:</b> Determination of Refined Averaged Prandtl Number Exponent	<b>104</b>
<b>Figure 9.8:</b> Determination of Refined Densities Ratio Exponent	<b>105</b>
<b>Figure 9.9:</b> Comparison of Data Fit with Experimental Data	<b>106</b>
<b>Figure 9.10:</b> Temperature and Heat Transfer Coefficient Variations along a 4-m Circular Tube at Various Heat Fluxes ( $ID=10\text{ mm}$ ): Normal Operating Conditions – $P_{in}=24.0\text{ MPa}$ , $G=200\text{ kg/m}^2\text{s}$	<b>107</b>
<b>Figure 9.11:</b> Temperature and Heat Transfer Coefficient Variations along a 4-m Circular Tube at Various Heat Fluxes ( $ID=10\text{ mm}$ ): Normal Operating Conditions – $P_{in}=24.0\text{ MPa}$ , $G=500\text{ kg/m}^2\text{s}$	<b>109</b>
<b>Figure 9.12:</b> Temperature and Heat Transfer Coefficient Variations along a 4-m Circular Tube at Various Heat Fluxes ( $ID=10\text{ mm}$ ): Normal Operating Conditions – $P_{in}=24.0\text{ MPa}$ , $G=1000\text{ kg/m}^2\text{s}$	<b>110</b>
<b>Figure 9.13:</b> Temperature and Heat Transfer Coefficient Variations along a 4-m Circular Tube at Various Heat Fluxes ( $ID=10\text{ mm}$ ): Normal Operating Conditions – $P_{in}=24.0\text{ MPa}$ , $G=1500\text{ kg/m}^2\text{s}$	<b>111</b>
<b>Figure 9.14:</b> Temperature and Heat Transfer Coefficient Profiles along Heated Length of Bare Vertical Tube: $G=500\text{ kg/m}^2\text{s}$ and $q=290\text{ kW/m}^2$	<b>112</b>
<b>Figure 9.15:</b> Temperature and Heat Transfer Coefficient Profiles along Heated Length of Bare Vertical Tube: $G=1000\text{ kg/m}^2\text{s}$ and $q=480\text{ kW/m}^2$	<b>112</b>
<b>Figure 9.16:</b> Temperature and Heat Transfer Coefficient Comparisons Between Final Correlation and CFD Code Calculations along a 4-m Circular Tube ( $ID= 10\text{ mm}$ ): Operating Conditions – $P_{in}=24.0\text{ MPa}$ , $G=1000\text{ kg/m}^2\text{s}$	<b>113</b>
<b>Figure 9.17:</b> Temperature and Heat Transfer Coefficient Variations along a Circular Tube at Various Heat Fluxes: Nominal Operating Conditions – $P_{in} = 25.5\text{ MPa}$	<b>116</b>

**Figure 9.18:** Temperature and Heat Transfer Coefficient Variations along a Tube at Various Heat Fluxes: Nominal Operating Conditions –  $P_{in} = 24.5 \text{ MPa}$

**117**

**Figure 9.19:** Temperature and Heat Transfer Coefficient Variations along a Circular Tube at Various Heat Fluxes: Nominal Operating Conditions –  $P_{in} = 24.5 \text{ MPa}$

**118**

## LIST OF TABLES

<b>Table 3.1:</b> <i>Critical Parameters of Water</i>	<b>17</b>
<b>Table 3.2:</b> <i>Value of Pseudocritical Temperatures and Corresponding Specific Heat Peak Values</i>	<b>18</b>
<b>Table 3.3:</b> <i>Peak Values of Specific Heat, Volume Expansivity and Thermal Conductivity in Critical and Near Pseudocritical Points</i>	<b>19</b>
<b>Table 3.4:</b> <i>Major Parameters of Supercritical Water CANDU (Canada) and VVER-SCP (Russia) Nuclear-Reactor Concepts</i>	<b>23</b>
<b>Table 4.1:</b> <i>Major Parameters of Selected Current and Upcoming Hitachi Supercritical Plants</i>	<b>25</b>
<b>Table 4.2:</b> <i>Thermal Efficiency of Supercritical Water NPP Cycles</i>	<b>34</b>
<b>Table 4.3:</b> <i>Selected Parameters of Proposed Supercritical Water NPP Cycles A and C</i>	<b>35</b>
<b>Table 4.4:</b> <i>Selected Parameters of Proposed SCWR Fuel-Channels</i>	<b>35</b>
<b>Table 4.5:</b> <i>Chemical Reaction Steps and Basic Parameters of the Copper-Chlorine Cycle</i>	<b>38</b>
<b>Table 5.1:</b> <i>Fuel-Channel Major Parameters used in Calculations</i>	<b>43</b>
<b>Table 6.1:</b> <i>Dyadyakin and Popov Test Bundle Parameters</i>	<b>61</b>
<b>Table 7.1:</b> <i>Uncertainties of Primary Parameters</i>	<b>71</b>
<b>Table 7.2:</b> <i>Dataset Test Matrix</i>	<b>72</b>
<b>Table 9.1:</b> <i>Description of Various Parameters of Heat Transfer</i>	<b>95</b>
<b>Table 9.2:</b> <i><math>\Pi</math> Terms of the Empirical Correlation</i>	<b>96</b>
<b>Table 9.3:</b> <i>Test Matrix for Mokry et al. Correlation</i>	<b>106</b>
<b>Table 9.4:</b> <i>Other Datasets and Corresponding Test Matrices</i>	<b>115</b>

## LIST OF APPENDICES

<b>Appendix A:</b> Supercritical Carbon Dioxide	<b>131</b>
<b>Appendix B:</b> Other Datasets Graph Comparisons	<b>156</b>
<b>Appendix C:</b> Conferences Attended, Papers Presented and Awards Received	<b>164</b>
<b>Appendix D:</b> Publications of S. Mokry	<b>167</b>

## NOMENCLATURE

$A$	area, m <sup>2</sup>
$a$	coefficient
$c_p$	specific heat, J/kg·K
$\bar{c}_p$	average specific heat, J/kg·K, $\left( \frac{H_w - H_b}{T_w - T_b} \right)$
$D$	diameter, m
$E$	electrical energy, J
$G$	mass flux, kg/m <sup>2</sup> s
$H$	enthalpy, J/kg
$HL$	heat loss, W
$h$	heat transfer coefficient, W/m <sup>2</sup> K
$I$	Current, A
$K$	Temperature, K
$k$	thermal conductivity, W/m·K
$L$	length, m
$M$	mass, kg
$\dot{m}$	mass flow rate, kg/s
$P$	pressure, Pa
POW	power, W
$p$	perimeter, m
$Q$	thermal energy, J
$\dot{q}$	heat transfer rate, W
$q$	heat flux, W/m <sup>2</sup>

$R$	electrical resistance, $\Omega$
$R_a$	surface roughness, $\mu\text{m}$
$T$	time, $\text{s}$
$T$	temperature, $^{\circ}\text{C}$
$V$	velocity, $\text{m/s}$
$V$	volume, $\text{m}^3$
$V$	voltage, $\text{V}$
$x$	axial location, $\text{m}$

### Greek letters

$\Delta$	difference
$\mu$	dynamic viscosity, $\text{Pa}\cdot\text{s}$
$\rho$	density, $\text{kg}/\text{m}^3$
$\sigma$	thickness, $\text{m}$

### Dimensionless numbers

$\text{Nu}$	Nusselt number $\left( \frac{h \cdot D}{k} \right)$
$\text{Pr}$	Prandtl number $\left( \frac{\mu \cdot c_p}{k} \right)$
$\overline{\text{Pr}}$	averaged Prandtl number $\bar{c}_p \left( \frac{\mu_b}{k_b} \right)$
$\text{Re}$	Reynolds number $\left( \frac{G \cdot D}{\mu} \right)$

### Subscripts

ave	average
b	bulk
calc	calculated
central	central
ch	channel
clad	cladding
CO <sub>2</sub>	carbon dioxide
cr	critical
dht	deteriorated heat-transfer
el	electrical
exp	experimental
ext	external
flow	flow
fuel	fuel
h	heated
hy	hydraulic
in	inlet
int	internal
l	local
main	main (loop)
max	maximum
mixer	mixing chamber
out	outlet

pc	pseudocritical
pt	pressure tube
reheat	reheat (loop)
th	thermal
TS	test section
v	volumetric
W	water
w	wall
wet	wet

Abbreviations:

AECL	Atomic Energy Canada Limited
AHFD	Axial Heat Flux Distribution
AHFP	Axial Heat Flux Profile
BWR	Boiling Water Reactor
CANDU	CANada Deuterium Uranium (reactor)
CEP	Condensate Extraction Pump
CFD	Computational Fluid Dynamics
CHF	Critical Heat Flux
CO <sub>2</sub>	Carbon Dioxide
CRL	Chalk River Laboratories
DAS	Data Acquisition System
DHT	Deteriorated Heat Transfer (regime)

GFR	Gas-cooled Fast Reactor
GIF	Generation IV International Forum
HHV	Higher-Heating Value
HP	High Pressure
HTC	Heat Transfer Coefficient
HTR	HeaTeR
HWR	Heavy Water Reactor
ID	Internal Diameter
IHT	Improved Heat Transfer (regime)
IP	Intermediate Pressure
KP-SKD	Pressure-tube nuclear reactor at supercritical pressure (in Russian abbreviations)
LFR	Lead-cooled Fast Reactor
LHV	Lower-Heating Value
LP	Low Pressure
LWR	Light Water Reactor
MSR	Molten Salt Reactor
MSRH	Moisture Separator ReHeater
N <sub>2</sub>	Nitrogen Gas
NHT	Normal Heat Transfer
NIST	National Institute of Standards and Technology
NPP	Nuclear Power Plant
OD	Outside Diameter
PT	Pressure Tube (reactor)
PV	Pressure Vessel (reactor)

PWR	Pressurized Water Reactor
RDIPE	Research & Development Institute of Power Engineering (Moscow) (NIKIET in Russian abbreviations)
RFP	Reactor Feedwater Pump
SCWR	SuperCritical Water Reactor
SFR	Sodium-cooled Fast Reactor
SHS	SuperHeated Steam
SRH	Steam ReHeat
TS	Test Section
UOIT	University of Ontario Institute of Technology
USA	United States of America
USSR	Union of Soviet Socialist Republics
VHTR	Very-High Temperature Reactor
VVER-SCP	Supercritical Water-Water Power Reactor (in Russian Abbreviations)

# CHAPTER 1

## INTRODUCTION

### 1.1 First Concepts

Investigation of heat transfer at supercritical pressures began as early as the 1930s. Schmidt et al. (Schmidt et al., 1946; Schmidt, 1960) determined that a fluids' free convection Heat Transfer Coefficient (HTC) was higher within the critical point. Their utilization of a working fluid at the near-critical point in single-phase thermosyphons arose from this finding (Pioro and Pioro, 1997).

In the 1950s, the concept of using supercritical "steam" to increase the thermal efficiency of fossil-fired power plants became an attractive option. At supercritical pressures, there is no liquid-vapour phase transition; therefore, dryout or Critical Heat Flux (CHF) does not occur. Deterioration in heat transfer may occur, only at high heat fluxes and low mass fluxes. This deterioration is gradual, and does not result in the same dramatic drop in heat transfer that is associated with the dryout in boiling fluids. The USA and the former USSR intensively studied supercritical heat transfer during the 1950s till the 1980s. Research primarily focused around circular water-cooled tube flow geometry.

Near the end of the 1950s and at the beginning of the 1960s, several studies were conducted to investigate the potential of using supercritical water as a coolant in nuclear reactors. Several concepts of SuperCritical Water-cooled nuclear Reactors (SCWRs) were subsequently developed (Pioro and Duffey, 2007). Unfortunately, this idea was abandoned, likely due to material constraints. However, in the 1990s, almost 30 years later, SCWR concepts became attractive again as a means to improve upon the performance of current operating reactors.

The primary objectives for using supercritical water as a coolant in nuclear reactors are: (1) to increase the thermal efficiency of modern Nuclear Power

Plants (NPPs), which is currently 30 – 35%, to approximately 45% or higher, and (2) to decrease the operational and capital costs by eliminating the steam generators, steam separators, steam dryers, etc. that are currently used in modern plants.

Once SCWR concepts regained momentum, many countries including Canada, China, Germany, Japan, Korea, Russia, the USA and others started to work on developing these concepts. Recently, the Generation IV International Forum (GIF) identified SCWRs as one of six promising emerging nuclear-reactor technologies. As a result, there are currently a number of SCWR concepts under development worldwide.

In support of the development of an SCWR, it is necessary to perform a heat-transfer analysis. As a first step in this process, heat-transfer to supercritical water in bare vertical tubes can be investigated as a conservative approach (in general, heat-transfer in fuel bundles will be enhanced with various types of appendages, i.e. bearing pads, end plates, fins, ribs, spacers, etc.).

Therefore, a large set of experimental data, obtained in Russia, was analyzed. This experimental dataset was obtained within conditions similar to those for proposed SCWR concepts. The dataset was obtained for supercritical water flowing upward in a 4-m-long vertical bare tube. The data was collected at pressures of approximately 24 MPa for several combinations of wall and bulk-fluid temperatures that were below, at, or above the pseudocritical temperature. The values for mass flux ranged from 200 – 1500 kg/m<sup>2</sup>s, for heat flux up to 1250 kW/m<sup>2</sup> and inlet temperatures from 320 to 350°C.

Previous study (Pioro et al., 2008a) confirmed that there are three heat-transfer regimes for forced convective heat transfer to water flowing inside tubes at supercritical pressures: (1) Normal heat-transfer regime; (2) Deteriorated heat-transfer regime, characterized by lower than expected HTCs values than in the

normal heat-transfer regime; and (3) Improved heat-transfer regime with higher-than-expected HTC values within some part of a test section compared to those of the normal heat-transfer regime. Building on the first steps and conservative approach basis, only heat-transfer within the normal heat-transfer regime was considered in this thesis.

Pioro and Duffey (2007) have shown that there are a number of supercritical water heat-transfer correlations available in the open literature. However, a comparison of selected correlations has shown that their results may differ from one another by more than 200%. A comparison between the Bishop et al. (1964), Dittus-Boelter (1930), Jackson (2002) and Swenson et al. (1965) correlations and the experimental dataset was conducted. As well, experimental HTC values within the normal heat-transfer regime were compared to those calculated using the Computational Fluid Dynamics (CFD) code FLUENT 6.0.

The results showed that the Dittus-Boelter correlation significantly overestimates the experimental HTC values within the pseudocritical range. The Bishop et al. and Jackson correlations tended also to deviate substantially from the experimental data within the pseudocritical range. The Swenson et al. correlation provided a better fit for the experimental data than the previous three correlations within some flow conditions, but did not follow closely the experimental data within others. Also, HTC and wall temperature values calculated with the FLUENT CFD code might deviate significantly from the experimental data, for example, the  $k$ - $\varepsilon$  model (wall function). However, the  $k$ - $\varepsilon$  model (low Reynolds numbers) shows a better fit within some flow conditions.

## 1.2 Objectives

Based on these comparisons, it became evident that there is a need for a reliable, accurate and wide range supercritical water heat-transfer correlation to be used:

1. For preliminary calculations of supercritical-water-cooled fuel bundles, as a conservative approach in relation to SCWRs;
2. For calculations of supercritical water heat-transfer in heat exchangers in SCWR indirect cycle concepts;
3. For calculations of heat-transfer in heat exchangers for the co-generation of hydrogen at supercritical water NPPs;
4. For calculations of supercritical water heat-transfer in heat exchangers for other Generation IV reactor concepts with an indirect cycle;
5. For future comparisons with other independent datasets;
6. For comparisons with bundle data, as the reference case;
7. For the verification of computer codes for SCWR core thermalhydraulics; and
8. For the verification of scaling parameters between water and modeling fluids ( $\text{CO}_2$ , refrigerants, etc.).

Therefore, the objective of this thesis is to develop a new correlation for the normal heat-transfer regime in a bare vertical tube to improve upon the fundamental knowledge of heat transport processes.

## Chapter 2

### GENERATION IV NUCLEAR-ENERGY SYSTEMS

#### 2.1 Generation IV Reactor Systems

In 2001, ten countries, including Canada, initiated the GIF to collaboratively develop the next generation of nuclear-energy systems, which will provide competitively-priced and reliable energy in a safe and sustainable manner. Over 100 potential nuclear reactor concepts (or "systems") were reviewed by an international panel of experts. This panel selected six reactor types that best matched the Generation IV objectives of sustainability, economics, safety and reliability and proliferation resistance and physical protection. Figure 2.1 shows the evolution timeframe of nuclear reactor technology (GIF, 2002).

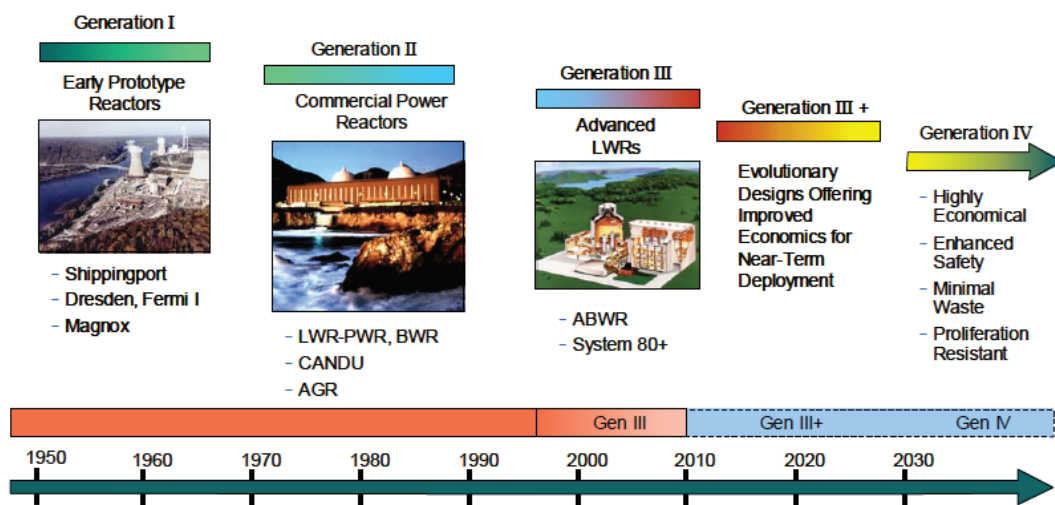


**Figure 2.1. Nuclear Reactor Technology Progression Timeframe (GIF, 2002).**

Goals for Generation IV Reactors, as presented in A Technology Roadmap for Generation IV Nuclear Energy Systems (GIF, 2002) are:

- **Sustainability** – Generation IV nuclear-energy systems will provide sustainable energy generation that meets clean-air objectives and promotes long-term availability of systems and effective fuel utilization for worldwide energy production. In addition, Generation IV nuclear-energy systems will

minimize and manage their nuclear waste and notably reduce the long-term stewardship burden, thereby improving protection for public health and the environment.

- **Economics** – Generation IV nuclear-energy systems will have a clear life-cycle cost advantage over other energy sources. As well, Generation IV nuclear-energy systems will have a level of financial risk comparable to other energy projects.
- **Safety and Reliability** – Generation IV nuclear-energy system operations will excel in safety and reliability. These systems will have a very low likelihood and degree of reactor-core damage. Generation IV nuclear-systems will eliminate the need for offsite emergency response.
- **Proliferation Resistance and Physical Protection** – Generation IV nuclear-energy systems will increase the assurance that they are a very unattractive and the least desirable route for diversion or theft of weapons-usable materials, and provide increased physical protection against acts of terrorism.

These goals had three objectives: First, they served as the basis for developing criteria to assess and compare Generation IV systems. Second, they were challenging and stimulated the search for innovative nuclear-energy systems — through both fuel cycles and reactor technologies. Third, they served to motivate and guide the Research and Development of Generation IV systems as collaborative efforts got underway.

## **2.2 Descriptions of the Generation IV Systems**

After review and evaluation, the GIF panel identified six reactor systems to be developed for future generations of nuclear-energy systems. A summary (GIF, 2002) of these systems follows:

- **Gas-cooled Fast Reactors (GFRs)** – these systems will have a fast-neutron spectrum and a closed-fuel cycle. They will use a direct Brayton-cycle helium turbine for electricity production and can use process heat for the thermochemical production of hydrogen. The current reference reactor design operates at 9 MPa with an outlet temperature of 850°C.
- **Lead-cooled Fast Reactors (LFRs)** – these systems will use molten lead or lead-bismuth eutectic coolant and feature a fast-neutron spectrum. The LFR system is cooled via natural convection and has a reactor outlet coolant temperature within a range of 550 – 800°C. LFR systems will operate on a closed-fuel cycle with long refueling intervals of approximately 15 – 20 years.
- **Molten Salt Reactors (MSRs)** – these systems will use a molten salt mixture as the primary coolant for the reactor. MSRs have a high-temperature operation (inlet 565°C and outlet up to 850°C) which holds the potential for hydrogen production. The nuclear fuel for these reactors can either be solid fuel rods or dissolved in the coolant itself.
- **Sodium-cooled Fast Reactors (SFRs)** – these systems will operate with a closed-fuel recycle system and a fast spectrum. The outlet temperature ranges from 530 – 550°C. One of the primary goals for the development of SFR systems is the efficient management of reactor fuel through nearly full actinide recovery and recycle.
- **Very-High-Temperature Reactors (VHTRs)** – these systems are graphite-moderated, helium-cooled and will operate with a thermal neutron spectrum. The coolant inlet temperature is approximately 640°C while the outlet temperature is up to 1000°C. VHTR can produce a co-generation of heat and power, allowing for hydrogen production as well as for process heat which would have numerous industrial applications.
- **Super-Critical Water-cooled Reactors (SCWRs)** – these systems are high-temperature, high pressure reactors. They will use supercritical water as the

working fluid and will operate above the thermodynamic critical point of water (22.1 MPa and 374°C). These plants offer a high thermal efficiency of up to 45 – 50% in addition to plant simplification.

The majority of these Generation IV reactor concepts will be linked to the **supercritical water Rankine cycle**, through heat exchangers, due to their high outlet temperatures in the primary circuit. Even helium cooled reactors have two concept options that may be connected through heat exchangers to the supercritical water Rankine Cycle if helium gas turbines are not designed or are not reliable in operation.

Also, SCWRs are considered to be a conventional way of developing ultimate water-cooled reactors. The thermal power industry went through the transition to supercritical water 50 years ago. Accounting on the extensive work already established for supercritical power plants, Canada is participating in the development of an SCWR, which is also a natural evolution of the current Canadian CANDU<sup>1</sup> technology.

### **2.3 Supercritical Water-Cooled Reactor Concepts**

There are two types of SCWRs currently being developed as part of the GIF initiative: (a) A large reactor Pressure Vessel (PV) (see Figure 2.2), with a wall thickness of about 0.5 m, to contain the reactor core analogous to conventional Light Water Reactors (LWRs); or (b) Distributed Pressure Tubes (PTs) (see Figure 2.3) analogous to conventional Heavy Water Reactors (HWRs). Within these two main classes, the PT reactors are designed to be more flexible to flow, flux and density changes when compared to the PV-type reactors.

---

<sup>1</sup> CANDU® (CANada Deuterium Uranium) is a registered trademark of Atomic Energy of Canada Limited (AECL).

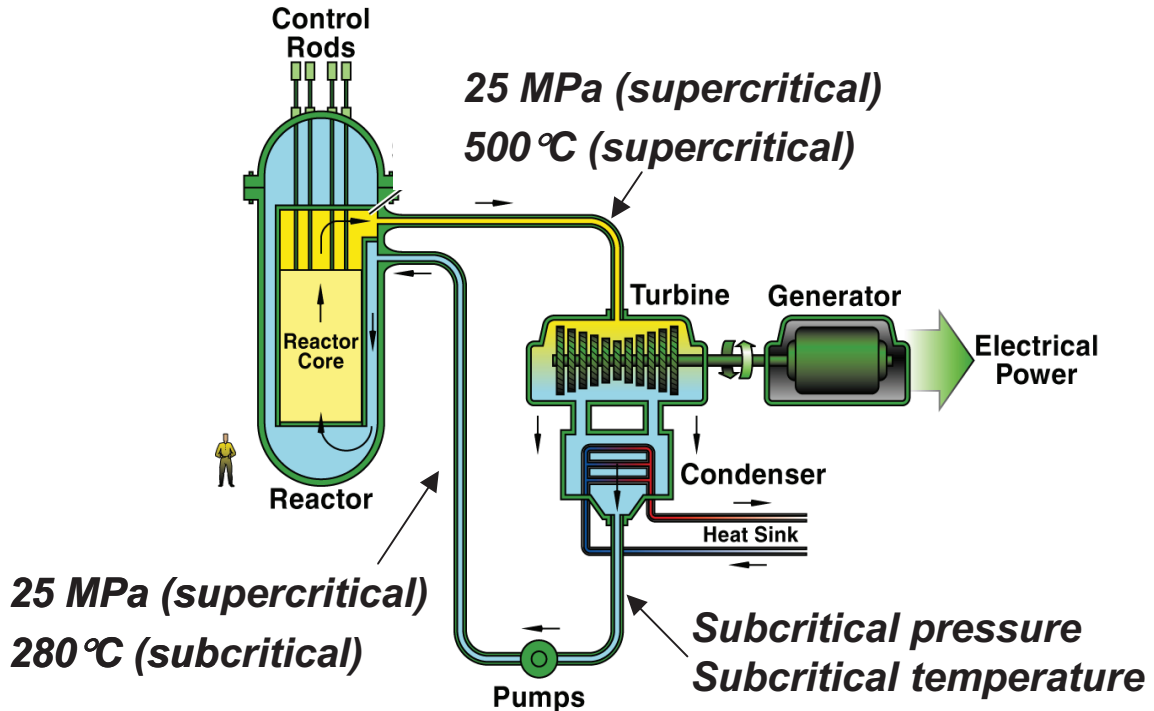


Figure 2.2. Pressure Vessel SCWR Concept  
(courtesy of Professor J. Buongiorno (MIT) (Buongiorno and MacDonald 2003)).

## Multiple products are key to sustainable future and competitive designs

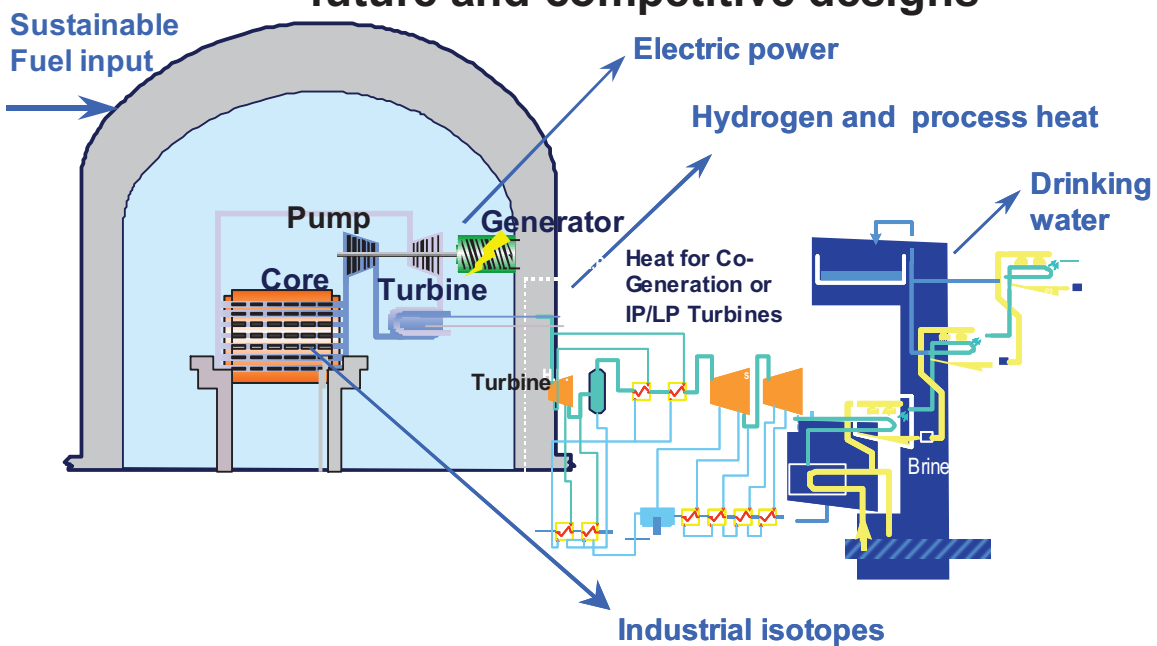
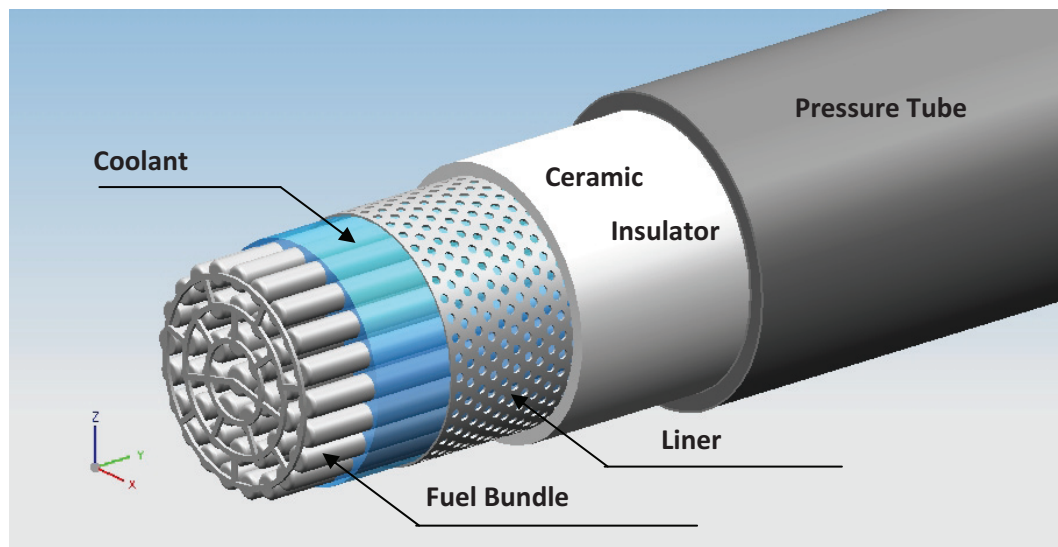


Figure 2.3. Pressure-Tube Supercritical Water CANDU Nuclear Reactor Concept  
(courtesy of Dr. R. Duffey (AECL) (Pioro and Duffey, 2007)).

Atomic Energy of Canada Limited (AECL) and the Research and Development Institute of Power Engineering (RDIPE or NIKIET in Russian abbreviations) are currently developing concepts of the PT SCWRs. However, only the Canadian concept is considered in this study.

A fuel-channel design, for proposed SCWR concepts (Chow and Khartabil, 2008) is shown in Figure 2.4. The fuel-channel consists of a bundle, liner tube, ceramic layer, and pressure tube.



**Figure 2.4. Supercritical Water CANDU Fuel-Channel Design**  
(courtesy of W. Peiman) (Pioro et al., 2010).

The outer surface of the pressure tube will be in direct contact with the moderator while the inner surface of the pressure tube is covered with a ceramic layer to protect the pressure tube from exposure to high temperature coolant. In addition, a perforated metal liner covers and protects the insulator from damage during fueling and/or refueling and from erosion by the coolant flow.

Supercritical Water NPPs will have much higher operating parameters (i.e., pressures of about 25 MPa and outlet temperatures up to 625°C) compared to current NPPs (Pioro and Duffey, 2007). These temperatures and pressures are similar to supercritical thermal power plants, and will offer higher plant efficiency.

Similar to Boiling Water Reactors (BWRs), SCWRs will operate on a direct cycle where the coolant in the reactor is also used in the turbines, thus, eliminating the need for steam generators, steam separators, seam dryers, and recirculation and jet pumps.

A key feature of SCWRs is that the supercritical water coolant is only a single-phase fluid. This is similar to current Pressurized Water Reactors (PWRs). However, SCWRs operate at much higher pressures and temperatures than either PWRs or BWRs. Water at these supercritical conditions will have properties between those of a liquid and a gas. An analysis of properties of fluids in critical and pseudocritical regions is provided in the following Chapter.

## CHAPTER 3

### GENERAL FEATURES OF SUPERCRITICAL FLUIDS

#### 3.1 General Definitions of Selected Terms and Expressions Related to Fluids at Critical and Supercritical Pressures

Prior to a discussion on thermophysical properties of supercritical fluids and SCWR concepts, it is important to define special terms and expressions used at these conditions. Therefore, general definitions of selected terms and expressions related to critical and supercritical pressures, as presented in Pioro and Duffey (2007), are listed below. In order to illustrate these terms and expressions a thermodynamic diagram for water is shown in Figure 3.1.

**Compressed fluid** is a fluid at a pressure above the critical pressure, but at a temperature below the critical temperature.

**Critical point** (also called a *critical state*) is the point where the distinction between the liquid and gas (or vapor) phases disappears, i.e., both phases have the same temperature, pressure and volume. The *critical point* is characterized by the phase state parameters  $T_{cr}$ ,  $P_{cr}$  and  $V_{cr}$ , which have unique values for each pure substance.

**Deteriorated heat transfer (DHT)** is characterized by lower values of the wall heat transfer coefficient compared to those at the normal heat transfer regime and hence has higher values of wall temperature within some part of a test section or within the entire test section.

**Improved heat transfer (IHT)** is characterized by higher values of the wall heat transfer coefficient compared to those at the normal heat transfer regime and hence lower values of wall temperature within some part of a test section or within the entire test section.

**Near-critical point** is actually a narrow region around the critical point where all the thermophysical properties of a pure fluid exhibit rapid variations.

**Normal heat transfer (NHT)** can be characterized by wall heat transfer coefficients similar to those of subcritical convective heat transfer far from the critical or pseudocritical regions, when are calculated according to the conventional single-phase Dittus-Boelter type correlations.

**Pseudo-boiling** is a physical phenomenon similar to subcritical pressure nucleate boiling, which may appear at supercritical pressures. Due to heating of the supercritical fluid with a bulk-fluid temperature below the pseudocritical temperature (high-density fluid, i.e., “liquid”), some layers near a heating surface may attain temperatures above the pseudocritical temperature (low-density fluid, i.e., “gas”). This low-density “gas” leaves the heating surface in the form of variable density (bubble) volumes. During the pseudo-boiling, the wall heat transfer coefficient usually increases (improved heat-transfer regime).

**Pseudocritical point** (characterized with  $P_{pc}$  and  $T_{pc}$ ) is a point at a pressure above the critical pressure and at a temperature ( $T_{pc} > T_{cr}$ ) corresponding to the maximum value of the specific heat for this particular pressure.

**Pseudo-film boiling** is a physical phenomenon similar to subcritical pressure film boiling, which may appear at supercritical pressures. At pseudo-film boiling, a low-density fluid (a fluid at temperatures above the pseudocritical temperature, i.e., “gas”) prevents a high-density fluid (a fluid at temperatures below the pseudocritical temperature, i.e., “liquid”) from contacting (“rewetting”) a heated surface. Pseudo-film boiling leads to the deteriorated heat transfer regime.

**Supercritical fluid** is a fluid at pressures and temperatures that are higher than the critical pressure and critical temperature. However, in the current thesis, the term *supercritical fluid* includes both terms – *supercritical fluid* and *compressed fluid*.

**Supercritical steam (“steam”)** is actually supercritical water because at supercritical pressures there is no difference between phases. However, this term is widely used in literature in relation to supercritical steam generators and turbines.

**Superheated steam** is a steam at pressures below the critical pressure, but at temperatures above the critical temperature.

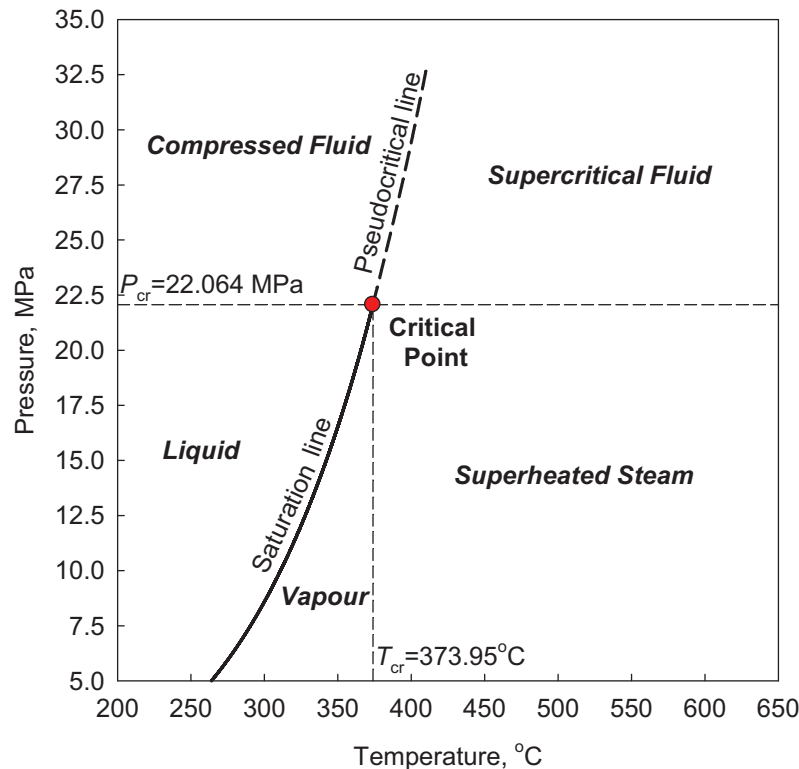


**Figure 3.1. Pressure-Temperature Diagram for Water in the Critical Region**  
**(Mokry et al., 2009a).**

Figure 3.2 and 3.3 outline the differences in the operating conditions (pressures, temperatures and entropy) of current generation reactor systems in comparison to SCWRs. Compared to existing PWRs, SCWRs would involve increasing the coolant pressure from 10 – 16 MPa to about 25 MPa, the inlet temperature to about 350°C, and the outlet temperature to 625°C. The coolant would pass through the pseudocritical region before reaching the channel outlet (Pioro and Duffey, 2007).

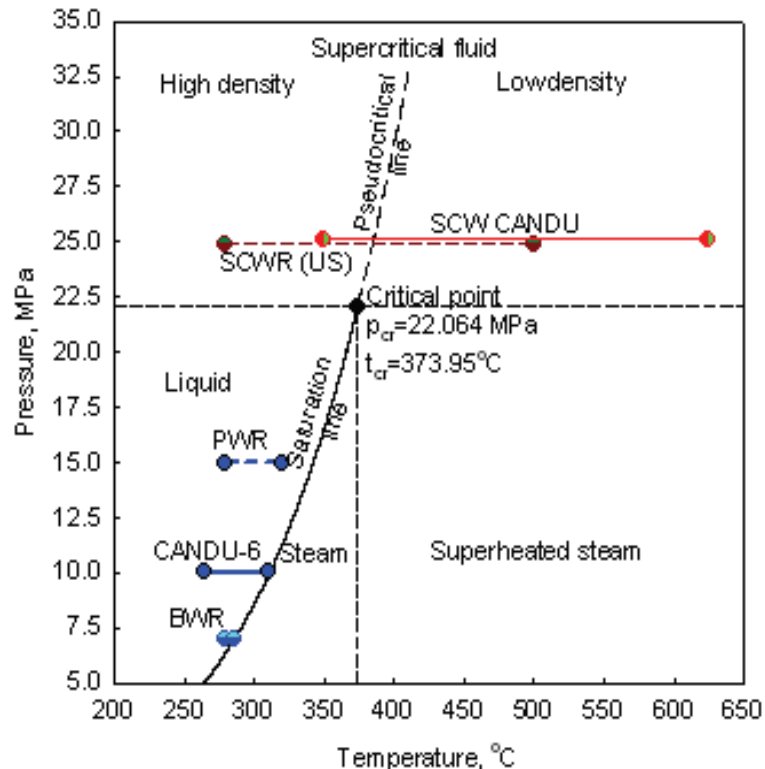


**Figure 3.2. Pressure-Temperature Diagram of Water for Typical Operating Conditions of SCWRs, PWRs, CANDU-6 Reactors and BWRs (Pioro and Duffey, 2007).**

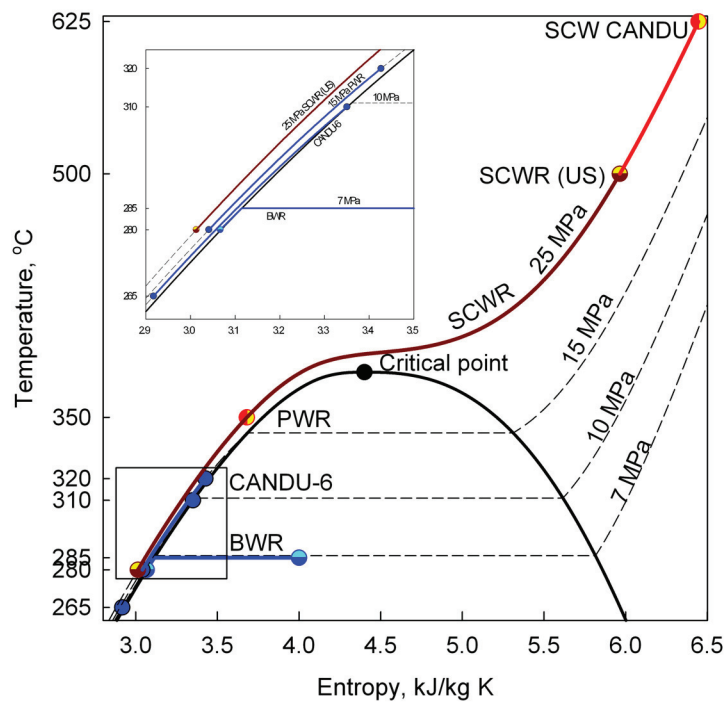


**Figure 3.3. Temperature-Entropy Diagram Comparison of Current Generation Nuclear Reactors and SCWRs (Pioro and Duffey, 2007).**

### 3.2 Physical Properties of Fluids in Critical and Pseudocritical Regions

Supercritical fluids have unique properties (Pioro et al., 2004; Pioro and Duffey, 2003). It is well established that thermophysical properties of any fluid, including water, experience significant changes within critical and pseudocritical regions. Beyond the critical point, the fluid becomes a supercritical fluid, or dense gas (see Figure 3.4, calculated with NIST (2009)). Crossing from high-density fluid to low-density fluid does not involve a distinct phase change.

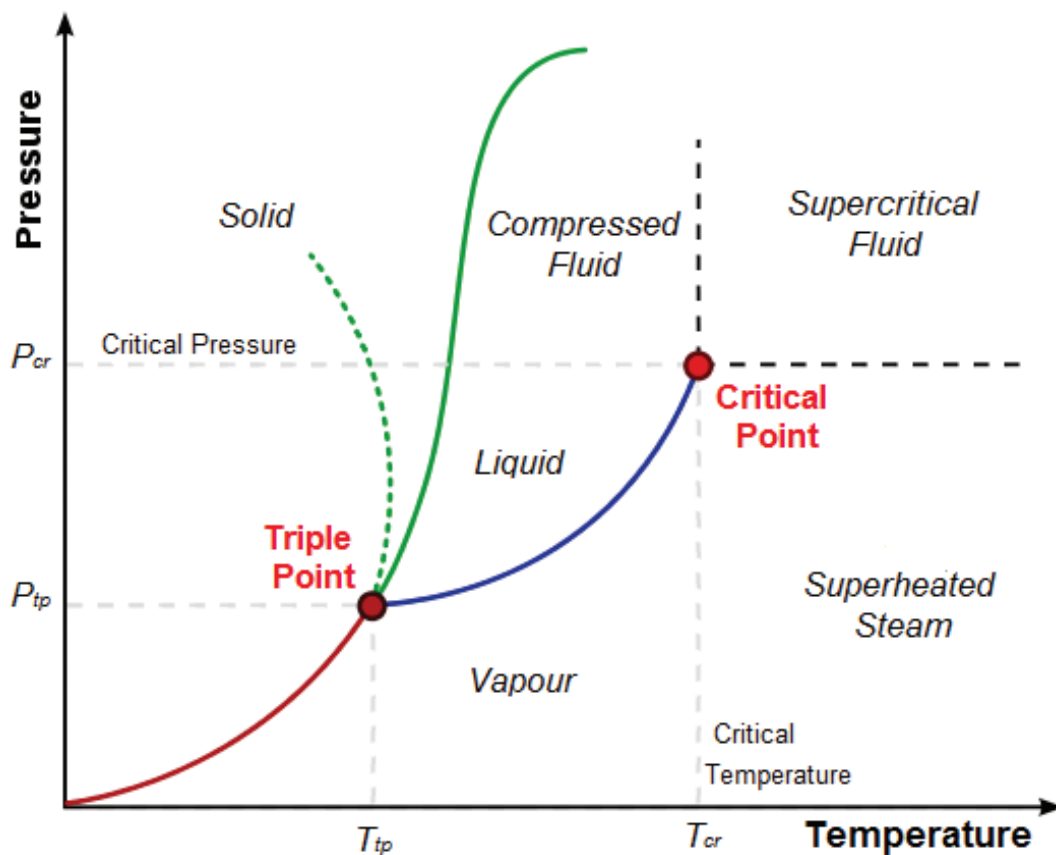


Figure 3.4. General Pressure-Temperature Phase Diagram.

#### 3.2.1 Thermophysical Properties

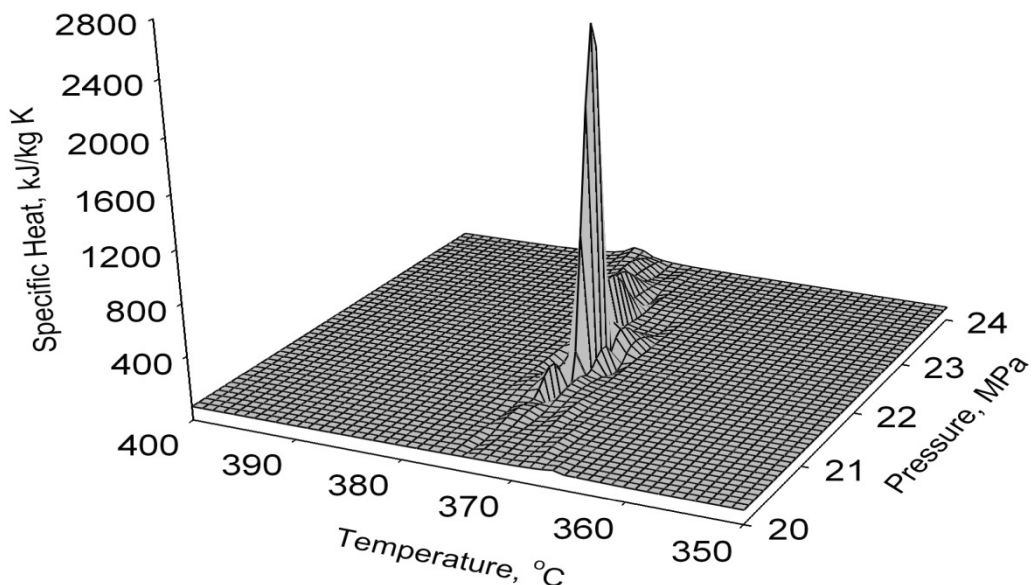
The specific heat of water has the maximum value at the critical point. The exact temperature that corresponds to the specific heat peak above the critical pressure is known as the pseudocritical point (Pioro and Duffey, 2007). Table 3.1 presents the critical parameters of water.

**Table 3.1. Critical Parameters of Water (NIST, 2009).**

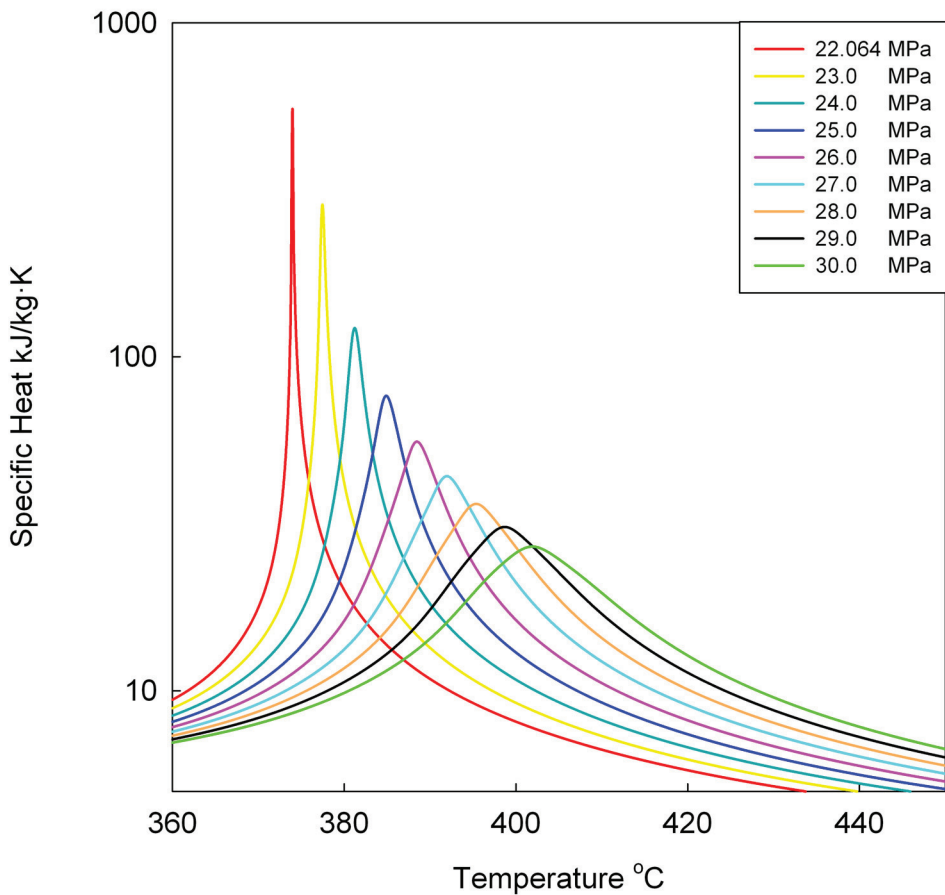
Parameter	Unit	Water
Critical Pressure	MPa	22.064
Critical Temperature	°C	373.95
Critical Density	kg/m <sup>3</sup>	322.0

Figure 3.5 shows the dependence of specific heat on temperature and pressure.

At the critical point, specific heat has its maximum value. In addition, it can be noted that there is a local maximum value of specific heat capacity for each pressure (Figures 3.5 and 3.6). Table 3.2 provides the pseudocritical temperature and corresponding specific heat peak values for selected pressures above the critical pressure (Figures and Tables calculated using NIST 2009).



**Figure 3.5. Specific Heat Peak vs. Temperature and Pressure.**



**Figure 3.6. Effect of Pressure on Specific Heat Peaks for Water.**

It can be seen that as a pressure increases, the pseudocritical temperature increases; however, the peak value in specific heat decreases (see Figure 3.6 and Table 3.2).

**Table 3.2. Values of Pseudocritical Temperatures and Corresponding Specific Heat Peak Values.**

Pressure, MPa	Pseudocritical Temperature, °C	Specific Heat Peak Value, kJ/kg·K
22.064	373.95	3885.8
23	377.5	286.1
24	381.2	122.0
25	384.9	76.4
26	388.5	55.8
27	392.0	43.9
28	395.4	36.3
29	398.7	31.0
30	401.9	27.0

### 3.2.2 Parametric Trends

Figure 3.7 shows a comparison of the basic thermophysical properties of water at the near-critical ( $P_{cr} = 22.064$  MPa) and pseudocritical ( $P = 25.0$  MPa) points, calculated according to NIST (2009).

In general, all thermophysical properties undergo significant changes near the critical and pseudocritical points (see Table 3.3). Near the critical point, these changes are dramatic (see Figure 3.7). In the vicinity of pseudocritical points, with an increase in pressure, these changes become less distinct.

It can also be seen from Figure 3.7 that properties such as density and dynamic viscosity undergo a significant drop (near the critical point, this drop is almost vertical) within a very narrow temperature range, while specific enthalpy and kinematic viscosity undergo a sharp increase. Volume expansivity, specific heat, thermal conductivity and Prandtl Number have a peak near the critical and pseudocritical points. The magnitude of these peaks decrease very quickly with an increase in pressure (Pioro and Duffey, 2007).

**Table 3.3. Peak Values of Specific Heat, Volume Expansivity and Thermal Conductivity in Critical and Near Pseudocritical Points (Pioro and Duffey, 2007).**

Pressure, MPa	Pseudocritical Temperature, °C	Temperature, °C	Specific Heat, kJ/kg·K	Volume Expansivity, 1/K	Thermal Conductivity, W/m·K
$P_{cr}=22.064$	$T_{cr}=374.1$	-	$\infty$	$\infty$	$\infty$
22.5	375.6	-	690.6	1.252	0.711
23.0	-	377.4	-	-	0.538
	377.5	-	284.3	0.508	-
23.5	-	379.2	-	-	0.468
	-	379.3	-	0.304	-
	379.4	-	171.9	-	-
24.0	-	381.0	-	-	0.429
	381.2	-	121.9	0.212	-
24.5	-	382.6	-	-	0.405
	-	383.0	-	0.161	-
	383.1	-	93.98	-	-
25.0	-	384.0	-	-	0.389
	384.9	-	76.44	-	-
	-	385.0	-	0.128	-
25.5	386.7	-	64.44	0.107	No peak

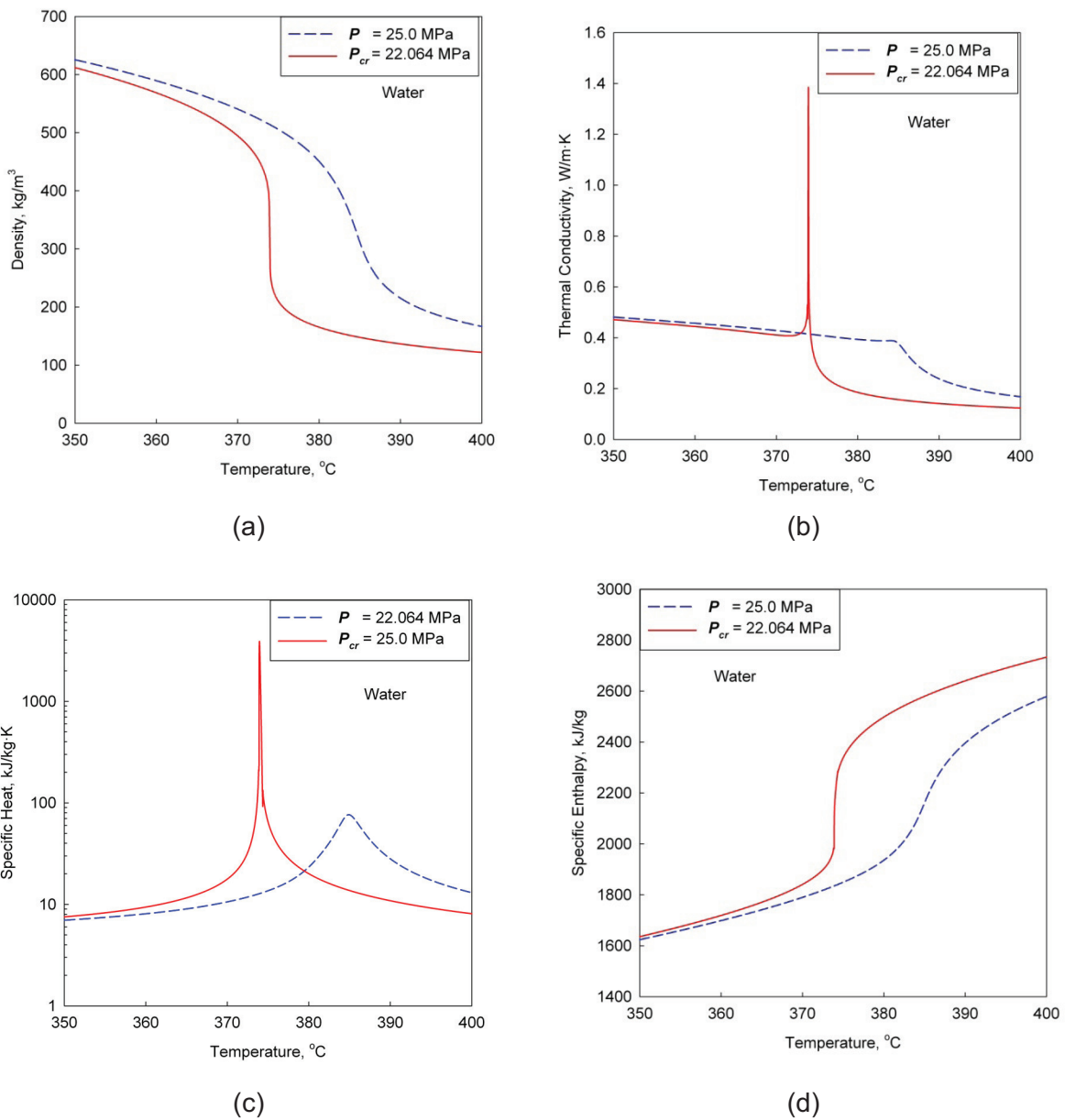


**Figure 3.7 (a-d). Basic Thermophysical Properties of Water Near the Critical and Pseudocritical Points (a) Density vs. Temperature; (b) Thermal Conductivity vs. Temperature (c) Specific Heat vs. Temperature; and (d) Specific Enthalpy vs. Temperature.**

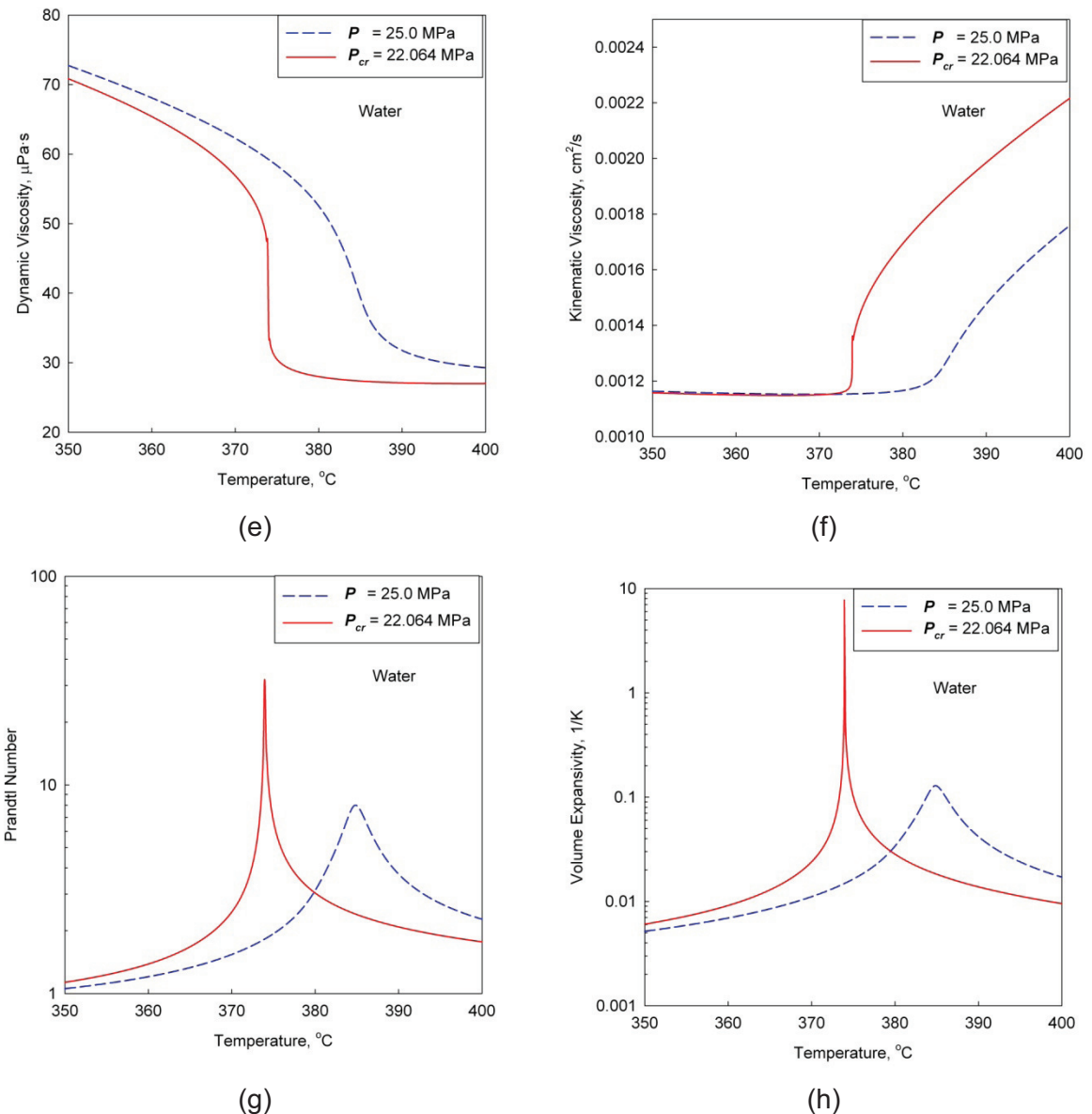


**Figure 3.7 (e-h). Basic Thermophysical Properties of Water Near the Critical and Pseudocritical Points (e) Dynamic Viscosity vs. Temperature; (f) Kinematic Viscosity vs. Temperature; (g) Prandtl Number vs. Temperature; and (h) Volume Expansivity vs. Temperature.**

Figure 3.8 shows thermophysical properties variations for water passing through the pseudocritical point at 25 MPa, the proposed operating pressure for SCWRs. The most significant changes in properties occur within  $\pm 25^\circ\text{C}$  from the pseudocritical temperature ( $384.9^\circ\text{C}$ ). The drop in density can be seen, as the fluid changes from a high-density fluid to low-density fluid and the specific heat peaks in the pseudocritical point. Additionally, thermal conductivity (at pressures up to 26 MPa thermal conductivity experiences a peak in the pseudocritical point) and viscosity drop as they pass through the pseudocritical region.

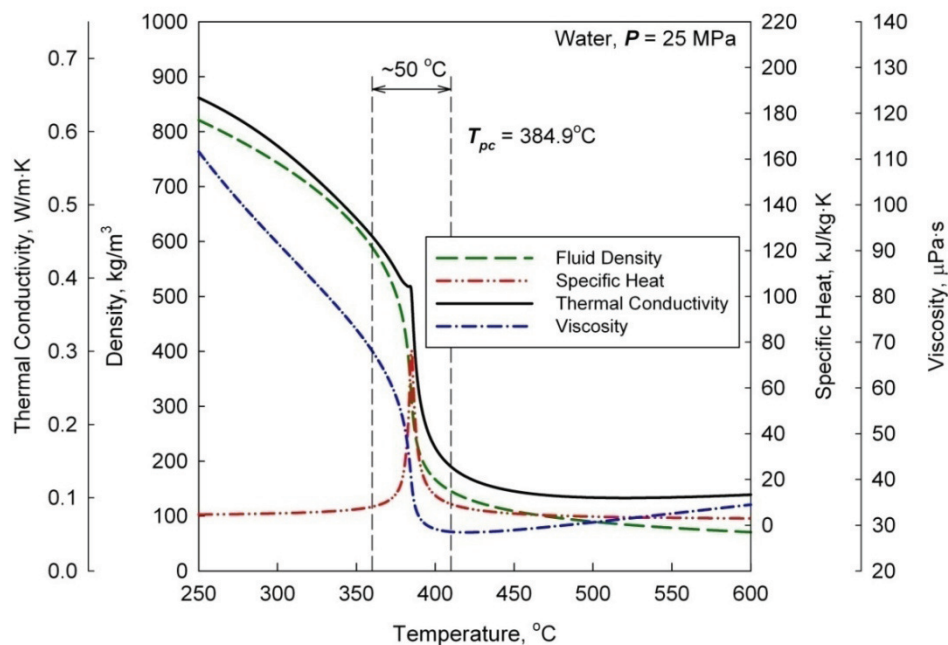


**Figure 3.8. Selected Properties for Supercritical Water within the Pseudocritical Region (Mokry et al., 2009a, b).**

Due to the high operating pressure and temperature requirements of supercritical water, current fuel-channel designs consisting just of a calandria and pressure tube are not feasible. Current alternatives include a SCWR fuel-channel comprised of a bundle, perforated liner, ceramic insert and pressure tube, which would enable the pressure tube to function at similar temperatures as the moderator, and a re-entrant fuel-channel design, which could allow the pressure tube to operate at the supercritical water inlet temperature.

The main design parameters of the supercritical water PT reactor are listed in Table 3.4. These parameters are preliminary and are subject to change, depending on the outcome of research efforts (Khartabil et al., 2005).

**Table 3.4. Major Parameters of Supercritical Water CANDU (Canada) and VVER-SCP (Russia) Nuclear-Reactor Concepts (Mokry et al., 2008; Pioro and Duffey, 2007).**

Parameters	SCW CANDU®	VVER-SCP
Reactor type	PT	PV
Reactor spectrum	Thermal	Fast
Thermal power, MW	2540	3830
Electric power, MW	1220	1700
Thermal efficiency, %	48	44
Pressure, MPa	25	25
Inlet temperature, °C	350	280
Outlet temperature, °C	625	530
Mass flow rate, kg/s	1320	1860
Number of fuel-channels	300	241
Number of fuel elements per bundle	43	252
Length of a bundle string, m	6	4

There are many advantages related to the development of SCWRs, primarily is an increase in thermal efficiency. Current generation NPPs operate with efficiencies from 30 – 35%. SCWRs can offer an increase in efficiency to approximately 45 – 50%. In addition, there is a simplified flow circuit in which steam generators, steam dryers, steam separators, etc. can be eliminated. This will facilitate a decrease in the capital and operational costs, and in doing so, decrease electrical energy costs (Pioro and Duffey, 2007). Also, the power required for pumping the coolant is decreased. Another advantage is the elimination of fuel-sheath dryout, which is the boiling phenomenon that could potentially lead to burnout of the fuel-sheath. Furthermore, SCWRs operating at higher temperatures can facilitate an economical production of hydrogen through thermochemical cycles or high-temperature electrolysis (Naidin et al., 2009b); Mokry et al., 2008).

In support of developing an SCWR, studies are being conducted into heat transfer at supercritical conditions using carbon dioxide as a modelling fluid as a less expensive alternative to using supercritical water and to aid in the improvement of fundamental knowledge of the transport processes and handling of supercritical fluids. For more details, see Appendix A.

## CHAPTER 4

### GENERAL CONSIDERATIONS FOR SUPERCRITICAL WATER NPP CYCLES

#### 4.1 Review of Supercritical Turbines

Currently, there are about 560 operating supercritical units around the world. Supercritical-“steam” turbines of medium and large capacities (450 – 1200 MW<sub>el</sub>) (Duffey et al., 2008; Naidin et al., 2008; Pioro and Duffey, 2007) have been used very successfully at many fossil power plants worldwide for more than fifty years. Their gross steam-cycle thermal efficiencies have reached nearly 54%, which is equivalent to a net plant efficiency of approximately 40 – 43% on a Higher-Heating Value (HHV) basis.

It should be noted that the absolute leaders among large-scale power plants, in terms of thermal efficiencies, are combined-cycle (i.e., tandem arrangement of gas turbine and subcritical-pressure steam turbine) gas-fired power plants with about 60% net plant efficiency on a Lower-Heating Value (LHV) basis or net-plant efficiencies of up to 54% on a HHV basis. Table 4.1 lists selected current and upcoming supercritical turbines manufactured by Hitachi for reference purposes.

**Table 4.1. Major Parameters of Selected Current and Upcoming Hitachi Supercritical Plants (Naidin et al., 2009a, c; Pioro et al., 2008b ).**

First Year of Operation	Power Rating, MW <sub>el</sub>	P, MPa	T <sub>main</sub> / T <sub>reheat</sub> , °C
2011	495	24.6	566/566
2010	677	25.5	566/566
	809	25.4	579/579
	790	26.4	600/620
2009	677	25.5	566/566
	600	25.5	600/620
2008	1000	24.9	600/600
	870	24.7	566/593
	870	24.7	566/593
2007	1000	24.9	600/600
	870	25.3	566/593

An analysis of supercritical-turbine data (Duffey et al., 2008; Naidin et al., 2008; Pioro and Duffey, 2007) showed that:

- The vast majority of modern and upcoming supercritical turbines are single-reheat-cycle turbines;
- Major “steam” inlet parameters of these turbines are: main or primary supercritical “steam” –  $P = 24 - 25 \text{ MPa}$  and  $T = 540 - 600^\circ\text{C}$ ; and the reheat or secondary subcritical-pressure steam –  $P = 3 - 5 \text{ MPa}$  and  $T = 540 - 620^\circ\text{C}$ .
- Usually, the main “steam” and reheat-steam temperatures are the same or very close (for example, 566/566°C; 579/579°C; 600/600°C; 566/593°C; and 600/620°C).
- Only very few double-reheat-cycle turbines were manufactured. The market demand for double-reheat turbines disappeared, due to economic reasons, after the first few units were built.

#### **4.2 Direct-, Indirect- and Dual-Cycle Options**

Since the “steam” parameters of supercritical water NPPs are much higher than those of current NPPs, several conceptual designs have been investigated to determine the optimum configuration. As such, direct-, indirect- and dual-cycles have been considered.

In the direct cycle, supercritical “steam” from a nuclear reactor is fed directly to a supercritical turbine (Duffey et al., 2008). This concept eliminates the need for complex and expensive equipment such as steam generators. From a thermodynamic perspective, this allows for high “steam” pressures and temperatures, and results in the highest cycle efficiency for the given parameters. Current BWR NPPs are based on this concept.

The indirect- and dual-cycles utilize heat exchangers (steam generators) to transfer heat from the reactor coolant to a secondary loop. They are currently used in PWRs and CANDU power plants. The indirect-cycle has the safety benefit of containing the potential radioactive particles inside the primary coolant. However, the heat-transfer process through heat exchangers reduces the maximum temperature of the secondary-loop coolant, thus lowering the thermal efficiency of the cycle.

Since increasing the thermal efficiency is one of the main objectives in the development of supercritical water NPPs, the direct-cycle was analyzed further.

#### 4.3 Reheating Options

A preliminary investigation of supercritical water NPP reheat options (Mokry et al., 2008; Naidin et al., 2008) revealed the following:

- The no-reheat cycle offers a simplified supercritical water NPP layout, contributing to lower capital costs. However, the efficiency of this cycle was the lowest of all the considered configurations.
- The single-reheat cycle has the advantage of high thermal efficiency (compared to that of the no-reheat cycle) and reduced development costs due to a wide variety of single-reheat supercritical turbines manufactured by companies worldwide. The major disadvantage was the increased design complexity associated with the introduction of steam-reheat channels to the reactor core.
- While the double-reheat cycle had the highest thermal efficiency, it was deemed that the complicated nuclear-steam reheat configuration would significantly increase the design and construction costs of such a facility.

In conclusion, the double-reheat configuration was no longer considered of interest, while the most viable options are the single-reheat and no-reheat supercritical water NPPs.

#### 4.4 Regenerative Cycle

Another way of increasing the average temperature during heat addition is to increase the temperature of feedwater entering the SCWR. Since the reactor inlet temperature is approximately 350°C, it is obvious that a regenerative cycle needs to be implemented to increase the feedwater temperature from the condenser outlet (about 40°C) to the reactor inlet conditions (350°C).

In practice, regeneration is accomplished through feedwater heaters. Steam extracted from the turbine, at various points, is used to heat the feedwater to the desired temperature. The regeneration process does not only improve the cycle efficiency, but also improves the quality of the feedwater system by removing air and other non-condensable gases.

#### 4.5 Turbine Options

The no-reheat and single-reheat cycles were both deemed to be viable, thus, a suitable turbine arrangement must be chosen as well. In a single-reheat configuration, the supercritical “steam” coming from the reactor flows to the High Pressure (HP) turbine, where it expands and is exhausted back to the subcritical-pressure Steam-ReHeat (SRH) channels. Here, the steam temperature is increased to the supercritical temperature, and the steam is allowed to expand through an Intermediate-Pressure (IP) turbine. Furthermore, the steam is carried through a cross-over pipe to the Low-Pressure (LP) turbine and is exhausted to a condenser. However, for a no-reheat cycle, the IP turbine is eliminated and the steam is transferred directly from the HP turbine to the LP turbines.

The LP turbines have large exhaust areas because the steam is expanded to very low pressures, for the purpose of extracting as much useful energy as reasonably possible. Due to the large volume of steam, the LP turbines have a double-flow configuration. The single-reheat cycle IP turbine is also a double-flow configuration as the expected flow rate of steam is quite high.

From a design point, the turbine-generator module can be classified as a tandem compound or cross-compound. Generally, the cross-compound configuration consists of the HP and IP turbines located on the same shaft and driving one generator, while the LP turbines are on a different shaft driving a separate generator. The speed of the HP and IP turbine shaft is generally 3600 rpm, while that of the LP turbine shaft is 1800 rpm (in a 60 Hz electrical grid). The slower speed of the LP turbine allows the implementation of longer last-turbine blades with expansion to higher moisture percentages and less exhaust losses, thus increasing the overall cycle efficiency (Black and Veatch, 1995). Therefore, the proposed turbine arrangement for the supercritical water NPP single-reheat cycle is the cross-compound option. However, it is to be noted that there is a higher cost associated with cross-compound turbine arrangements.

## 4.6 Supercritical Water NPP Cycles Description

### 4.6.1 Single-Reheat Cycles System Description

The proposed cycle layouts for a supercritical water NPP with a single-reheat option are shown in Figures 4.1 and 4.2 (Cycles A and B, respectively) (Naidin et al., 2009c). As per the previous sections, the cycles have direct single-reheat, regenerative configurations. As such, the supercritical “steam” exiting the reactor is expanded through a single-flow HP turbine.

As shown in Figure 4.1, for Cycle A the steam is sent back to the reheat (SRH channels inside the reactor), where the temperature is raised to a supercritical level. Furthermore, the subcritical-pressure SuperHeated Steam (SHS) is expanded in the IP turbine and transferred, through a cross-over pipe, to the LP

turbines. Since the volume of the steam at the exhaust of the IP turbine is quite high, two LP turbines are utilized. In Figure 4.1, the turbine-generator arrangement is a cross-compound: the HP and IP turbines are located on the same shaft, while the LP turbines are located on a separate shaft.

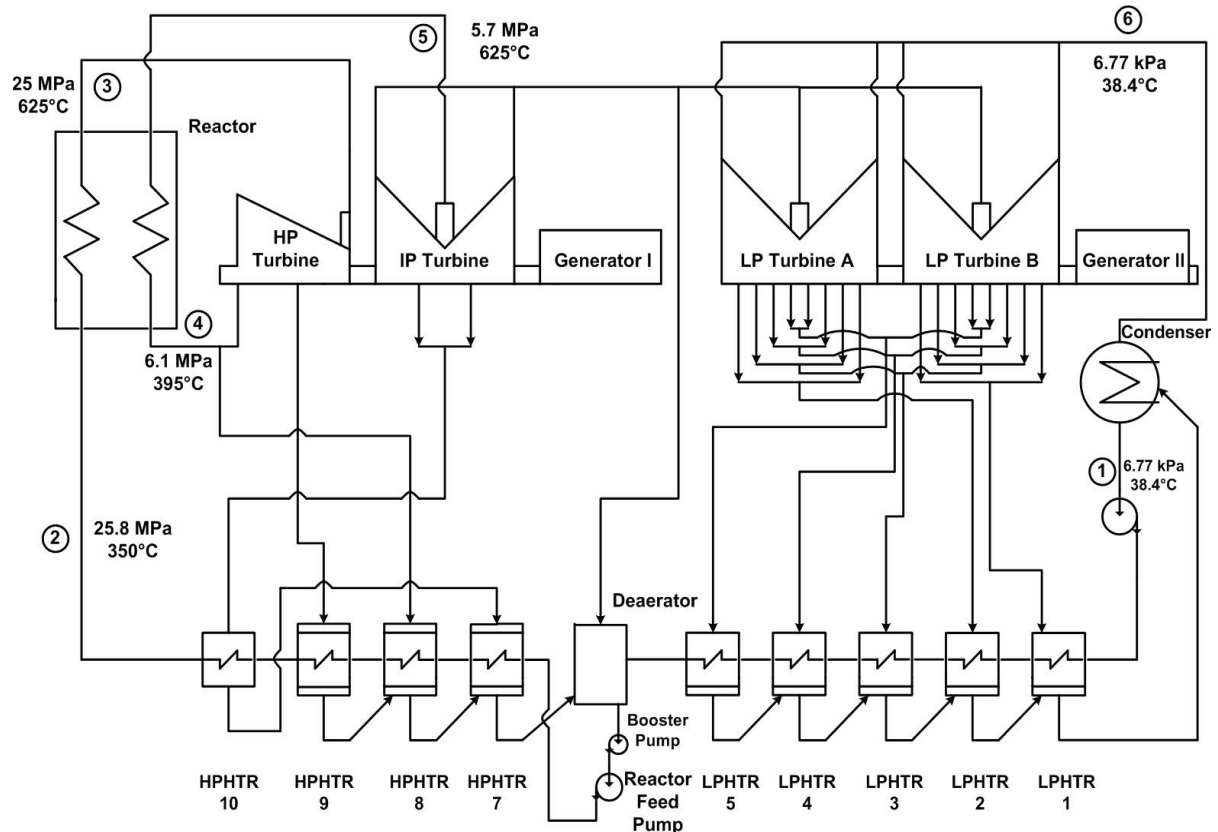


**Figure 4.1. Single-Reheat Cycle A for Supercritical Water NPP**  
(Naidin et al., 2009c).

Cycle B, shown in Figure 4.2, follows a slightly different arrangement. As such, the steam expanded in the HP turbine is sent to the IP turbine where it expands to saturated conditions (approximately 98% steam quality). Furthermore, the steam is passed through a Moisture-Separator-ReHeater (MSRH) unit that contains one stage of moisture separation and two stages of reheat. From here, superheated steam exiting the MSHR unit is sent to the inlet of the LP turbines where it is expanded to saturated conditions. The steam is exhausted from the

turbine to the condenser, suffering exhaust losses, which depend on the exhaust area and steam velocity.

The saturated steam undergoes a phase change and is condensed, at a constant pressure and temperature, by a cooling medium inside the condenser. The Condensate Extraction Pump (CEP) takes its suction from the condenser outlet. It pumps the condensate from the hotwell, through a series of LP-feedwater heaters (HTRs) (LP HTR 1 to 5 for Cycle A, LP HTR 1 to 4 for Cycle B), to the deaerator. The feedwater temperature differentials across the LP heaters are assumed to be approximately the same. These LP heaters are tube-in-shell, closed-type heat exchangers. On the steam side, they contain condensing and subcooling zones.

The deaerator is an open-type feedwater heater, where the feedwater, extraction steam and HP heater drains come into direct contact. The feedwater is heated (at constant pressure) to the saturation temperature, and leaves the deaerator as saturated liquid. The Reactor Feedwater Pump (RFP) takes its suction from the deaerator and raises the feedwater pressure to the required value at the reactor inlet.

Furthermore, the feedwater is passed through 3 HP heaters (HP HTR 7 to 9) and a topping de-superheater (HP HTR 10) for the configuration described in Cycle A. Similarly, the feedwater passes through 4 HP heaters (HP HTR 6 to HP HTR 9) in the case of Cycle B. The HP heaters are tube-in-shell, closed-type heat exchangers with de-superheating, condensing and subcooling zones.

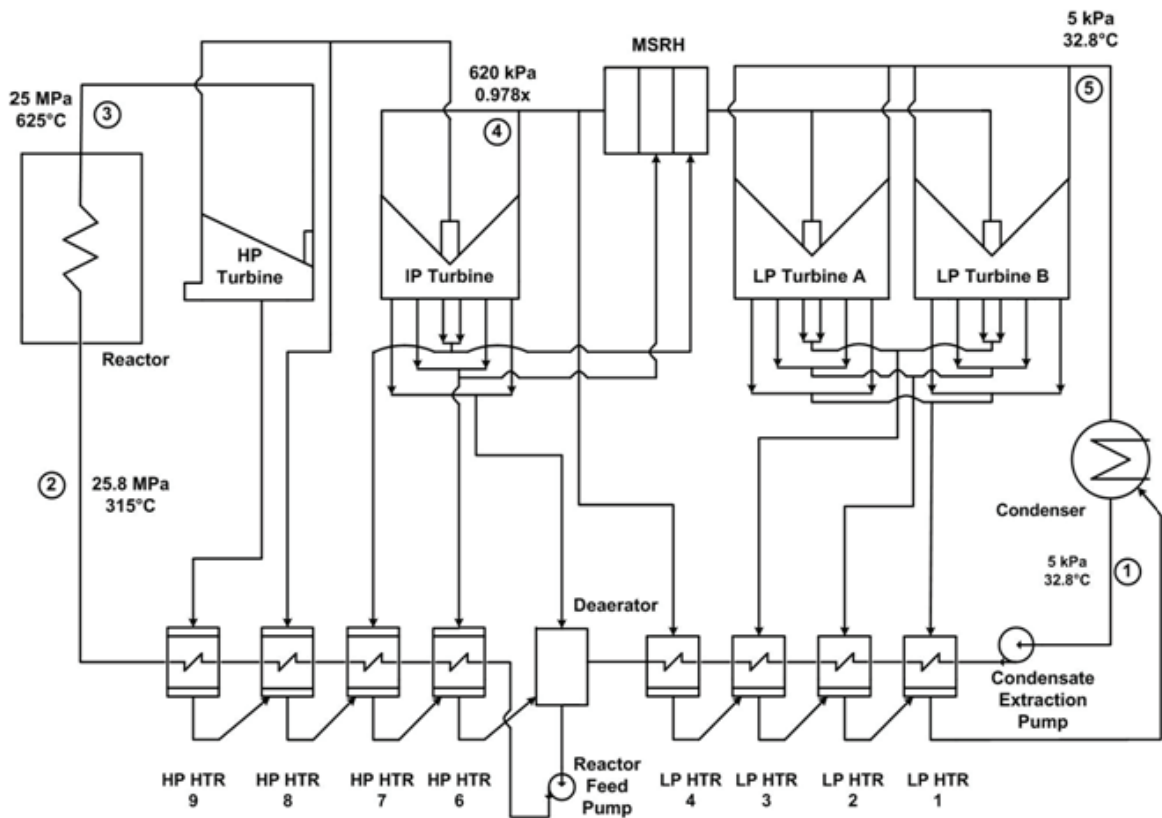


**Figure 4.2. Single-Reheat Cycle B for Supercritical Water NPP (Duffey et al., 2008).**

#### 4.6.2 No-Reheat Cycles System Description

The single-reheat cycle introduces nuclear SRH channels, thus increasing the complexity of the reactor-core design. Although preliminary results show that the thermal efficiency of the no-reheat cycle is approximately 1 – 2% lower than that of single-reheat cycles, the less complex core configuration might prove to be a major factor when selecting the most suitable design. Therefore, it is worth analyzing the possibility of a no-reheat supercritical water NPP cycle such as the following proposed cycle.

The proposed no-reheat supercritical water NPP cycle consists of five LP-feedwater heaters, one deaerator, three HP-feedwater heaters and one topping

de-superheater (see Figure 4.3). This cycle has a direct, no-reheat, regenerative configuration. As such, the supercritical “steam” exiting the reactor is expanded through a double-flow HP turbine to superheated conditions. Since the volume of steam at the exhaust of the HP turbine is quite high, two IP/LP turbines are utilized. Furthermore, the steam is exhausted from the IP/LP turbine to the condenser. The saturated steam undergoes a phase change and is condensed at constant pressure and temperature by a cooling medium inside a condenser.

The CEP takes its suction from the condenser hotwell. It pumps the condensate through a series of five LP-feedwater heaters (LP HTR 1 to 5) to the deaerator. The feedwater is heated at constant pressure, and leaves the deaerator as saturated liquid. The RFP takes its suction from the deaerator and raises the feedwater pressure to the required value at the reactor inlet (25 MPa). Furthermore, the feedwater is passed through three HP heaters (HP HTR 7 to 9) and a topping de-superheater (HP HTR 10).

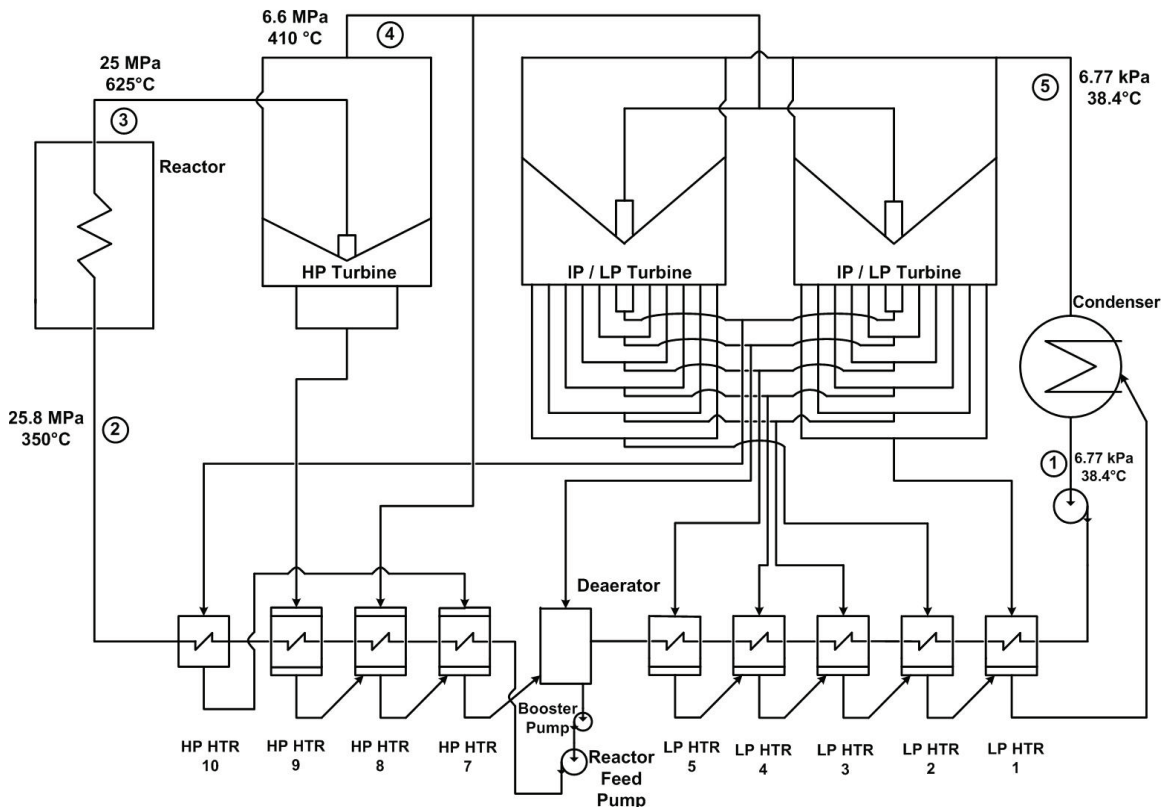


**Figure 4.3. No-Reheat Cycle C for Supercritical Water NPP (Naidin et al., 2009c).**

## 4.7 Supercritical Water NPP Cycles Analysis and Results

Table 4.2 lists values of thermal efficiency for the proposed supercritical water NPP single-reheat and no-reheat cycles. Table 4.3 illustrates major parameters of the proposed thermal cycles, while Table 4.4 presents PT SCWR major parameters.

**Table 4.2. Thermal Efficiency of Supercritical Water NPP Cycles (Naidin et al., 2009c).**

Cycle	Thermal Efficiency (%)
A	52
B	52
C	51

**Table 4.3. Selected Parameters of Proposed Supercritical Water NPP Cycles A and C (Naidin et al., 2009c).**

Parameters	Unit	Description / Value	Description / Value
Cycle type	–	Single-Reheat (A)	No-Reheat (C)
Reactor type	–	Pressure Tube	
Reactor spectrum	–	Thermal	
Fuel	–	$\text{UO}_2$ ( $\text{ThO}_2$ )	
Cladding material	–	Inconel or Stainless steel	
Reactor coolant	–	$\text{H}_2\text{O}$	
Moderator	–	$\text{D}_2\text{O}$	
Power Thermal	$\text{MW}_{\text{th}}$	2300	2340
Power Electrical	$\text{MW}_{\text{el}}$	1200	1200
Thermal Efficiency	%	52	51
Pressure of supercritical water at inlet	MPa	25.8	25.8
Pressure of supercritical water at outlet (estimated)	MPa	25	25
$T_{\text{in}}$ coolant (supercritical water)	°C	350	350
$T_{\text{out}}$ coolant (supercritical water)	°C	625	625
Pressure of SHS at inlet	MPa	6.1	–
Pressure of SHS at outlet (estimated)	MPa	5.7	–
$T_{\text{in}}$ coolant (SHS)	°C	400	–
$T_{\text{out}}$ coolant (SHS)	°C	625	–
Power thermal supercritical water channels	$\text{MW}_{\text{th}}$	1870	2340
Power thermal SRH channels	$\text{MW}_{\text{th}}$	430	–

Parameters	Unit	Description / Value	Description / Value
Power thermal / supercritical water channel	MW <sub>th</sub>	8.5	8.5
Power thermal / SRH channel	MW <sub>th</sub>	5.5	—
# of fuel-channels (total)	—	300	270
# of SCW channels	—	220	270
# of SRH channels	—	80	—
Total flow rate of supercritical water	kg/s	960	1190
Total flow rate of SHS	kg/s	780	—
Flow rate / supercritical water channel	kg/s	4.37	4.37
Flow rate / SRH channel	kg/s	10	—

**Table 4.4. Selected Parameters of Proposed SCWR Fuel-Channels (Naidin et al., 2009c).**

Parameters	Unit	Description / Value		
$T_{\max}$ cladding (design value)	°C	850		
$T_{\max}$ fuel centerline (industry accepted limit)	°C	1850		
Heated fuel-channel length	m	5.772		
# of bundles per fuel-channel	—	12		
# of fuel rods per bundle	—	43		
Bundle type*	—	CANFLEX	Variant-18	Variant-20
# of heated fuel rods	—	43	42	42
# of unheated fuel rods	—	—	1	1
Diameter of heated fuel rods (# of rods)	mm	11.5 (35) & 13.5 (8)	11.5	11.5
Diameter of unheated fuel rod	mm	—	18	20
$D_{hy}$ of fuel-channel	mm	7.52	7.98	7.83
$D_h$ of fuel-channel	mm	9.04	9.98	9.83
Heated area of fuel-channel	m <sup>2</sup>	9.26	8.76	8.76
Flow area of fuel-channel	mm <sup>2</sup>	3625	3788	3729
Pressure tube inner diameter	mm	103.45		
<b>Average parameters of fuel-channels in single-reheat (A) and no-reheat (B) options</b>				
Heat flux in supercritical water channel (A&B cycles)	kW/m <sup>2</sup>	918	970	970
Heat flux in SRH channel (A cycle)	kW/m <sup>2</sup>	594	628	628
Mass flux in supercritical water channel (A&B cycles)	kg/m <sup>2</sup> s	1206	1154	1172
Mass flux in SRH channel (A cycle)	kg/m <sup>2</sup> s	2759	2640	2682

\*for details, see Leung, 2008.

#### 4.8 Single-Reheat Option with Two Heat Exchangers

This indirect-cycle differs from the direct-cycle by the addition of two heat exchangers (see Figure 4.4). The first heat exchanger is for the reactor primary loop supercritical water (inlet: 25 MPa and 625°C) / secondary loop supercritical water (outlet: 25 MPa and 550°C). The second heat exchanger is for the reactor primary loop supercritical water (inlet: 25 MPa and 625°C) / secondary loop supercritical superheated steam (outlet: 4.5 MPa and 550°C).

Thus, the development of a supercritical water heat-transfer correlation, based on the latest experimental dataset, would be applicable for heat-transfer calculations in both heat exchangers of the indirect cycle on the supercritical-water side (i.e., from the reactor side), because it would be valid within the operating range of such heat exchangers.

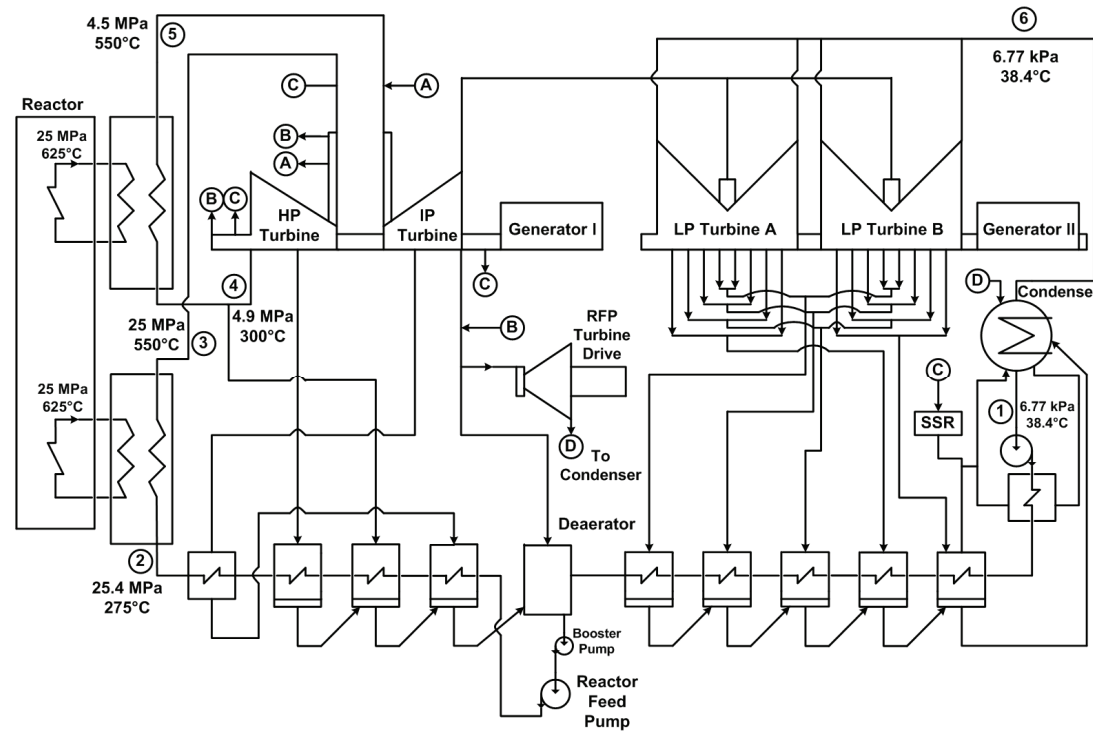


**Figure 4.4. Single-Reheat Cycle with Two Heat Exchangers (Pioro et al., 2010).**

#### **4.9 Co-Generation of Hydrogen**

Greenhouse gas emissions, generated by fossil fuels, are well-known contributors to global warming. As such, worldwide research is currently being conducted to identify a clean energy carrier. Through these studies, hydrogen ( $H_2$ ) was identified as one of the promising options. However, most of the hydrogen supply currently available is obtained from fossil fuels through reforming processes, which release greenhouse gases (Naidin et al., 2009b; Naterer et al., 2009).

Hydrogen is needed in large quantities for use in many industrial sectors, (Canadian oil sands, petroleum products, agriculture, and transportation). Thus, a technology suitable for large-scale sustainable production of hydrogen needs to be developed and implemented. Water splitting by thermochemical reaction is one of the most promising technologies for hydrogen generation without the negative consequences of pollutants (Naidin et al., 2009b; Naterer et al., 2009). By using intermediate compounds, a series of chemical and physical processes decompose water into its two constituents, hydrogen and oxygen. Thermochemical hydrogen production is also much more efficient than other methods, such as electrolysis, because the heat is used directly to produce hydrogen, rather than being converted first into electrical energy.

Although over 200 thermochemical cycles have been identified (Naidin et al., 2009b; Naterer et al., 2009), proof-of-principle demonstrations have only been completed for a few of them. However, most of these processes use process heat above  $800^{\circ}C$ , and require very high temperatures that are not currently available in nuclear or thermal power plants. The copper-chlorine (Cu-Cl) cycle is the only demonstrated cycle that functions at a lower temperature, of approximately  $500^{\circ}C$ , which makes it suitable for linkage with a supercritical water NPP cycle. The relatively lower operating temperature can also lead to a reduction in material and maintenance costs.

Currently, UOIT (University of Ontario Institute of Technology), in collaboration with AECL and other partners, is developing the Cu-Cl cycle with a maximum temperature in the cycle of up to 500°C (for details, see Table 4.5). Therefore, using the high-temperature heat from a SCWR to heat water and endothermic reactors in the hydrogen-production loop is a viable option. Heat exchangers of a recuperator-type would be used for this purpose.

**Table 4.5. Chemical Reaction Steps and Basic Parameters of the Copper-Chlorine Cycle (Naidin et al., 2009b; Mokry et al., 2008).**

Step	Reaction	Temp. Range (°C)	Feed/Output	
1	$2\text{Cu(s)} + 2\text{HCl(g)} \rightarrow \text{CuCl(l)} + \text{H}_2\text{(g)}$	430 – 475	Feed:	Electrolytic Cu + dry HCl + Q
			Output:	$\text{H}_2 + \text{CuCl(l)}$ salt
2	$2\text{CuCl(l)} \rightarrow 2\text{CuCl(aq)}$ $\rightarrow \text{CuCl}_2\text{(aq)} + \text{Cu(s)}$	Ambient (electrolysis)	Feed:	Powder/granular CuCl and HCl + E
			Output:	Cu and slurry containing HCl and CuCl <sub>2</sub>
3	$\text{CuCl}_2\text{(aq)} \rightarrow \text{CuCl}_2\text{(s)}$	<100	Feed:	Slurry containing HCl and CuCl <sub>2</sub> + Q
			Output:	Powder/granular CuCl <sub>2</sub> + H <sub>2</sub> O/HCl vapour
4	$2\text{CuCl}_2\text{(s)} + \text{H}_2\text{O(g)} \rightarrow \text{CuO}^*\text{CuCl}_2\text{(s)} + 2\text{HCl(g)}$	400	Feed:	Powder/granular CuCl <sub>2</sub> + H <sub>2</sub> O(g) + Q
			Output:	Powder/granular CuO <sup>*</sup> CuCl <sub>2</sub> + 2HCl (g)
5	$\text{CuO}^*\text{CuCl}_2\text{(s)} \rightarrow 2\text{CuCl(l)} + 1/2\text{O}_2\text{(g)}$	500	Feed:	Powder/granular CuO <sup>*</sup> CuCl <sub>2</sub> (s) + Q
			Output:	Molten CuCl salt + oxygen

Figure 4.5 provides a layout of a hydrogen co-generation plant that can be linked to an SCWR through one or two heat exchangers. One of these heat exchangers would be a supercritical water / low-pressure superheated-steam heat exchanger, and the other a medium-pressure superheated steam / low-pressure superheated-steam heat exchanger.

High-quality steam can be extracted from the main supercritical “steam” lines coming from the reactor core. The high-temperature and high-pressure fluid (625°C and 25 MPa) would then be used to heat the process water in the hydrogen co-generation loop using a heat exchanger. The fluid returning to the supercritical water NPP loop from the H<sub>2</sub> co-generation heat exchangers would be added to the feedwater heating system at a suitable location. The second possibility would be to use the superheated steam at 8.8 MPa and 625°C returning from the nuclear reheat channels. However, since the design of a heat exchanger able to handle the high pressure differential between the supercritical

“steam” and the process water in the H<sub>2</sub> loop could be technically challenging, the first option is likely more suitable for practical application.

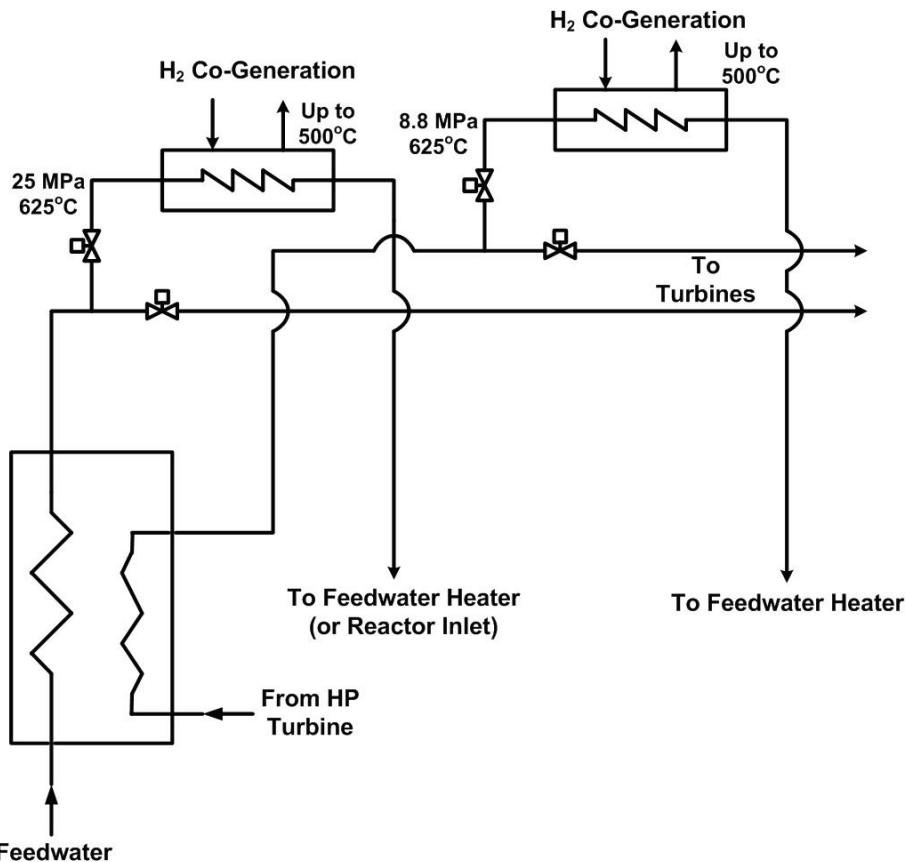


**Figure 4.5. Layout for H<sub>2</sub> Co-Generation Associated with Proposed Single-Reheat Supercritical Water NPP (Naidin et al., 2009b; Mokry et al., 2008).**

For the development of such heat exchangers, two heat-transfer correlations would need to be identified: 1) for supercritical water and 2) for superheated steam. Pioro and Duffey (2007) have shown that there are a number of supercritical-water heat-transfer correlations available in the open literature. However, a comparison of selected correlations has shown that their results may differ from one another by more than 200%.

Thus, the development of a supercritical water heat-transfer correlation, based on the latest experimental dataset, would be applicable for heat-transfer calculations in the first heat exchanger for hydrogen co-generation on the supercritical-water side (i.e., from the reactor side), because it would be valid within the operating range of such a heat exchanger.

## CHAPTER 5

### HEAT TRANSFER CALCULATIONS FOR AN SCWR FUEL-CHANNEL

SCWR technology is currently in its early design phase. A demonstration unit has yet to be designed and constructed. Fuel materials and configurations suited for supercritical conditions are currently being studied. Thermophysical properties and thermal-design options of fuel bundles, with respect to the maximum fuel centerline temperature and the maximum sheath temperature (Mokry et al., 2008; Chow and Khartabil, 2008), will need to be analyzed.

#### 5.1 SCWR Fuel-Channel Design

The current Canadian SCWR concept includes fuel-channels comprised of a pressure tube insulated internally with a ceramic insert, which would enable the pressure tube to operate at temperatures close to that of the moderator, and a fuel-bundle string (for details, see Table 5.1.) This fuel-channel design was considered for supercritical water heating from 350 to 625°C at a pressure of 25 MPa (for details, see Gopaul et al., 2007.) Water would pass through a pseudocritical point ( $T_{pc} = 384.9^\circ\text{C}$  at  $P = 25 \text{ MPa}$ ) in which all thermophysical properties experience rapid variations (see Figure 3.7).

Temperature, HTC and thermophysical properties profiles along a heated length of a channel are important for a better understanding of heat-transfer processes inside the fuel-channel. However, to be able to design an SCWR, including the fuel-channel design, some preliminary heat-transfer / thermalhydraulic calculations should be performed. In this case, the preliminary calculations can be based on supercritical water bare tube heat-transfer correlations as a conservative approach. Based on these calculations the sheath temperature must be below the design limit of 850°C (Pioro and Khartabil, 2005). Also, another important parameter is the fuel centerline temperature. In this case, the fuel centerline temperature should be below the industry accepted limit of about 1850°C.

The model used in the current thermal-design analysis was a generic PT SCWR with 300 fuel-channels and 1200-MW<sub>el</sub> power. A heated-channel length of 5.772 m was assumed. The anticipated fuel string consists of 12 bundles. Calculations consider the fuel-rod length to be equal to the heated-channel length, i.e., end-plates and end-caps of a bundle are not considered. Pressure drop along the channel was not accounted for, and the channel pressure was assumed to be a constant 25 MPa. The contact resistance between a fuel pellet and sheath was considered to be negligible. A linear, averaged heat flux was used along the heated pressure channel. A coolant mass-flow rate per channel was assumed to be a constant 4.4 kg/s, and the produced power per channel to be 8.5 MW<sub>th</sub>.

Several correlations were identified to be used for these calculations. The Bishop et al. correlation (1964) (see Chapter 6, (Eq. 6.3)) was used, because the range over which the correlation is applicable closely matches that of the proposed SCWR concepts.

First, the temperature of the fuel along the heated channel was obtained. To obtain the fuel centerline temperature, a constant value for thermal conductivity for the fuel and the cladding was used. The values used for conductivities were chosen to be the lowest possible, as part of a conservative approach. The obtained results gave an over-estimation of the fuel centerline temperature, providing a basis for future comparisons. The existing 43-element fuel bundle design was used as a basis for various calculations. An Axial Heat Flux Profile (AHFP) was considered to be non-uniform and close to a cosine-type profile. Based on the general supercritical water CANDU reactor design parameters (Table 3.4), fuel-channel average parameters were calculated (for details, see Table 5.1).

**Table 5.1 Fuel-Channel Major Parameters used in Calculations.**

Parameter, (Unit)	Value	
<b>Bundle</b>		
No. of Elements	43	
No. of Elements per Ring	Center	1
	Inner	7
	Intermediate	14
	Outer	21
No. of Fuelled Elements	42	
Center Rod with Low Heat Flux	1	
Fuelled Element OD, (mm)	11.5	
Center Rod OD, (mm)	23.6	
Fuel Pellet OD, (mm)	10.72	
Heated Length, (mm)	481	
<b>Bundle String</b>		
No. of Bundles	12	
Heated Length , (m)	5.772	
<b>Pressure-Tube</b>		
ID, (mm)	103.38	
Cross-Section Area, (mm <sup>2</sup> )	8394	
Flow Area, (mm <sup>2</sup> )	3600	
<b>Other Parameters</b>		
Hydraulic-Equivalent Diameter, (mm)	7.5	
Axial Heat Flux Profile	Non-Uniform Cosine	
Fuel	UO <sub>2</sub>	
Cladding Material	Inconel-718	
Total Heated Area Without Center Rod, (m <sup>2</sup> )	8.758	
Mass Flow Rate, (kg/s)	4.4	
Mass Flux, (kg/m <sup>2</sup> s)	1224	
Fuel-Channel Power, (MW <sub>th</sub> )	8.5	
Average Linear Heat Flux, (kW/m)	1473	

The following parameters were calculated:

$$\text{Mass flow rate per channel, kg/s: } \frac{\dot{m}}{\# \text{channels}} \quad (5.1)$$

Flow area, m<sup>2</sup>:

$$A_{fl} = \frac{\pi}{4} (D_{pt}^2 - 42 \cdot D_{fuel}^2 - D_{central}^2) \quad (5.2)$$

Mass flux, kg/s·m<sup>2</sup>

$$G = \frac{\dot{m}_{ch}}{A_{fl}} \quad (5.3)$$

Fuel-channel Power, MW:

$$\frac{\text{ThermalPower}}{\# \text{channels}} \quad (5.4)$$

Heated area, m<sup>2</sup>:

$$A_h = \pi D_{fuel} \times 42 \quad (5.5)$$

Local heat flux, W/m<sup>2</sup>:

$$q_\ell = \frac{Q_\ell}{A_h} \quad (5.6)$$

Wetted perimeter, m

$$p_{wet} = \pi (D_{pt} + 42 \cdot D_{fuel} + D_{central}) \quad (5.7)$$

Hydraulic-equivalent diameter, m:

$$D_{hy} = \frac{4A_{fl}}{p_{wet}} \quad (5.8)$$

## 5.2 Axial Heat Flux Profiles

A 43-element fuel bundle AHFP was assumed to be a cosine type similar to that used by Hwang, et al. (2006). To obtain the cosine heat-flux shape along the heated channel, the data were fitted with an 8<sup>th</sup>-order polynomial equation:

$$y = a_0 + a_1 \cdot z + a_2 \cdot z^2 + a_3 \cdot z^3 + a_4 \cdot z^4 + a_5 \cdot z^5 + a_6 \cdot z^6 + a_7 \cdot z^7 + a_8 \cdot z^8 \quad (5.9)$$

The coefficients for this relationship were obtained using SigmaPlot's regression analysis:

$$\begin{aligned} a_0 &= 0.086; \\ a_1 &= 0.559; \\ a_2 &= 1.019; \\ a_3 &= -1.366; \\ a_4 &= 0.788; \\ a_5 &= -0.256; \\ a_6 &= 0.048; \\ a_7 &= -4.843 \times 10^{-3}; \text{ and} \\ a_8 &= 2.037 \times 10^{-4}. \end{aligned}$$

This equation gave a proper shape for an axial heat flux, but it is non-dimensional and needed to be scaled to match the channel power. For all future calculations, the heated length of the channel was divided into 577 increments, i.e., 10-mm length each, to represent the approximate length of a heated channel of 5.77 m. The given channel power was 8.5 MW<sub>th</sub> (Table 5.1); therefore, the AHFP had to be scaled in order to represent the required power. This was accomplished by integrating the axial heat flux shape and finding the ratio between the area under the curve and the desired area that represented an 8.5 MW<sub>th</sub> power output for the channel. The result gave the linear heat flux along a heated-channel profile, and the area under the curve was the total channel power output (Figure 5.1).

$$Q_{loc} = y_{loc} \times \frac{Q_{total}}{\int_0^{577} y_{loc} dz}, \quad (5.10)$$

where  $Q_{total} = 8.5 \text{ MW}_{th}$ , and  $\int_0^{577} y_{loc} dz = 560.78$

$$\frac{Q_{total}}{\int_0^{577} y_{loc} dz} = 15.16 \quad (5.11)$$

$$\text{Heat transfer rate: } Q_{loc} = y_{loc} \times 15.16 \quad (5.12)$$

Linear heat flux, kW/m:

$$q = \frac{Q_{loc}}{L}, \quad (5.13)$$

where  $L = 0.01 \text{ m}$  was the increment.

$Q_{loc}$  was the heat transfer rate within the increment in kW.  $Q_{total}$  was the total heat transfer rate for the channel in kW.  $y_{loc}$  was the value of  $y$  within each increment.  $z$  was the axial position along the heated channel in m.

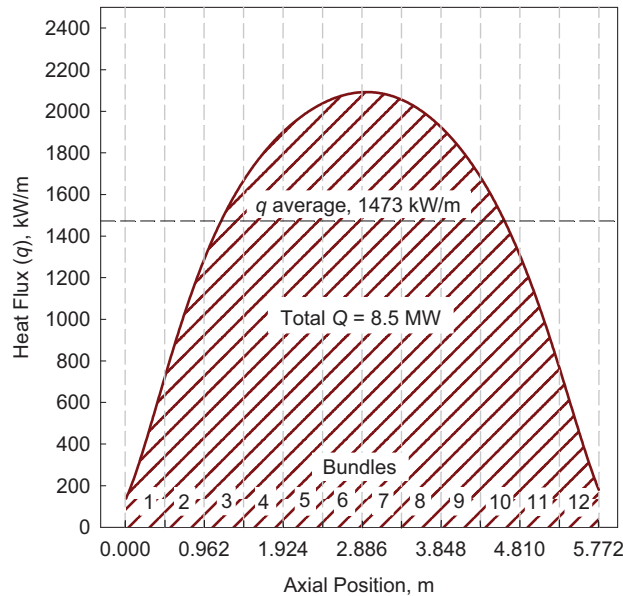


**Figure 5.1. Axial Heat Flux Distribution Along a Heated Channel.**

### 5.3 Parametric Trends

A comparison of selected thermophysical properties profiles for water along the fuel-channel heated length are shown in Figures 5.2 and 5.3 (Mokry et al., 2008). These figures are drawn for a non-uniform cosine axial heat-flux distribution at a pressure of 25 MPa. For calculation in the supercritical range, an averaged Prandtl number (**Pr**) and specific heat ( $c_p$ ) are used to account for thermophysical properties variations (for details, see Figure 5.3).

As discussed previously, all thermophysical properties undergo variations near the critical and pseudocritical points. For this case, (i.e., non-uniform cosine AHFP), the pseudocritical region occurs within Bundles 4 and 5. It can be observed in Figure 5.2 that properties such as density ( $\rho$ ), thermal conductivity ( $k$ ), and dynamic viscosity ( $\mu$ ) undergo a significant drop along the heated channel. Dynamic viscosity has a minimum value within Bundles 7 and 8, beyond which it is slightly increasing. Specific heat, thermal conductivity, and Prandtl number have peaks in the pseudocritical point (Figure 5.3). The magnitude of these peaks decreases very quickly with an increase in pressure (Pioro and Duffey, 2007). The peak in thermal conductivity had not been discovered prior to the 1990s (Pioro and Duffey, 2007), and for this reason, many early studies did not take this peak into account.

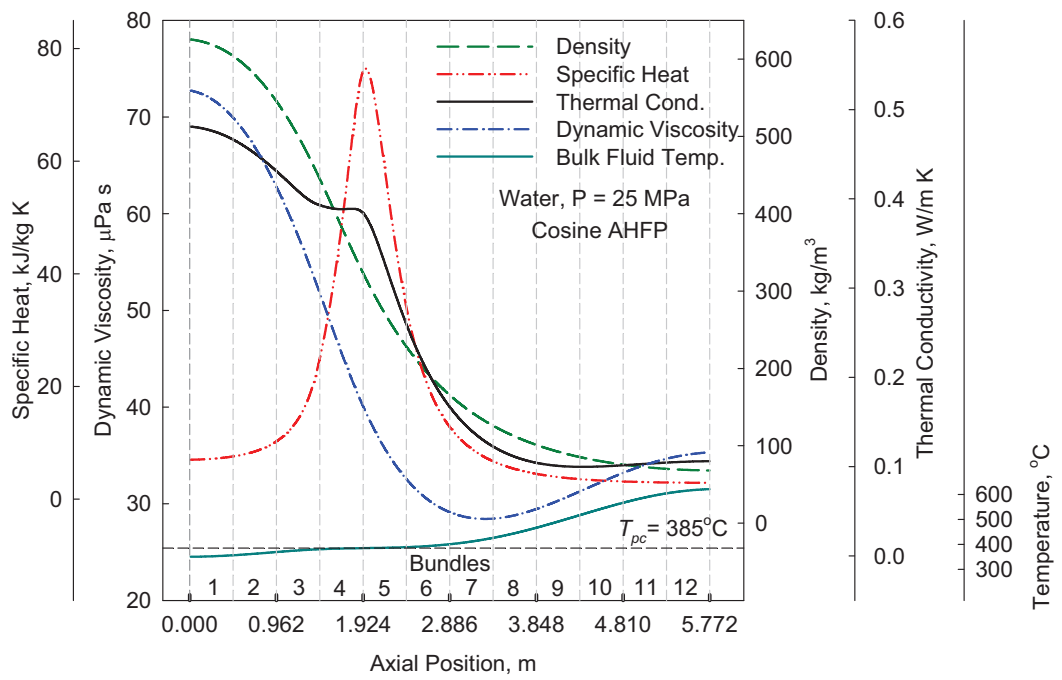


**Figure 5.2. Bulk-Fluid Temperature and Thermophysical Properties Profiles for Water along Heated Length of Fuel-Channel (Mokry et al., 2008).**

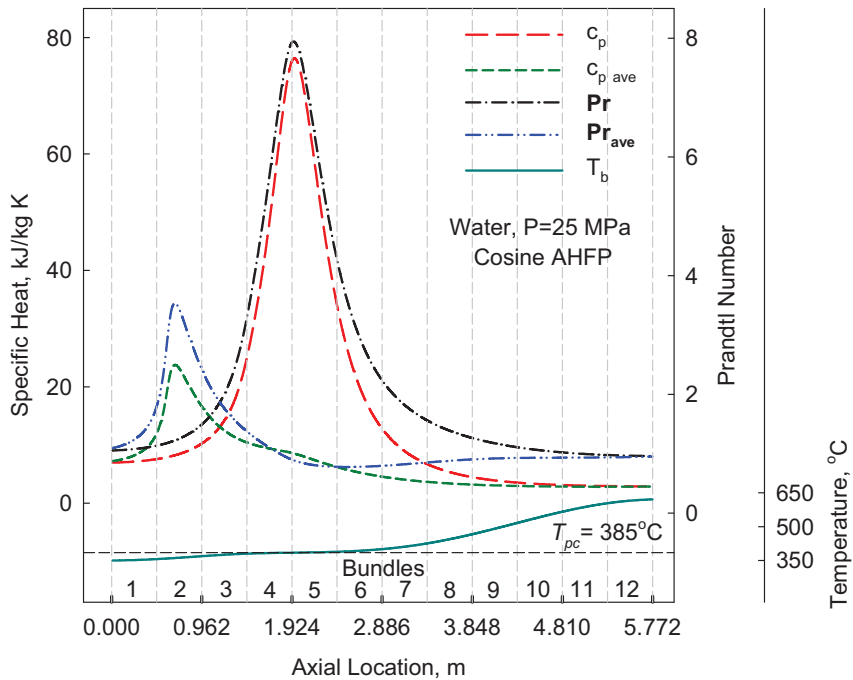


**Figure 5.3. Prandtl Number and Specific Heat Profiles for Water along Heated Length of Fuel-Channel (Mokry et al., 2008).**

The determination of fuel cladding and fuel centerline temperatures relies on the HTC. An accurate HTC is essential for thermalhydraulic analysis of the fuel channel. This is due to the fact that the HTC and fluid properties are used in calculating the maximum fuel and cladding temperatures. The determination of the feasibility of design of an SCWR will be based on the comparison of these values with their maximum allowable temperatures.

Searching through open literature, the only correlation for fuel bundles was developed by Dyadyakin and Popov (1977) (see Eq. 6.1). Experiments were conducted with a tight 7-rod helically-finned bundle; however, this bundle appeared to be a prototype for a transport reactor. Thus, this bundle is very dissimilar in design from that of the potential fuel bundles for power SCWRs, and other correlations have to be used. A better correlation, although still only approximate, is the Bishop et al. correlation (1964), which should prove to be sufficiently adequate.

The Bishop et al. (1964) heat-transfer correlation is based on experiments conducted with supercritical water flowing upwards inside tubes and annuli. The operating parameters were: pressure 22.8 – 27.6 MPa, bulk-fluid temperature 282 – 527°C, mass flux 651 – 3662 kg/m<sup>2</sup>s, and heat flux 0.31 – 3.46 MW/m<sup>2</sup>. This range of parameters is relevant to the SCWR operating range. The Bishop et al. correlation is given below:

$$\text{Nu} = 0.0069 \text{Re}^{0.9} \overline{\text{Pr}}^{0.66} \left( \frac{\rho_w}{\rho_b} \right)^{0.43} \left( 1 + 2.4 \frac{D_{hy}}{x} \right), \quad (5.14)$$

where **Re** and **Pr** refer to Reynolds and Prandtl numbers.

However, the Bishop et al. correlation was obtained over 40 years ago. Therefore, it is necessary for this correlation to be updated, on the basis of the latest thermophysical properties of water, i.e., NIST software, and a recent dataset collected within SCWR ranges.

#### 5.4 Bulk-Fluid Temperature Profile

A bulk-fluid-temperature profile was calculated based on an average cross-sectional temperature and invariable pressure along the fuel-channel. The bulk-fluid-temperature values were calculated based on a heat-balance method.

The inlet bulk-fluid enthalpy was calculated through NIST REFPROP (2007), based on a pressure of 25 MPa and an inlet bulk-fluid temperature of 350°C. Taking this inlet enthalpy value as a starting point, enthalpies along the fuel-channel were determined using the following equation:

$$H_{i+1} = H_i + \frac{POW_\ell}{\dot{m}}, \quad (5.15)$$

where  $H_i$  is the initial enthalpy in kJ/kg;  $H_{i+1}$  is the successive enthalpy along the length of the channel in kJ/kg;  $POW_\ell$  is the local power in kW; and  $\dot{m}$  is the mass-flow rate per channel in kg/s (see Table 5.1). In this manner, enthalpies for the entire fuel-channel were determined.

Bulk-fluid temperature values were then calculated based on enthalpy values and the constant pressure of 25 MPa. Figure 5.4 shows bulk-fluid-temperature and bulk-fluid-enthalpy profiles along the heated length of the fuel-channel (10-mm axial increments were used).

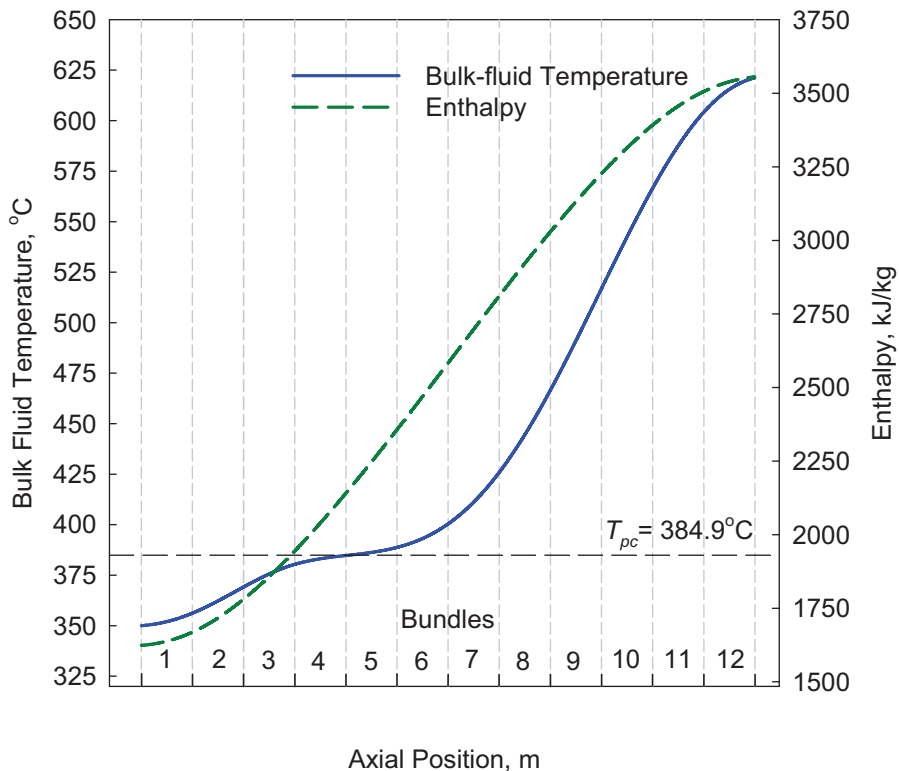


**Figure 5.4. Bulk-Fluid Temperature and Enthalpy Profiles along Heated Fuel-Channel.**

## 5.5 Thermal Conductivity of the Cladding

Higher operating conditions require that the cladding for the reactor fuel be made of a material that can withstand the high temperatures and stresses that it will be subjected to. Today, the most commonly assumed material for use in SCWRs is Inconel-718 (for details on Inconel-718, see Special Metals, 2007). The thermal conductivity of Inconel-718 changes with temperature within the operating range. This relationship was determined as follows:

$$k_{clad} = 6.806601 + 0.015842 T_{clad}, \quad (5.16)$$

where  $T_{clad}$  is the temperature at the fuel element surface in °C.

This equation was obtained by linear regression of the thermal conductivity values of Inconel-718 at certain points using tabulated data (Incropera et al., 2007).

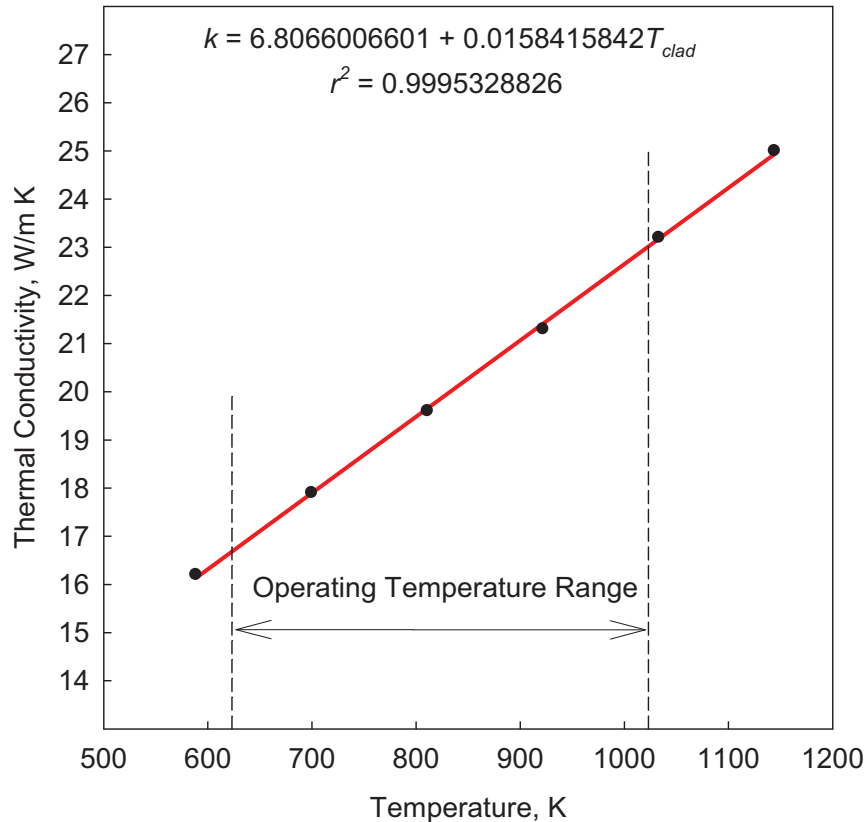


**Figure 5.5. Thermal Conductivity of Inconel-718.**

## 5.6 Thermal Conductivity of the Fuel

To obtain the relationship for the thermal conductivity of the fuel, a 5<sup>th</sup>-order polynomial was found to be the best representation of the relationship, within the range of ~500 to 2500 K:

$$k_{fuel} = a_0 + a_1 \cdot T_{fuel} + a_2 \cdot T_{fuel}^2 + a_3 \cdot T_{fuel}^3 + a_4 \cdot T_{fuel}^4 + a_5 \cdot T_{fuel}^5 \quad (5.17)$$

The coefficients for this relation (Eq. 5.17) were determined using SigmaPlot's regression analysis and are as follows:

$$\begin{aligned}a_0 &= 15.637; \\a_1 &= -0.029; \\a_2 &= 2.899E-5; \\a_3 &= -1.628E-8; \\a_4 &= 4.709E-12; \\a_5 &= -5.331E-16;\end{aligned}$$

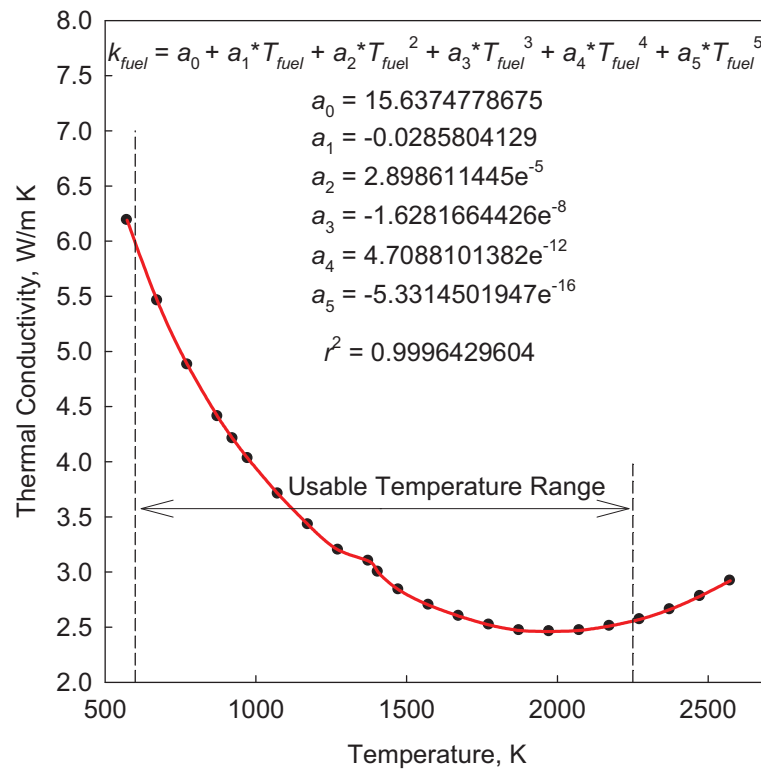
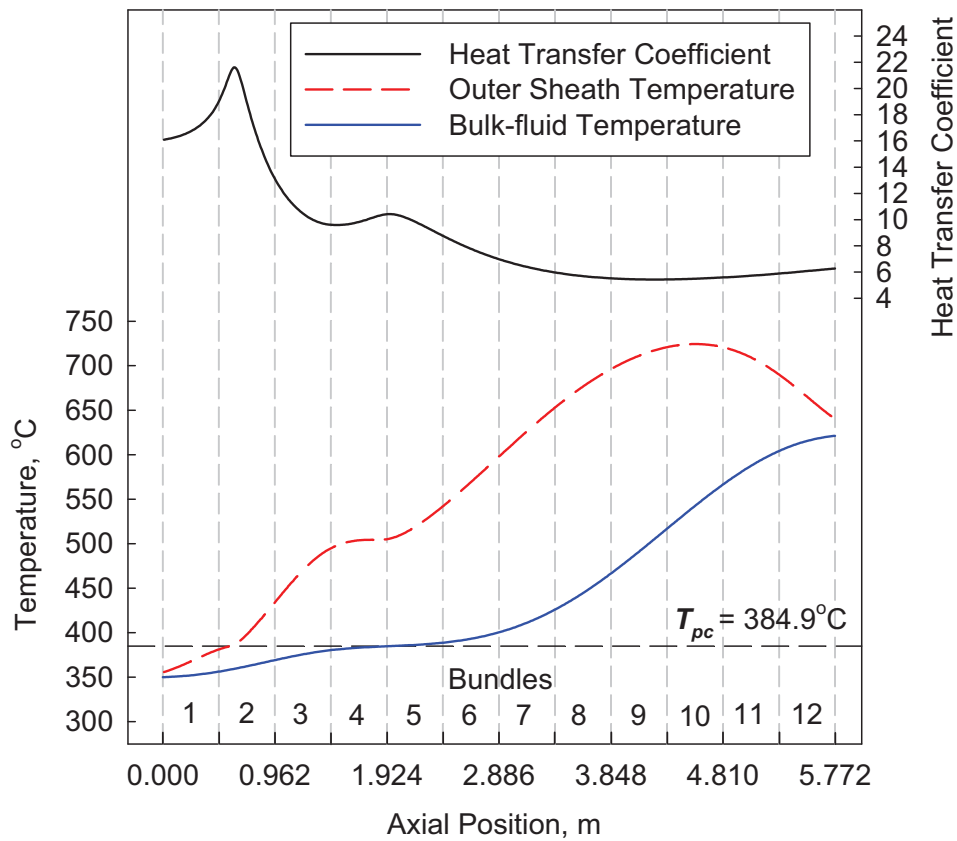


Figure 5.6. Thermal Conductivity of Uranium Oxide ( $\text{UO}_2$ ).

## 5.7 Heat Transfer and Surface Temperature of the Fuel Elements

Using the heat-transfer rate and bulk-fluid temperature profiles along the heated channel, the HTC and surface temperature of the fuel elements were obtained through iterations. A MATLAB (2007) code was written and set-up to interact with

the NIST REFPROP software, such that corresponding water properties were obtained. The fuel cladding element temperature was initially assumed to be 50°C above the bulk-fluid temperature. The MATLAB code then used iterations until the surface temperature of the fuel element converged to a single value.



**Figure 5.7. Fuel Element Temperature and Heat Transfer Coefficient Profiles.**

The HTC profile in Figure 5.7 appears to have two distinctive peaks. The first peak appears as a result of an averaged Prandtl number, which is part of the Bishop et al. (1964) correlation used (Eq. 5.14). The averaged Prandtl number (see Section 5.3) depends on the averaged specific heat capacity in the channel cross section. Due to a large difference between the bulk-fluid temperature and the temperature of fluid near the fuel element sheath, this peak is shifted upstream of the pseudocritical point (see Figure 5.7). The reason for the second peak appears to be a result of thermal conductivity in the HTC expression. This

peak is smaller compared to the averaged specific heat and Prandtl number; however, it is in the pseudocritical region.

Using the variable conductivity of the cladding, fuel element surface temperature and a non-uniform linear heat flux, the temperature difference through the cladding was obtained along the heated channel.

$$\Delta T_{clad} = \frac{q \cdot \ln\left(\frac{r_{outer}}{r_{inner}}\right)}{2\pi \cdot k_{clad}}, \quad (5.18)$$

where  $q$  is the linear heat flux, in  $\text{W/m}^2$ .

The result gave the temperature difference through the cladding along the heated length of the fuel-channel. Adding this difference to the outer cladding temperature produced the temperature profile for the outer surface of the Uranium Dioxide ( $\text{UO}_2$ ) (Table 5.1) on the inner surface of the Inconel-718 cladding.

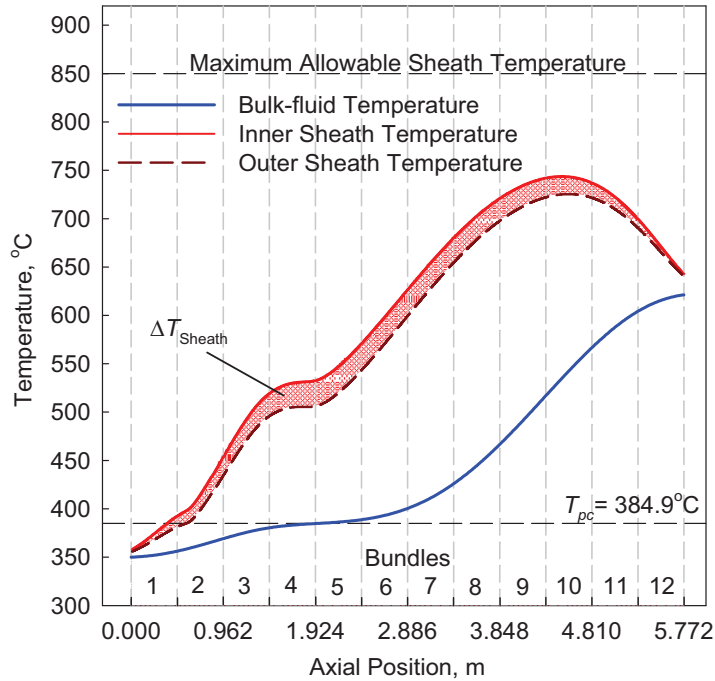


**Figure 5.8. Bulk-Fluid Temperature, Sheath Temperature and HTC Profiles.**

## 5.8 Fuel Centerline Temperature

To calculate the fuel centerline temperature, variable thermal conductivity was used along the heated length of the channel only. Then, to improve accuracy, variable thermal conductivity was also used in the fuel cross-section. The fuel pellet was modeled as if it was comprised of five layers, each of a 1-mm thickness, in addition to a 0.72-mm diameter central section. For calculations of the temperature difference across each layer, the thermal conductivity was taken at the temperature of the outer radius of each layer. It was assumed that uniform heat generation took place within the volume of the fuel.

Next, a program was written (MATLAB) to repeat the layer by layer calculations. This allowed for the closest reasonable approximation of the fuel centerline temperature.

$$\text{Volumetric heat flux: } q_{vl} = \frac{\frac{1}{42} Q_{loc}}{V_{xsect}} \quad (5.19)$$

$$\text{Volume of the cross-section: } V_{xsect} = \pi r_{fuel,pellet}^2 L \quad (5.20)$$

where  $L=0.01$  m

$$\text{Fuel centerline temperature: } T_{fuel,centerline} = T_{fuel,surface} + \frac{q_{vl} r_{fuel,surface}^2}{4 k_{fuel}} \quad (5.21)$$

Since the fuel surface temperature was used to compute the fuel centerline temperature, the resulting temperature profile was much lower than the actual temperature and required further analysis. Therefore, calculations proceeded with the layers approach.

For each layer,  $r_2$  was the outer radius for the layer and  $r_1$  was the inner radius. The temperature jump across each layer was calculated using the following formulas:

Temperature of fuel at the inner radius for the current layer:

$$T_{fuel,1} = T_{fuel,2} + \frac{q_{vl,layer}}{4k_{fuel}} (r_{fuel,2}^2 - r_{fuel,1}^2) \quad (5.22)$$

Volumetric heat flux of the current layer at the cross section:

$$q_{vl,layer} = \frac{\frac{1}{42} Q_{loc} \cdot \frac{r_{fuel,2}^2 - r_{fuel,1}^2}{r_{fuel,surf}^2}}{V_{xsect}} \quad (5.23)$$

Volume of the current layer, in the current cross section:

$$V_{xsect} = \pi (r_{fuel,2}^2 - r_{fuel,1}^2) L, \quad \text{where } L = 0.01 \text{ m} \quad (5.24)$$

Simplifying resulted in the following expression:

$$T_{fuel,1} = T_{fuel,2} + \frac{\frac{1}{42} Q_{loc}}{4k_{fuel} \pi L} \frac{(r_{fuel,2}^2 - r_{fuel,1}^2)}{r_{fuel,surf}^2} \quad (5.25)$$

Once the temperature on the inside of the last layer was obtained, the centerline temperature was found through:

$$T_{fuel,centerline} = T_{fuel,1} + \frac{q_{vl,center} r_{fuel,1}^2}{4 k_{fuel}} \quad (5.26)$$

Volumetric heat flux at the central section:

$$q_{vl,center} = \frac{1}{42} \frac{Q_{loc}}{V_{xsect}} \frac{r_{fuel,1}^2}{r_{fuel,pellet}^2} \quad (5.27)$$

$$V_{xsect} = \pi r_{fuel,1}^2 L, \quad \text{where } L=0.01 \text{ m} \quad (5.28)$$

Simplifying resulted with:

$$T_{fuel,centerline} = T_{fuel,1} + \frac{1}{42} \frac{Q_{loc}}{4 k_{fuel} \pi L} \frac{r_{fuel,1}^2}{r_{fuel,pellet}^2} \quad (5.29)$$

Calculating the centerline fuel temperature by layers gave a closer approximation. The same approach was repeated, using layers of a much smaller thickness. It was found that 0.01 mm was the smallest layer thickness that was reasonable to take. At this point, the temperature profile was so close to that of the final temperature that there was no benefit to using smaller increments for the cross-section.

As it can be seen from Figure 5.9, the maximum centerline temperature was just above 2000°C. The melting point of Uranium Dioxide is approximately 2800°C and the optimal operating conditions for existing reactors is between 1800 – 1900°C. In this case, the centerline temperature appears far below the fuel

melting point, but is slightly above the industry accepted maximum operating temperature of 1850°C.

An additional calculation of the fuel centerline temperature was conducted, again using a conservative approach, taking the smallest value for thermal conductivity of UO<sub>2</sub>. The maximum centerline temperature found using this method was approximately 2240°C. This is significantly larger than the maximum centerline temperature obtained using the variable thermal conductivity. Using the layer by layer calculations with variable thermal conductivity gave the better estimate for the centerline fuel temperature.

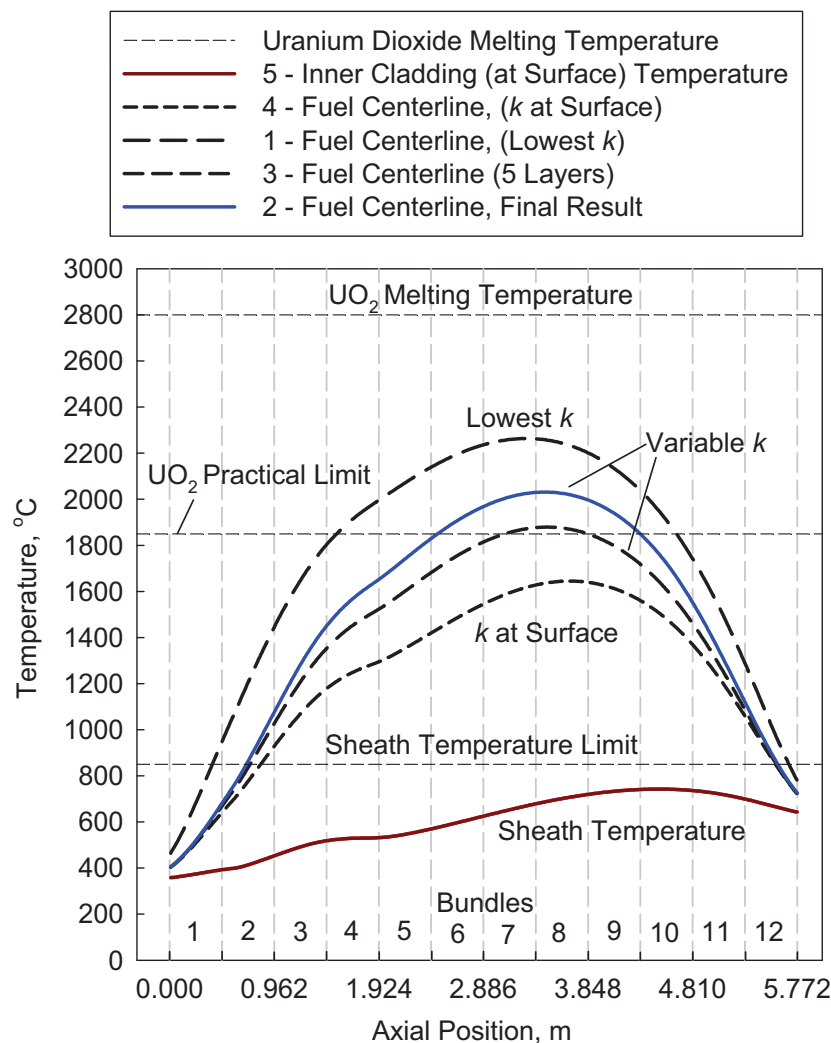


**Figure 5.9. Profiles for Fuel Centerline Temperature.**

Unfortunately, there are no correlations available for the HTC in fuel bundles cooled with supercritical water. Based on the performed calculations, using the Bishop et al. (1964) correlation, the maximum centerline fuel temperature is just above 2000°C. This temperature was based on a conservative approach. A number of possible ways to lower the centerline temperature have been identified. They include:

- Use of hollow fuel pellets;
- Decrease in fuel element diameter; and
- Turbulization of flow.

However, the most important task will be to develop a new reliable and accurate heat transfer correlation for these first step calculations.

## CHAPTER 6

### HEAT TRANSFER CORRELATIONS AT SUPERCRITICAL PRESSURES

Currently, there is just one supercritical-water heat-transfer correlation for fuel bundles, developed by Dyadyakin and Popov (1977) (Pioro and Duffey, 2007).

$$Nu_x = 0.021 Re_x^{0.8} Pr_x^{0.7} \left( \frac{\rho_w}{\rho_b} \right)_x^{0.45} \left( \frac{\mu_b}{\mu_{in}} \right)_x^{0.2} \left( \frac{\rho_b}{\rho_{in}} \right)_x^{0.1} \left( 1 + 2.5 \frac{D_{hy}}{x} \right) \quad (6.1)$$

Where  $x$  is the axial location along the heated length in meters, and  $D_{hy}$  is the hydraulic-equivalent diameter (equals four times the flow area, divided by the wetted perimeter) in meters.

This correlation was obtained through experimentation with a tight-lattice 7-element helically-finned bundle cooled with water. Five test bundles with different flow areas were examined. Table 6.1 provides the parameters for these bundles.

**Table 6.1. Dyadyakin and Popov Test Bundle Parameters (Pioro and Duffey, 2007).**

Test Section #	1	2	3	4	5
$A_{fl}$ , mm <sup>2</sup>	112	134	113	121	102
$D_{hy}$ , mm	2.35	2.77	2.38	2.53	2.15

However, heat-transfer correlations for bundles are generally very sensitive to bundle design, and the investigated design appears to be for a mobile-type (i.e. submarine or ship) reactor. Therefore, this correlation cannot be applied to other bundle geometries and used for fuel bundles of SCWRs.

To overcome this problem, a wide-range heat-transfer correlation based on bare-tube data should be developed, as a conservative approach. This process is based on the fact that HTC values for bare tubes are generally lower than those

having bundle geometries where heat transfer is enhanced with appendages (endplates, bearing pads, spacers, button, etc.).

A number of empirical generalized correlations, based on experimentally obtained datasets, have been proposed to calculate HTCs in forced convection for various fluids, including water, at supercritical pressures. These bare-tube-based correlations are available in various literature sources. However, analysis and comparison of these correlations by Pioro and Duffey (2007) has shown that differences in HTC values can be up to several hundred percent.

## 6.1 Existing Heat Transfer Correlations

The most widely used heat-transfer correlation at subcritical pressures for forced convection is the Dittus-Boelter correlation (1930). McAdams (1942) proposed the use of the Dittus-Boelter correlation in the following form for forced-convective heat transfer in turbulent flows at subcritical pressures (this statement was based on the recent study by Winterton (1998)):

$$\text{Nu}_b = 0.0243 \text{Re}_b^{0.8} \text{Pr}_b^{0.4} \quad (6.2)$$

Later, Eq. (6.2) was also used at supercritical conditions. According to Schnurr et al. (1976), Eq. (6.2) showed good agreement with experimental data for supercritical water, flowing inside circular tubes, at a pressure of 31 MPa with low heat fluxes. However, it was noted that Eq. (6.2) might produce unrealistic results within some flow conditions, especially within the critical and pseudocritical points, because it is very sensitive to properties variations. In general, this classical correlation was used extensively as a basis for various supercritical heat-transfer correlations.

An analysis performed by Pioro and Duffey (2007) showed that the two following correlations: 1) Bishop et al. (1964) and 2) Swenson et al. (1965); were obtained within the same range of operating conditions as those for SCWRs.

Bishop et al. (1964) conducted experiments in supercritical water flowing upward inside bare tubes and annuli within the following range of operating parameters: pressure 22.8 – 27.6 MPa, bulk-fluid temperature 282 – 527°C, mass flux 651 – 3662 kg/m<sup>2</sup>s and heat flux 0.31 – 3.46 MW/m<sup>2</sup>. Their data for heat transfer in tubes was generalized using the following correlation with a fit of ±15%:

$$\text{Nu}_b = 0.0069 \text{Re}_b^{0.9} \overline{\text{Pr}}_b^{0.66} \left( \frac{\rho_w}{\rho_b} \right)^{0.43} \left( 1 + 2.4 \frac{D}{x} \right), \quad (6.3)$$

where  $x > 0$ . Equation (6.3) uses the cross-sectional averaged Prandtl number, as mentioned in an earlier chapter. The last term in the correlation accounts for entrance-region effects.

The Bishop et al. correlation is often used without the entrance-region term, Eq. (6.4), because this term depends significantly on the particular design of the inlet of the bare test section:

$$\text{Nu}_b = 0.0069 \text{Re}_b^{0.9} \overline{\text{Pr}}_b^{0.66} \left( \frac{\rho_w}{\rho_b} \right)^{0.43} \quad (6.4)$$

In addition, the Dittus-Boelter correlation was used in the following form, for reference purposes:

$$\text{Nu}_b = 0.023 \text{Re}_b^{0.8} \text{Pr}_b^{0.4} \quad (6.5)$$

Equation (6.5) is the most widely used interpretation of the original Dittus-Boelter correlation (Incropera et al., 2007).

Swenson et al. (1965) found that conventional correlations, which use the bulk-fluid temperature as a basis for calculating the majority of thermophysical properties, did not work well. They suggested the following correlation in which thermophysical properties are based mainly on wall temperature:

$$\text{Nu}_w = 0.00459 \text{Re}_w^{0.923} \overline{\text{Pr}}_w^{0.613} \left( \frac{\rho_w}{\rho_b} \right)^{0.231} \quad (6.6)$$

Equation (6.6) was obtained within the following range: pressure 22.8 – 41.4 MPa, bulk-fluid temperature 75 – 576°C, wall temperature 93 – 649°C and mass flux 542 – 2150 kg/m<sup>2</sup>s; and predicts the experimental data within ±15%.

Jackson (2002) modified the original correlation of Krasnoshchekov et al. (1967) (for details, see Pioro and Duffey (2007)), for forced-convective heat transfer in water and carbon dioxide at supercritical pressures, to employ the Dittus-Boelter type form for  $\text{Nu}_o$ . Finally, the following correlation was obtained:

$$\text{Nu}_b = 0.0183 \text{Re}_b^{0.82} \overline{\text{Pr}}_b^{0.5} \left( \frac{\rho_w}{\rho_b} \right)^{0.3} \left( \frac{c_p}{c_{pb}} \right)^n \quad (6.7)$$

Where the exponent  $n$  is defined as following:

$$n = 0.4 \quad \text{for } T_b < T_w < T_{pc} \text{ and for } 1.2T_{pc} < T_b < T_w ;$$

$$n = 0.4 + 0.2 \left( \frac{T_w}{T_{pc}} - 1 \right) \quad \text{for } T_b < T_{pc} < T_w ; \text{ and}$$

$$n = 0.4 + 0.2 \left( \frac{T_w}{T_{pc}} - 1 \right) \left[ 1 - 5 \left( \frac{T_b}{T_{pc}} - 1 \right) \right] \quad \text{for } T_{pc} < T_b < 1.2T_{pc} \text{ and } T_b < T_w .$$

## 6.2 Comparison of Heat Transfer Correlations

Figure 6.1 shows two sample experimental runs at supercritical pressures and provides experimentally measured HTC values. A comparison between experimental HTCs and the calculated HTCs using the Dittus-Boelter, Bishop et al., Jackson, and Swenson et al. correlations are plotted.

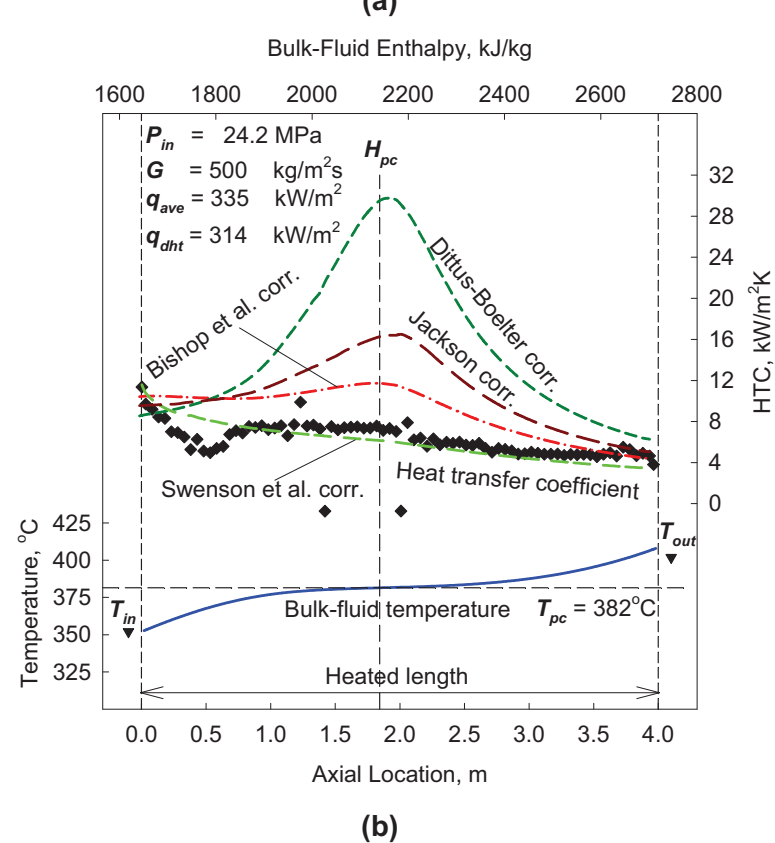
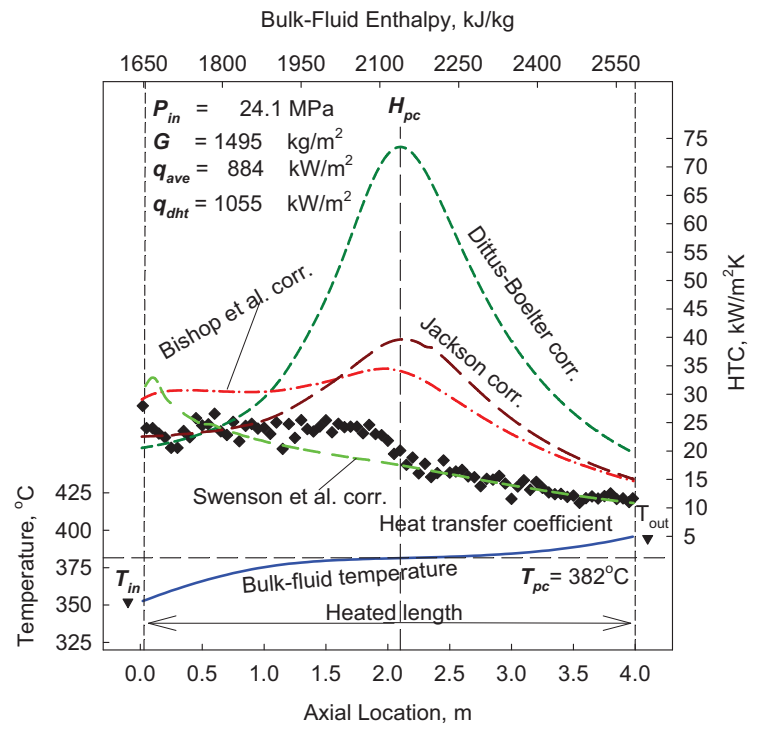


**Figure 6.1. Temperature and HTC (Experimental and Calculated Values) Profiles along Heated Length of Bare Vertical Tube: (a)  $G = 1500 \text{ kg/m}^2\text{s}$  and  $q = 884 \text{ kW/m}^2$ ; (b)  $G = 500 \text{ kg/m}^2\text{s}$  and  $q = 335 \text{ kW/m}^2$  (Mokry et al., 2009b).**

As can be seen from Figure 6.1, the Dittus-Boelter correlation provides a significant overestimation of the HTC within the pseudocritical region, and thus, this correlation is unusable within a wide range of parameters. The Bishop et al. and Jackson correlations also tend to deviate substantially from the experimental data within the pseudocritical range. The Swenson et al. correlation provides a better fit for the experimental date than the previous three correlations within some flow conditions, but does not closely follow the experimental data within others (Mokry et al., 2009b).

It should be noted that all heat-transfer correlations presented in this thesis are intended only for normal heat-transfer regime calculations. Neither the Dittus-Boelter nor the Bishop et al. correlations can be used for the prediction of HTCs within the deteriorated heat-transfer regime.

An empirical correlation was proposed for heat flux calculations at which the deteriorated heat-transfer regime appears (for details, see Gabaraev et al., 2007):

$$q_{dht} = 7.9 \cdot 10^{-4} G \left( \frac{P}{P_{cr}} \right)^{1.5}, \text{ MW/m}^2 \quad (6.8)$$

A more thorough discussion and comparison of heat-transfer correlations can be found in Pioro and Duffey (2007).

### 6.3 Final Objective

The majority of the reviewed empirical correlations were proposed in the 1960s and 1970s, when experimental techniques were not at the same level (i.e., advanced level) as they are today. Also, thermophysical properties of water have since been updated (for example, a peak in thermal conductivity in critical and pseudocritical points, within a range of pressures from 22.1 to 25 MPa, was not officially recognized until the 1990s (Pioro and Duffey, 2007)).

Thus, this further emphasizes the necessity to develop a new or an updated correlation based on a new set of heat-transfer data and the latest thermophysical properties of water (NIST, 2009) within the SCWRs operating range.

Through analysis and consideration, it is clear that there are urgent needs for a reliable, accurate and wide range supercritical water heat transfer correlation to be used for bare tubes:

1. For preliminary thermalhydraulics calculations of supercritical-water-cooled fuel bundles as a conservative approach in relation to SCWRs;
2. For calculations of supercritical water heat transfer in heat exchangers at supercritical water NPPs using an indirect cycle;
3. For calculations of heat transfer in heat exchangers for co-generation of hydrogen at supercritical water NPPs;
4. For calculations of heat transfer in heat exchangers for all other Generation IV reactor concepts (GFRs, LFRs, MSRs, SFRs and VHTRs) even including HTGRs if the supercritical Rankine Cycle will be used;
5. For future comparisons with other independent datasets;
6. For comparisons with bundle data, as the reference case;
7. For the verification of computer codes for SCWR core thermalhydraulics; and
8. For the verification of scaling parameters between water and modeling fluids ( $\text{CO}_2$ , refrigerants, etc.).

Therefore, the proposed objective of this study to develop a new heat-transfer correlation for the normal heat-transfer regime to improve fundamental knowledge of the heat-transport processes and handling of supercritical fluids was deemed to be both necessary and relevant.

## Chapter 7

### EXPERIMENTAL DATASET

The experimental data used in the current thesis was obtained at the State Scientific Center of Russian Federation – Institute for Physics and Power Engineering Supercritical-Test Facility (Obninsk, Russia). This set of data was obtained within operating conditions close to those of SCWRs, including the hydraulic-equivalent diameter ( $D_{hy}$ ) (Mokry et al., 2009a, b). In addition, this dataset was collected recently, thus experimental techniques would have been at a more advanced level than those of the correlations previously discussed.

#### **7.1 Test Facility**

The Supercritical-Pressure Test Facility SKD-1 loop (Kirillov et al., 2005) is a high-temperature and high-pressure pumped loop. This loop was intended for supercritical water heat-transfer testing in bare tubes and other flow geometries, within a wide range of parameters (operating pressures up to 28 MPa at outlet water temperatures up to 500°C and power up to 0.6 MW). All components of the experimental setup were made of stainless steel and distilled and de-ionized water was used as a coolant in the loop.

Water passes from a pump through a flowmeter, a preheater, a test section, a mixing cooler, main coolers and back to the pump. Pressurization was achieved with a high-pressure gas ( $N_2$ ) (see Figure 7.1).

The test section is installed vertically with an upward flow. Power was delivered to the test section by a 600 kW (AC) power supply, and cooling was achieved just downstream of the test section using a mixing cooler. While some of the heat from the test section was removed using this mixing cooler, a large portion was removed using the main loop heat exchangers in the discharge circuit of the pump.

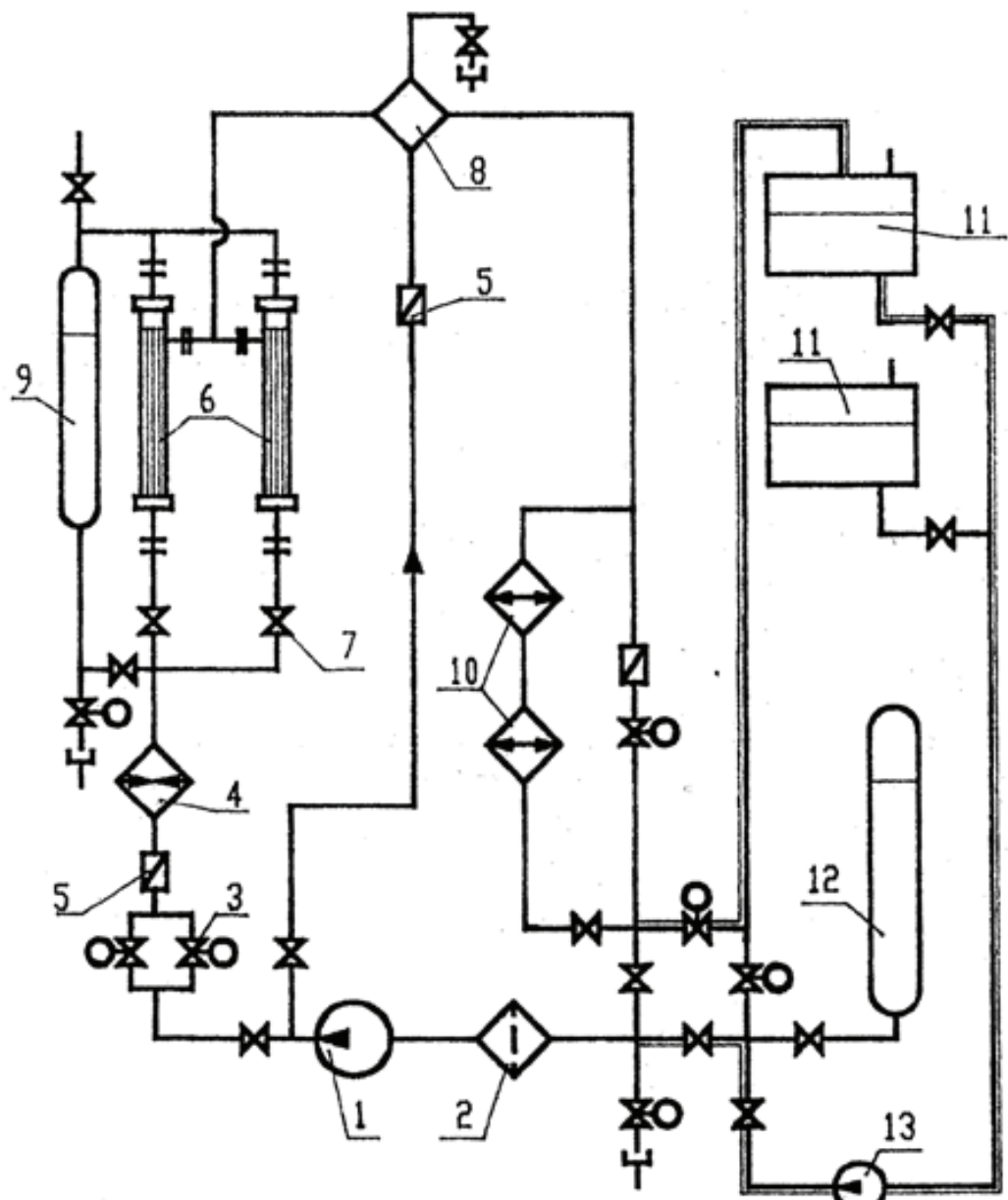


**Figure 7.1. Schematic of the SKD-1 Loop  
(Pioro et al., 2010; Kirillov et al., 2005).**

1 – circulating pump, 2 – mechanical filter, 3 – regulating valves,  
4 – electrical heater, 5 – flow meter, 6 – test section,  
7 – throttle valve, 8 – mixer, 9 – discharge tank,  
10 – heat exchanger, 11 – feedwater tank, 12 – volume compensator,  
13 – feedwater pump.

## 7.2 Test-Section Design

The test section was a vertical stainless steel (12Cr18Ni10Ti) smooth circular tube with upward flow (10-mm ID, 2-mm wall thickness and tube internal arithmetic-averaged surface roughness  $R_a = 0.63 - 0.8 \mu\text{m}$ ). The diameter of the test section is close to the proposed hydraulic-equivalent diameter of an SCWR fuel bundle. Two heated lengths were utilized: 1) 1-m-long and 2) 4-m-long. Upon evaluation, the experimental dataset collected through use of the 1-m-long test section proved to be very limited and was determined to be insufficient for analysis. Therefore, only the dataset collected with the 4-m-long test section is presented in this thesis.

Water was heated by means of an AC electric current passing through the tube wall from the inlet to the outlet power terminals (copper clamps). In order to minimize heat losses, the test section was wrapped with thermal insulation. A schematic of the test section is provided in Figure 7.2.

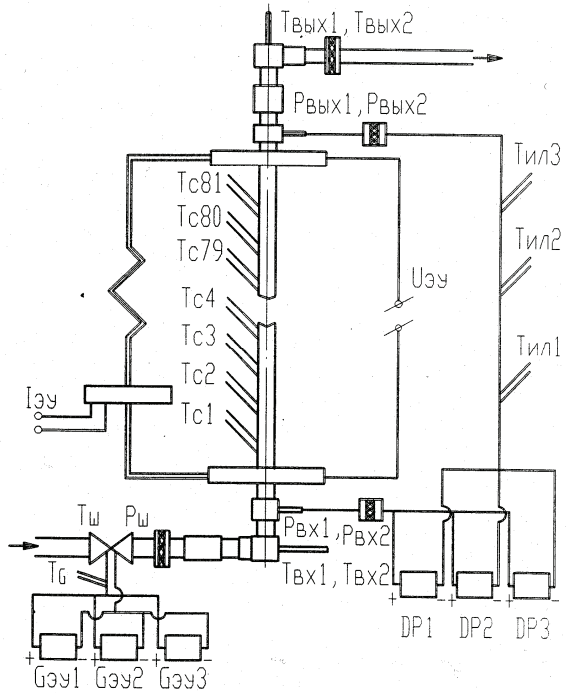


Figure 7.2. SKD-1 Loop Test Section Schematic (Kirillov et al., 2005)  
(courtesy of Professor P.L. Kirillov).

### 7.3 Instrumentation and Test Matrix

The following test-section parameters were measured or calculated during the experimental runs:

- Test-section current and voltage were used to calculate the power;
- Pressure at the test-section inlet;
- Temperatures at the test-section inlet and outlet. These temperatures were measured using ungrounded sheathed thermocouples (K-type) inserted into the fluid stream. The thermocouples were installed just downstream of the mixing chambers, which were used to minimize non-uniformity in the cross-sectional temperature distribution. These thermocouples were calibrated *in situ*;
- Outside wall temperatures at equal intervals (50 mm) along the test section. Eighty-one thermocouples, attached to the 4-m-long test section, were contact welded onto the outside wall surface. These thermocouples were isolated by glass cord and were calibrated *in situ*;
- Water mass-flow rate was calculated based on the measured pressure drop over a small orifice plate, which was monitored with a differential-pressure cell; and
- Ambient temperature.

The instrumentation used to measure the loop and test-section parameters was thoroughly checked and calibrated. Uncertainties of primary parameters are summarized in Table 7.1.

**Table 7.1. Uncertainties of Primary Parameters (Mokry et al., 2009a, b; Kirillov et al., 2005).**

Parameter	Maximum Uncertainty
Test-section Power	±1.0%
Inlet Pressure	±0.25%
Wall Temperature	±3.0%
Mass-flow Rate	±1.5%
Heat Loss	±3.0%

## 7.4 Experimental Procedure

The test-section was heated by the application of an alternating current through the tube. The specified operating parameters (pressure, mass flux and water temperature at the tube inlet) were set at the test section. The experimental dataset was recorded by a Data Acquisition System (DAS) when the desired flow conditions and power level had been reached and stabilized. Next, a new power level and/or new set of flow conditions were setup. The test matrix covered in the experiments is listed in Table 7.2. These test matrix values are close to the operating conditions of SCWRs (pressure of 24 – 25 MPa, inlet temperature of up to 350°C, outlet temperature of up to 625°C, mass flux within 800 – 1500 kg/m<sup>2</sup>s and heat flux of up to 1000 – 1200 kW/m<sup>2</sup>). The experimental runs were carried out under steady-state operating conditions, at forced water circulation, with vertical upward flow in the test section.

**Table 7.2. Dataset Test Matrix (Mokry et al., 2009a, b; Kirillov et al., 2005).**

<b>P</b> MPa	<b>T<sub>in</sub></b> °C	<b>T<sub>out</sub></b> °C	<b>T<sub>w</sub></b> °C	<b>q</b> kW/m <sup>2</sup>	<b>G</b> kg/m <sup>2</sup> s
24	320 – 350	380 – 406	<700	70 – 1250	200; 500; 1000; 1500

The heat-loss tests, conducted at the beginning of the experimental program, were used to determine the heat-loss characteristics of the test section. Heat loss was estimated by comparing the electrical heat input against the actual heat transfer to water. The test results showed that heat-loss from the test section was minor, within 3% of the electrical heat input. The power used in the heat-transfer calculations were adjusted for this heat loss.

## 7.5 Data Reduction

In general, the data reduction procedure is based on local parameters, which were measured or calculated at each cross-section corresponding to the external-wall thermocouples. The external-wall temperatures, inlet and outlet bulk-fluid temperatures and electrical current were used as the basis for local parameters calculations. These local parameters include thermal conductivity and electrical resistivity of the wall material, electrical resistance, power, heat flux, volumetric heat flux, internal wall temperature, heat loss, bulk-fluid temperature and pressure. The general and local parameters are defined as follows (Gospodinov et al., 2008; Pioro et al., 2008a).

### General Parameters:

- Flow area:
- $$A_{flow} = \frac{\pi D^2}{4} \quad (7.1)$$

- Mass flux:

$$G = \frac{\dot{m}}{A_{flow}} \quad (7.2)$$

- Total heated area:

$$A_h = \pi D L \quad (7.3)$$

- Measured power:

$$POW = VI \quad (7.4)$$

where  $V$  is the test-section voltage drop, and  $I$  is the electrical current.

- Average heat flux:

$$q = \frac{POW}{A_h} \quad (7.5)$$

- Outlet pressure:

$$P_{out} = P_{in} - \Delta P_{TS}, \quad (7.6)$$

where  $\Delta P_{TS}$  is the total pressure drop across the test section.

### Local Parameters:

- Heated area:

$$A_{h\ell} = \pi D L_\ell, \quad (7.7)$$

where  $L_\ell$  is the local heated length. For wall thermocouples, the local heated length was 50 mm. It was assumed that within the local heated length the external wall temperature is constant and equal to the value measured by wall thermocouples.

- Power:

$$POW_\ell = I^2 R_{\ell\ell}, \quad (7.8)$$

Where  $R_{\ell\ell}$  is the local electrical resistance within the local heated length, calculated using a local value of electrical resistivity.

- Heat flux:

$$q_\ell = \frac{POW_\ell - HL_\ell}{A_{h\ell}}, \quad (7.9)$$

where  $HL_\ell$  is the local heat loss based on the corresponding external wall temperature measurements. There is a minor change in axial heat flux due to direct AC heating and the effect of wall temperature on electrical resistivity of material.

- Tube wall thermal conductivity ( $k_{w\ell}$ ) was calculated using the average wall

temperature.

$$T_w^{ave} = \frac{T_w^{ext} - T_w^{int}}{2} \quad (7.10)$$

- Volumetric heat flux:

$$q_{v\ell} = \frac{POW_\ell}{\frac{\pi}{4}(D_{ext}^2 - D^2)L_\ell}. \quad (7.11)$$

- Internal wall temperature (Incropera et al., 2007):

$$T_w^{int} = T_w^{ext} + \frac{q_{v\ell}}{4k_{w\ell}} \left[ \left( \frac{D_{ext}}{2} \right)^2 - \left( \frac{D}{2} \right)^2 \right] - \frac{q_{v\ell}}{2k_{w\ell}} \left( \frac{D_{ext}}{2} \right)^2 \ln \frac{D_{ext}}{D} \quad (7.12)$$

This equation accounts for the uniformly distributed heat-generating sources inside the tube wall, i.e., heating with AC current passing through the tube wall.  $T_w^{ext}$  was a measured value from thermocouples along the tube.

- Thermophysical properties of water were calculated using NIST software (2002). These properties at a particular cross-section were calculated according to local pressure and local bulk-fluid temperature. The

pseudocritical temperature was evaluated at the inlet pressure for reference. The range of pseudocritical temperatures for each flow condition is quite narrow, because  $T_{pc}$ , which depends on pressure, decreases slightly from inlet to outlet.

- Bulk-fluid temperature was calculated using local pressure and local enthalpy in the cross-section, where the external-wall thermocouple was located. However, the average heat flux was used because variations in heat flux along the heated length were quite small.

The dataset includes 89 experimental runs, with 81 data points per run. In total, over 7,200 points were collected. Abnormalities, such as defective thermocouple readings were removed from the dataset (for details, see Figure 7.3.)

The primary objective of this study was to develop an updated heat-transfer correlation for the Normal Heat Transfer (NHT) regime. Therefore, data points in the Deteriorated Heat Transfer (DHT) region as well as points in the Improved Heat Transfer (IHT) region were also removed from the dataset (for details, see Figure 7.4.). These regions are subject to further study and investigation. Also, the very first and the last points of most experimental runs were removed. Temperatures at these outlying points were likely affected by test-section clamps, which were at a lower temperature than the heated part of the tube. Overall, approximately 91% of the experimental dataset was used for the development of a heat transfer correlation.

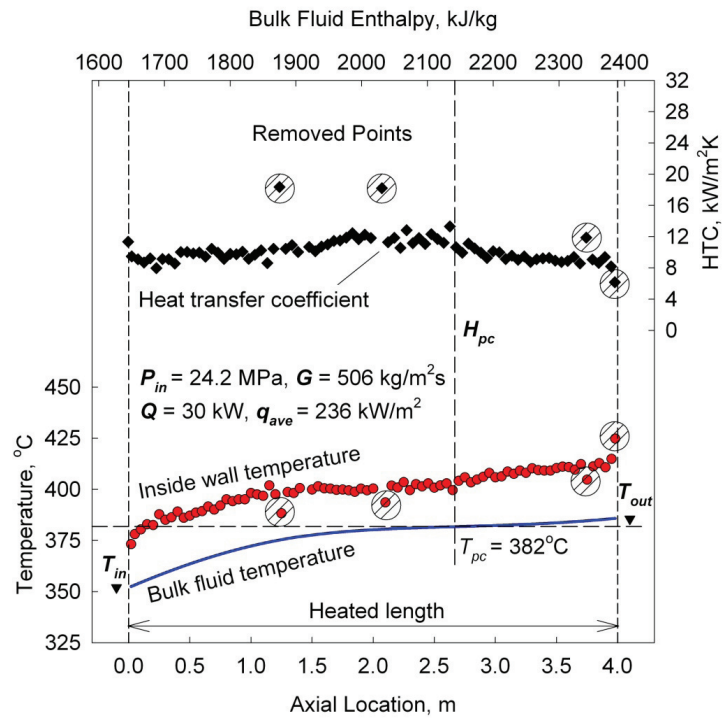


**Figure 7.3. Sample Experimental Run with Removed Outliers (Mokry et al., 2009a).**

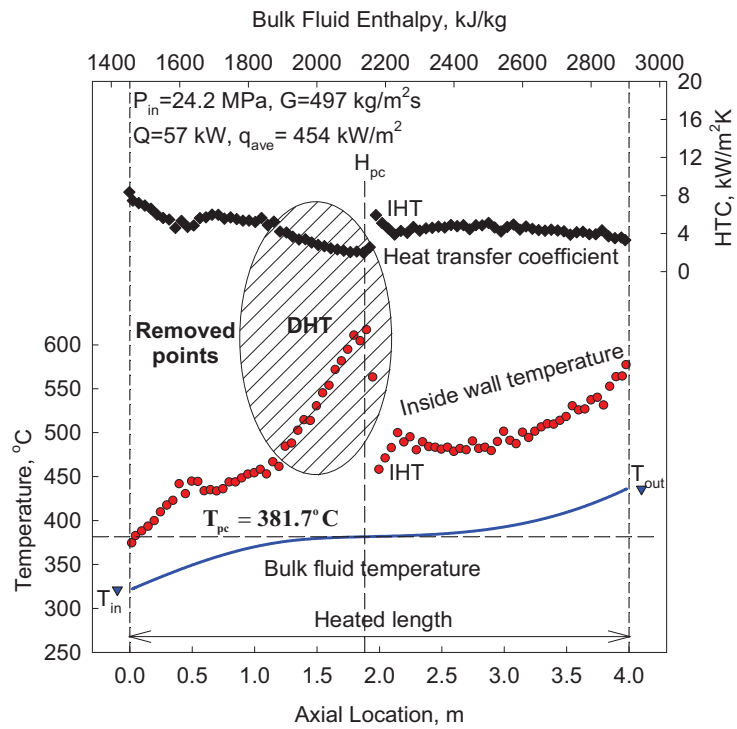


**Figure 7.4. Sample Experimental Run with Removed Points in the Deteriorated Heat Transfer and Improved Heat Transfer Regimes (Mokry et al., 2009a).**

## Chapter 8

### EXPERIMENTAL RESULTS

Selected experimental results (Mokry et al., 2010; Gospodinov et al., 2008) in supercritical water flowing upward in the vertical bare circular tube are summarized in Figures 8.1 - 8.4, to illustrate the key findings.

In general, the following supercritical heat-transfer cases were covered:

Within a certain heated length:

1.  $T_w^{in} < T_{pc}$ ,  $T_w^{in} = T_{pc}$ ,  $T_w^{in} > T_{pc}$  and
  - (a)  $T_b < T_{pc}$  or (b)  $T_b < T_{pc}$ ,  $T_b = T_{pc}$  and  $T_b > T_{pc}$
2.  $T_w^{in} > T_{pc}$  and (a)  $T_b < T_{pc}$  and  $T_b = T_{pc}$  or  
(b)  $T_b < T_{pc}$ ,  $T_b = T_{pc}$  and  $T_b > T_{pc}$ .

Typically, at the entrance region (i.e.,  $L/D \leq 30$ ), the wall temperature rises sharply (Figures. 8.1 – 8.4). In general, this temperature profile is due to the thermal-boundary-layer development.

At the inlet and outlet, power clamps may have affected the nearby heated-wall temperature. Therefore, any data, i.e., affected with the power-clamp effect, was eliminated from consideration. The same applies to some data points, which were outliers of the general trend due to the various reasons previously described (faulty thermocouples, IHT and DHT regimes).

Experimental data for supercritical water obtained at higher mass fluxes ( $G = 500 - 1500 \text{ kg/m}^2\text{s}$ ) (see Figures 8.1 – 8.3) showed good agreement between the calculated value of the last downstream bulk-fluid temperature, which was calculated through incremental heat-balances, and the measured outlet bulk-fluid temperature just downstream of the outlet mixing chamber.

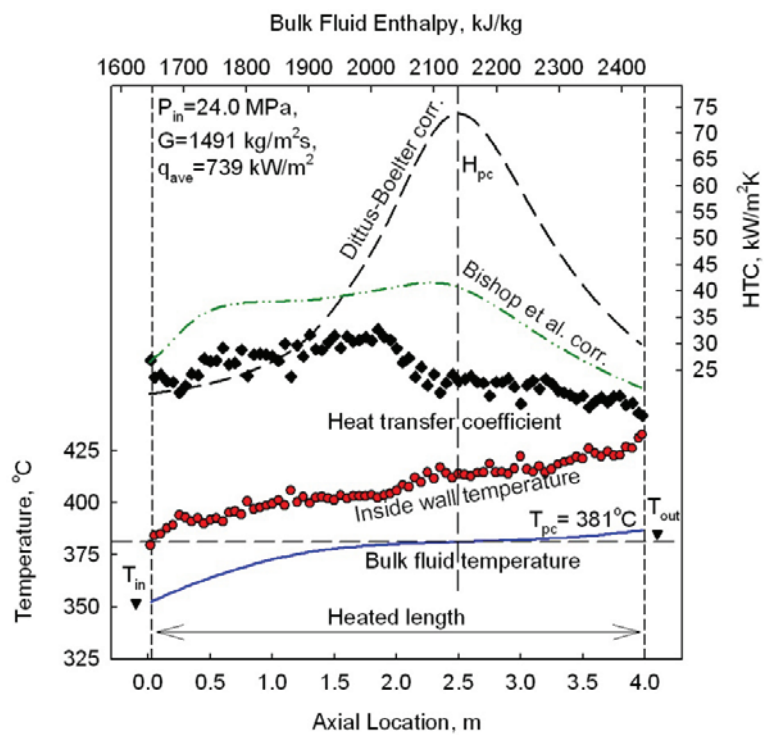
However, at lower mass flux ( $G = 200 \text{ kg/m}^2\text{s}$ ), there is a noticeable difference between the measured and calculated outlet bulk-fluid temperatures (see Figure 8.4). This effect seems to be due to the increased measurement uncertainty at low mass-flow rates.

Experimental data shown in Figures 8.1 – 8.3 are mainly within the normal heat-transfer regime. Exceptions are some data shown in Figure 8.1c (points inside shaded areas), which belong to the IHT regime; and some data shown in Figure 8.2c; 8.3b and 8.3d, which belong to the deteriorated heat-transfer regime (points inside shaded areas). All data shown in Figure 8.4 appears to be of the DHT regime.

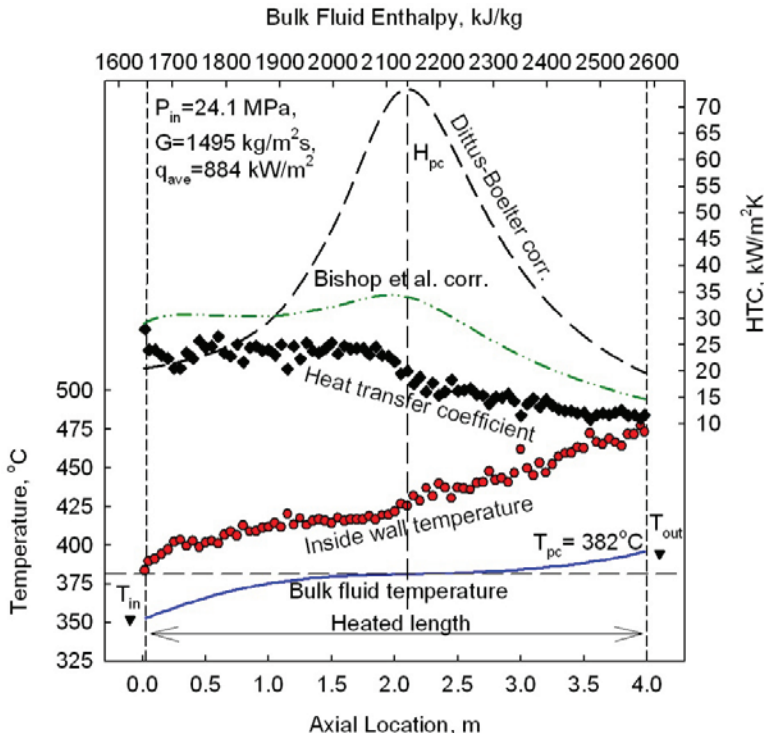
A comparison of the HTC experimental data (some unreliable points were not considered, for details, see Figure 8.2a, points inside shaded areas) with those calculated according to the heat-transfer correlations by Bishop et al. (Eq. (6.4)) and Dittus-Boelter (Eq. (6.5)) shows that, in general, the Bishop et al. correlation has a good agreement with the experimental HTCs outside the pseudocritical region (see Figures 8.1 – 8.4). However, this correlation over predicts the experimental HTCs within the pseudocritical region. Figure 8.5 shows a comparison of all experimental HTC values with those calculated.

The Dittus-Boelter correlation can also predict the experimental HTCs outside the pseudocritical region, but deviates significantly from the experimental data within the pseudocritical region (see Figures 8.1 – 8.4).

It should be noted that usually both these correlations cannot be used for prediction of HTCs within the deteriorated heat-transfer regime. All these observations are similar to those reported and reviewed in the literature by Pioro and Duffey (2007).



(a)



(b)

**Figure 8.1 (a-b). Temperature and Heat Transfer Coefficient Variations along a 4-m Circular Tube at Various Heat Fluxes: Nominal Operating Conditions –  $P_{in} = 24.0 \text{ MPa}$  and  $G = 1500 \text{ kg/m}^2\text{s}$  (Mokry et al., 2010).**

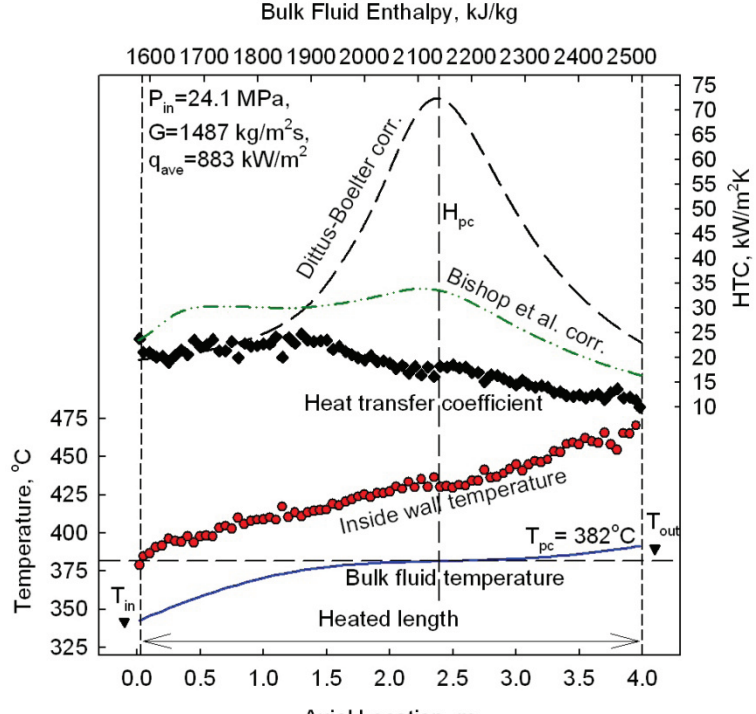
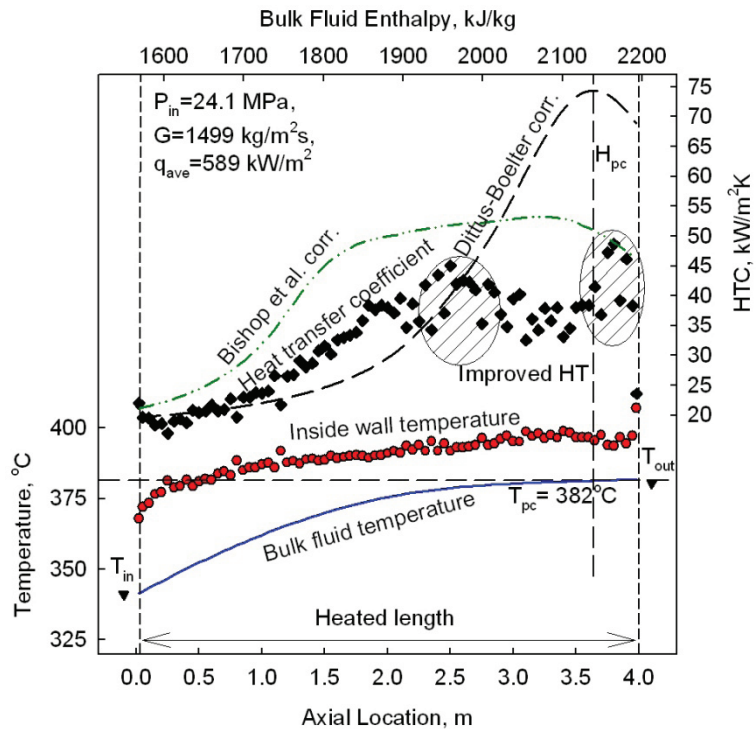
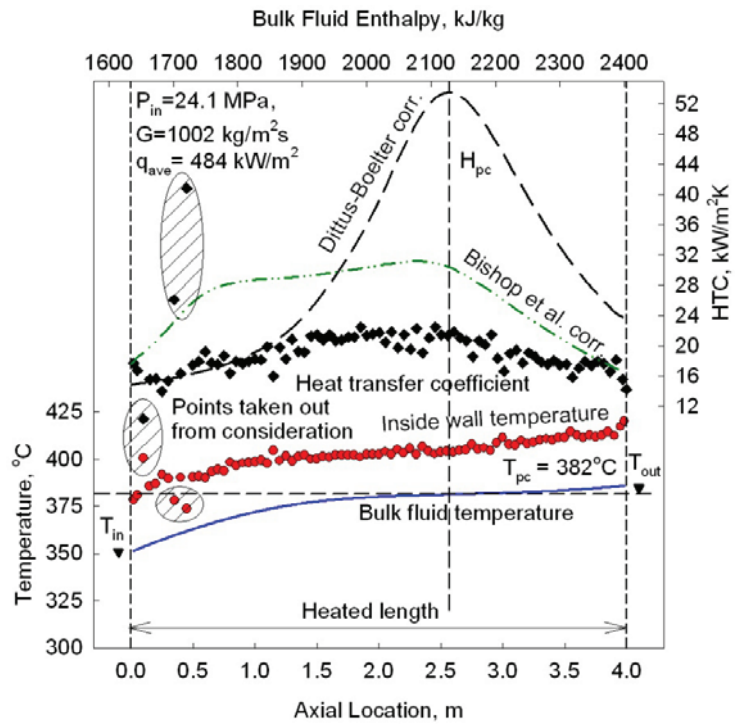
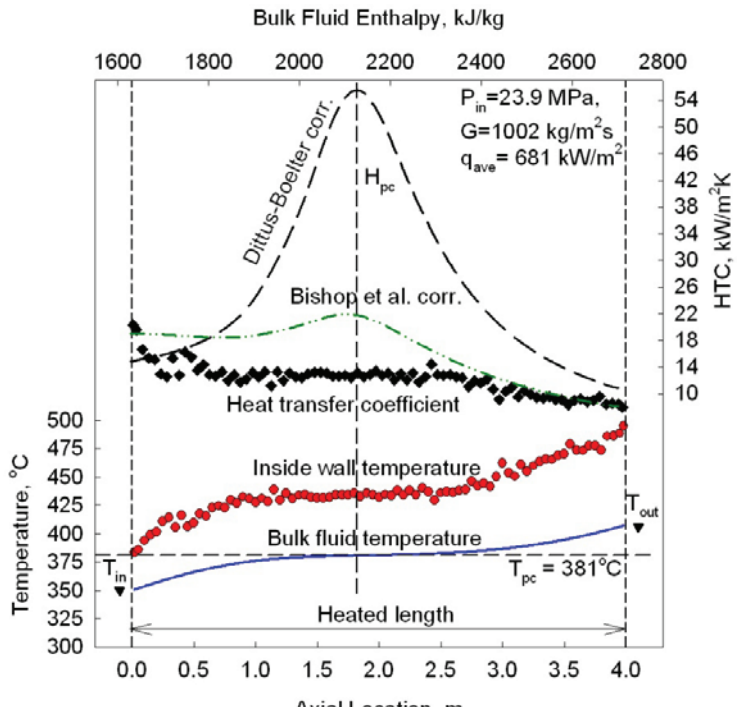


**Figure 8.1 (c-d). Temperature and Heat Transfer Coefficient Variations along a 4-m Circular Tube at Various Heat Fluxes: Nominal Operating Conditions –  $P_{in} = 24.0 \text{ MPa}$  and  $G = 1500 \text{ kg/m}^2\text{s}$  (Mokry et al., 2010).**

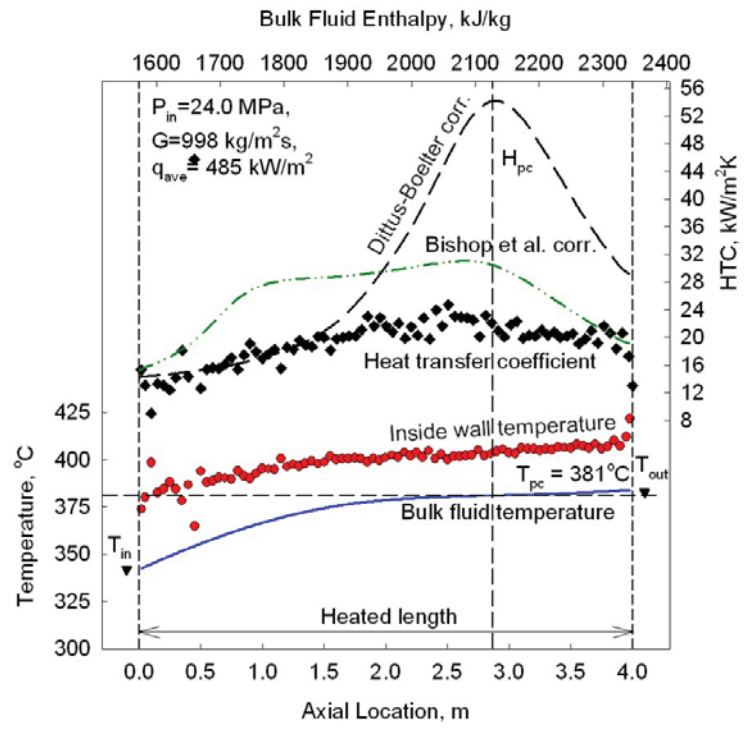


(a)

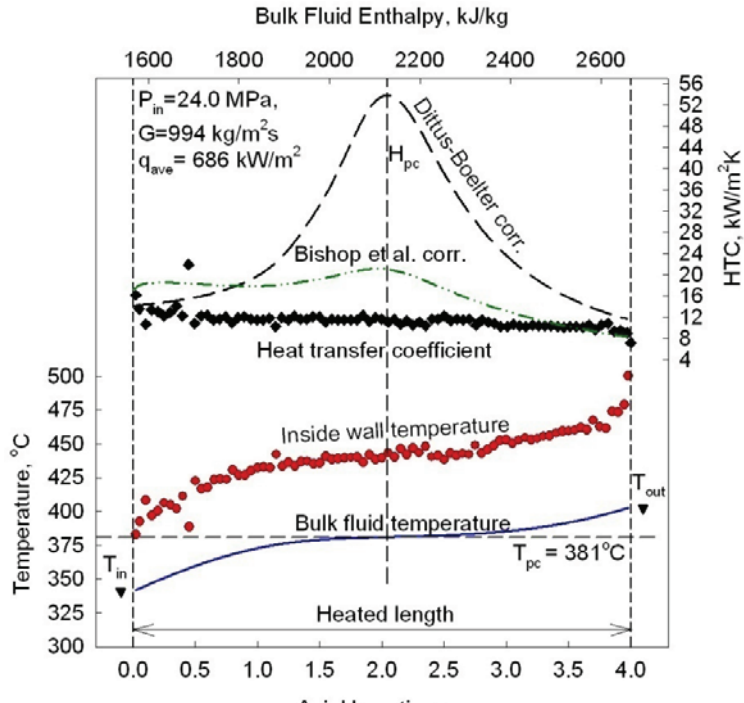


(b)

**Figure 8.2 (a-b).** Temperature and Heat Transfer Coefficient Variations along a 4-m Circular Tube at Various Heat Fluxes: Nominal Operating Conditions –  $P_{in} = 24.0 \text{ MPa}$ ,  $G = 1000 \text{ kg/m}^2\text{s}$  (Mokry et al., 2010).

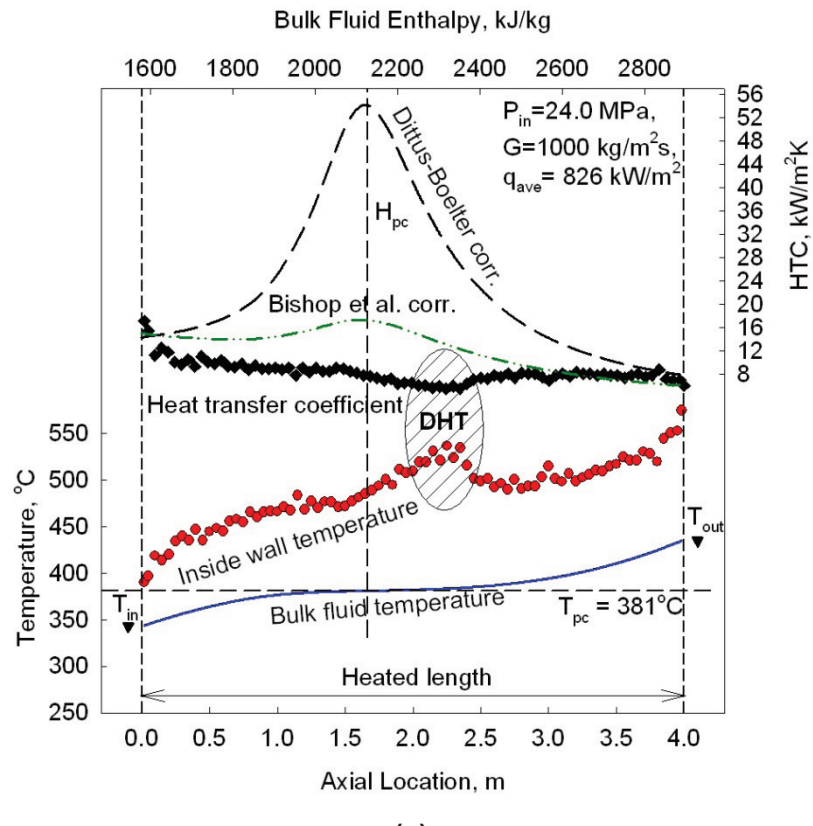


(c)



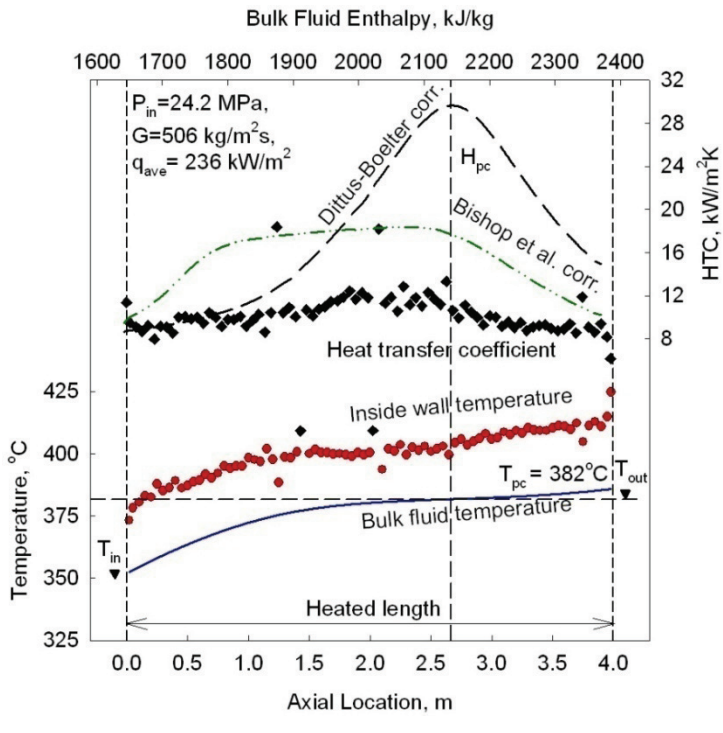
(d)

**Figure 8.2 (c-d). Temperature and Heat Transfer Coefficient Variations along a 4-m Circular Tube at Various Heat Fluxes: Nominal Operating Conditions –  $P_{in} = 24.0 \text{ MPa}$ ,  $G = 1000 \text{ kg/m}^2\text{s}$  (Mokry et al., 2010).**

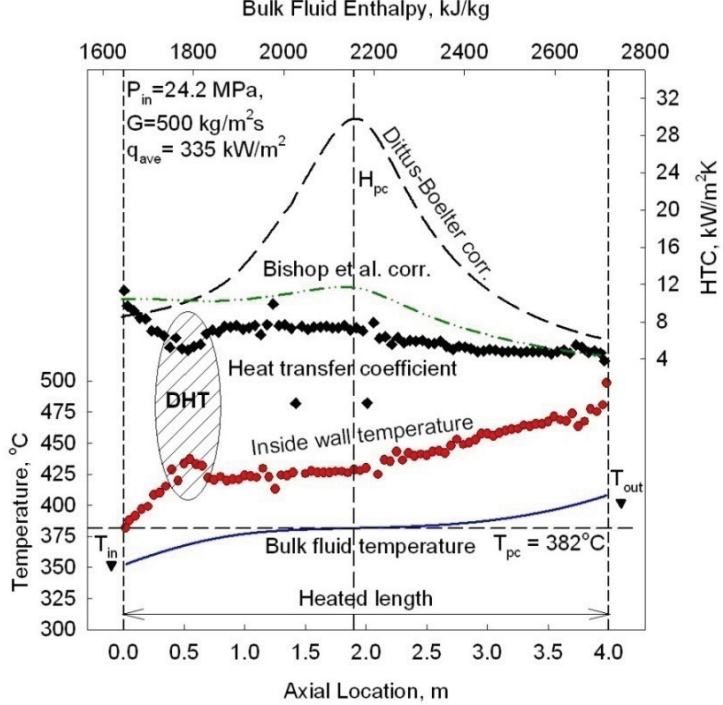


(e)

**Figure 8.2 (e). Temperature and Heat Transfer Coefficient Variations along a 4-m Circular Tube at Various Heat Fluxes: Nominal Operating Conditions –  $P_{in} = 24.0 \text{ MPa}$ ,  $G = 1000 \text{ kg/m}^2\text{s}$  (Mokry et al., 2010).**

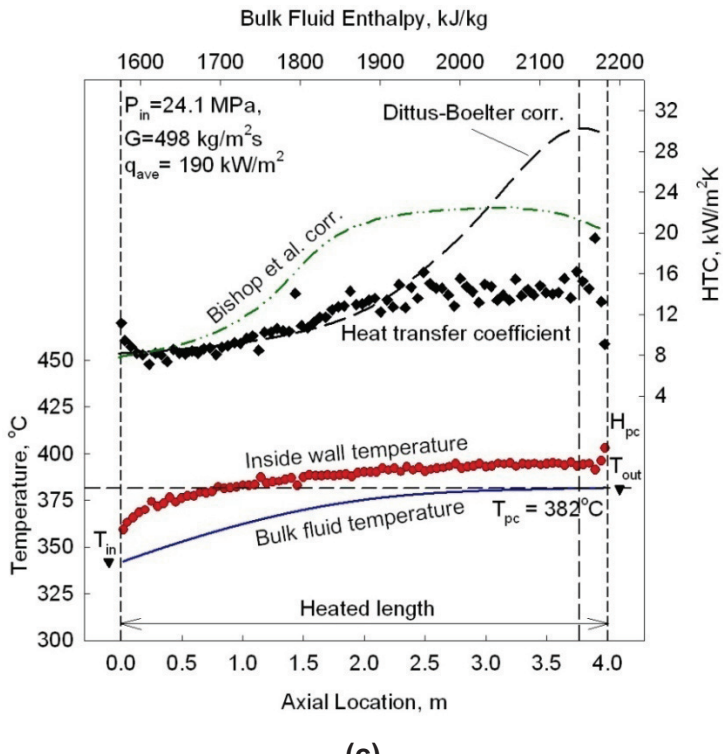


(a)

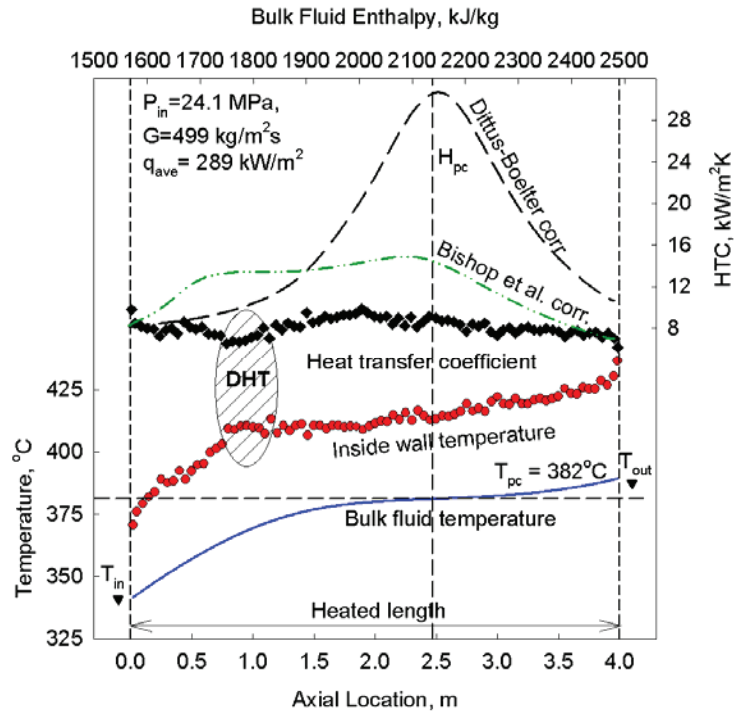


(b)

**Figure 8.3 (a-b). Temperature and Heat Transfer Coefficient Variations along a 4-m Circular Tube at Various Heat Fluxes: Nominal Operating Conditions –  $P_{in} = 24.0 \text{ MPa}$ ,  $G = 500 \text{ kg/m}^2\text{s}$  (Mokry et al., 2010).**

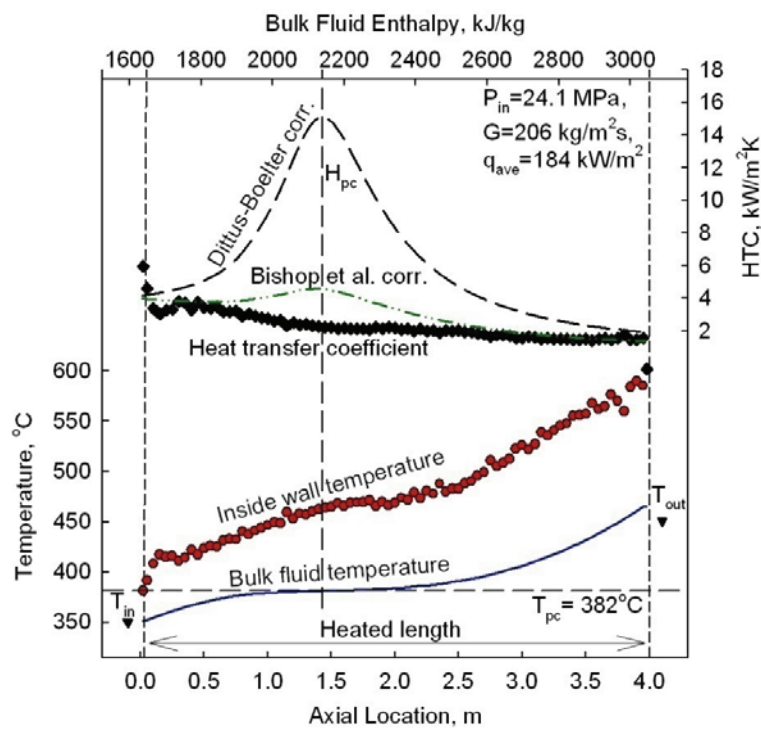


(c)

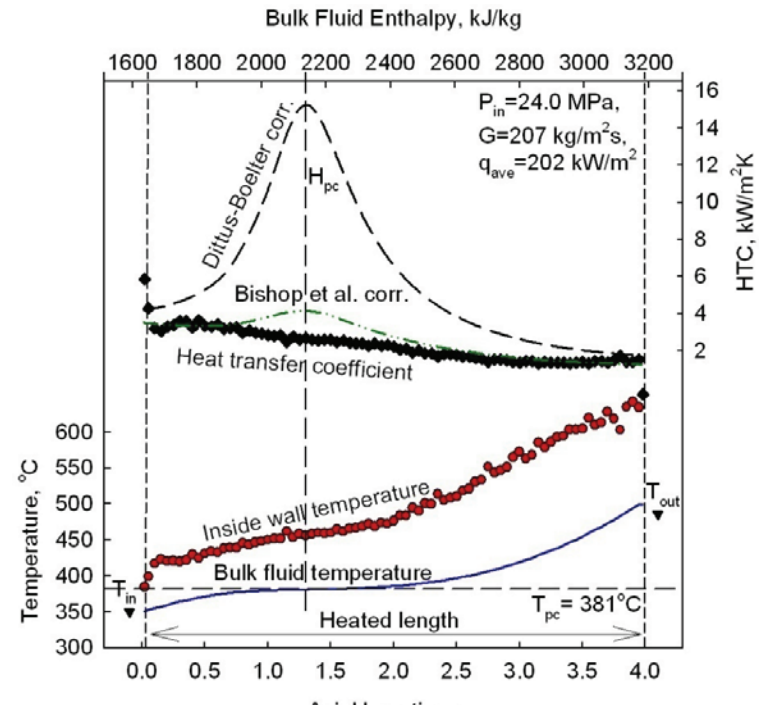


(d)

**Figure 8.3 (c-d).** Temperature and Heat Transfer Coefficient Variations along a 4-m Circular Tube at Various Heat Fluxes: Nominal Operating Conditions –  $P_{in} = 24.0 \text{ MPa}$ ,  $G = 500 \text{ kg/m}^2\text{s}$  (Mokry et al., 2010).



(a)



(b)

**Figure 8.4 (a-b). Temperature and Heat Transfer Coefficient Variations along a 4-m Circular Tube at Various Heat Fluxes: Nominal Operating Conditions –  $P_{in} = 24.0 \text{ MPa}$ ,  $G = 200 \text{ kg/m}^2\text{s}$  (Mokry et al., 2010).**

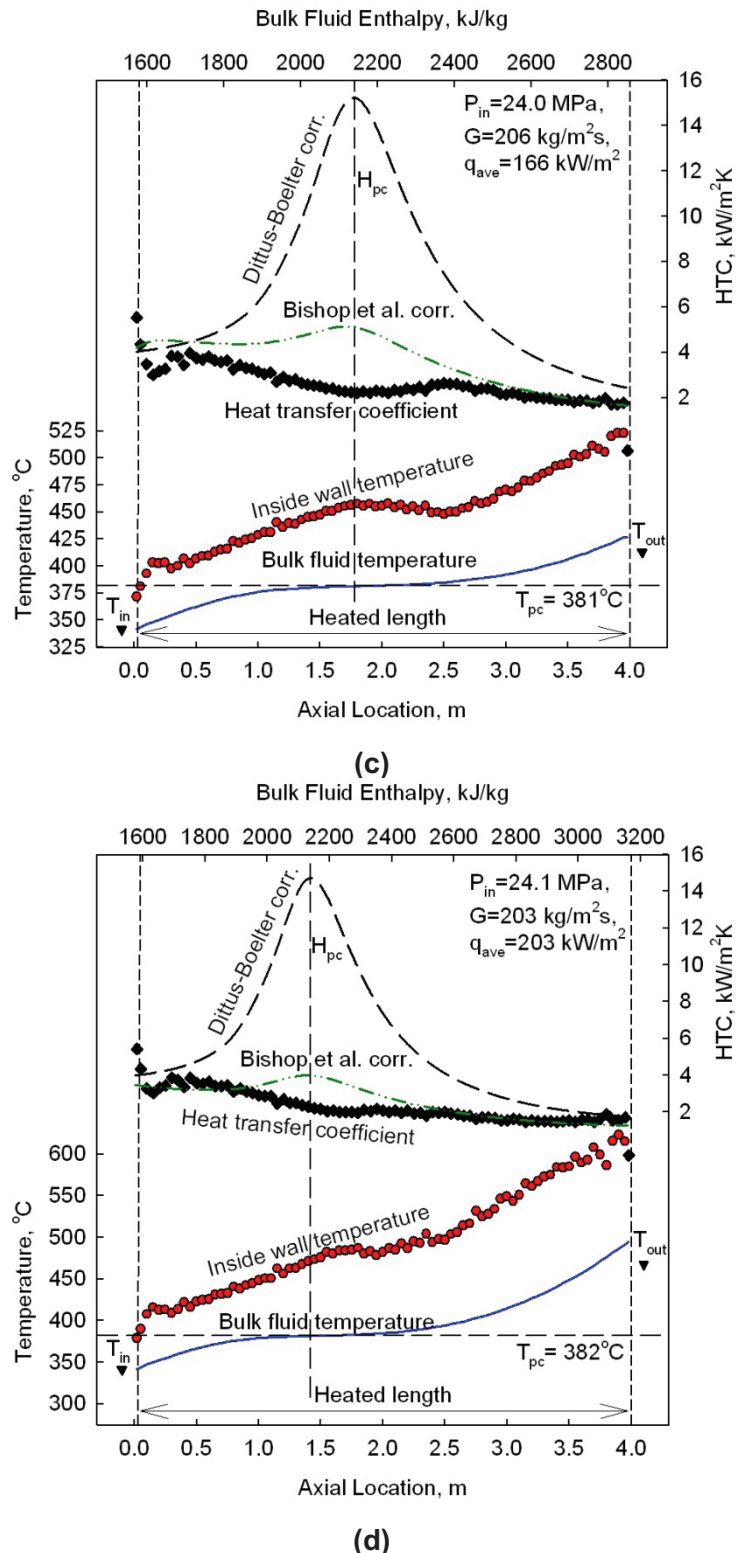


**Figure 8.4 (c-d). Temperature and Heat Transfer Coefficient Variations along a 4-m Circular Tube at Various Heat Fluxes: Nominal Operating Conditions –  $P_{in} = 24.0 \text{ MPa}$ ,  $G = 200 \text{ kg/m}^2\text{s}$  (Mokry et al., 2010).**

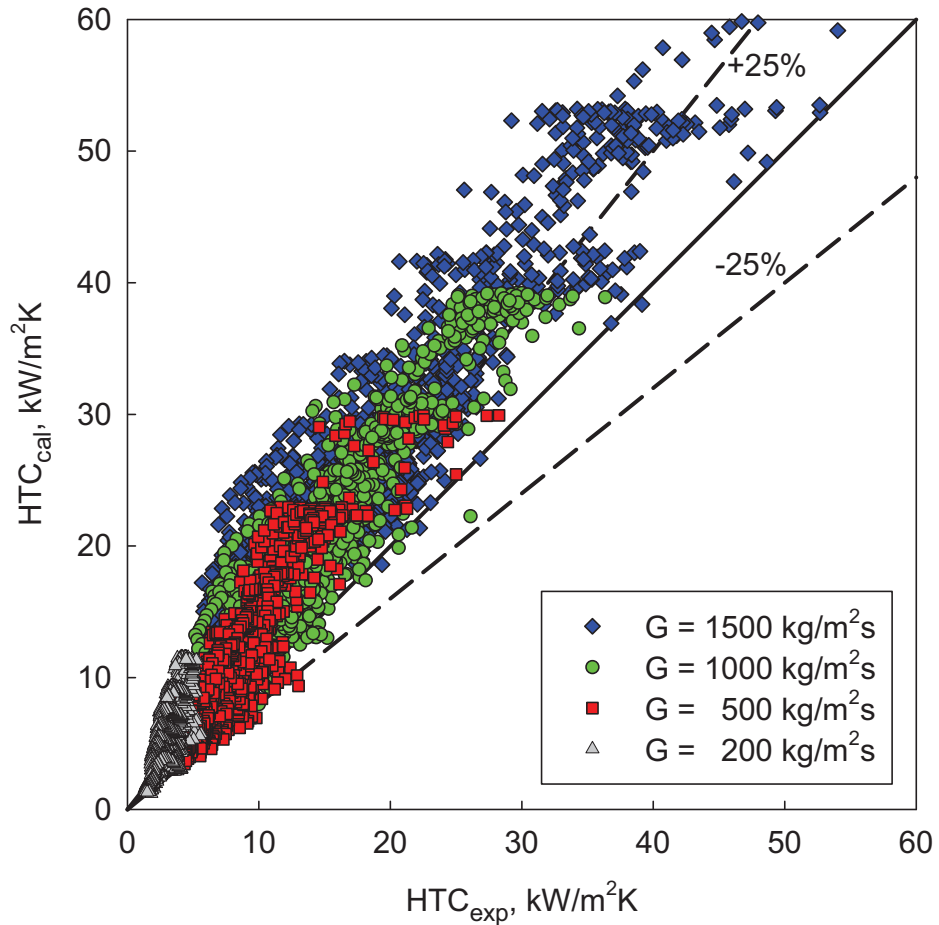


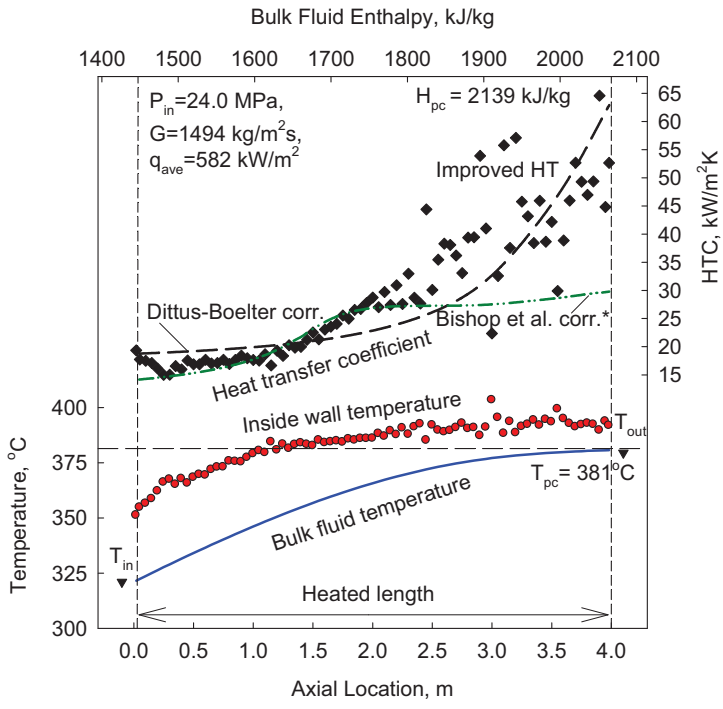
**Figure 8.5. Comparison of Experimental Heat Transfer Coefficient Values with Those Calculated Through Bishop et al. Correlation (1964) (Mokry et al., 2010).**

Later, Kirillov (2005) proposed a new constant to be used in the Bishop et al. Correlation (Eq. (6.4)):

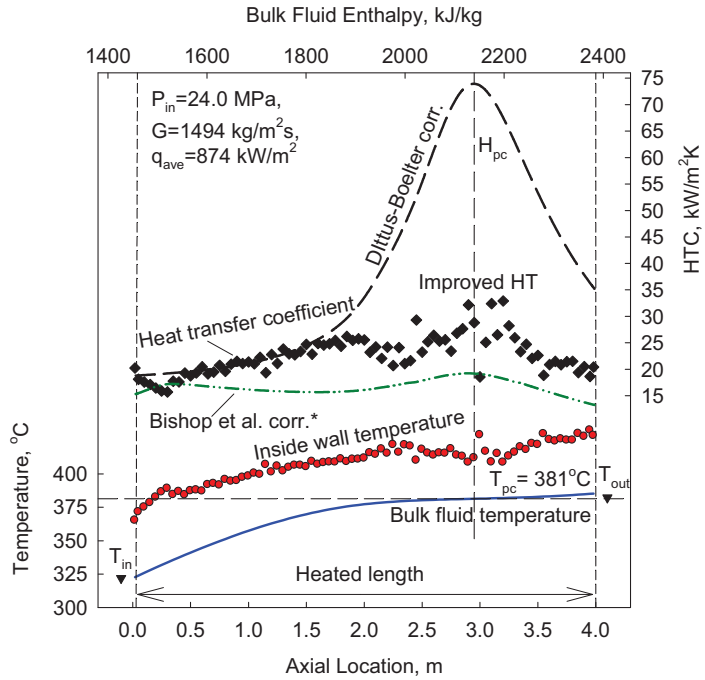
$$Nu_x = 0.0052 Re_x^{0.9} \overline{Pr}_x^{0.66} \left( \frac{\rho_w}{\rho_b} \right)_x^{0.43} \quad (8.1)$$

A comparison of the HTC experimental data with those calculated according to this modified Bishop et al. correlation\* (Eq. (8.1)) and the Dittus-Boelter correlation (Eq. (6.5)) shows that, in general, the Bishop et al. correlation\* has a good agreement with the experimental HTCs outside the pseudocritical region (see Figures 8.1 – 8.4). However, this correlation was also found to slightly

under predict the experimental HTCs within the pseudocritical region. Therefore, the modified Bishop et al. correlation\* (i.e. with Kirillov's coefficient) can be used for preliminary calculations of HTCs at supercritical pressures within the range of operating conditions of supercritical water nuclear reactors. Results for this correlation are shown in Figures 8.6 – 8.9 (Pioro et al., 2008a). However this correlation is still insufficient for the design-development calculations that are necessary for SCWRs. Therefore it is necessary for a new correlation to be developed.

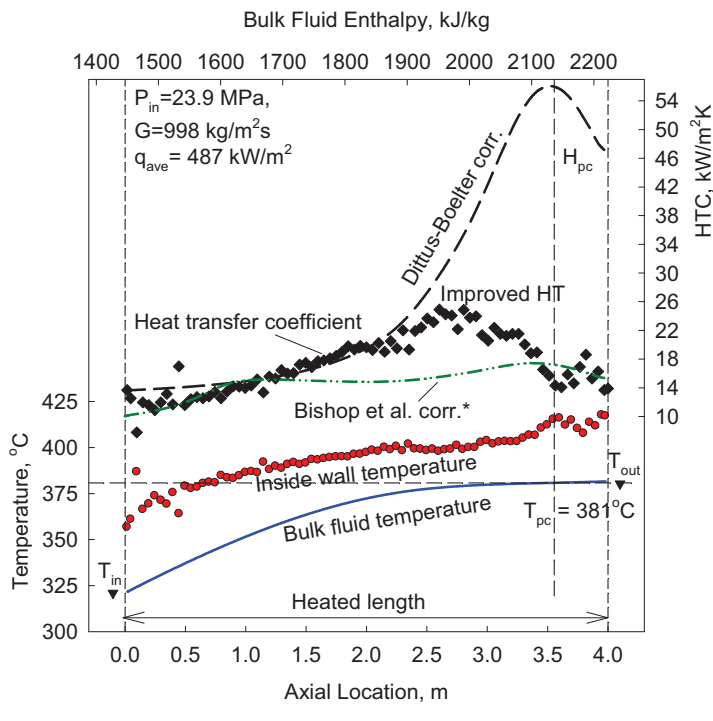


(a)

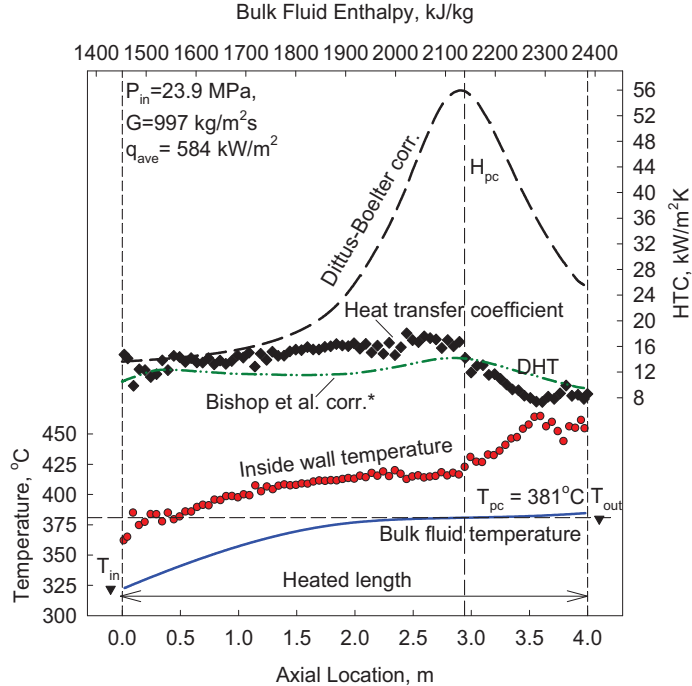


(b)

**Figure 8.6 (a-b). Temperature and Heat Transfer Coefficient Variations along a 4-m****Circular Tube at Various Heat Fluxes: Nominal Flow Conditions –** **$P_{in} = 24.0 \text{ MPa}$ ,  $G = 1500 \text{ kg/m}^2\text{s}$  (Pioro et al., 2008a).**

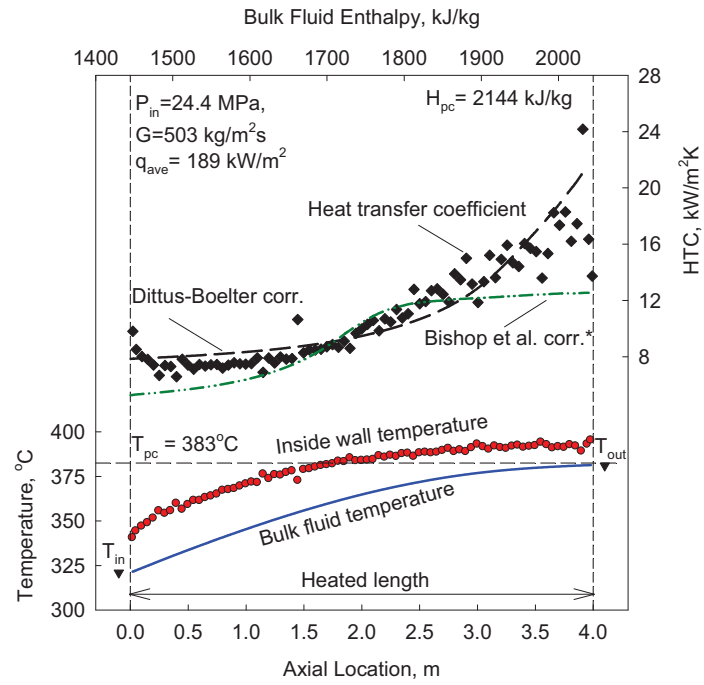


(a)

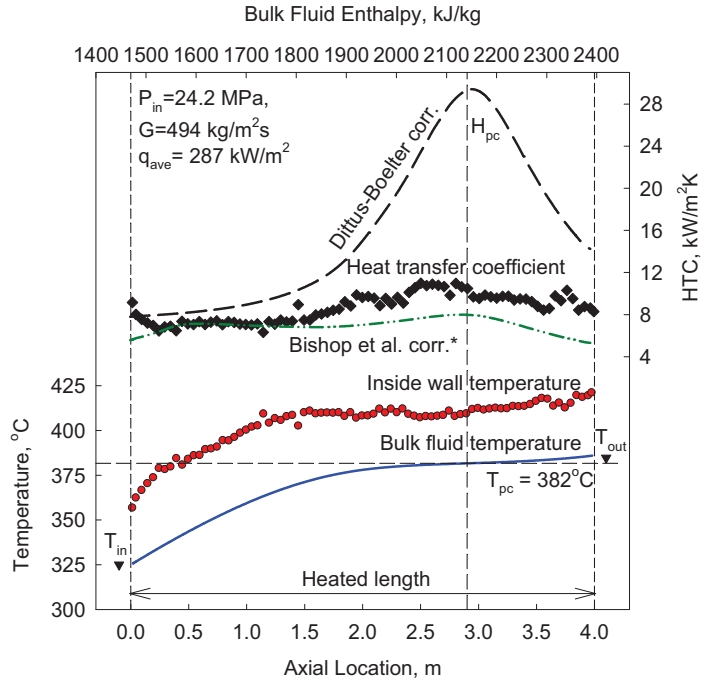


(b)

**Figure 8.7 (a-b). Temperature and Heat Transfer Coefficient Variations along a 4-m Circular Tube at Various Heat Fluxes: Nominal Operating Conditions –**  
 $P_{in} = 24.0 \text{ MPa}$ ,  $G = 1000 \text{ kg/m}^2\text{s}$  (Pioro et al., 2008a).

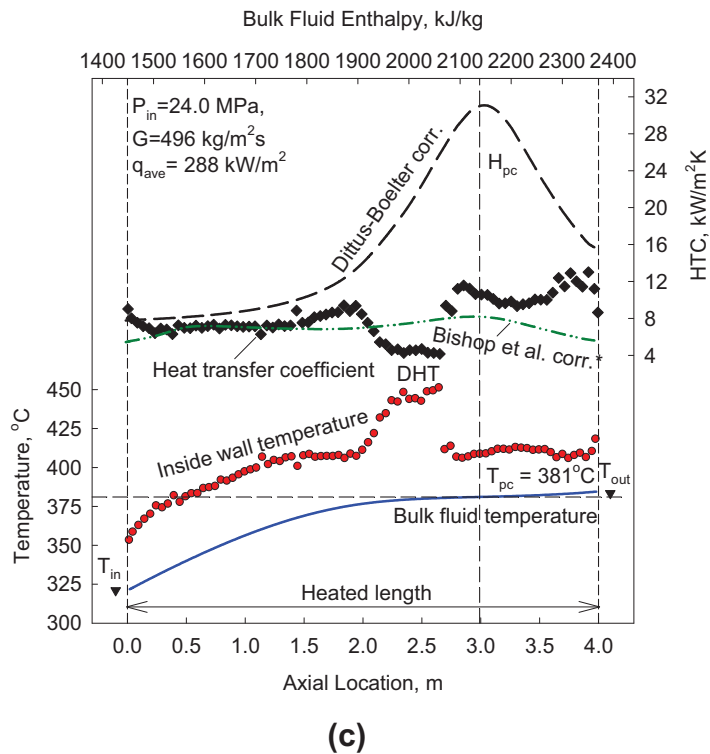


(a)

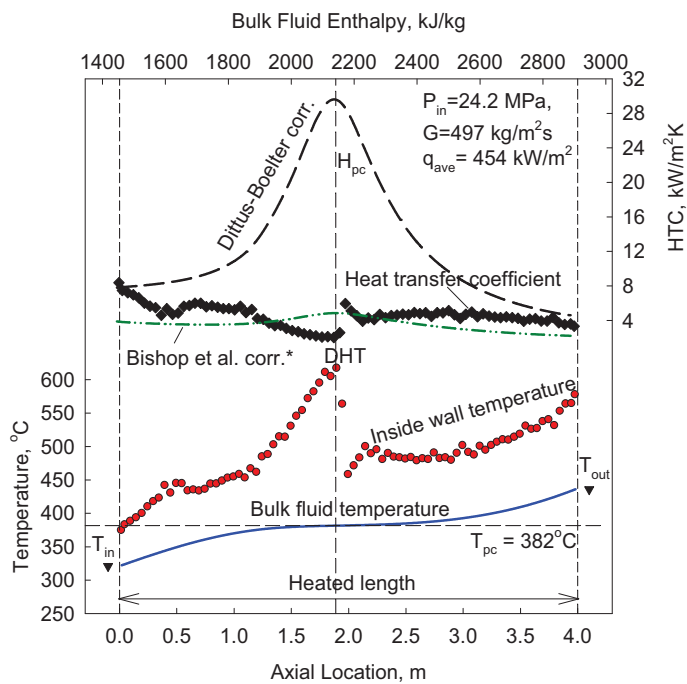


(b)

**Figure 8.8 (a-b). Temperature and Heat Transfer Coefficient Variations along a 4-m Circular Tube at Various Heat Fluxes: Nominal Operating Conditions –  $P_{in}=24.0 \text{ MPa}$ ,  $G=500 \text{ kg/m}^2\text{s}$  (Pioro et al., 2008a).**

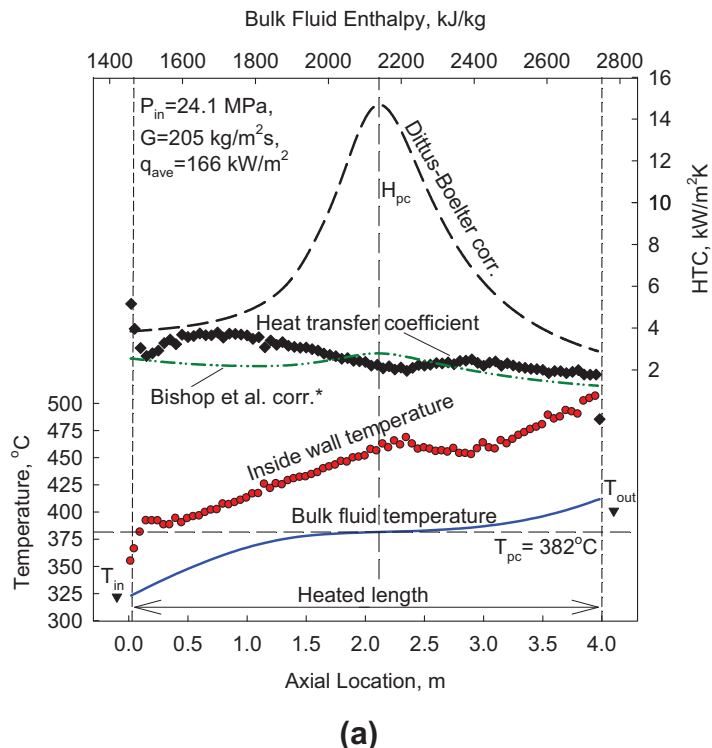


(c)

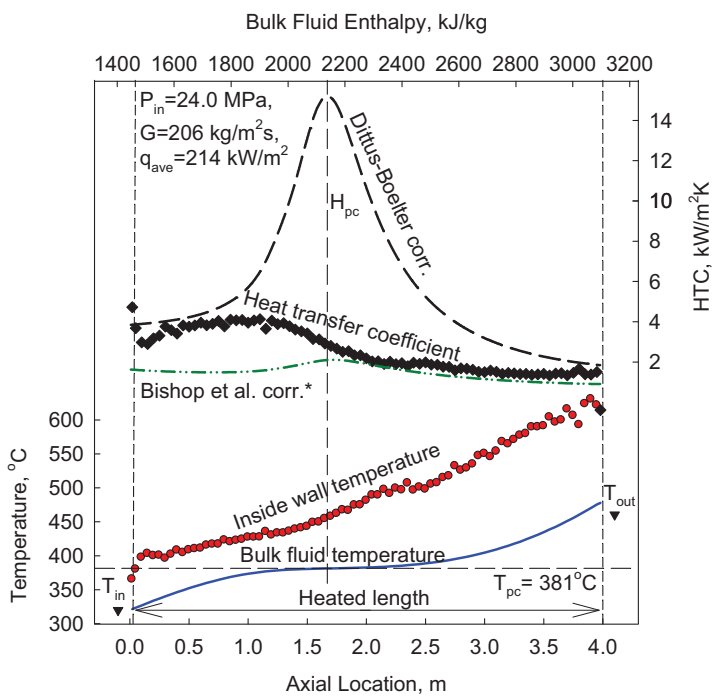


(d)

**Figure 8.8 (c-d). Temperature and Heat Transfer Coefficient Variations along a 4-m Circular Tube at Various Heat Fluxes: Nominal Operating Conditions –**  
 $P_{in} = 24.0 \text{ MPa}, G = 500 \text{ kg/m}^2\text{s}$  (Pioro et al., 2008a).



(a)



(b)

**Figure 8.9 (a-b). Temperature and Heat Transfer Coefficient Variations along a 4-m Circular Tube at Various Heat Fluxes: Nominal Operating Conditions –  $P_{in} = 24.0 \text{ MPa}$ ,  $G = 200 \text{ kg/m}^2\text{s}$  (Pioro et al., 2008a).**

## CHAPTER 9

### DEVELOPING THE CORRELATION

#### 9.1 Dimensional Analysis

It is well established that the general form of a correlation takes the following form:

$$y = C_o \cdot t_1^{C_1} t_2^{C_2} \dots t_n^{C_n}, \quad (9.1)$$

where  $t$  represents the various parameters that affect heat transfer and  $C$  represents the various coefficients and exponents.

In order to obtain a general empirical form of an equation governing heat transfer coefficients, a dimensional analysis was conducted. It is well known that HTC is not an independent variable, and that HTC values are affected by fluid velocity, inside diameter and thermophysical properties variations. A review of trends in correlating heat transfer data at supercritical pressures determined that there are nine parameters affecting heat transfer (Pioro and Duffey, 2007). Table 9.1 lists the parameters identified as essential for the analysis of heat-transfer processes for forced convection at supercritical conditions.

**Table 9.1. Description of the Various Parameters of Heat Transfer (Mokry et al., 2009b).**

Variable	Description	SI units	Dimensions
HTC	Heat Transfer coefficient	W/(m <sup>2</sup> K)	MT <sup>-3</sup> K <sup>-1</sup>
D	Diameter of the tube	m	L
$\rho_w$	Density of water	kg/m <sup>3</sup>	ML <sup>-3</sup>
$\rho_b$	Density of bulk-fluid	kg/m <sup>3</sup>	ML <sup>-3</sup>
$\mu_w$	Dynamic viscosity of water	Pa·s	ML <sup>-1</sup> T <sup>-1</sup>
$\mu_b$	Dynamic viscosity of bulk-fluid	Pa·s	ML <sup>-1</sup> T <sup>-1</sup>
$k_w$	Thermal conductivity of water	W/(m·K)	MLT <sup>-3</sup> K <sup>-1</sup>
$k_b$	Thermal conductivity of bulk-fluid	W/(m·K)	MLT <sup>-3</sup> K <sup>-1</sup>
$c_p$	Specific heat	J/(kg·K)	L <sup>2</sup> T <sup>-2</sup> K <sup>-1</sup>
V	Characteristic velocity	m/s	LT <sup>-1</sup>

The Buckingham  $\Pi$ -Theorem (Munson et al., 2005), using dimensionless  $\Pi$  terms, was chosen for this analysis. This theorem is based on dimensional homogeneity, in which dimensionless  $\Pi$  terms can be formed from the correlation variables. Thus, the following expression was produced for HTCs as a function of the identified heat-transfer parameters:

$$\text{HTC} = f(D, \rho_w, \rho_b, \mu_w, \mu_b, k_w, k_b, c_p, V) \quad (9.2)$$

Each of the identified parameters was broken down into the four primary dimensions of mass (M), length (L), time (T), and temperature (K) (see Table 9.1). Through consideration of these primary dimensions, six unique dimensionless  $\Pi$  terms were determined. These terms are listed in Table 9.2.

**Table 9.2.  $\Pi$  Terms of the Empirical Correlation (Mokry et al., 2009b).**

$\Pi$ Terms	Dimensionless Group	Name
$\Pi_1$	$\frac{\text{HTC} \cdot D}{k_b}$	Nusselt number
$\Pi_2$	$\frac{\rho \cdot V \cdot D}{\mu_b}$	Reynolds number
$\Pi_3$	$\frac{c_p \cdot \mu_b}{k_b}$	Prandtl number
$\Pi_4$	$\frac{\rho_w}{\rho_b}$	Density ratio
$\Pi_5$	$\frac{\mu_w}{\mu_b}$	Viscosity ratio
$\Pi_6$	$\frac{k_w}{k_b}$	Thermal conductivity ratio

The resulting relationship based on this analysis is as follows:

$$\Pi_1 = f(\Pi_2, \Pi_3, \Pi_4, \Pi_5, \Pi_6) \quad \text{or,} \quad (9.3)$$

$$\mathbf{Nu}_b = C \cdot \mathbf{Re}_b^{n_1} \mathbf{Pr}_b^{n_2} \left( \frac{\rho_w}{\rho_b} \right)^{n_3} \left( \frac{\mu_w}{\mu_b} \right)^{n_4} \left( \frac{k_w}{k_b} \right)^{n_5} \quad (9.4)$$

Equation 9.4 provided a starting point for the development of a correlation, where HTC can be calculated from the following equation:

$$\text{HTC} = \frac{\mathbf{Nu} \cdot k_b}{D_{hy}}, \quad (9.5)$$

where  $D_{hy}$  and  $k_b$  denote hydraulic diameter and thermal conductivity of the bulk-fluid, respectively. The various exponents and coefficient for the resulting relationship needed to be determined for the final correlation.

A number of correlations at supercritical pressures use an averaged specific heat ( $\bar{c}_p$ ) and Prandtl number ( $\bar{\mathbf{Pr}}$ ). As previously discussed, significant peaks in thermophysical properties occur within the pseudocritical range. Thus, averaging specific heat and Prandtl number over the ranges accounts for these thermophysical properties variations. Figure 9.1 shows the differences between the regular and averaged specific heats and regular and averaged Prandtl numbers.

The average Prandtl number ( $\bar{\mathbf{Pr}}$ ) is given by the follow equation:

$$\bar{\mathbf{Pr}} = \frac{\mu_b \cdot \bar{c}_p}{k_b}, \quad (9.6)$$

and averaged specific heat ( $\bar{c}_p$ ) is given by:

$$\bar{c}_p = \frac{H_w - H_b}{T_w - T_b}, \quad (9.7)$$

where  $H_w$  and  $H_b$  refer to the enthalpy at the channel wall and bulk-fluid enthalpy, respectively.

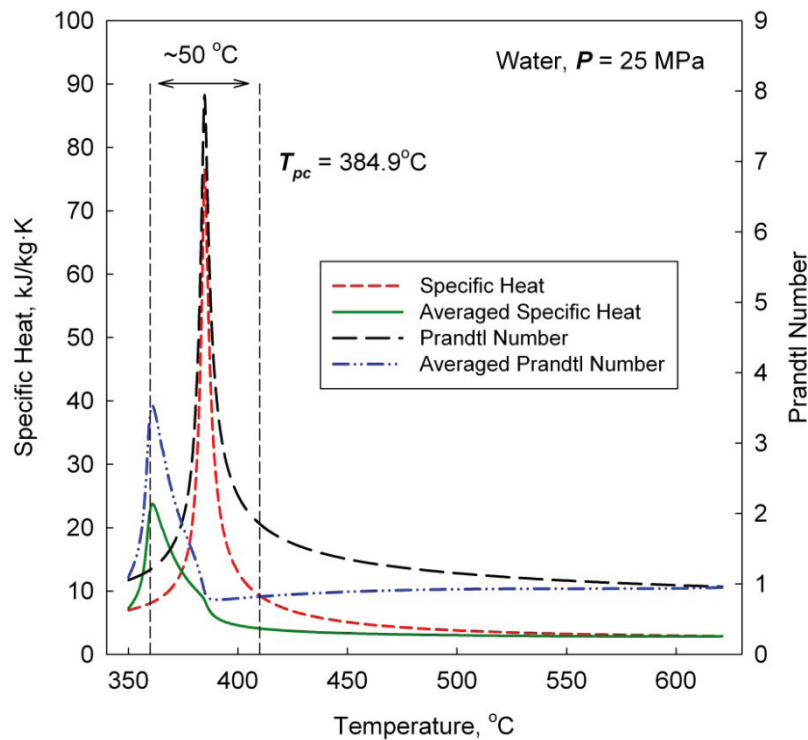


**Figure 9.1. Regular and Averaged Specific Heat and Prandtl Number Values.**

From Figure 9.1, it can be seen that the regular specific heat and Prandtl number both have peaks in the pseudocritical point. However, the averaged specific heat and the averaged Prandtl number have smaller peaks, occurring before the pseudocritical region. Thus, it was decided to replace the regular (thermophysical properties table based) specific heat and Prandtl number with these cross-sectional averaged values.

## 9.2 Manual Iterations

In order to determine the coefficients in the general correlation relationship, manual iterations were performed. The experimental dataset, with removed outliers and points in the DHT and IHT regimes, was compiled into an MS Excel spreadsheet. The required thermophysical properties data was retrieved using NIST (2002) software. Scatter plots were then created and analyzed using linear regression on a log-log scale. The resulting slope of this regression line provided the exponent for the associated scatter plot.

The first step of the manual iterations was performed for the first two  $\Pi$  terms.

### Manual Iteration Step 1:

$$\mathbf{Nu}_b \text{ vs. } \mathbf{Re}_b \quad (9.8)$$

Figure 9.2 shows the resulting scatter plot for this first step.

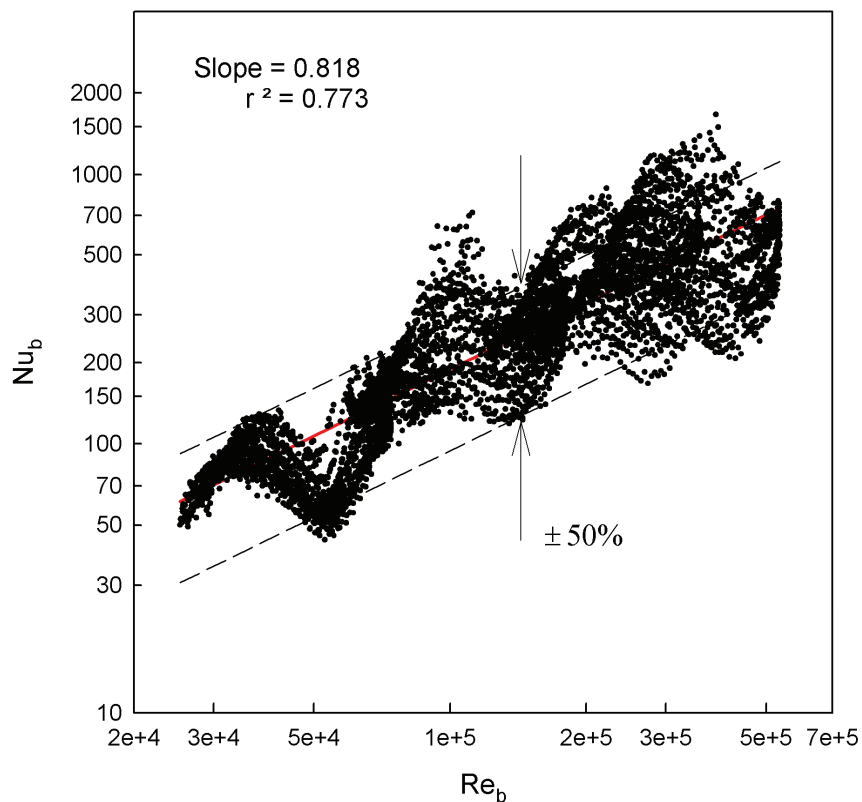


**Figure 9.2. Scatter Plot for  $\mathbf{Re}_b$  versus  $\mathbf{Nu}_b$ .**

Thus, the slope of the linear regression line (0.818) becomes the exponent for the  $\text{Re}_b$  term in the correlation. The statistical R-squared value was 0.773, which is a good indication that the data correlates at this point. Also, the majority of the data lies within a  $\pm 50\%$  interval. This value is expected to be drastically reduced as further steps and iterations are performed.

The next step was to determine the exponent for the average Prandtl number through the creation of a second scatter plot. At this point, the effect of  $\text{Re}_b$  can be accounted for in this second plot.

#### **Manual Iteration Step 2:**

$$\frac{\text{Nu}_b}{\text{Re}_b^{0.818}} \text{ vs. } \overline{\text{Pr}}_b \quad (9.9)$$

As with the first plot, the slope of the linear regression line provides the exponent for the averaged Prandtl number. Figure 9.3 shows the resulting scatter plot for this step and provides the slope and R-squared values.

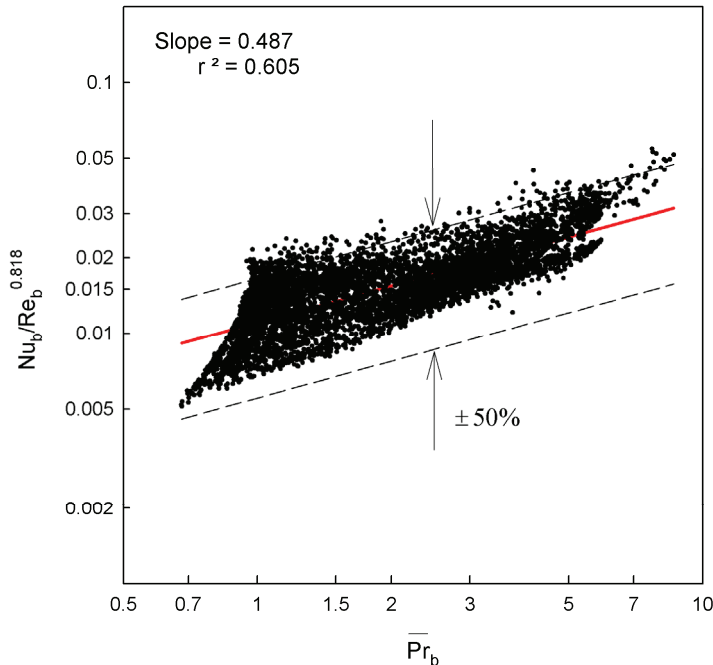


**Figure 9.3. Determination of the Exponent of the Average Prandtl Number.**

Thus, the exponent for the average Prandtl number was taken to be 0.487. The third step was to obtain the exponent for the ratio of densities of the coolant at the wall and the bulk fluid temperatures (Figure 9.4). The effects of the Reynolds number and the averaged Prandtl number from the first two steps were accounted for in this step.

### Manual Iteration Step 3:

$$\frac{\text{Nu}_b}{\text{Re}_b^{0.818} \overline{\text{Pr}}_b^{0.487}} \text{ vs. } \frac{\rho_w}{\rho_b} \quad (9.10)$$

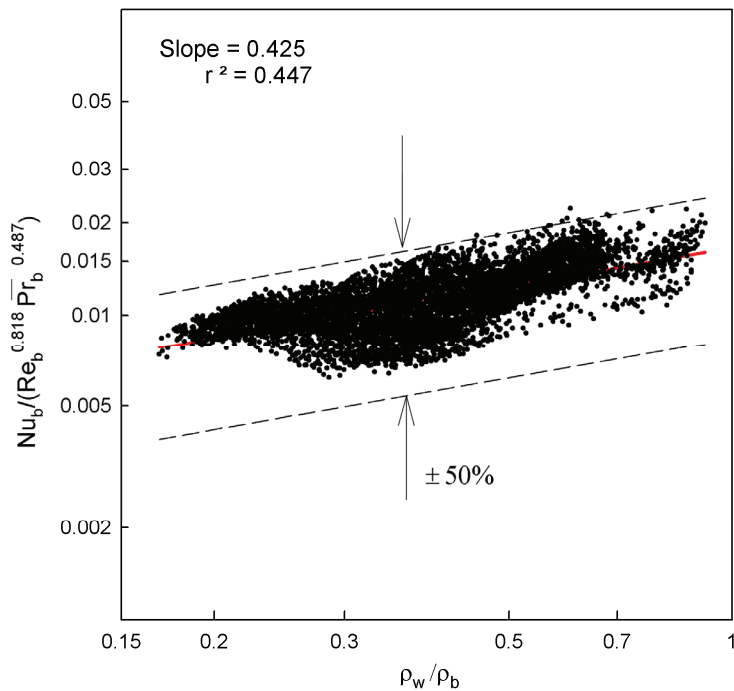


**Figure 9.4. Determination of the Exponent of the Ratio of Densities.**

In the fourth step, the exponent for the ratio of the viscosities of the coolant at wall and bulk-fluid temperatures was determined (Figure 9.5). Again, the effect of the parameters determined in the previous steps were accounted for.

#### Manual Iteration Step 4:

$$\frac{\mathbf{Nu}_b}{\mathbf{Re}_b^{0.818} \overline{\mathbf{Pr}}_b^{0.487} \left( \frac{\rho_w}{\rho_b} \right)^{0.425}} \text{ vs. } \frac{\mu_w}{\mu_b} \quad (9.11)$$

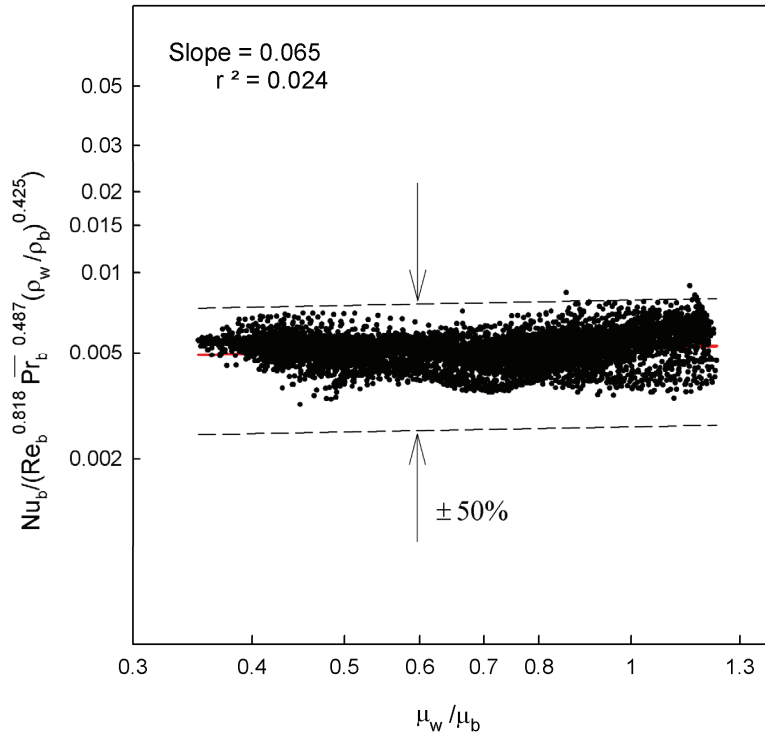


**Figure 9.5. Determination of the Exponent of the Ratio of Viscosities.**

From Figure 9.5, it can be seen that both the slope and R-squared values are small and close to zero. Therefore, the affect of the ratio of viscosities was not considered in further iterations. Similarly, the ratio of thermal conductivity at the wall and for the bulk-fluid was found to have an insignificant result, and thus was not considered in further iterations. At this point, the following correlation had been attained:

$$\mathbf{Nu}_b = \mathbf{Re}_b^{0.818} \overline{\mathbf{Pr}}_b^{0.487} \left( \frac{\rho_w}{\rho_b} \right)^{0.425} \quad (9.12)$$

### 9.3 Second Iterations

Once the approximate coefficient and exponents had been obtained, a MATLAB code was prepared and used to perform a number of iterations for the exponents such that they converged to steady values. At iteration 7, convergence had been achieved and subsequent iterations did not change the coefficient values. The iteration equations, new coefficients and plots are show in Figures 9.6 – 9.8.

#### Second iteration Step 1:

$$\frac{\text{Nu}_b}{\overline{\text{Pr}}_b^{0.487} \left( \frac{\rho_w}{\rho_b} \right)^{0.425}} \text{ vs. } \text{Re}_b \quad (9.13)$$

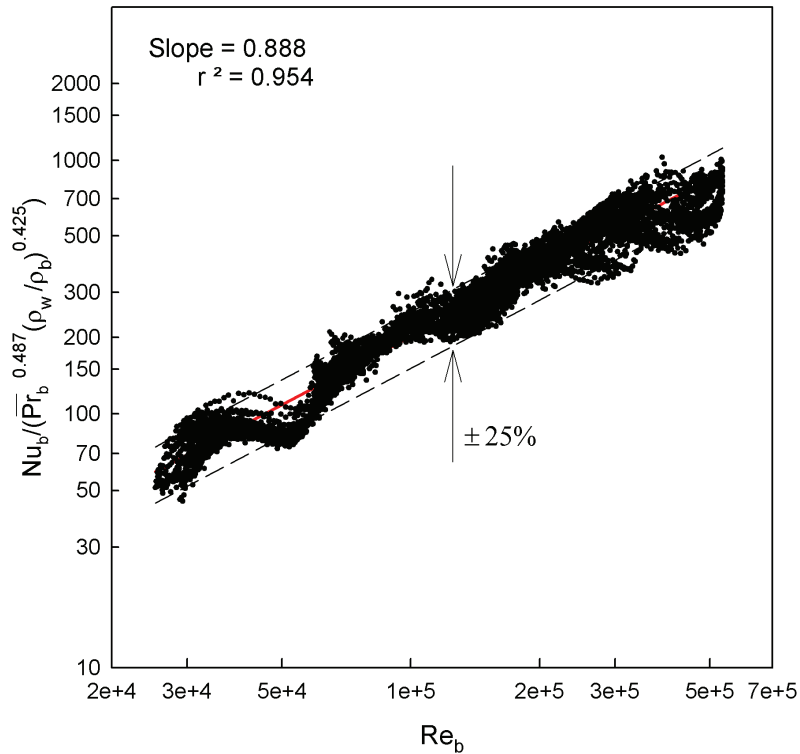


**Figure 9.6. Determination of Refined Reynolds Number Exponent.**

**Second iteration Step 2:**

$$\frac{\text{Nu}_b}{\text{Re}_b^{0.888} \left( \frac{\rho_w}{\rho_b} \right)^{0.425}} \text{ vs. } \overline{\text{Pr}}_b \quad (9.14)$$

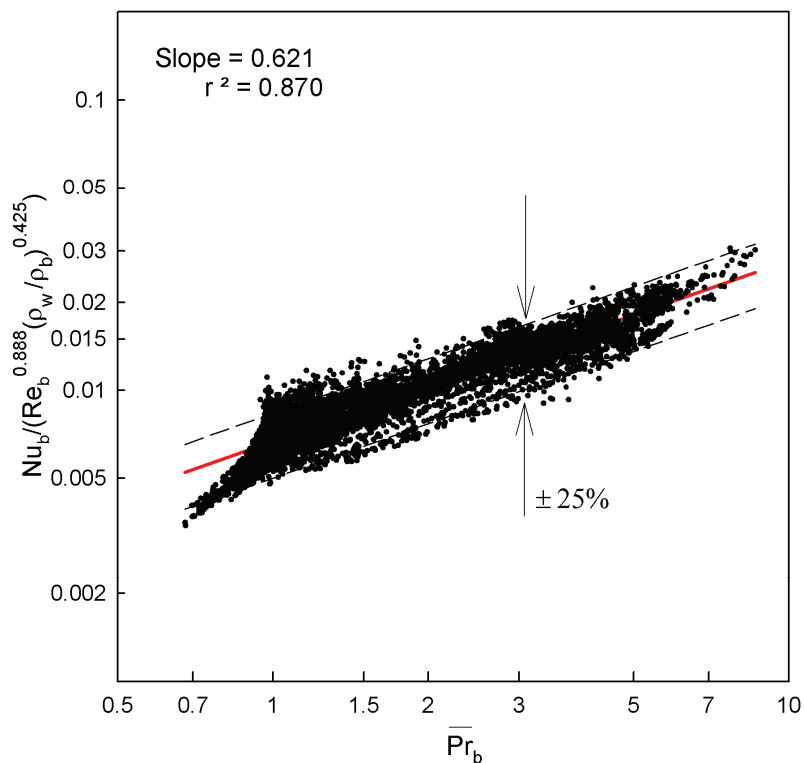


**Figure 9.7. Determination of Refined Averaged Prandtl Number Exponent.**

**Second iteration Step 3:**

$$\frac{\text{Nu}_b}{\text{Re}_b^{0.888} \overline{\text{Pr}}_b^{0.621}} \text{ vs. } \left( \frac{\rho_w}{\rho_b} \right) \quad (9.15)$$

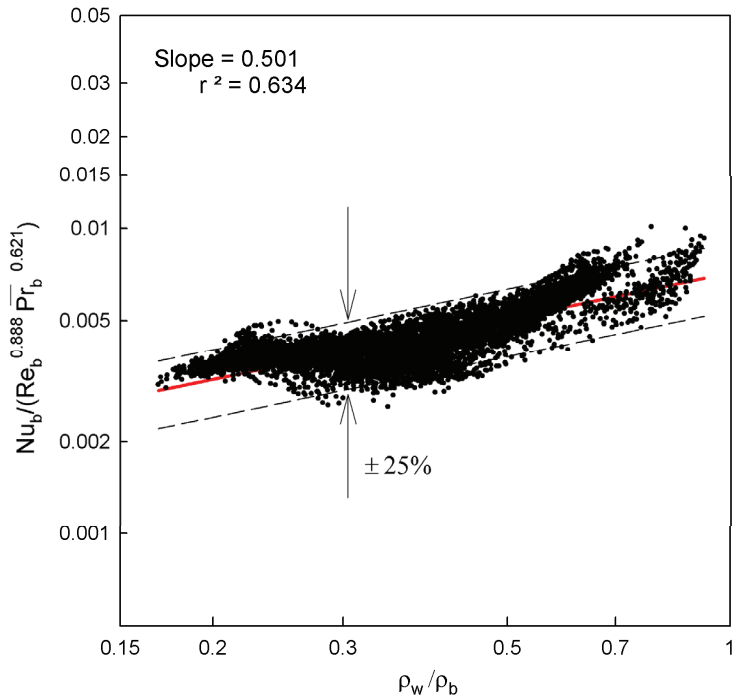


**Figure 9.8. Determination of Refined Densities Ratio Exponent.**

From Figure 9.8, it can be seen that the R-squared value has increased to 0.634 (from 0.447), thus showing an improvement in the data fit. Also, the majority of the data can be seen to fall within a  $\pm 25\%$  range. Iterations three through seven were conducted in the same manner, resulting in refinement of exponents and an improvement in R-squared values.

#### 9.4 Finalizing the Correlation

As a result of the experimental data analysis described, the following preliminary and final correlations for heat transfer to supercritical water were obtained.

Preliminary Correlation:

$$\text{Nu}_b = 0.0053 \text{ Re}_b^{0.914} \overline{\text{Pr}}_b^{0.654} \left( \frac{\rho_w}{\rho_b} \right)^{0.518} \quad (9.16)$$

Final Correlation:

$$\text{Nu}_b = 0.0061 \text{ Re}_b^{0.904} \overline{\text{Pr}}_b^{0.684} \left( \frac{\rho_w}{\rho_b} \right)^{0.564} \quad (9.17)$$

The test matrix shown in Table 9.3 provides the range of applicability for the new Mokry et al. correlation. This matrix is the result of comparison with Kirillov's (2005) experimental data, described in earlier chapters, in addition to a comparison with other datasets for supercritical water (see Table 9.4 and Appendix B).

**Table 9.3. Test Matrix for Mokry et al. Correlation.**

Pressure, MPa	Heat Flux, kW/m <sup>2</sup>	Mass Flux, kg/m <sup>2</sup> s	Diameter, mm
22.8 – 29.4	70 – 1250	200 – 1500	3 – 38

Even though the final exponents slightly deviate from the preliminary correlation, both correlations fit the data in nearly the same manner. Figure 9.9 provides scatter plots of the experimentally obtained HTC and wall temperature values versus the calculated HTC and wall temperature values for each of the previously mentioned correlations. The final correlation (Eq. (9.17), Mokry et al. correlation) has an uncertainty of about  $\pm 25\%$  for HTC values and about  $\pm 15\%$  for calculated wall temperature.

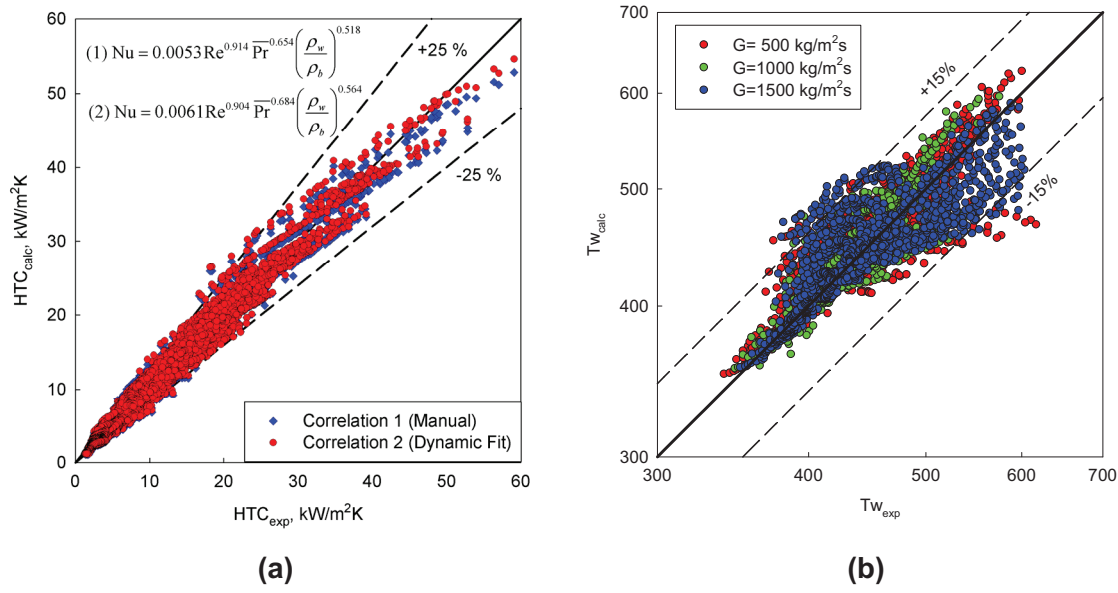


**Figure 9.9 (a-b). Comparison of Data Fit with Experimental Data: (a) for Heat Transfer Coefficient and (b) for  $T_w$  (Mokry et al., 2009b).**

## 9.5 Verifying the Correlation

In order to verify the correlation and the data fit, samples of experimental runs from the dataset, with the final correlation, are shown in Figures 9.10 through 9.13. The graphs shown are for a pressure of ~24 MPa and vary in mass flux from 200 – 1500 kg/m<sup>2</sup>s, and heat fluxes up to 1250 kW/m<sup>2</sup>.

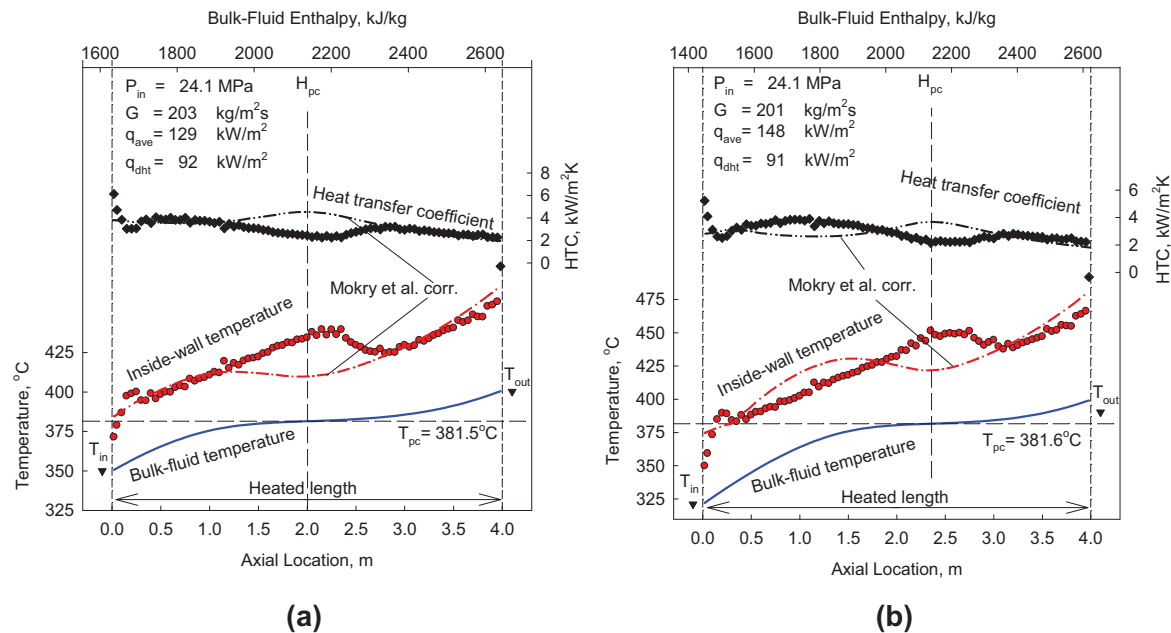


**Figure 9.10 (a-b). Temperature and Heat Transfer Coefficient Variations along a 4-m Circular Tube at Various Heat Fluxes (ID = 10 mm): Nominal Operating Conditions –  $P_{in} = 24.0 \text{ MPa}$ ,  $G = 200 \text{ kg/m}^2\text{s}$  (Mokry et al., 2009b).**

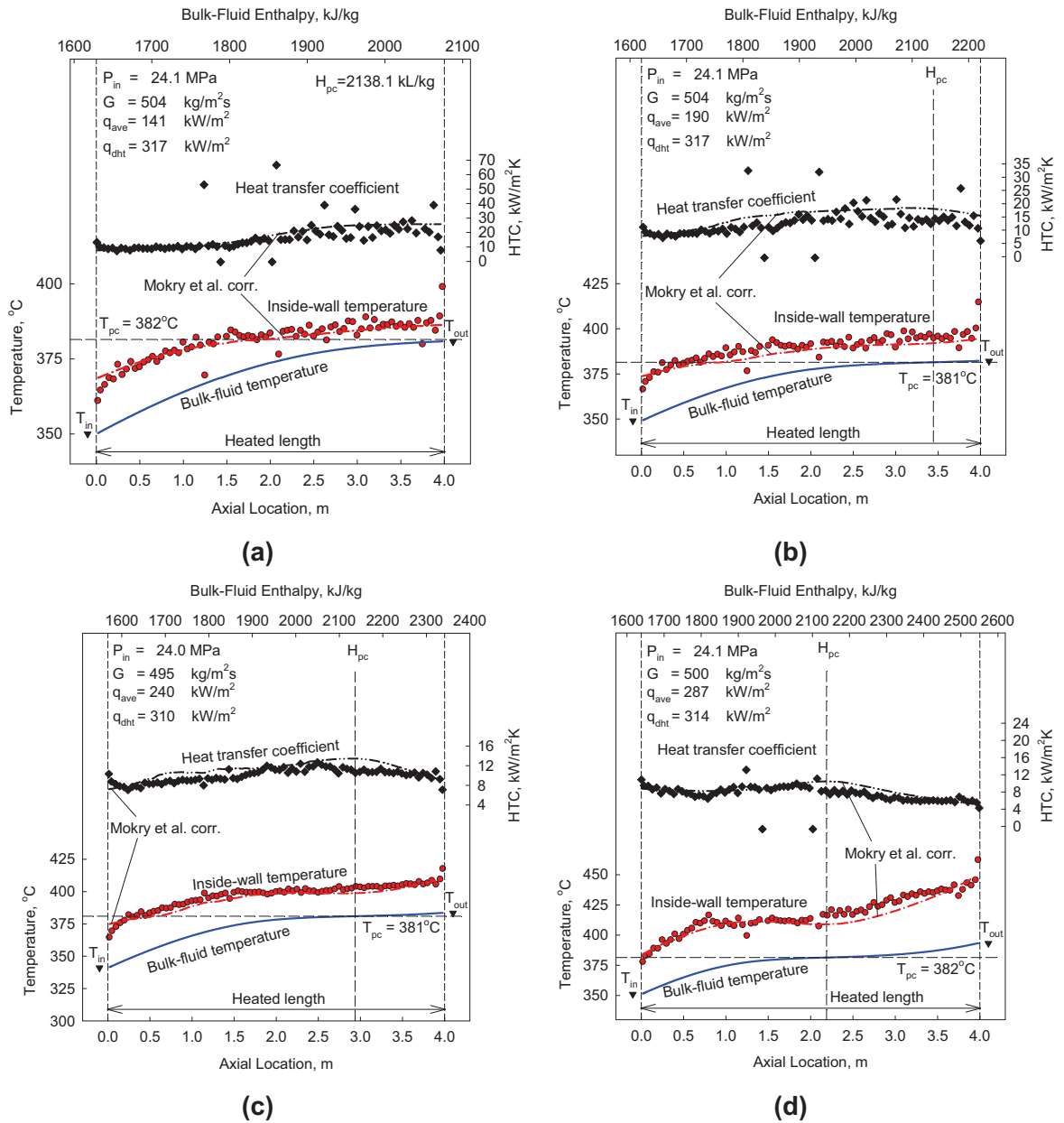
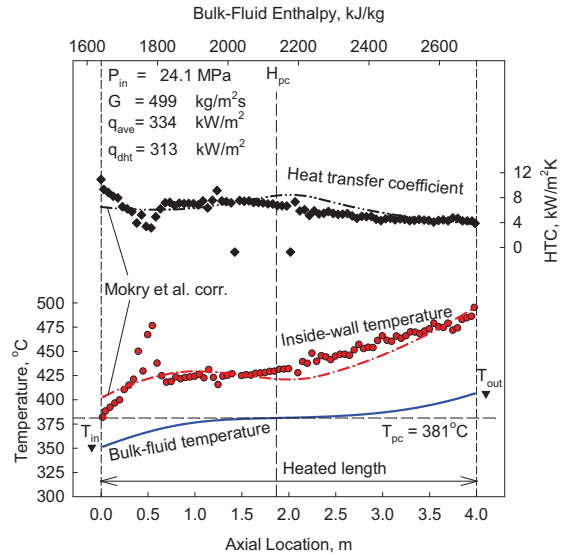


**Figure 9.11 (a-d). Temperature and Heat Transfer Coefficient Variations along a 4-m Circular Tube at Various Heat Fluxes (ID = 10 mm): Nominal Operating Conditions –  $P_{in} = 24.0 \text{ MPa}$ ,  $G = 500 \text{ kg/m}^2\text{s}$  (Mokry et al., 2009b).**



(e)

**Figure 9.11 (e). Temperature and Heat Transfer Coefficient Variations along a 4-m Circular Tube at Various Heat Fluxes (ID = 10 mm): Nominal Operating Conditions –  $P_{in} = 24.0 \text{ MPa}$ ,  $G = 500 \text{ kg/m}^2\text{s}$  (Mokry et al., 2009b).**

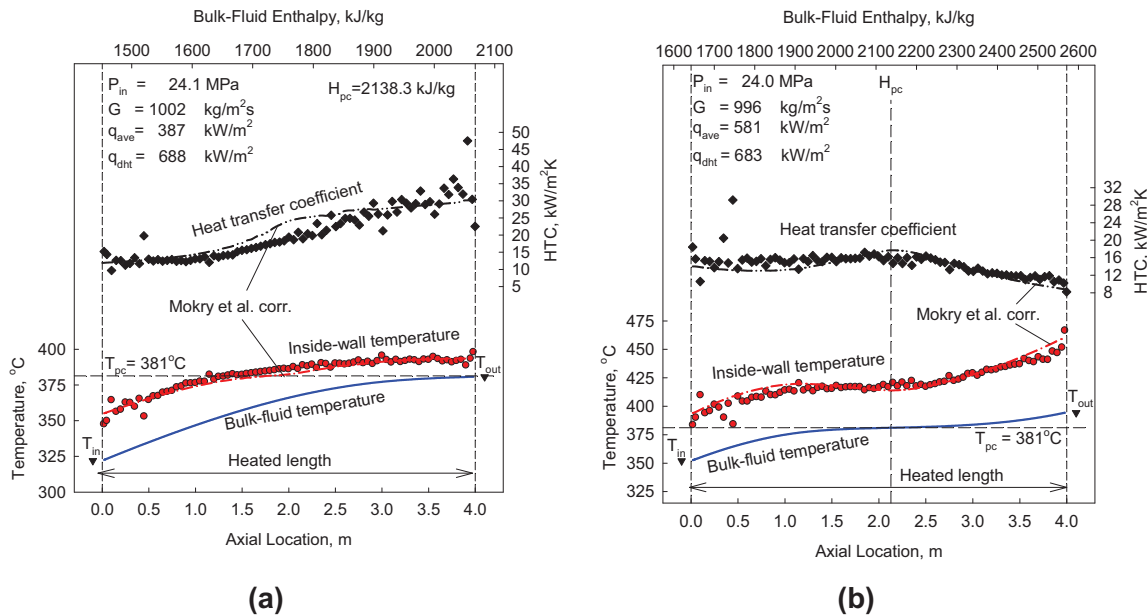


**Figure 9.12 (a-b). Temperature and Heat Transfer Coefficient Variations along a 4-m Circular Tube at Various Heat Fluxes (ID = 10 mm): Nominal Operating Conditions –  $P_{in} = 24.0 \text{ MPa}$ ,  $G = 1000 \text{ kg/m}^2\text{s}$  (Mokry et al., 2009b).**

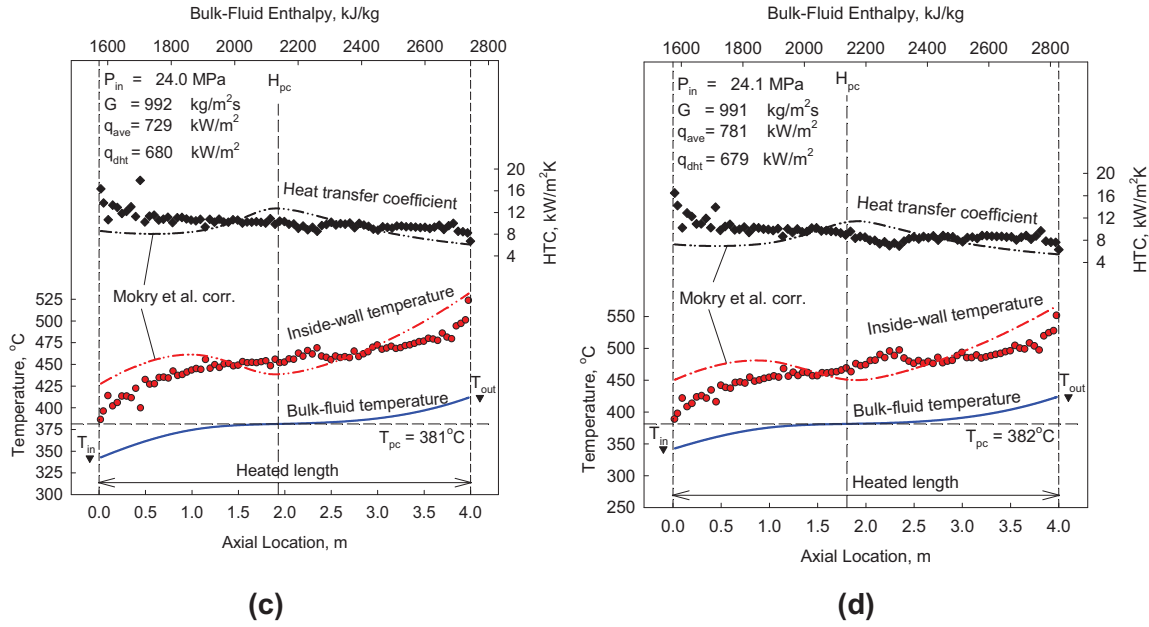


**Figure 9.12 (c-d). Temperature and Heat Transfer Coefficient Variations along a 4-m Circular Tube at Various Heat Fluxes (ID = 10 mm): Nominal Operating Conditions –  $P_{in} = 24.0 \text{ MPa}$ ,  $G = 1000 \text{ kg/m}^2\text{s}$  (Mokry et al., 2009b).**

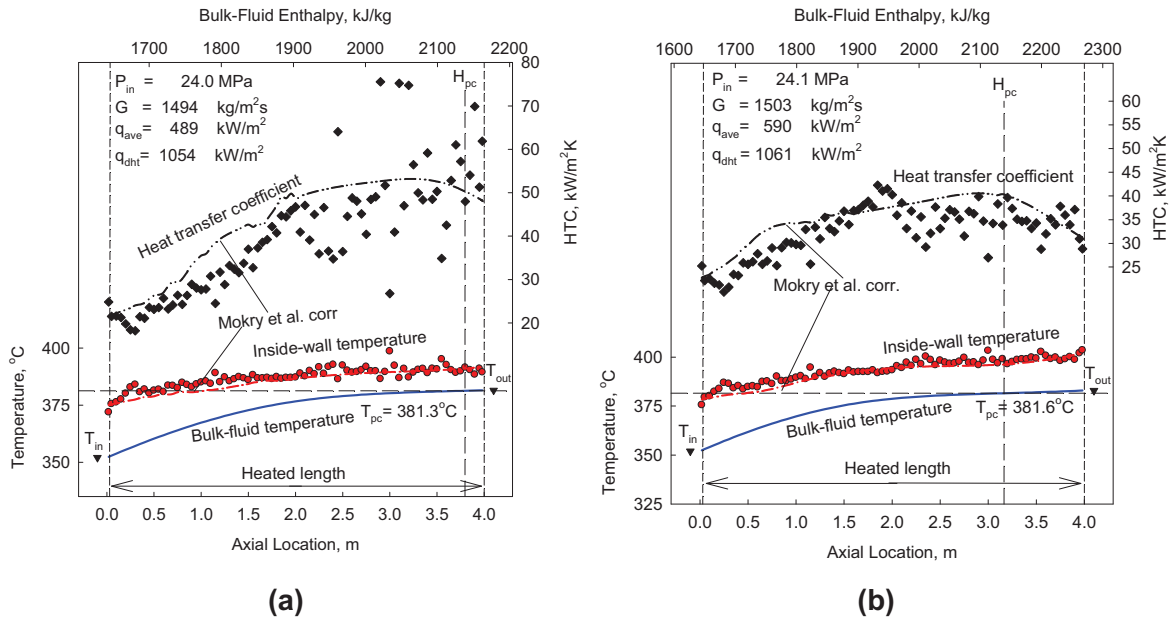
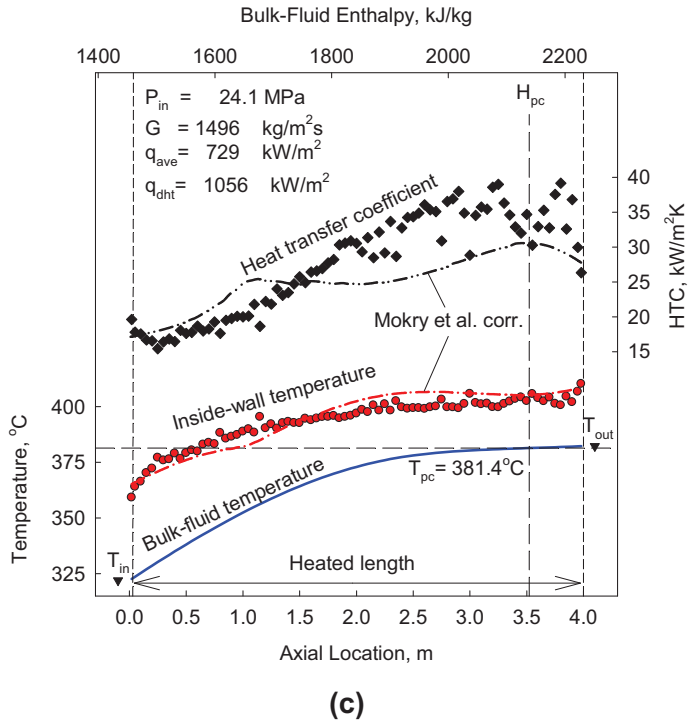


**Figure 9.13 (a-b). Temperature and Heat Transfer Coefficient Variations along a 4-m Circular Tube at Various Heat Fluxes (ID = 10 mm): Nominal Operating Conditions –  $P_{in} = 24.0 \text{ MPa}$ ,  $G = 1500 \text{ kg/m}^2\text{s}$  (Mokry et al., 2009b).**



(c)

**Figure 9.13 (c). Temperature and Heat Transfer Coefficient Variations along a 4-m Circular Tube at Various Heat Fluxes (ID = 10 mm): Nominal Operating Conditions**  
 $- P_{in} = 24.0 \text{ MPa}, G = 1500 \text{ kg/m}^2\text{s}$  (Mokry et al., 2009b).

## 9.6 Comparison Graphs

In order to evaluate the accuracy of the derived correlation, a comparison of the experimental data with the calculated HTC profiles, using the Bishop et al., Dittus-Boelter and the Mokry et al. correlations was conducted and is shown in Figures 9.14 and 9.15. As can be seen from these graphs, neither the original Bishop et al. nor the Dittus-Boelter correlations provide a good fit for the experimental data, whereas the final Mokry et al. correlation fits the data well and follows trends closely.

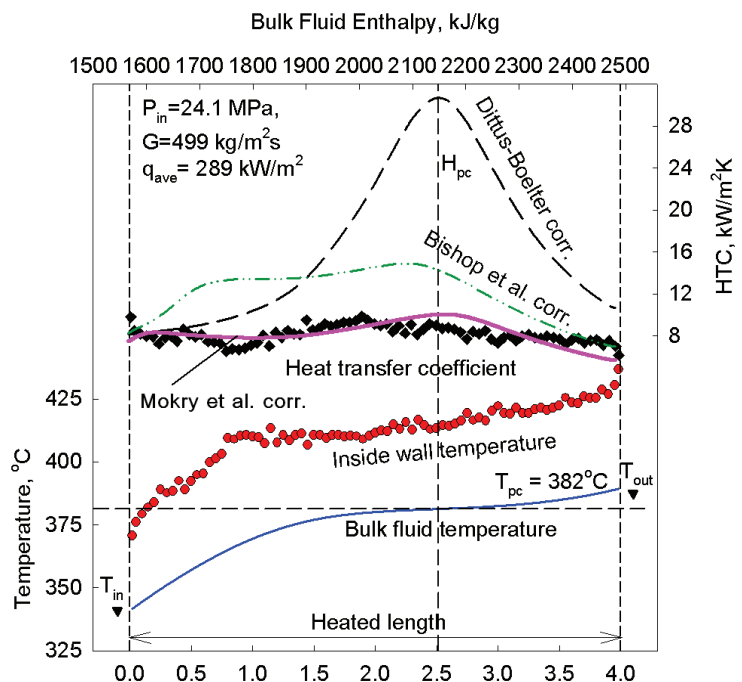


**Figure 9.14. Temperature and Heat Transfer Coefficient Profiles along Heated Length of Bare Vertical Tube:  $G = 500 \text{ kg/m}^2\text{s}$  and  $q = 290 \text{ kW/m}^2$  (Mokry et al., 2009b).**

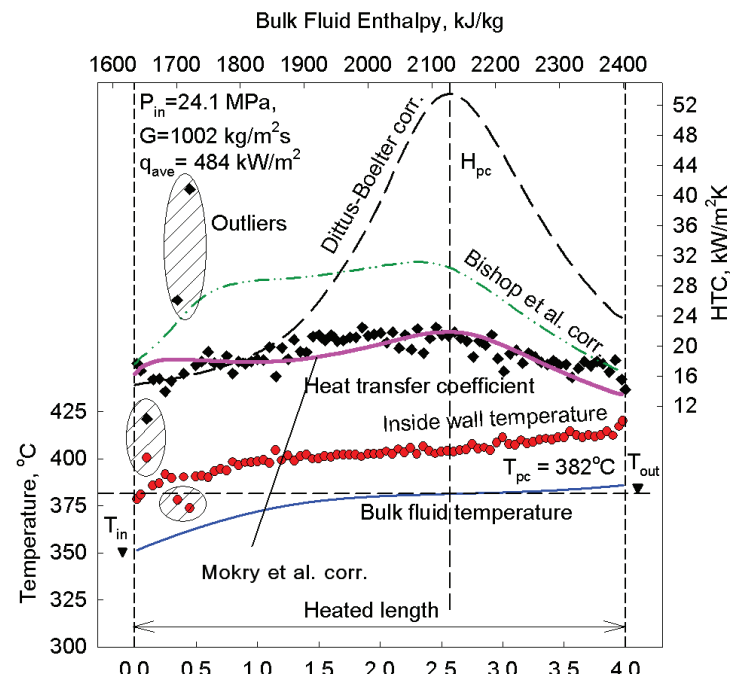


**Figure 9.15. Temperature and Heat Transfer Coefficient Profiles along Heated Length of Bare Vertical Tube:  $G = 1000 \text{ kg/m}^2\text{s}$  and  $q = 480 \text{ kW/m}^2$  (Mokry et al., 2009b).**

Another final comparison between the Mokry et al. correlation and calculations, using the CFD Code FLUENT-6.0 is shown, in Figure 9.16.

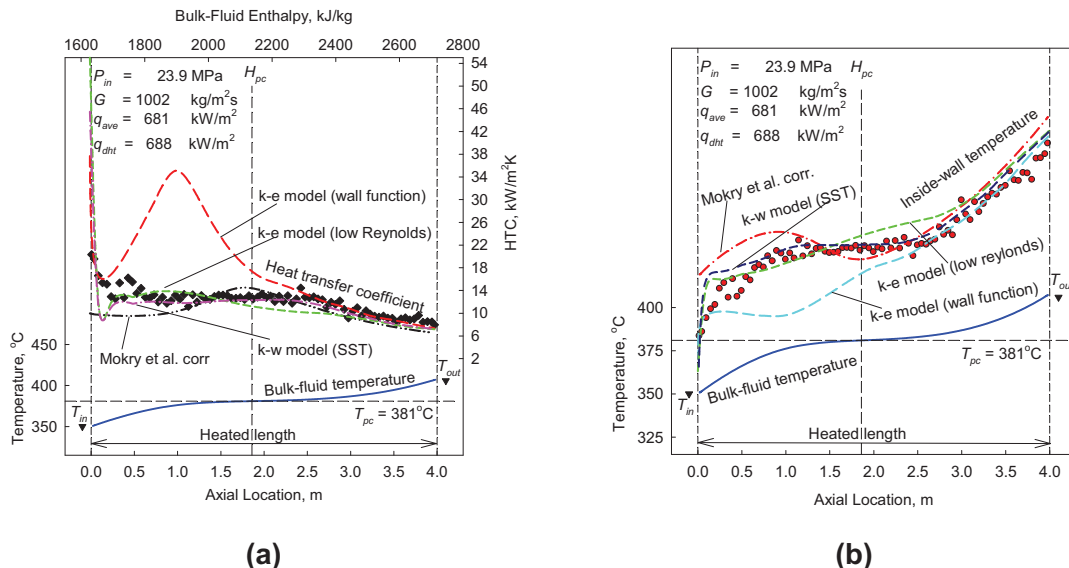


**Figure 9.16 (a-b). Temperature and Heat Transfer Coefficient Comparisons Between Final Correlation and CFD Code Calculations along a 4-m Circular Tube (ID = 10 mm): Operating Conditions –  $P_{in} = 24.0 \text{ MPa}$ ,  $G = 1000 \text{ kg/m}^2\text{s}$  (Mokry et al., 2009b; Vanyukova et al., 2009).**

An analysis of the plots in Figures 9.10 – 9.16 showed that in general the final correlation appeared to fit the general data trends. Deviations in the calculated HTC from the experimentally determined values were found, for the most part, at the test section inlet. Within this area, however, the flow was likely subject to an entrance effect. There were also slight deviations within the pseudocritical point, however, the most pronounced difference occurred at the lower mass fluxes.

The HTC and wall temperature values calculated with the FLUENT CFD code (Figure 9.16) may deviate significantly from the experimental data (for example, the *k*-*ε* model (wall function)). However, the *k*-*ε* model (low Reynolds numbers) shows a better fit within some flow conditions (Mokry et al., 2009b).

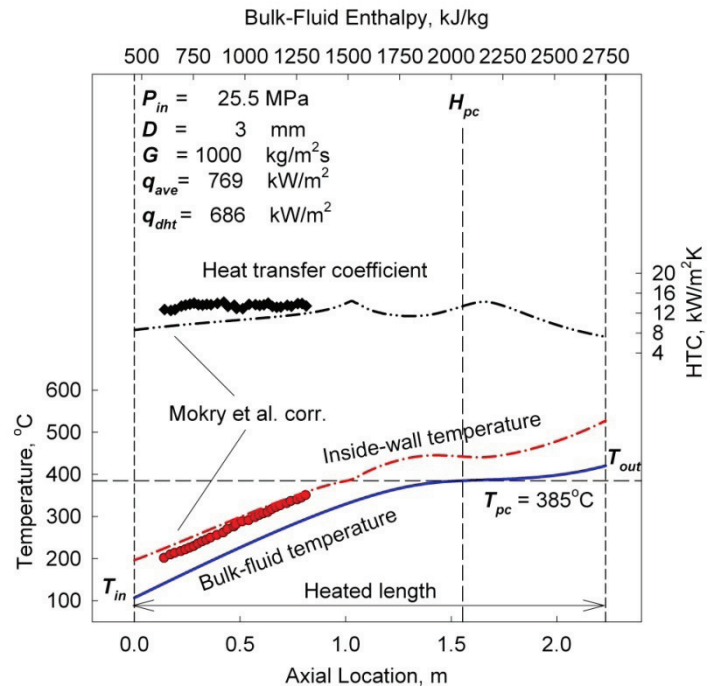
Nevertheless, the derived correlation showed the best fit for the experimental data within a wide range of flow conditions. This correlation has an uncertainty of about  $\pm 25\%$  for HTC values and about  $\pm 15\%$  for calculated wall temperatures.

Therefore, the derived correlation can be used for preliminary HTC calculations in SCWR fuel bundles, for heat exchangers, for future comparison with other datasets, for verification of computer codes and scaling parameters between water and modeling fluids.

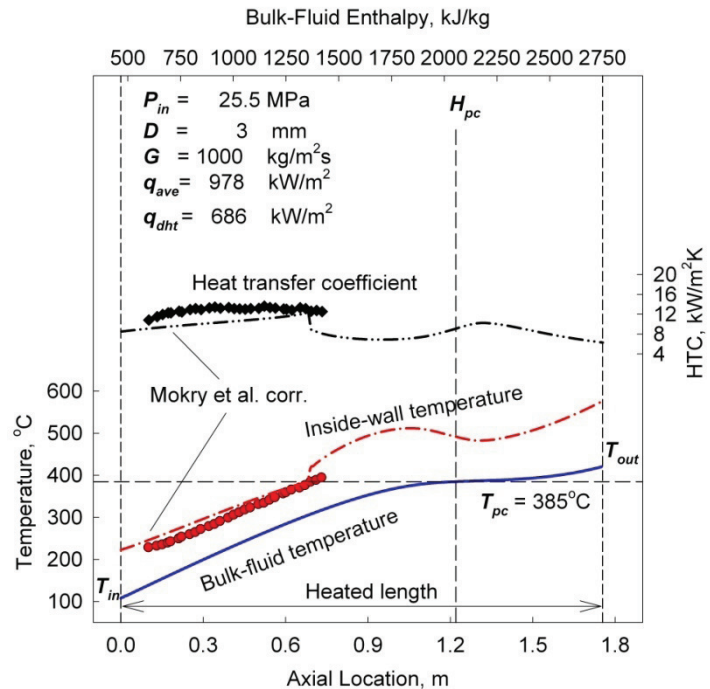
For a final verification of the correlation, a comparison with other datasets was completed (Figures 9.17 – 9.19, for additional Figures, see Appendix B). From the presented Figures, it can be seen that the new correlation closely represents the experimental data and follows trends closely, even within the pseudocritical range. Table 9.4 lists the test matrices for these datasets against which the Mokry et al. correlation was compared.

**Table 9.4. Other Datasets and Corresponding Test Matrices.**

Reference	P, MPa	q, MW/m <sup>2</sup>	G, kg/m <sup>2</sup> s	Flow geometry
Alferov et al., 1976	26.5	0.48	447	Tube ( $D=20$ mm, $L/D=185$ ), ascending flow, $\rho_w=447$ kg/m <sup>2</sup> ·s
Petukhov and Polyakov, 1988	29.4	0.50	675	Tube ( $D=3$ mm)
Bishop et al., 1964	22.8 – 27.6	0.31 – 3.46	651 – 3662	Tube ( $D=5$ mm,) upward flow
Shitsman, 1963	22.6 – 24.5	0.28 – 1.1	300 – 1500	SS tube ( $D=8$ mm, $L=1.5$ m)
Vikhrev et al., 1967	24.5; 26.5	0.23 – 1.25	485 – 1900	SS tube ( $D=7.85$ ; 20.4 mm, $L=1.515$ ; 6 m) (selected data are shown in Figure B.5)
Ornatsky et al., 1970	22.6; 25.5; 29.4	0.28 – 1.2	450 – 3000	Five SS parallel tubes ( $D=3$ mm, $L=0.75$ m), upward stable and pulsating flows
Pis'mennyy et al., 2005	23.5	Up to 0.515	250; 500	Vertical SS tubes ( $D=6.28$ mm, $L_h=600$ ; 360 mm; $D=9.50$ mm, $L_h=600$ ; 400mm) (for more details, see Section B.6)
Polyakov, 1975	29.4	0.50	675	Tube ( $D=8$ mm)
Lee and Haller, 1974	24.1	0.25 – 1.57	542 – 2441	SS tubes ( $D=38.1$ ; 37.7 mm, $L=4.57$ m), tube with ribs
Shiralkar and Griffith, 1969 and 1968	22.8	0.32	461	Tube ( $D=10$ mm)
Shitsman, 1968	10 – 35	0.27 – 0.7	400	Vertical and horizontal SS tubes ( $D/L=3/0.7$ ; 8/0.8; 8/3.2; 16/1.6 mm/m), upward, downward and horizontal flows
Yamagata et al., 1972	22.6 – 29.4	0.12 – 0.93	310 – 1830	Vertical and horizontal SS tubes ( $D/L=7.5/1.5$ ; 10/2 mm/m), upward, downward and horizontal flows (selected data are shown in Figure 9.18)
Yoshida and Mori, 2000	24.5	0.23 - 0.33	376, 1180	Tube ( $D=10$ mm, $D=16$ )

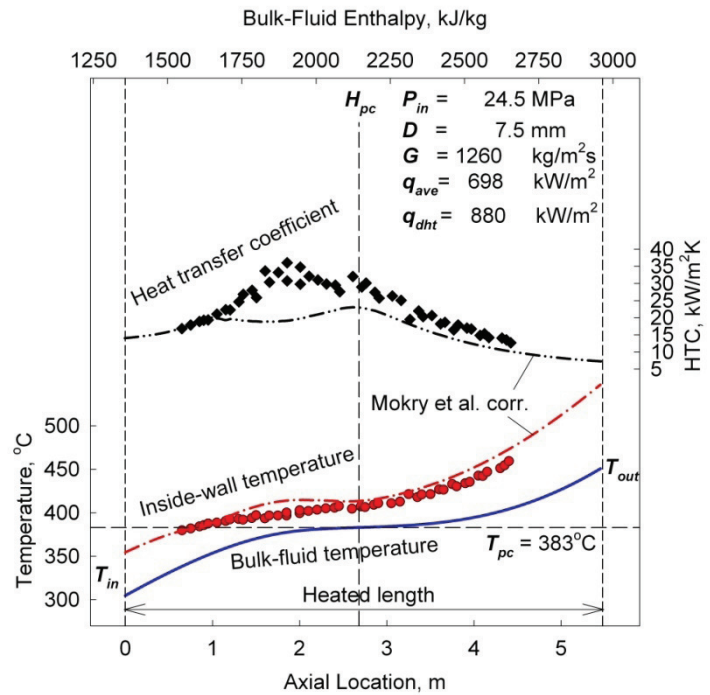


(a)

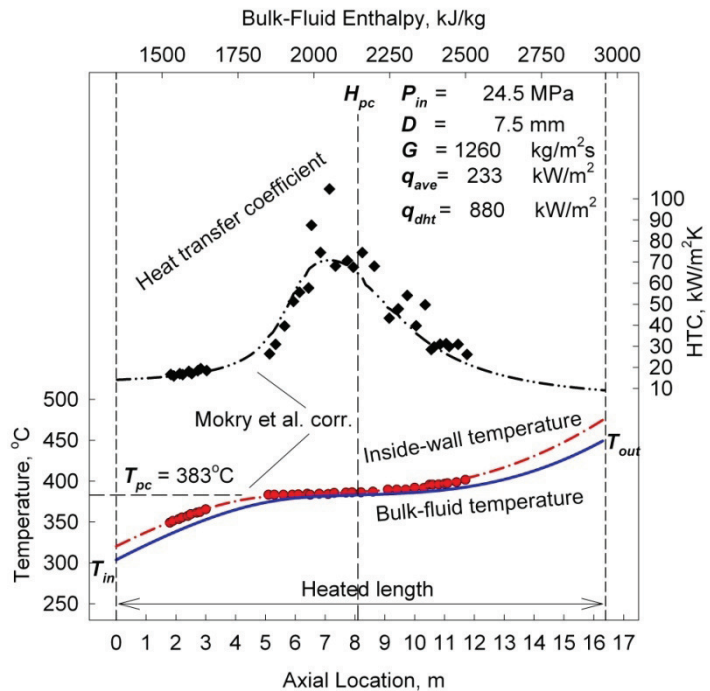


(b)

**Figure 9.17. Temperature and Heat Transfer Coefficient Variations along a Circular Tube at Various Heat Fluxes: Nominal Operating Conditions –  $P_{in} = 25.5 \text{ MPa}$ , (a)  $G = 769 \text{ kg/m}^2\text{s}$ ; (b)  $G = 978 \text{ kg/m}^2\text{s}$  (Ornatsky et al. 1970).**

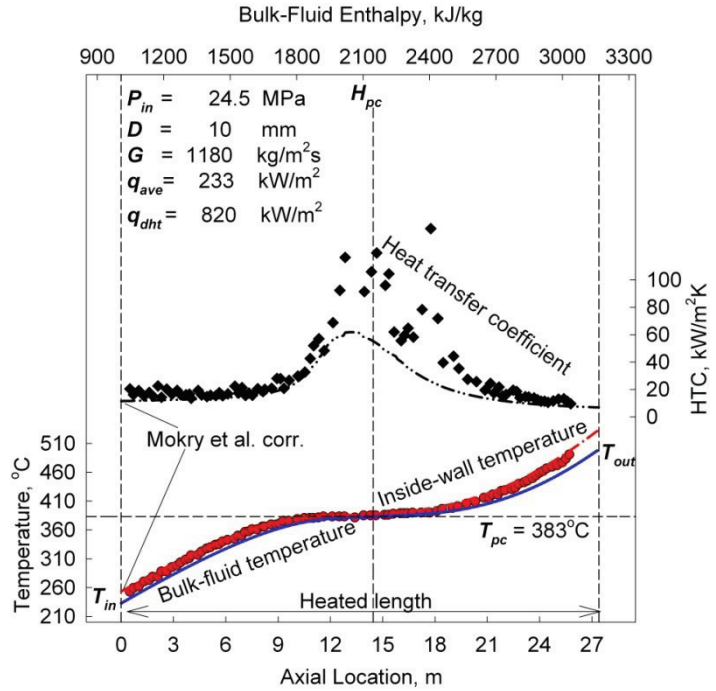


(a)

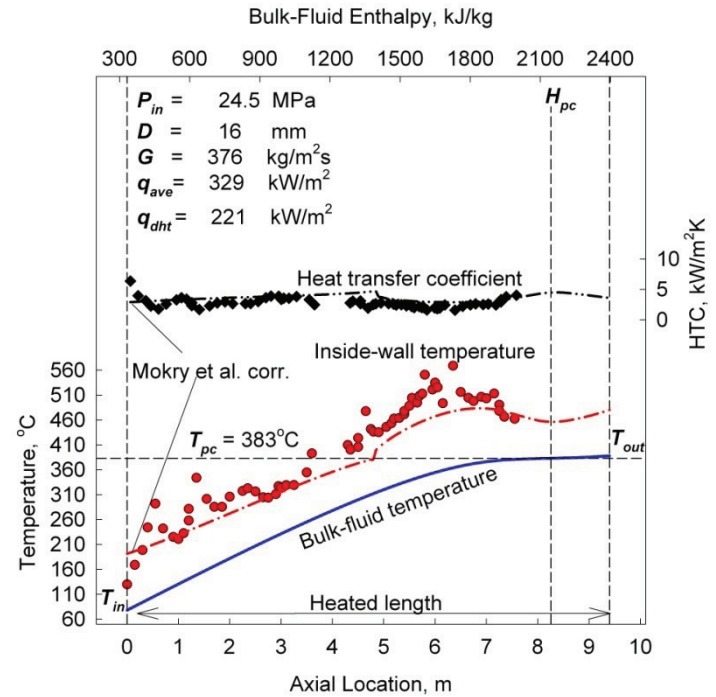


(b)

**Figure 9.18. Temperature and Heat Transfer Coefficient Variations along a Tube at Various Heat Fluxes: Nominal Operating Conditions –  $P_{in} = 24.5 \text{ MPa}$ ,  $G = 1260 \text{ kg/m}^2\text{s}$ ; (a)  $q_{ave} = 698 \text{ kW/m}^2$  (b)  $q_{ave} = 233 \text{ kW/m}^2$  (Yamagata, 1972).**



(a)



(b)

**Figure 9.19. Temperature and Heat Transfer Coefficient Variations along a Circular Tube at Various Heat Fluxes: Nominal Operating Conditions –  $P_{in} = 24.5 \text{ MPa}$ , (a)  $G = 1180 \text{ kg/m}^2\text{s}$ ; (b)  $G = 376 \text{ kg/m}^2\text{s}$  (Yoshida and Mori, 2000).**

## CHAPTER 10

### CONCLUSIONS

Supercritical water heat-transfer data for a vertical bare circular tube were obtained within the proposed SCWR operating conditions: pressure of ~24 MPa, mass fluxes from 200 to 1500 kg/m<sup>2</sup>s, heat fluxes up to 1250 kW/m<sup>2</sup> and inlet temperatures from 320 to 350°C. Supercritical heat transfer was investigated for several combinations of wall and bulk-fluid temperatures, i.e., internal wall temperatures and bulk-fluid temperatures below, at, or above the pseudocritical temperature.

The obtained correlation for forced convective heat transfer to supercritical water in a bare vertical tube showed a good fit ( $\pm 25\%$ ) for the analyzed dataset. In addition, the calculated wall temperature resulted in a slightly more accurate fit for the analyzed dataset ( $\pm 15\%$ ).

Thus, this new correlation can be used: (1) for preliminary calculations of supercritical-water-cooled fuel bundles, as a conservative approach in relation to SCWRs; (2) for calculations of supercritical water heat-transfer in heat exchangers in SCWR indirect cycle concepts; (3) for calculations of heat-transfer in heat exchangers for the co-generation of hydrogen at supercritical water NPPs; (4) for calculations of supercritical water heat-transfer in heat exchangers for other Generation IV reactor concepts with an indirect cycle; (5) for future comparison with other independent datasets; (6) for comparison with bundle data, as the reference case; (7) for the verification of computer codes for SCWR core thermalhydraulics; and (8) for verification of scaling parameters between water and modeling fluids such as carbon dioxide, refrigerant R-134a, and others.

## **CHAPTER 11**

### **FUTURE WORK**

Future work on this topic includes correlating larger supercritical-water datasets with the proposed correlation, developing correlation(s) for modeling fluids (supercritical carbon dioxide and refrigerants), developing a correlation for supercritical-water bundle data, and developing a correlation for deteriorated heat-transfer regimes.

## REFERENCES

- Alferov, N.S., Balunov, B.F. and Rybin, R.A., 1976. The Effect of Natural Convection on the Heat Transfer of a Single-Phase Flow with Subcritical and Supercritical Pressures, *High Temperature*, May, 14(6), pp. 1087–1093.
- Bishop, A.A., Sandberg, R.O. and Tong, L.S., 1964. Forced Convection Heat Transfer to Water at Near-Critical Temperatures and Super-Critical Pressures, Report WCAP-2056, Westinghouse Electric Corporation, Atomic Power Division, Pittsburgh, PA, USA, December, 85 pages.
- Black and Veatch, 1995. *Power Plant Engineering*, Springer Science + Business Media, New York, NY, USA, 879 pages.
- Buongiorno, J. and MacDonald, Ph.E., 2003. Supercritical water reactor (SCWR). Progress report for the FY-03 Generation-IV R&D activities for the development of the SCWR in the U.S., Report INEEL/EXT-03-01210, Idaho National Engineering and Environmental Laboratory, USA, September, 38 pages.
- Chow, C. K. and Khatabil, H.F., 2008. Conceptual Fuel Channel Designs for CANDU-SCWR, *Nuclear Engineering and Technology*, 40(1), pp. 1–8.
- Dittus, F.W. and Boelter, L.M.K., 1930. Heat Transfer in Automobile Radiators of the Tubular Type, University of California, Berkeley, Publications on Engineering, Vol. 2(13), pp. 443-461.
- Duffey, R.B., Pioro, I., Zhou, T., Zirn, U., Kuran, S., Khatabil, H. and Nadin, M., 2008. Supercritical Water-Cooled Nuclear Reactors (SCWRs): Current and Future Concepts - Steam-Cycle Options, Proceedings of the 16<sup>th</sup> International Conference on Nuclear Engineering (ICON-E-16), Orlando, Florida, USA, May 11-15, Paper #48869, 9 pages.

Dyadyakin, B.V. and Popov, A.S., 1977. Heat transfer and thermal resistance of tight seven-rod bundle, cooled with water flow at supercritical pressures, (In Russian), Transactions of VTI (Труды ВТИ), No. 11, pp. 244–253.

Gabaraev, B.A., Kuznetsov, Yu.N., Pioro, I.L. and Duffey, R.B., 2007. Experimental Study on Heat Transfer to Supercritical Water Flowing in 6-m Long Vertical Tubes, Proceedings of the 15<sup>th</sup> International Conference on Nuclear Engineering (ICON-E-15), April 22-26, Nagoya, Japan, Paper #10692, 8 pages.

GIF – Generation IV International Forum, 2002. A Technology Roadmap for Generation IV Nuclear Energy Systems, Issued by the Generation IV international Forum and the U.S. DOE Nuclear Energy Research Advisory Board, 97 pages.

Gopaul, S., Hopps, V., Jacobs, Ch., Khan, M., Patkunam, R. and Pioro, I.L., 2007. Some Design Features of SCW Pressure-Tube Nuclear Reactor, Proceedings of the 15<sup>th</sup> International Conference on Nuclear Engineering (ICON-E-15), Nagoya, Japan, Apr. 22–26, Paper #10829, 9 pages.

Gorban', L.M., Pomet'ko, R.S. Khryaschev, O.A., 1990. Modeling of water heat transfer with Freon of supercritical pressure, (In Russian), ФЭИ-1766, Institute of Physics and Power Engineering (ФЭИ), Obninsk, Russia, 19 pages.

Gospodinov, Ye., Mokry, S., Pioro, I. and Kirillov, P.L., 2008. Supercritical Water Heat Transfer in a Vertical Bare Tube, Proceedings of the 16<sup>th</sup> International Conference on Nuclear Engineering (ICON-E-16), Orlando, FL, USA, May 11–15, Paper #48546, 11 pages.

Hwang, D.H., Seo, K.W., and Lee, C.C., 2006. Critical Heat Flux in Square- and Nonsquare-array Rod Bundles for Advanced Light Water Reactors, Nuclear Technology, 158, May, pp. 219-228.

Incropera, E.P., Dewitt, D.P., Bergman, T.L., and Lavine, A.S., 2007. Fundamentals of Heat and Mass Transfer, Sixth Edition, John Wiley & Sons., Hoboken, N.J., pp. 500-502.

Jackson, J.D., 2002. Consideration of the heat transfer properties of supercritical pressure water in connection with the cooling of advanced nuclear reactors, Proceedings of the 13<sup>th</sup> Pacific Basin Nuclear Conference, Shenzhen City, China, October 21–25, 6 pages.

Jackson, J.D. and Hall W.B., 1979. Forced convection heat transfer to fluids at supercritical pressure, In book: Turbulent Forced Convection in Channels and Bundles, Editors S. Kakaç and D.B. Spalding, Hemisphere Publishing Corp., New York, New York, USA, Vol. 2, pp. 563–612.

Khartabil, H.F., Duffey, R.D., Spinks, N., and Diamond, W., 2005. The pressure-tube concept of Generation IV Supercritical Water-Cooled Reactor (SCWR): Overview and status, Proceedings of the 2005 International Congress on Advances in Nuclear Power Plants (ICAPP'05), Seoul, Korea, May 15-19, Paper #5564, 7 pages.

Kirillov, P., Pometko, R., Smirnov, A., Grabezhnaia, V., Pioro, I., Duffey, R., and Khartabil, H., 2005. Experimental study on heat transfer to supercritical water flowing in 1- and 4-m-long vertical tubes, Proceedings of GLOBAL 2005 International Conference, Nuclear Energy Systems for Future Generation and Global Sustainability (GLOBAL'05), Tsukuba, Japan, Oct. 9-13, Paper No. 518, 8 pages.

Krasnoshchekov, E.A., Protopopov, V.S., Van, F. and Kuraeva, I.V., 1967. Experimental investigation of heat transfer for carbon dioxide in the supercritical region, Proceedings of the 2<sup>nd</sup> All-Soviet Union Conference on Heat and Mass Transfer, Minsk, Belarus', May, 1964, Published as Rand Report R-451-PR, Edited by C. Gazley, Jr., J.P. Hartnett and E.R.C. Ecker, Vol. 1, pp. 26–35.

Lee, R.A. and Haller, K.H., 1974. Supercritical water heat transfer developments and applications, Proceedings of the 5<sup>th</sup> International Heat Transfer Conference, Tokyo, Japan, September 3–7, Vol. IV, Paper No. B7.7, pp. 335–339.

Leung, L., 2008. Effect of CANDU Bundle-Geometry Variation on Dryout Power, Proc. ICONE-16, Orlando, Florida, USA, May 11-15, Paper #48827, 8 pages.

MATLAB version 7.4, R2007a, computer software, The MathWorks, Inc., Natick, Massachusetts, USA.

McAdams, W.H., 1942. Heat Transmission, 2<sup>nd</sup> edition, McGraw-Hill, New York, NY, USA, 459 pages.

Mokry, S., Pioro, I., Kirillov, P. and Gospodinov, Ye., 2010. Supercritical-Water Heat-Transfer in a Vertical Bare Tube, to be published in Nuclear Engineering and Design, 9 pages.

Mokry, S., Gospodinov, Ye., Pioro, I. and Kirillov, P., 2009a. Supercritical Water Heat-Transfer Correlation for Vertical Bare Tubes, Proceedings of the 17<sup>th</sup> International Conference on Nuclear Engineering (ICONE-17), Brussels, Belgium, July 12-16, Paper#76010, 8 pages.

Mokry, S., Farah, F., King, K., Gupta, S, Pioro, I. and Kirillov, P., 2009b. Development of Supercritical Water Heat-Transfer Correlation for Vertical Bare Tubes, Proceedings of the Nuclear Energy for New Europe 2009 International Conference, Bled, Slovenia, September 14-17, Paper#210, 13 pages.

Mokry, S., Pioro, I. and Duffey, R., 2009c. Experimental Heat Transfer to Supercritical CO<sub>2</sub> Flowing Upward in a Bare Vertical Tube, Proceedings of the Supercritical Carbon Dioxide Power Cycle Symposium 2009, Rensselaer Polytechnic Institute, Troy, New York, April 29 – 30, 2009, 15 pages.

Mokry, S., Naidin, M., Baig, F., Gospodinov, Ye., Zirn, U., Bakan, K., Pioro, I. and Naterer, G., 2008. Conceptual Thermal-Design Options for Pressure-Tube SCWRs with Thermochemical Co-Generation of Hydrogen, Proceedings of the 16<sup>th</sup> International Conference on Nuclear Engineering (ICON-E-16), Orlando, FL, USA, May 11–15, Paper #48313, 13 pages.

Munson, Bruce R., Young, Donald F., and Okiishi, Theodore H., 2005. Fundamentals of Fluid Mechanics. 5<sup>th</sup> ed. New York: Wiley, 816 pages.

Naidin, M., Pioro, I., Zirn, U., Mokry, S. and Naterer, G., 2009a. Supercritical Water-Cooled NPPs with Co-Generation of Hydrogen: General Layout and Thermodynamic-Cycles Options, Proceedings of the 4<sup>th</sup> International Symposium on Supercritical Water-Cooled Reactors, Heidelberg, Germany, March 8 – 11, 2009, Paper #78, 11 pages.

Naidin, M., Mokry, S., Monichan, R., Chop;a, K., Pioro, I., Naterer, G. and Gabriel, K., 2009b. Thermodynamic Analysis of SCW NPP Cycles with Thermo-Chemical Co-Generation of Hydrogen, Proceedings of the International Conference on Hydrogen Production, May 3 – 6, 2009, UOIT, Oshawa, Ontario, Canada, 15 pages.

Naidin, M., Pioro, I., Duffey, R., Mokry, S., Grande, L., Villamere, B., Allison, L., Rodriguez-Prado, A., Mikhael, S. and Chophla, K., 2009c. SuperCritical Water-Cooled Nuclear Reactors (SCWRs): Thermodynamic Cycle Options and Thermal Aspects of Pressure-Channel Design, International Conference on Opportunities and Challenges for Water Cooled Reactors in the 21st Century, Book of Extended Synopses, IAEA, Vienna, Austria, October 27-30, Paper 5S03, pp. 134-135.

Naidin, M., Mokry, S., Baig, F. and Gospodinov, Ye., 2008. Thermal-Design Options for Pressure-Channel SCWRs with Cogeneration of Hydrogen, Journal of Engineering for Gas Turbines and Power, 131(1), Paper #012901, 8 pages.

Naterer, G., Suppiah, S., Lewis, M., et al., 2009. Recent Canadian Advances in Nuclear-Based Hydrogen Production and the Thermochemical Cu-Cl Cycle, International Journal of Hydrogen Energy, 34(6), 17 pages.

National Institute of Standards and Technology (NIST), 2009. NIST Standard Reference Database 23: Reference Fluid Thermodynamic and Transport Properties-miniREFPROP, Version 8.1(06/01/2009), E.W. Lemmon, M.L. Huber, and M.O. McLinden, Standard Reference Data Program, Gaithersburg.

National Institute of Standards and Technology (NIST), 2007. NIST Standard Reference Database 23: Reference Fluid Thermodynamic and Transport Properties-miniREFPROP, Version 8.0, E.W. Lemmon, M.L. Huber, and M.O. McLinden, Standard Reference Data Program, Gaithersburg.

National Institute of Standards and Technology (NIST), 2002. NIST Standard Reference Database 23: Reference Fluid Thermodynamic and Transport Properties-REFPROP, Version 7.0, E.W. Lemmon, M.L. Huber and M.O. McLinden, Standard Reference Data Program, Gaithersburg.

Ornatsky, A.P., Glushchenko, L.P., Siomin, E.T. et al., 1970. The research of temperature conditions of small diameter parallel tubes cooled by water under supercritical pressures, Proceedings of the 4<sup>th</sup> International Heat Transfer Conference, Paris-Versailles, France, Elsevier Publishing Company, Vol. VI, Paper No. B 8.11

Petukhov, B.S. and Polyakov, A.F., 1988. Heat Transfer in Turbulent Mixed Convection, Hemisphere Publishing Corp., New York, NY, USA, Chapter 7.1. Heat Transfer at Supercritical Pressures, pp. 183–201.

Pioro, I.L. and Duffey, R.B., 2007. Heat Transfer and Hydraulic Resistance at Supercritical Pressures in Power Engineering Applications, ASME Press, New York, NY, USA, 334 pages.

Pioro, I.L. and Duffey, R.B., 2003. Literature Survey of the Heat Transfer and Hydraulic Resistance of Water, Carbon Dioxide, Helium and Other Fluids at Supercritical and Near-Critical Pressures, Report AECL-12137/FFC-FCT-409, CRL AECL, April, ISSN 0067-0367, 182 pages.

Pioro, I.L. and Khatabil, H.F., 2005. Experimental Study on Heat Transfer to Supercritical Carbon Dioxide Flowing Upward in a Vertical Tube, Proceedings of the 13<sup>th</sup> International Conference on Nuclear Engineering (ICON-E-13), Beijing, China, May 16–20, Paper # 50118, 9 pages.

Pioro, I.L., Khatabil, H.F. and Duffey, R.B., 2004. Heat Transfer to Supercritical Fluids Flowing in Channels – Empirical Correlations (Survey), Nuclear Engineering and Design, 230(1–3), pp. 69–91.

Pioro, I.L., Kirillov, P.L., Mokry, S.J. and Gospodinov, Y.K., 2010. Supercritical Water Heat Transfer in a Vertical Bare Tube: Normal, Improved and Deteriorated Regimes, to be published in Nuclear Technology, 31 pages.

Pioro, I.L., Kirillov, P.L., Mokry, S.J. and Gospodinov, Y.K., 2008a. Supercritical Water Heat Transfer in a Vertical Bare Tube: Normal, Improved and Deteriorated Regimes, Proceedings of the 2008 International Congress on Advances in Nuclear Power Plants (ICAPP'08), Anaheim, CA, USA, June 8 – 12, Paper #8333, 10 pages.

Pioro, L.S. and Pioro, I.L., 1997. Industrial Two-Phase Thermosyphons, Begell House, New York, NY, USA, 288 pages.

Pioro, I., Zirn, U., Duffey, R., Nadin, M., Mokry, S., Gospodinov, Ye. and Baig, F., 2008b. Supercritical Water-Cooled Nuclear Reactors: Thermodynamic-Cycles Options, Proceedings of the 6<sup>th</sup> International Conference on Heat Transfer, Fluid Mechanics and Thermodynamics, Pretoria, South Africa, June 30 – July 2, 2008, Paper #PI1, 9 pages.

Pis'menny, E.N., Razumovskiy, V.G., Maevskiy E.M. et al., 2005. Experimental study on temperature regimes to supercritical water flowing in vertical tubes at low mass fluxes, Proceedings of the International Conference GLOBAL-2005 Nuclear Energy Systems for Future Generation and Global Sustainability, Tsukuba, Japan, October 9–13, Paper No. 519, 9 pages.

Polyakov, A.F., 1975. Mechanism and limits on the formation of conditions for impaired heat transfer at a supercritical coolant pressure, High Temperatures (Теплофизика Высоких Температур, стр. 1210–1219), 13 (6), pp. 1119–1126.

Schmidt, E., 1960. Wärmetransport durch natürliche convection in Stoffen bei Kritischen zustand, International Journal of Heat & Mass Transfer, 1(1) pp. 92 - 101.

Schmidt, E., Eckert, E. and Grigull, V., 1946. Heat transfer by liquids near the critical state, AFF Translation, No. 527, Air Materials Command, Wright Field, Dayton, OH, USA, April.

Schnurr, N.M., Sastry, V.S. and Shapiro, A.B., 1976. A Numerical Analysis of Heat Transfer to Fluids near the Thermodynamic Critical Point Including the Thermal Entrance Region, *Journal of Heat Transfer, Transactions of ASME*, 98 (4), pp. 609–615.

Shiralkar, B.S. and Griffith, P., 1969. Deterioration in Heat Transfer to Fluids at Supercritical Pressures and High Heat Fluxes, *Journal of Heat Transfer, Transactions of the ASME*, 91(1), February, pp. 27-36.

Shiralkar, B. and Griffith, P., 1968. The Deterioration in Heat Transfer to Fluids at Supercritical Pressures and High Heat Fluxes, Report, Engineering Projects Laboratory, Department of Mechanical Engineering, Massachusetts Institute of Technology, Cambridge, MA, USA, June, 185 pages.

Shitsman, M.E., 1968. Temperature Conditions in Tubes at Supercritical Pressures, *Thermal Engineering* (Теплоэнергетика, стр. 57–61), 15(5), pp.72-77.

Shitsman, M.E., 1963. Impairment of the heat transmission at supercritical pressures, High Temperatures (Теплофизика Высоких Температур, стр. 267–275), 1 (2), pp. 237–244.

Special Metals, 2007. Inconel Alloy 718SPF, A Precision Castparts Corp. Company, 16 pages.

Swenson, H.S., Carver, J.R. and Kakarala, C.R., 1965. Heat transfer to supercritical water in smooth-bore tubes, *Journal of Heat Transfer, Transactions of the ASME, Series C*, 87 (4), pp. 477–484.

Vanyukova, G. V., Yu N. Kuznetsov, A. Ya Loninov, M. V. Papandin, V. P. Smirnov, and I. L. Pioro, 2009. Application of CFD-Code to Calculations of Heat Transfer in a fuel Bundle of SCW Pressure-Channel Reactor, *Proceedings of the 4<sup>th</sup> International Symposium on Supercritical Water-Cooled Reactors*, Germany, Heidelberg, 8 pages.

Vikhrev, Yu.V., Barulin, Yu.D. and Kon'kov, A.S., 1967. A study of heat transfer in vertical tubes at supercritical pressures, *Thermal Engineering* (Теплоэнергетика, стр. 80–82), 14 (9), pp. 116–119.

Winterton, R.H.S., 1998. Where did the Dittus and Boelter equation come from? *International Journal of Heat and Mass Transfer*, 41 (4–5), pp. 809–810.

Yamagata, K., Nishikawa, K., Hasegawa, S., et al., 1972. Forced Convective Heat Transfer to Supercritical Water Flowing in Tubes, *International Journal of Heat and Mass Transfer*, 15(12), pp. 2575–2593.

Yoshida, S. and Mori, H., 2000. Heat Transfer to Supercritical Pressures Fluids Flowing in Tubes, *Proceedings of the 1<sup>st</sup> International Symposium on Supercritical Water-Cooled Reactor Design and Technology (SCR-2000)*, Tokyo, Japan, November 6-8, Paper No. 106.

## APPENDIX A

### Supercritical Carbon Dioxide

In support of developing a SCWR reactor, studies are being conducted into heat transfer at supercritical conditions using carbon dioxide as a modelling fluid as a less expensive alternative to using supercritical water (Pioro and Khatabil, 2005). Another objective is to improve our fundamental knowledge of the transport processes and handling of supercritical fluids.

The MR-1 loop at Chalk River Laboratories (CRL) is a former steam/water loop that has been adapted for use with supercritical CO<sub>2</sub>. The objective of the experimental research was to obtain a detailed reference dataset on heat transfer in supercritical CO<sub>2</sub> flowing upward in a vertical tube at SCWR-equivalent operating conditions.

Supercritical CO<sub>2</sub> heat-transfer data were obtained at reactor-equivalent conditions at three pressures above the critical point (7.6, 8.4 and 8.8 MPa), mass fluxes from 840 to 3000 kg/m<sup>2</sup>s, heat fluxes up to 600 kW/m<sup>2</sup> and inlet temperatures from 20 to 40°C (Pioro and Khatabil, 2005).

Results are given for supercritical heat transfer for several combinations of wall and bulk-fluid temperatures that were below, at, or above the pseudocritical temperature. The experimental data on heat transfer are presented in the form of graphs of internal-wall and bulk-fluid temperatures and Heat Transfer Coefficient (HTC) vs. heated length and bulk-fluid enthalpy.

Two regimes of heat transfer at supercritical pressures have been recorded: (1) the so-called normal heat-transfer regime and (2) the deteriorated heat-transfer regime characterized with lower-than-expected HTC values than those in the normal heat-transfer regime.

A generalized heat-transfer correlation, for the normal heat-transfer regime, for supercritical carbon dioxide flowing in a vertical bare circular tube is proposed.

A comparison of selected thermophysical properties profiles for water along the fuel-channel heated length for a non-uniform Axial Heat Flux Distribution (AHFD) are shown in Figures A.1 and A.2 (Mokry et al., 2008). The following bulk-fluid thermophysical properties were calculated: (a) density; (b) specific heat; (c) thermal conductivity; (d) dynamic viscosity; and (e) Prandtl number. In addition to the regular bulk-fluid properties, the cross-sectional averaged specific heat and the corresponding averaged Prandtl number, which are used in various supercritical heat-transfer correlations (for details, see Pioro and Duffey (2007)), are shown in Figure A.2 for reference purposes. The coolant pressure used in the calculations was 25 MPa, and thus the pseudocritical temperature which corresponds to this pressure is 384.9°C. The bulk-fluid temperature was calculated based on the method of heat balances.

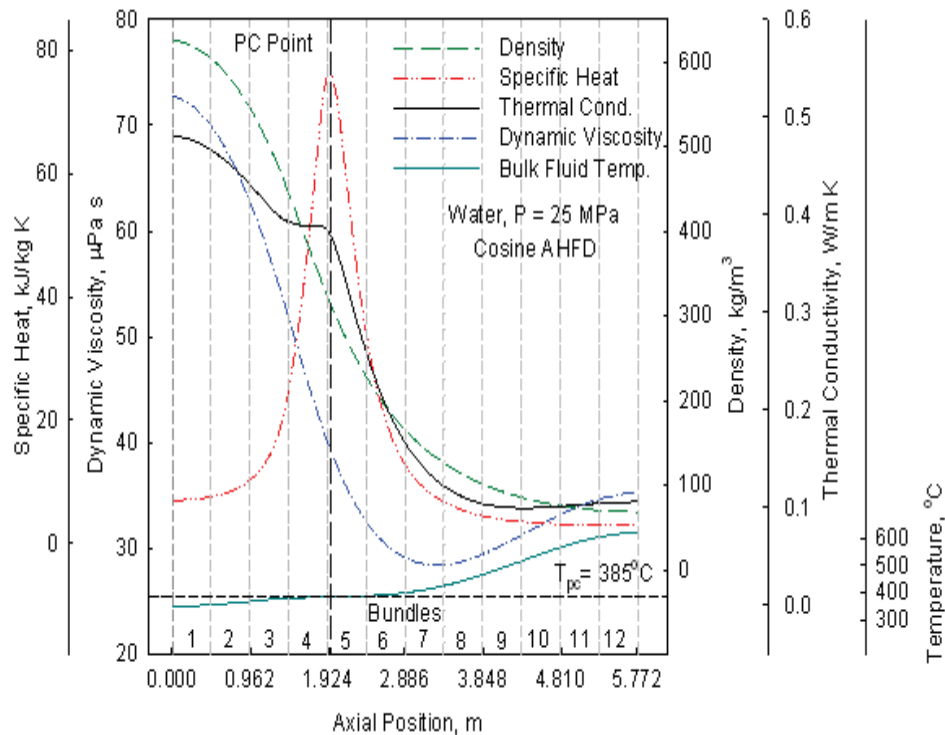


**Figure A.1. Bulk-Fluid Temperature and Thermophysical Properties Profiles for Water along Heated Length of SCWR Fuel-Channel (Mokry et al., 2009c).**

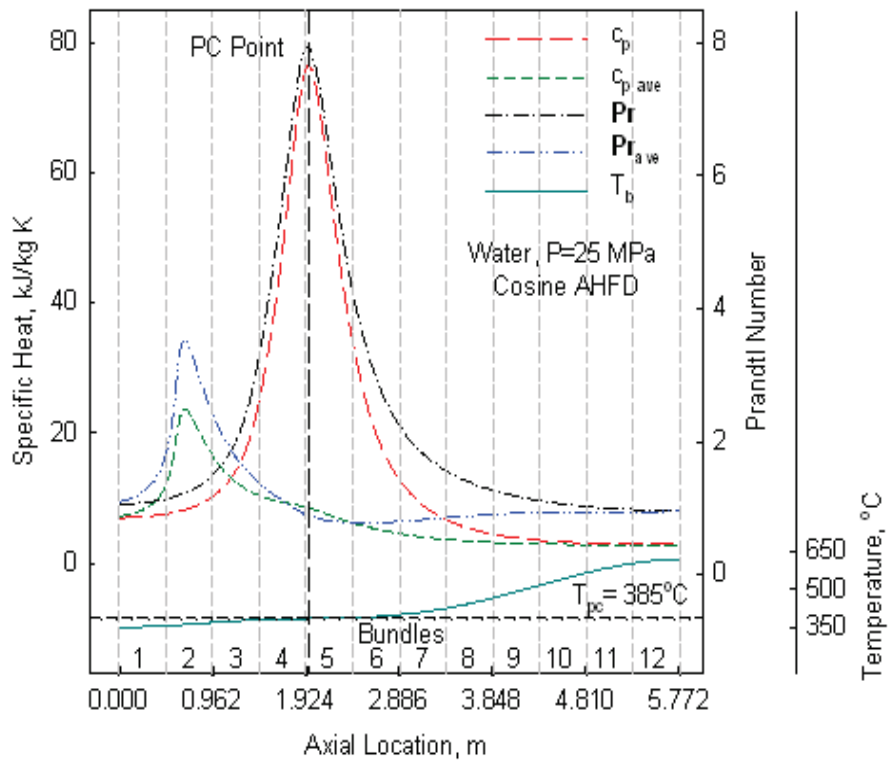


**Figure A.2. Prandtl Number and Specific Heat Profiles for Water along Heated Length of SCWR Fuel-Channel (Mokry et al., 2009c).**

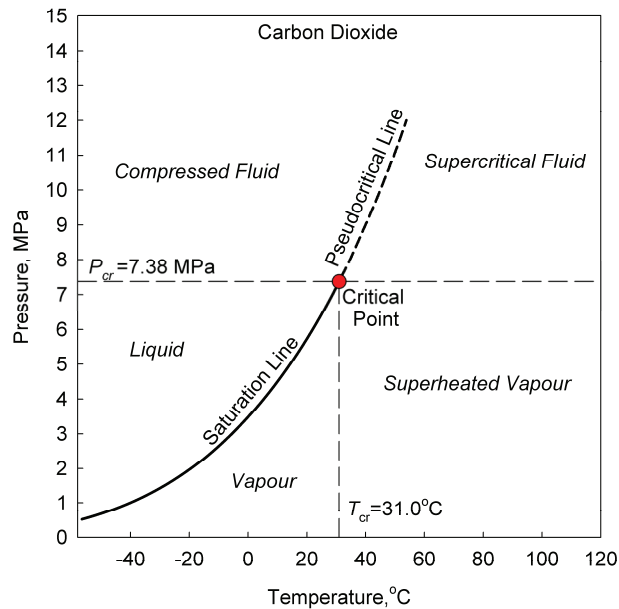


**Figure A.3. Pressure-Temperature Diagram for Carbon Dioxide (Mokry et al., 2009c).**

Compared to existing CANDU's, the SCWR (Pioro and Duffey, 2007) would involve increasing the coolant outlet pressure from 10 MPa to about 25 MPa, the inlet temperature from 260°C to about 350°C, and the outlet temperature from 310°C to 625°C. The coolant would pass through its pseudocritical temperature before reaching the channel outlet.

Preliminary parameters used for scaling nominal operating conditions of SCWRs (see Table 4.3) to carbon dioxide-equivalent values are listed in Table A.1. These scaling parameters (Pioro and Duffey, 2007) were deduced from those proposed by Jackson and Hall (1979) and Gorban' et al. (1990).

All thermophysical properties were calculated using the NIST REFPROP software (2008).

**Table A.1. Basic scaling parameters for fluid-to-fluid modeling at supercritical conditions (Mokry et al., 2009c).**

<b>Pressure</b>	$\left( \frac{P}{P_{cr}} \right)_{CO_2} = \left( \frac{P}{P_{cr}} \right)_W$
<b>Bulk-fluid temperature (K)</b>	$\left( \frac{T_b}{T_{cr}} \right)_{CO_2} = \left( \frac{T_b}{T_{cr}} \right)_W$

Table A.2 lists the critical parameters and nominal operating parameters of the supercritical water CANDU reactor concept in water and CO<sub>2</sub>-equivalent values.

**Table A.2. Critical and nominal operating parameters (Mokry et al., 2009c).**

Parameter	Unit	Water	CO <sub>2</sub>
<b>Critical parameters</b>			
Critical pressure	MPa	22.1	7.38
Critical temperature	°C	374.1	31.0
Critical density	kg/m <sup>3</sup>	315	468
<b>Operating parameters</b>			
Operating pressure	MPa	25	8.34
Inlet temperature	°C	350	20
Outlet temperature	°C	625	150

Carbon dioxide-equivalent operating parameters were used as a reference for the test matrix. The mass flux and heat flux were not scaled, because these parameters will be varied over different ranges.

Supercritical fluids have unique properties (Pioro and Duffey., 2007). Beyond the critical point, the fluid resembles a dense gas. Crossing from high-density fluid to low-density fluid does not involve a distinct phase change at these conditions. Phenomena such as dryout (critical heat flux) are therefore not relevant. However, at supercritical conditions, deteriorated heat transfer, i.e., lower HTC values compared to those of normal heat transfer, may exist (Duffey and Pioro, 2007).

### A.1 Thermophysical Properties of Supercritical Carbon Dioxide

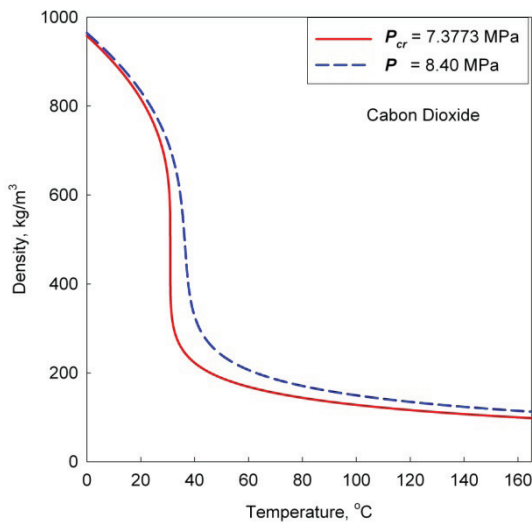
Figure A.4(a-i) of carbon dioxide (CO<sub>2</sub>) show thermophysical properties variations near the critical point and pseudocritical point, at a pressure which is equivalent to the water pressure of 25 MPa ( $p / p_{cr} = 1.133$ ). Data in these figures was obtained using the NIST REFPROP software, with temperature increments of

0.01°C. In these figures, the solid lines represent critical pressure properties while dashed lines represent pseudocritical pressure properties (for details, see Table A.3). The height of the peaks in specific heat, thermal conductivity, volume expansivity and Prandtl number in the critical and pseudocritical region near the critical point may vary with different temperature increment values.

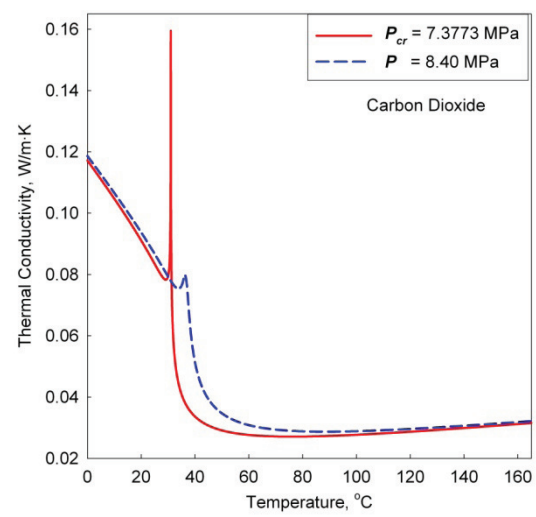
**Table A.3. Critical and pseudocritical (at  $p / p_{cr} = 1.133$ ) parameters comparison of water and carbon dioxide (based on NIST (2007)).**

Fluid	Type of Parameters	P, MPa	T, °C	H <sub>b</sub> , kJ/kg
<b>Water</b>	Critical	22.064	373.95	2146.6
	Pseudocritical	25	384.90	2152.2
<b>Carbon Dioxide</b>	Critical	7.3773	30.98	342.39
	Pseudocritical	8.36	36.60	340.75

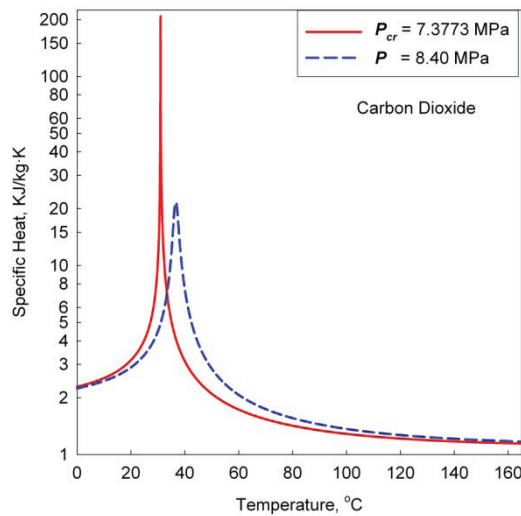
Figure A.4. shows major properties of carbon dioxide at a pressure of 8 MPa within the pseudocritical region. As it can be seen from the figure, density and viscosity sharply drop as they pass through the pseudocritical point. In general, thermal conductivity also experiences a drop. However, it exhibits a small peak at the pseudocritical point, and experiences a less drastic drop. Specific heat has a large peak in the pseudocritical point, but remains fairly constant outside the pseudocritical region.



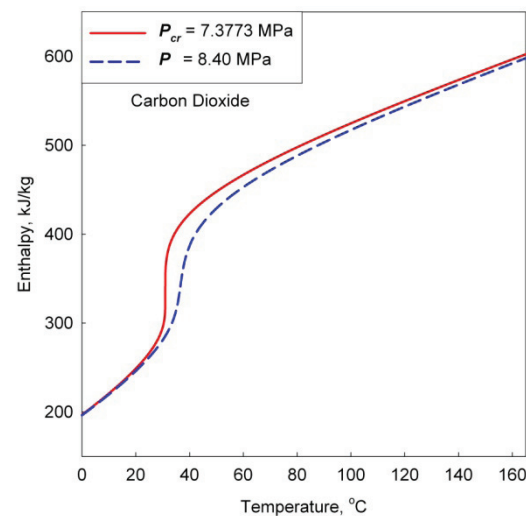
(a) Density vs. Temperature



(b) Thermal Conductivity vs. Temperature

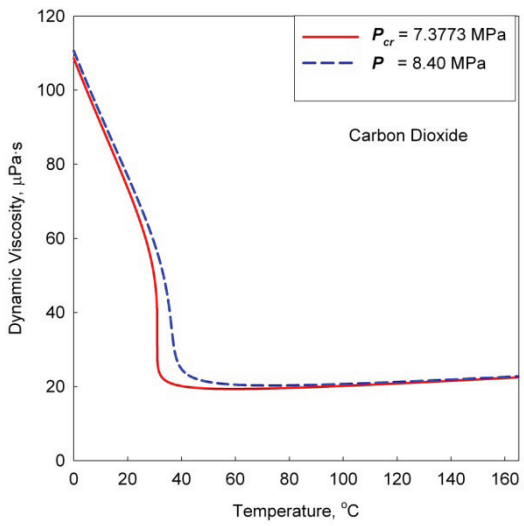


(c) Specific Heat vs. Temperature

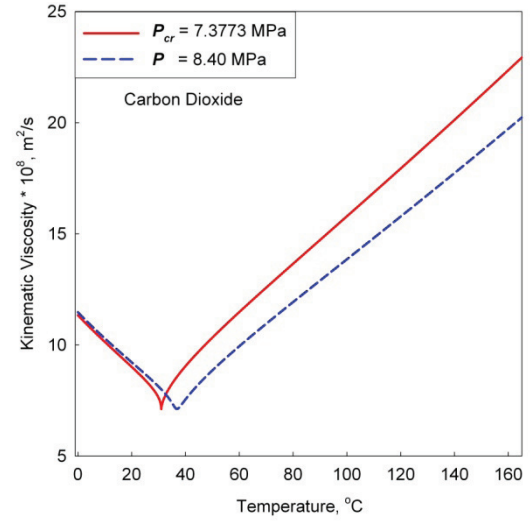


(d) Specific Enthalpy vs. Temperature

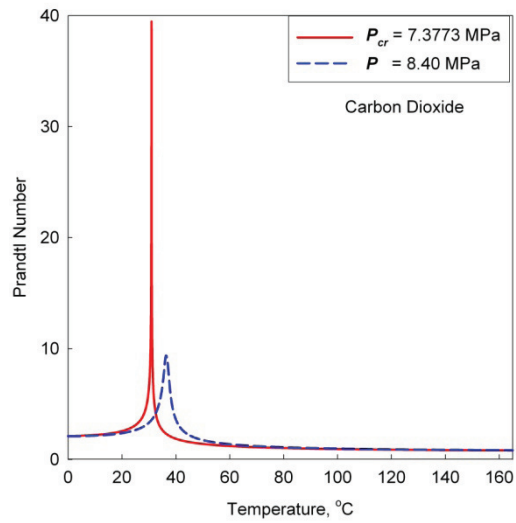
**Figure A.4 (a-d). Basic Thermophysical Properties of Carbon Dioxide Near the Critical and Pseudocritical Point (Mokry et al., 2009c).**



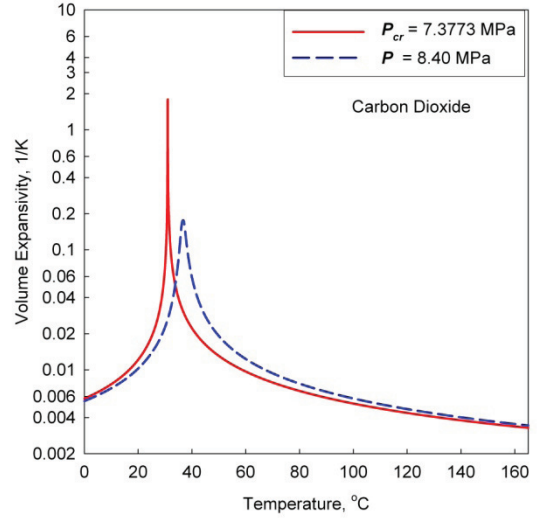
(e) Dynamic Viscosity vs. Temperature



(f) Kinematic Viscosity vs. Temperature

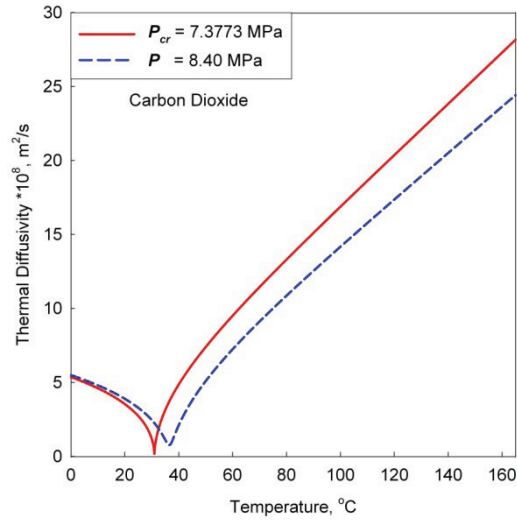


(g) Prandtl Number vs. Temperature



(h) Volume Expansivity vs. Temperature

**Figure A.4 (e-h). Basic Thermophysical Properties of Carbon Dioxide Near the Critical and Pseudocritical Point (Mokry et al., 2009c).**



(i) Thermal Diffusivity vs. Temperature

**Figure A.4 (i).** Basic Thermophysical Properties of Carbon Dioxide Near the Critical and Pseudocritical Point (Mokry et al., 2009c).

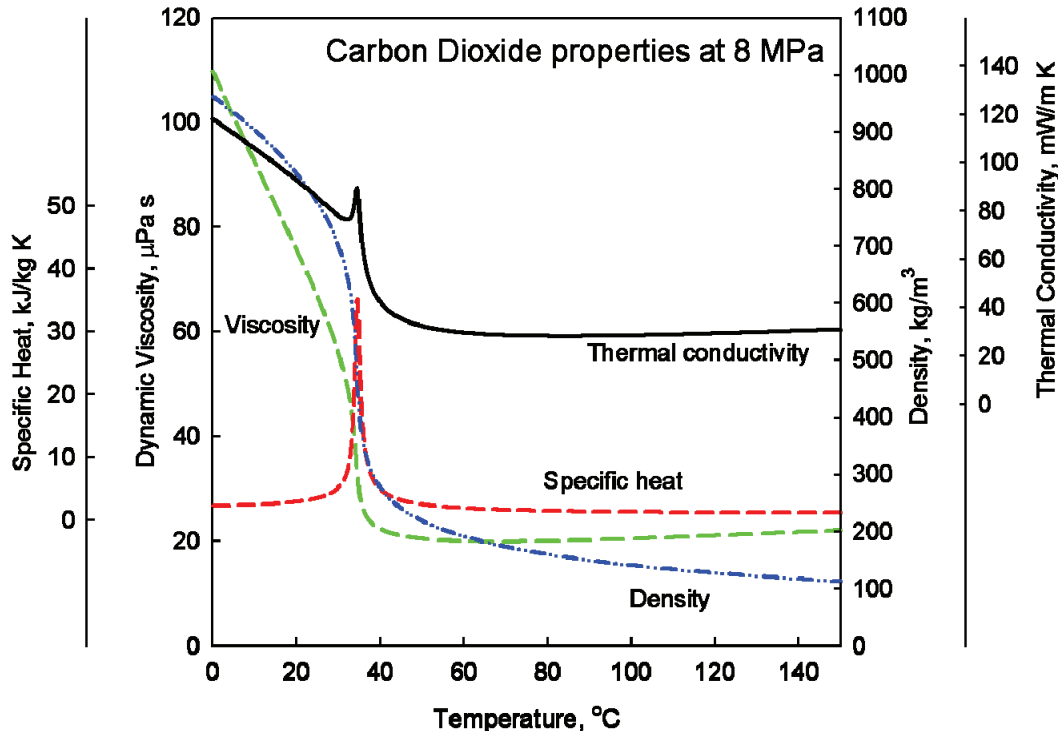


**Figure A.5.** Basic Thermophysical Properties of Carbon Dioxide across the Pseudocritical Point (Mokry et al., 2009c).

## A.2 Supercritical CO<sub>2</sub> Test Facility

The MR-1 loop is a high-temperature and high-pressure pumped loop (for more details, see Pioro and Duffey (2007) and Pioro and Khartabil (2005)). The operating pressure range is up to 10 MPa at temperatures up to 310°C. Carbon dioxide (99.9% purity, content of hydrocarbons 0.8 ppm) was charged into the loop. The fluid passed from the pump, through an orifice flowmeter, a preheater, a test section, a cooler and back to the pump. Pressurization was achieved by applying electrical power to the heating elements in two vessels – pressurizer.

The CO<sub>2</sub> fluid passed through a 25-kW electrical preheater before flowing into the test section. The test section was installed vertically with an upward flow of carbon dioxide. The test section design consisted of a 2.4-m-long, 8-mm-ID, Inconel-600 tube. The heated length was 2.208 m. The diameter of the test section was close to the equivalent-hydraulic diameter of a SCWR fuel bundle.

The instrumentation used to measure the loop parameters was thoroughly checked and calibrated. Uncertainties of primary parameters are summarized in Table A.4 (for details on the uncertainties and their estimation, see Pioro and Duffey, 2007).

**Table A. 4. Uncertainties of primary parameters (Pioro and Duffey, 2007).**

Parameter	Uncertainty
Test-section power	±0.5%
Outlet pressure	±0.2%
Local pressure drops	±0.8% at $\Delta P = 30$ kPa ±5.0% at $\Delta P = 5$ kPa
Temperatures	±0.3°C within 0 – 100°C ±2.2°C beyond 100°C
Mass-flow rate	±0.9% at 155 g/s ( $G=3084$ kg/m <sup>2</sup> s) ±8.2% at 46 g/s ( $G=915$ kg/m <sup>2</sup> s)

### A.3 Data Reduction

The data reduction procedure is based on local parameters, which were measured or calculated at each cross section corresponding to the external wall thermocouples. The external wall temperatures, inlet- and outlet-bulk-fluid temperatures and electrical current were used as the basis for local parameter calculations. These local parameters include thermal conductivity and electrical resistivity of the wall material, electrical resistance, power, heat flux, volumetric heat flux, internal wall temperature, heat loss, bulk-fluid temperature and pressure. The general and local parameters are defined as follows.

**Table A.5. Test Matrix for the Experimental Data (Mokry et al., 2009c).**

No of points	$P_{out}$	Mass flux	$T_{in}$	$T_{out}$	Heat flux
—	MPa	kg/m <sup>2</sup> s	°C	°C	kW/m <sup>2</sup>
158	7.36	900, 2000	25, 30	29–82	37.4–447
129		2000	21	29–94	115–480
664		295–2060	21–30	35–124	16–225
598		900, 2780–3200	25–40	32–139	26.5–616
416		1500, 2020	30–40	33–131	30–460
581		784–2000	20–40	39–120	221–466
182		750	31–40	35–136	18–209
108	8.8	900, 2000	31	37–107	28–225
181	8.83	2002, 3020	30	35–89	30–536

### A.4 Experimental Results

Experimental results in supercritical carbon dioxide are summarized in Figures A.6 – A.14 (Mokry et al., 2009c). The data shown in these figures are average values over a one-minute scan at nominal test flow conditions. Experimental data obtained at other operating parameters are shown in Pioro and Duffey (2007) and Pioro and Khartabil (2005).

In general, the following supercritical heat-transfer cases were covered:

Within a certain heated length –  $T_w^{in} < T_{pc}$ ,  $T_w^{in} = T_{pc}$ ,  $T_w^{in} > T_{pc}$  and  $T_b < T_{pc}$ ;  
 $T_w^{in} > T_{pc}$  and within a certain heated length  $T_b < T_{pc}$  and  $T_b = T_{pc}$ ;  
 $T_w^{in} > T_{pc}$  and within a certain heated length  $T_b < T_{pc}$ ,  $T_b = T_{pc}$  and  $T_b > T_{pc}$ ; and  
 $T_w^{in}$  and  $T_b > T_{pc}$ .

Within a short entrance region, the wall temperature rises sharply. This is probably due to the thermal boundary layer development.

Some thermocouples (see Figure A.6) show slightly lower temperature than the neighboring thermocouples just upstream. These thermocouples were located near the pressure drop impulse lines, which affect the wall-temperature measurements just downstream. Structural supports of the test section have no visible impact on wall-temperature measurements.

In general, experimental data of supercritical carbon dioxide obtained at higher mass fluxes show good agreement between the calculated value of the last downstream bulk-fluid temperature, which was calculated from incremental heat balances, and the measured outlet bulk-fluid temperature just downstream of the outlet mixing chamber.

However, at lower mass flux ( $G = 900 \text{ kg/m}^2\text{s}$ ) and with heat flux increase, the difference between the measured and calculated outlet bulk-fluid temperatures increases (see Figures A.8d and A.10d). This is due to the increased measurement uncertainty at low mass-flow rates (see Table A.4). In general, the difference between the measured and calculated outlet bulk-fluid temperatures was less than 10%.

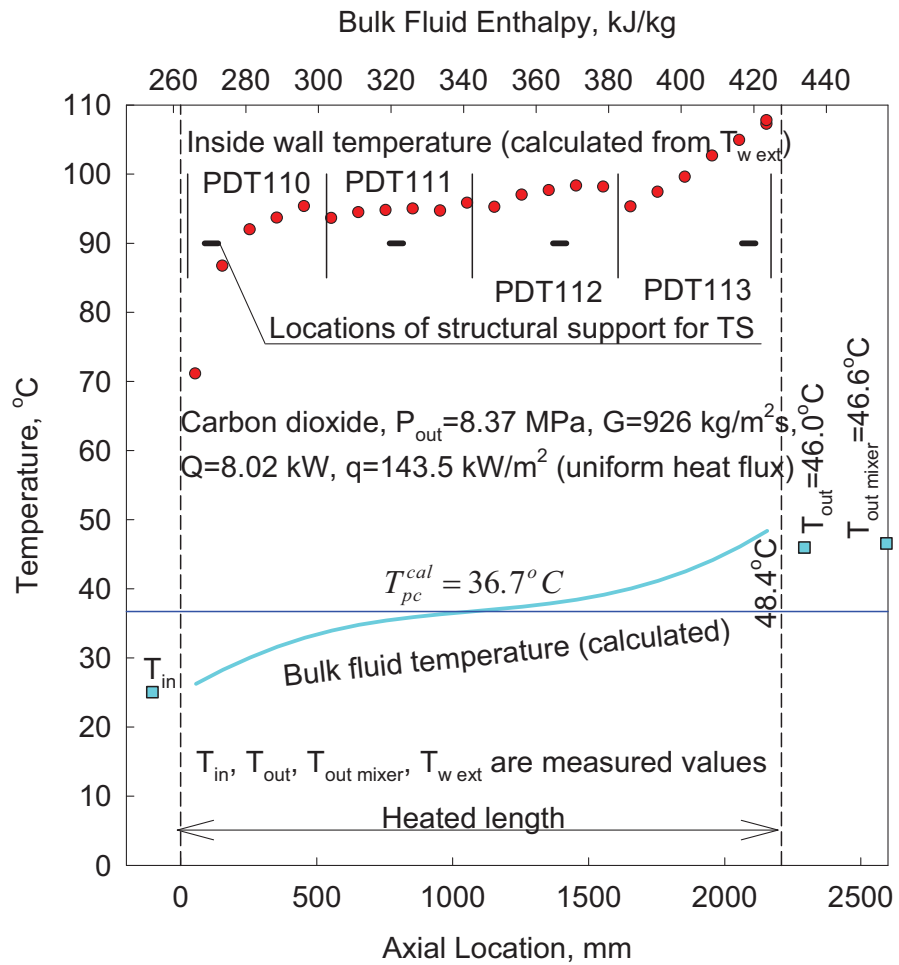


**Figure A.6. Temperature Variations along the Test Section at  $P_{out}=8.37 \text{ MPa}$  and  $G=926 \text{ kg/m}^2\text{s}$  (Mokry et al., 2009c).**

At high bulk-fluid outlet temperatures, the bulk-fluid temperature measured at the test section outlet was found to be lower than the temperature measured just downstream of the outlet mixing chamber (see Figures A.8d, A.9e, A.11e, A.13e,f, A.14c,d). This disagreement shows that mixing chambers improve bulk-fluid temperature uniformity in a cross section.

Some figures, for example Figures A.8d, A.9c,d,f, A.11f and A.12e show evidence of deteriorated heat transfer over a certain section of the tube. In

general, these observations are similar to those reported in the literature (Pioro and Duffey, 2007).

### A.5 Developing the Correlation

The general form of a heat-transfer correlation is:

$$y = C_o \times t_1^{C_1} t_2^{C_2} \dots t_n^{C_n} \quad (\text{A.1})$$

The desired parameter for the correlation is the HTC. Taking into consideration major parameters that play a role in convective heat transfer, the correlation then takes on the following form:

$$\text{Nu} = C_o \times \text{Re}^{C_1} \overline{\text{Pr}}^{C_2} \left( \frac{\rho_w}{\rho_b} \right)^{C_3} \dots t_n^{C_n} \quad (\text{A.2})$$

Nusselt, Reynolds and averaged Prandtl numbers are the basic key parameters involved in forced convection heat transfer. The ratio of density of the fluid at the wall temperature to the density of fluid at the bulk-fluid temperature was added to account for a large temperature gradient in the cross-section, and was calculated through iterations.

The coefficient  $C_o$  and the exponents  $C_1$ ,  $C_2$ , etc. needed to be determined, and it was necessary to check for additional terms that might affect the HTC.

### A.6 Finalizing Correlation

As a result of the experimental-data analysis, the following preliminary correlation for heat transfer to supercritical carbon dioxide was obtained:

$$\text{Nu}_b = 0.0345 \text{Re}_b^{0.77} \overline{\text{Pr}}_b^{0.17} \left( \frac{\rho_w}{\rho_b} \right)^{0.47} \quad (\text{A.3})$$

To finalize the development of the correlation, the complete set of primary data and Eq. (A.3) were fed into the SigmaPlot Dynamic Fit Wizard to perform final

adjustments. The final correlation is as follows:

$$\text{Nu}_b = 0.0121 \text{Re}_b^{0.86} \overline{\text{Pr}}_b^{0.23} \left( \frac{\rho_w}{\rho_b} \right)^{0.59} \quad (\text{A.4})$$

Figure A.7 shows a scatter plot of the experimental HTC versus the calculated HTC, according to Eq. (A.4). The data lies along a 45-degree line, with a spread of  $\pm 50\%$ . Due to this relatively high uncertainty, more thorough analysis of the experimental data is required.

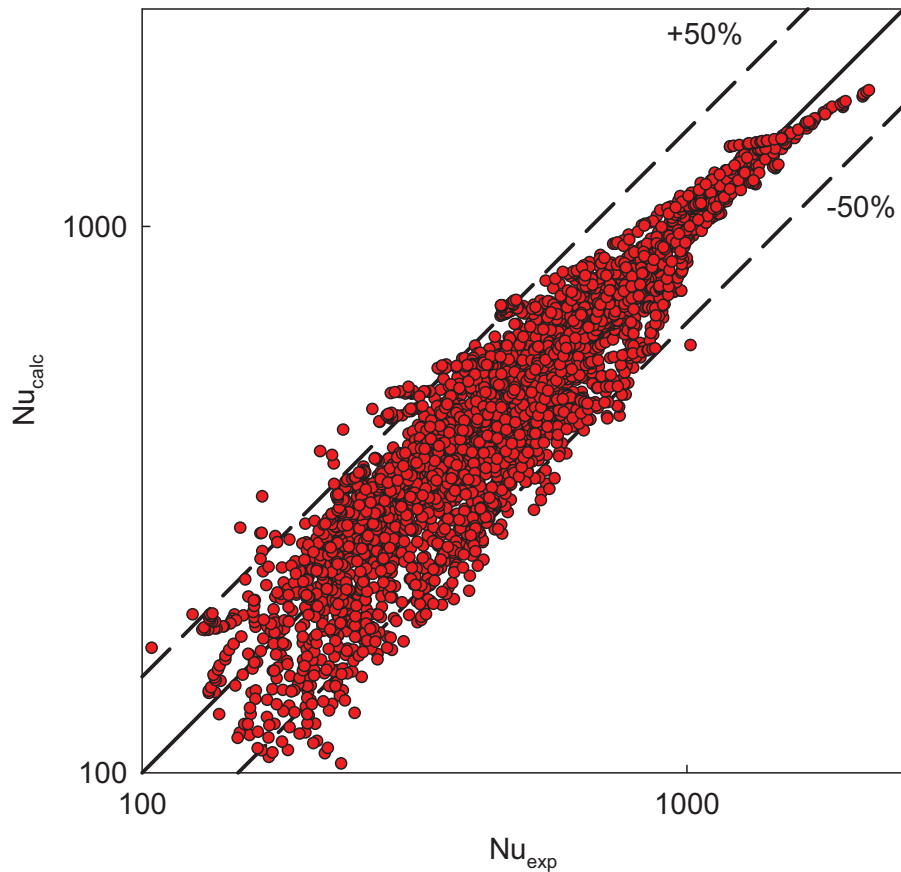


**Figure A.7. Verification of the Final Correlation (Mokry et al., 2009c).**

## A.7 Conclusions

Supercritical carbon dioxide heat-transfer data were obtained at three pressures above the critical point (7.6, 8.4 and 8.8 MPa), mass fluxes from 840 to 3000 kg/m<sup>2</sup>s, heat fluxes up to 600 kW/m<sup>2</sup> and inlet temperatures from 20 to 40°C. These conditions, scaled into water-equivalent values, are relevant to SCWR flow conditions.

Supercritical heat transfer was investigated for several combinations of wall and bulk-fluid temperatures, i.e., internal-wall temperatures and bulk-fluid temperatures below, at or above the pseudocritical temperature.

Two modes of heat transfer at supercritical pressures have been observed: normal and deteriorated heat transfer. The latter was observed within the entrance region and near the middle of the test section. The deteriorated heat transfer regime is characterized by higher wall temperatures (lower HTC values) than the normal heat transfer regime. This phenomenon is affected by pressure, bulk-fluid temperature, mass flux and heat flux.

The obtained correlation for forced convective heat transfer to supercritical carbon dioxide, in a bare vertical tube with upward flow, showed a reasonable fit for the analyzed dataset. This correlation can be used for future comparisons with other independent datasets and for the verification of scaling parameters between water and CO<sub>2</sub>.

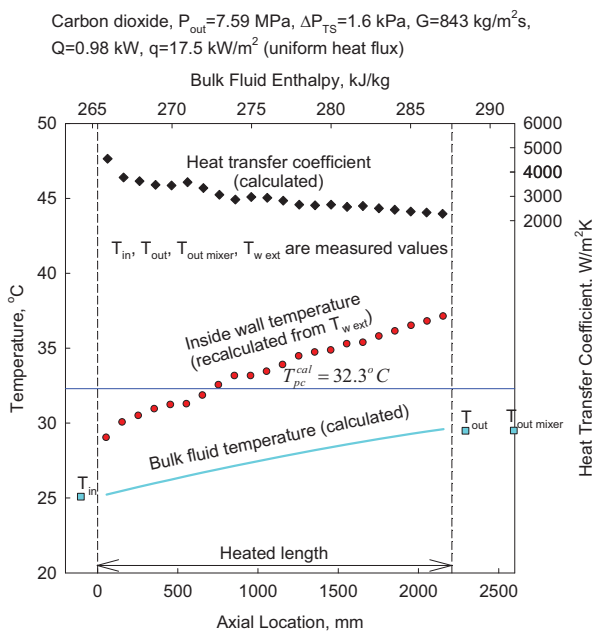


**Figure A.8a. Temperature Variations along Test Section at  $P_{out}=7.59$  MPa and  $G=843 \text{ kg/m}^2\text{s}$ .**

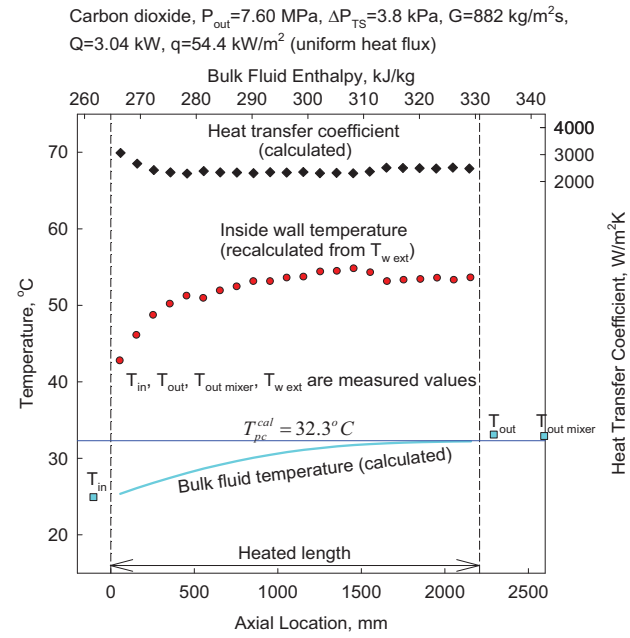


**Figure A.8b. Temperature Variations along Test Section at  $P_{out}=7.60$  MPa and  $G=882 \text{ kg/m}^2\text{s}$ .**

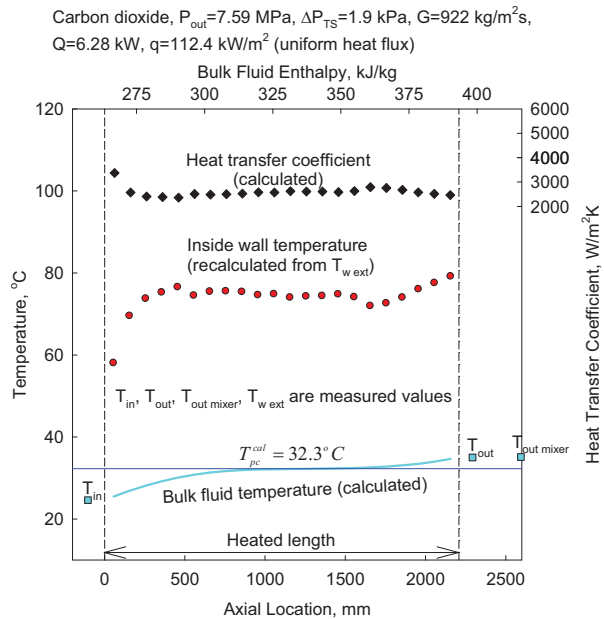


**Figure A.8c. Temperature Variations along Test Section at  $P_{out}=7.59$  MPa and  $G=922 \text{ kg/m}^2\text{s}$ .**

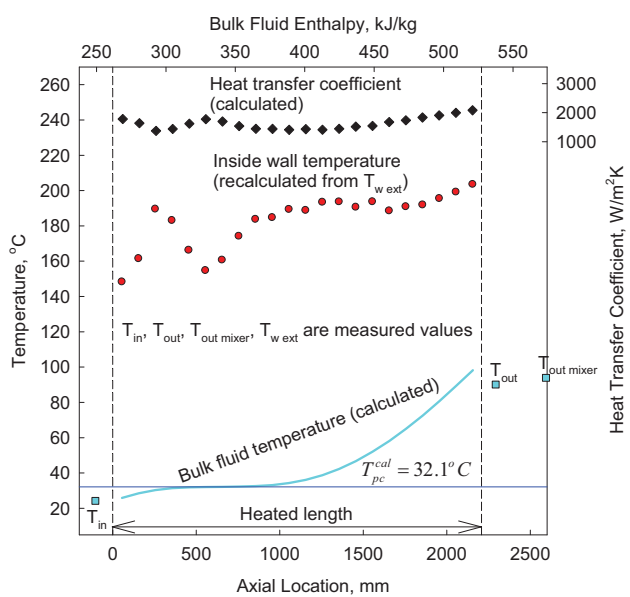


**Figure A.8d. Temperature Variations along Test Section at  $P_{out}=7.57$  MPa and  $G=902 \text{ kg/m}^2\text{s}$ .**

Carbon dioxide,  $P_{out}=7.59$  MPa,  $\Delta P_{TS}=7.3$  kPa,  $G=2000$  kg/m<sup>2</sup>s,  
 $Q=2.1$  kW,  $q=37.6$  kW/m<sup>2</sup> (uniform heat flux)

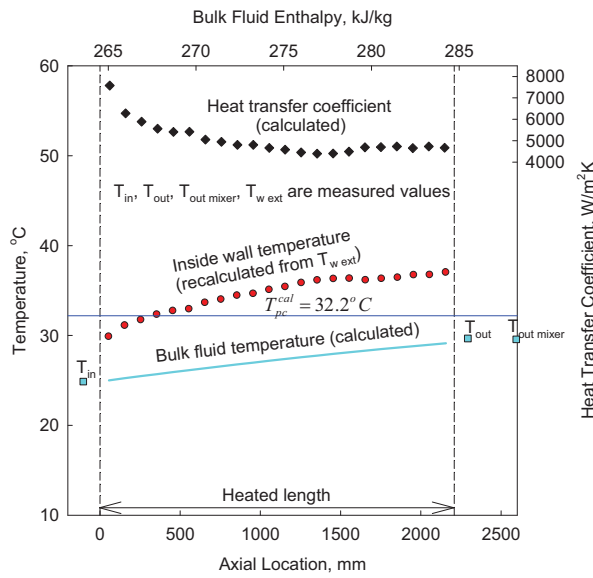


**Figure A.9a. Temperature Variations along Test Section at  $P_{out}=7.59$  MPa and  $G=2000$  kg/m<sup>2</sup>s.**

Carbon dioxide,  $P_{out}=7.59$  MPa,  $\Delta P_{TS}=9.3$  kPa,  $G=2000$  kg/m<sup>2</sup>s,  
 $Q=5.9$  kW,  $q=105.6$  kW/m<sup>2</sup> (uniform heat flux)

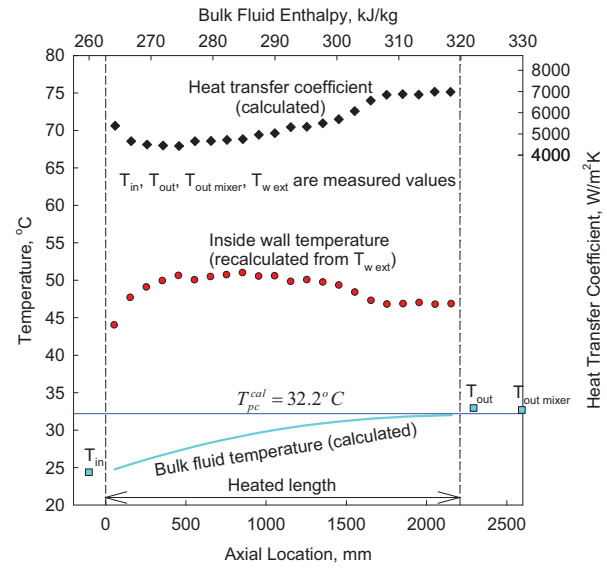


**Figure A.9b. Temperature Variations along Test Section at  $P_{out}=7.59$  MPa and  $G=2000$  kg/m<sup>2</sup>s.**

Carbon dioxide,  $P_{out}=7.63$  MPa,  $\Delta P_{TS}=9.4$  kPa,  $G=2020$  kg/m<sup>2</sup>s,  
 $Q=10.24$  kW,  $q=183.2$  kW/m<sup>2</sup> (uniform heat flux)

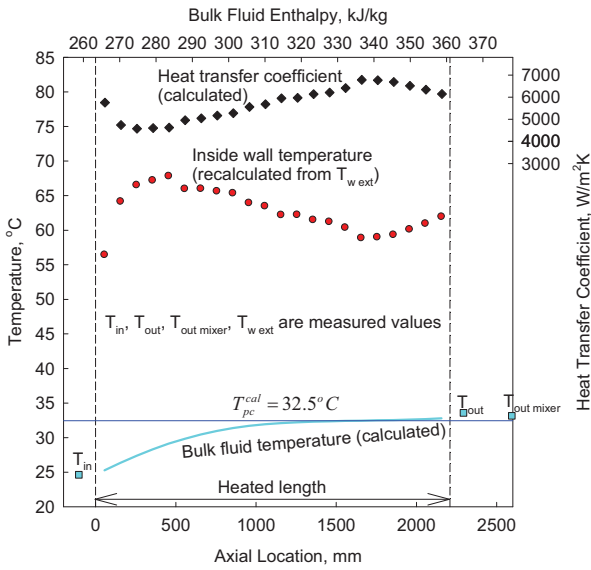


**Figure A.9c. Temperature Variations along Test Section at  $P_{out}=7.623$  MPa and  $G=2020$  kg/m<sup>2</sup>s.**

Carbon dioxide,  $P_{out}=7.58$  MPa,  $\Delta P_{TS}=6.4$  kPa,  $G=2039$  kg/m<sup>2</sup>s,  
 $Q=13.97$  kW,  $q=249.9$  kW/m<sup>2</sup> (uniform heat flux)

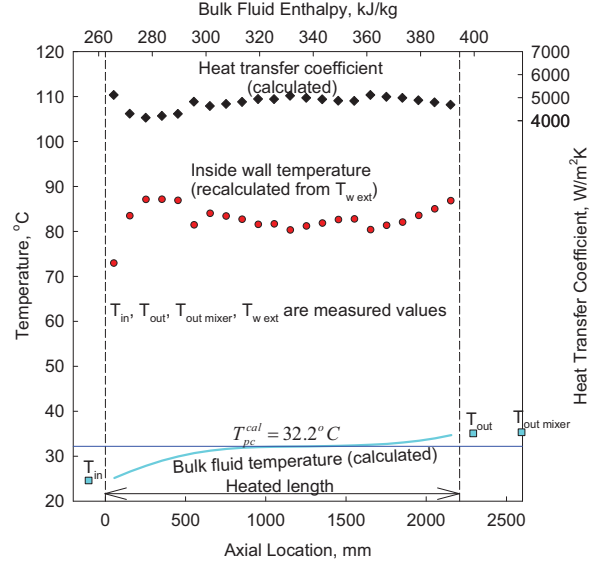


**Figure A.9d. Temperature Variations along Test Section at  $P_{out}=7.58$  MPa and  $G=2039$  kg/m<sup>2</sup>s.**

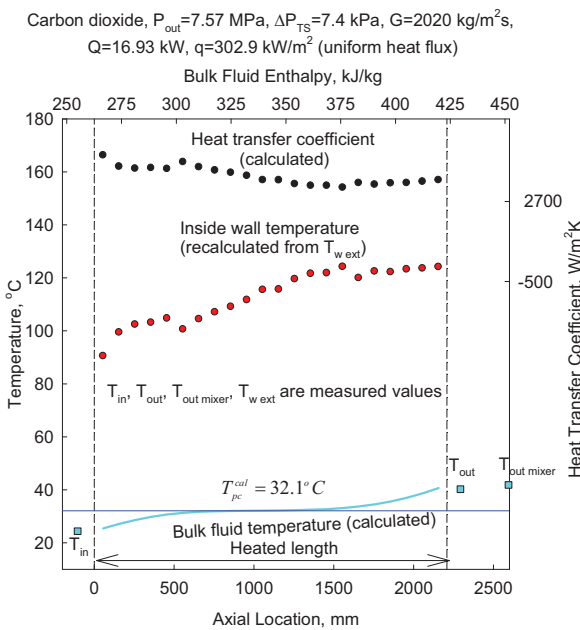


**Figure A.9e. Temperature Variations along Test Section at  $P_{out}=7.57$  MPa and  $G=2020$  kg/m<sup>2</sup>s.**

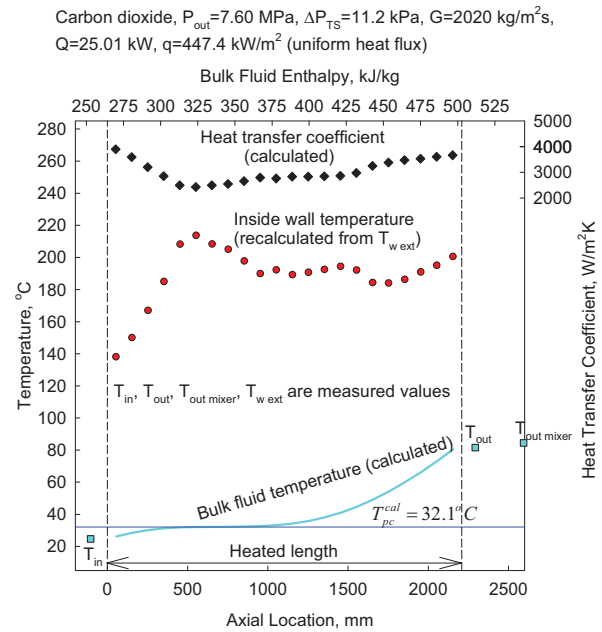


**Figure A.9f. Temperature Variations along Test Section at  $P_{out}=7.60$  MPa and  $G=2020$  kg/m<sup>2</sup>s.**

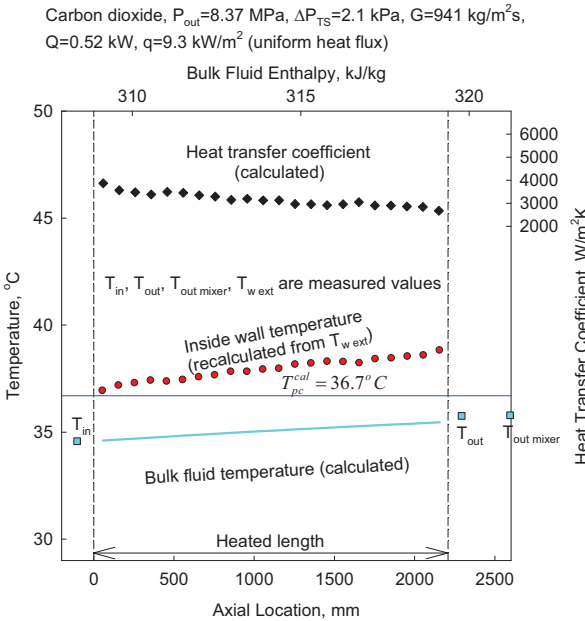


**Figure A.10a. Temperature Variations along Test Section at  $P_{out}=8.37$  MPa and  $G=941$  kg/m<sup>2</sup>s.**

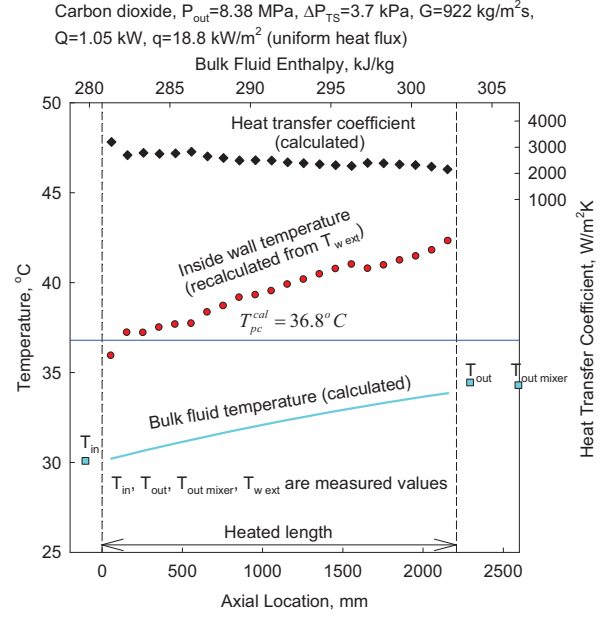


**Figure A.10b. Temperature Variations along Test Section at  $P_{out}=8.38$  MPa and  $G=922$  kg/m<sup>2</sup>s.**

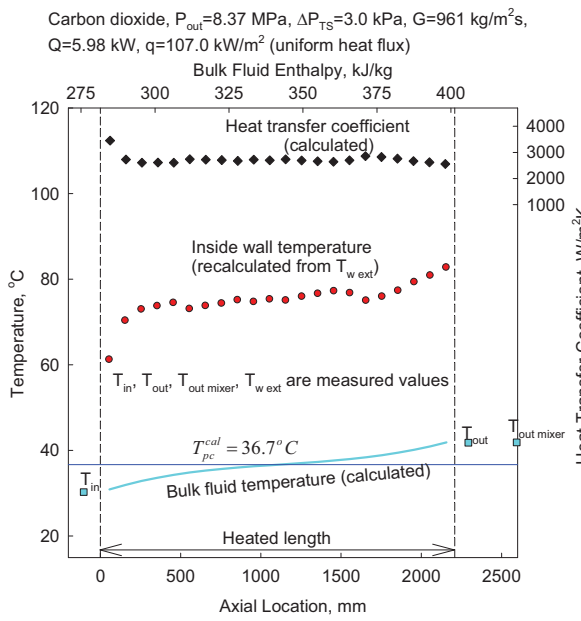


**Figure A.10c. Temperature Variations along Test Section at  $P_{out}=8.37 \text{ MPa}$  and  $G=961 \text{ kg/m}^2\text{s}$ .**

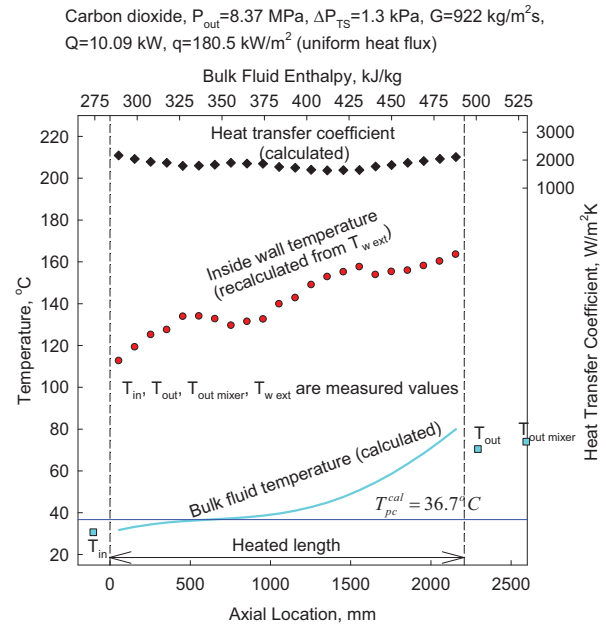


**Figure A.10d. Temperature Variations along Test Section at  $P_{out}=8.37 \text{ MPa}$  and  $G=922 \text{ kg/m}^2\text{s}$ .**

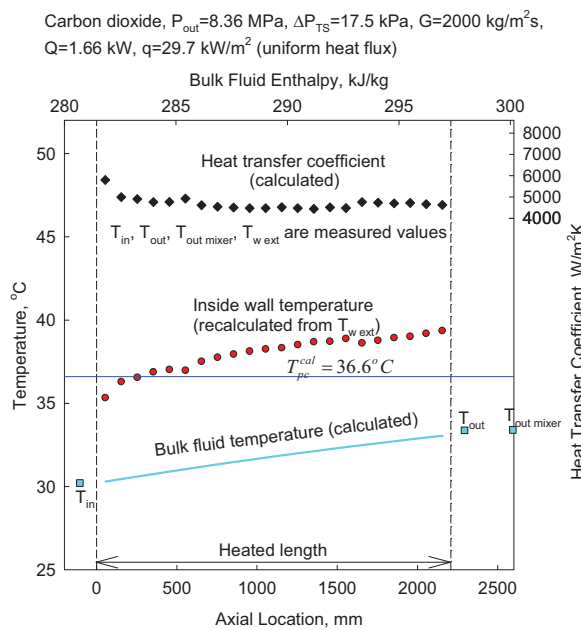


**Figure A.11a. Temperature Variations along Test Section at  $P_{out}=8.36 \text{ MPa}$  and  $G=2000 \text{ kg/m}^2\text{s}$ .**

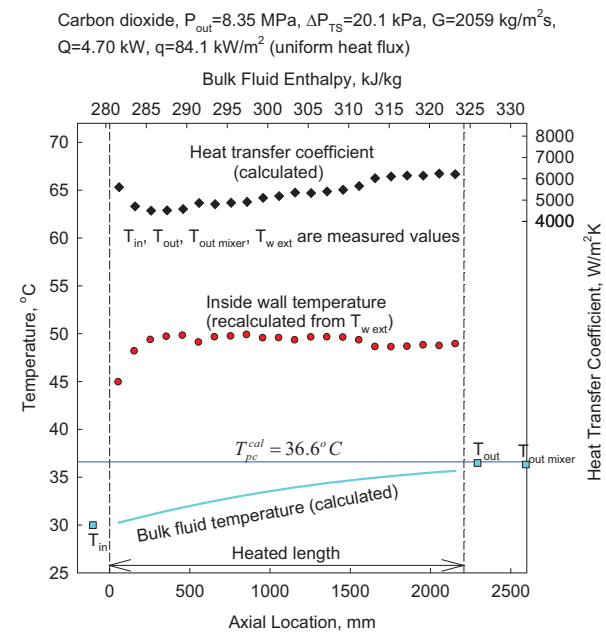


**Figure A.11b. Temperature Variations along Test Section at  $P_{out}=8.35 \text{ MPa}$  and  $G=2059 \text{ kg/m}^2\text{s}$ .**

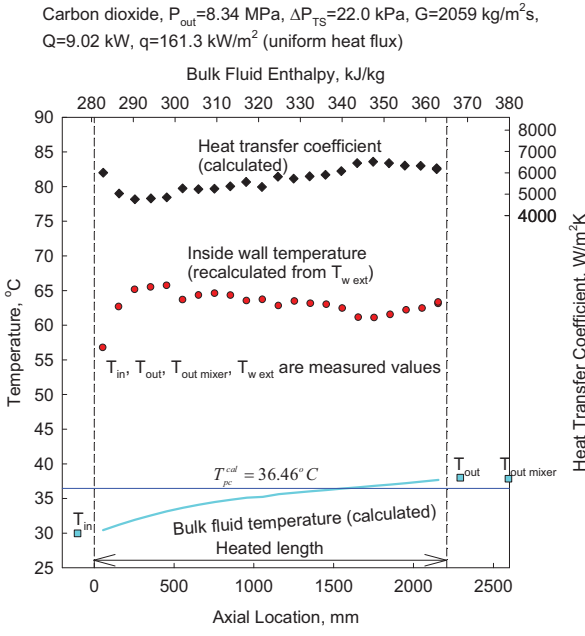


**Figure A.11c. Temperature Variations along Test Section at  $P_{out}=8.34$  MPa and  $G=2059 \text{ kg/m}^2\text{s}$ .**

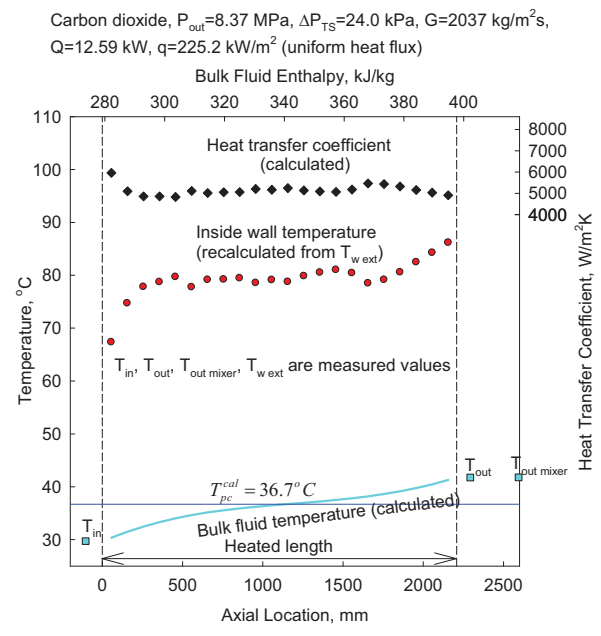


**Figure A.11d. Temperature Variations along Test Section at  $P_{out}=8.37$  MPa and  $G=2037 \text{ kg/m}^2\text{s}$ .**

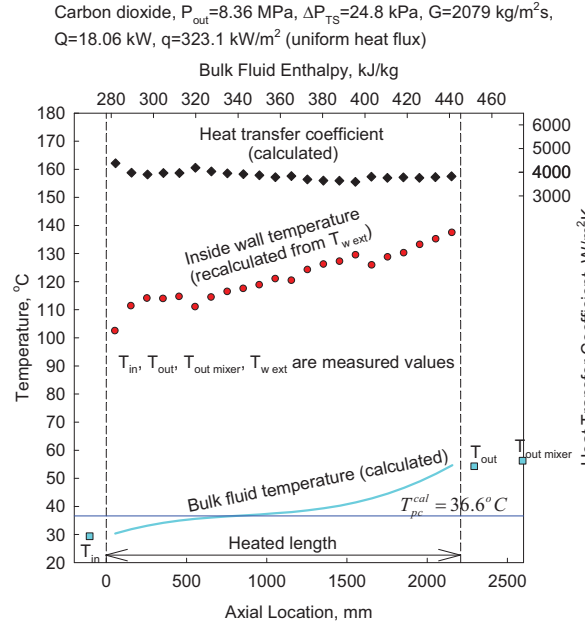


**Figure A.11e. Temperature Variations along Test Section at  $P_{out}=8.36$  MPa and  $G=2079 \text{ kg/m}^2\text{s}$ .**

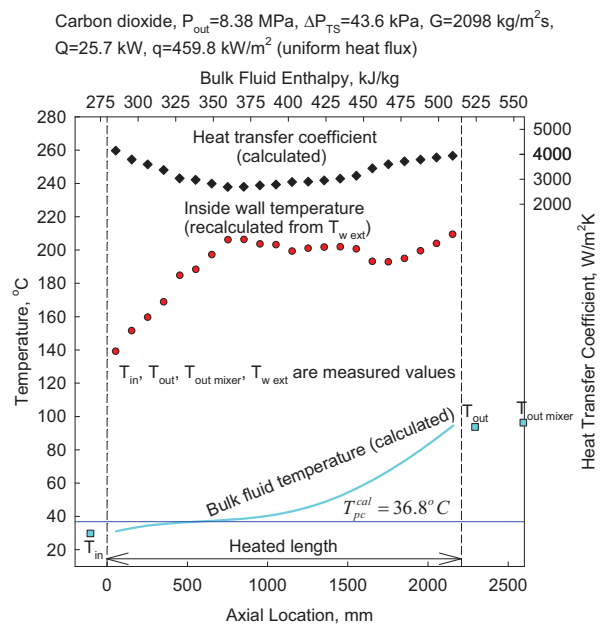


**Figure A.11f. Temperature Variations along Test Section at  $P_{out}=8.38$  MPa and  $G=2098 \text{ kg/m}^2\text{s}$ .**

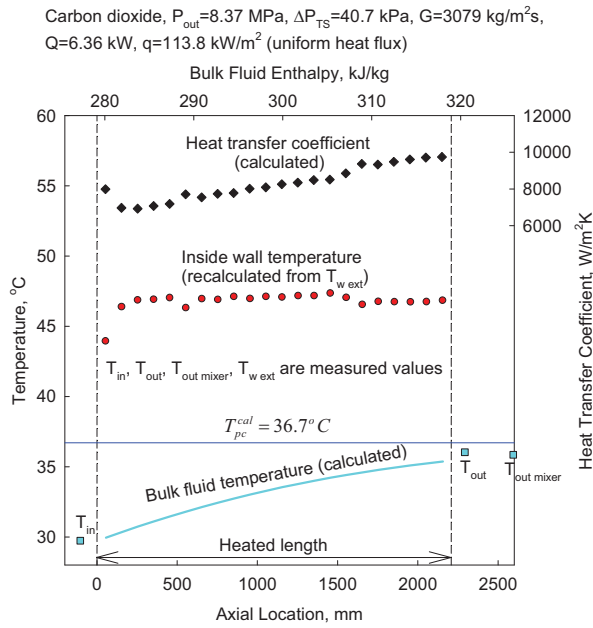


**Figure A.12a. Temperature Variations along Test Section at  $P_{out}=8.37$  MPa and  $G=3079$  kg/m<sup>2</sup>s.**

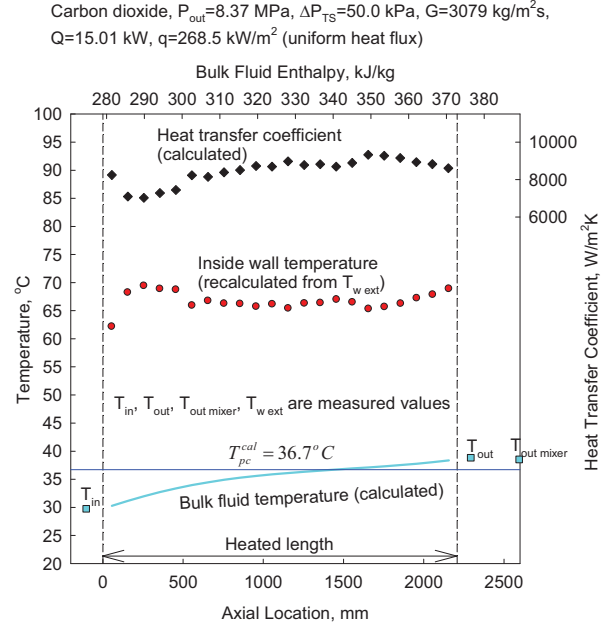


**Figure A.12b. Temperature Variations along Test Section at  $P_{out}=8.37$  MPa and  $G=3079$  kg/m<sup>2</sup>s.**

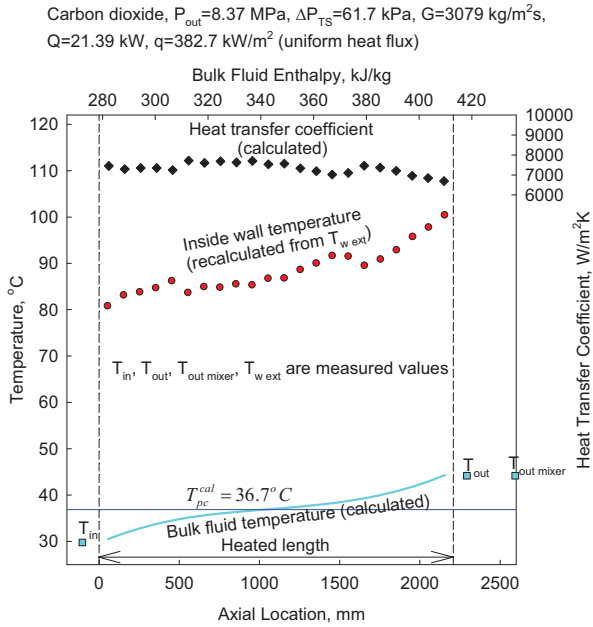


**Figure A.12c. Temperature Variations along Test Section at  $P_{out}=8.37$  MPa and  $G=3079$  kg/m<sup>2</sup>s.**

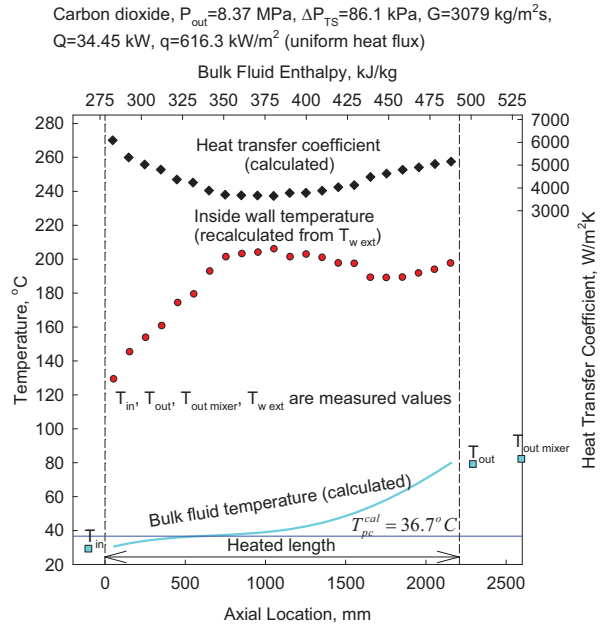


**Figure A.12d. Temperature Variations along Test Section at  $P_{out}=8.37$  MPa and  $G=3079$  kg/m<sup>2</sup>s.**

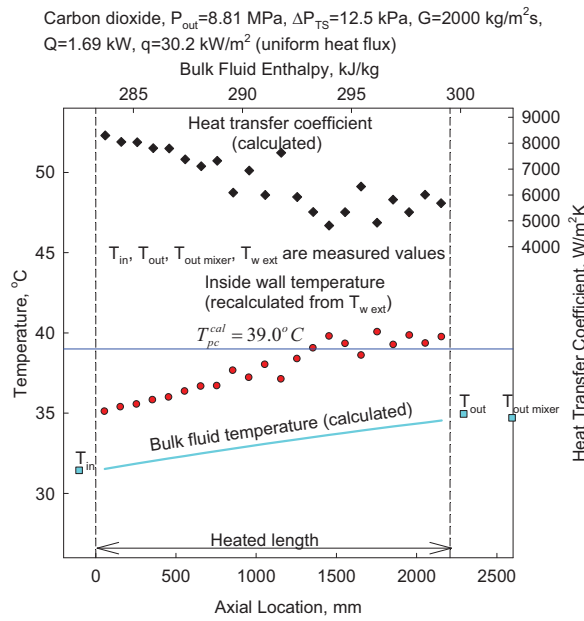


**Figure A.13a. Temperature Variations along Test Section at  $P_{out}=8.81 \text{ MPa}$  and  $G=2000 \text{ kg/m}^2\text{s}$ .**

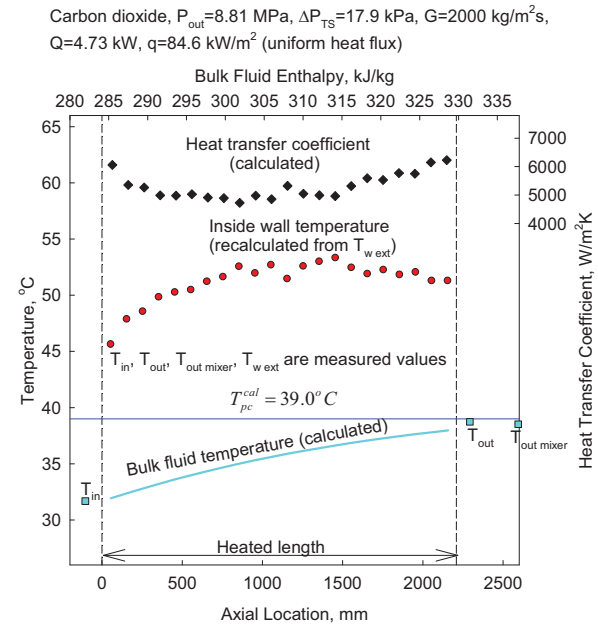


**Figure A.13b. Temperature Variations along Test Section at  $P_{out}=8.81 \text{ MPa}$  and  $G=2000 \text{ kg/m}^2\text{s}$ .**

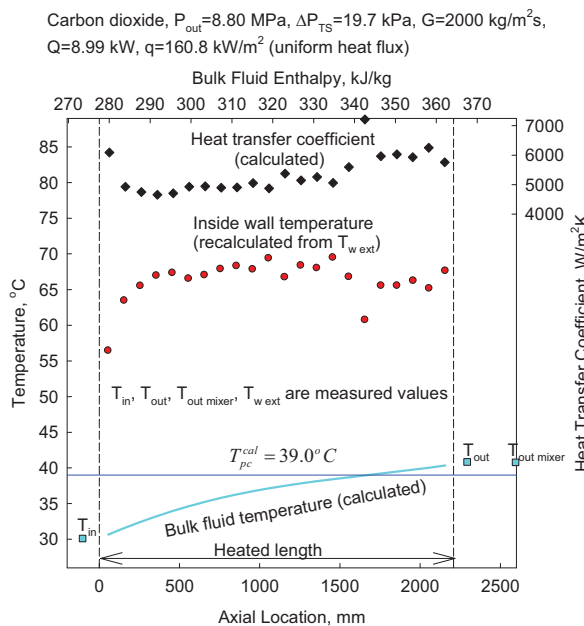


**Figure A.13c. Temperature Variations along Test Section at  $P_{out}=8.80 \text{ MPa}$  and  $G=2000 \text{ kg/m}^2\text{s}$ .**

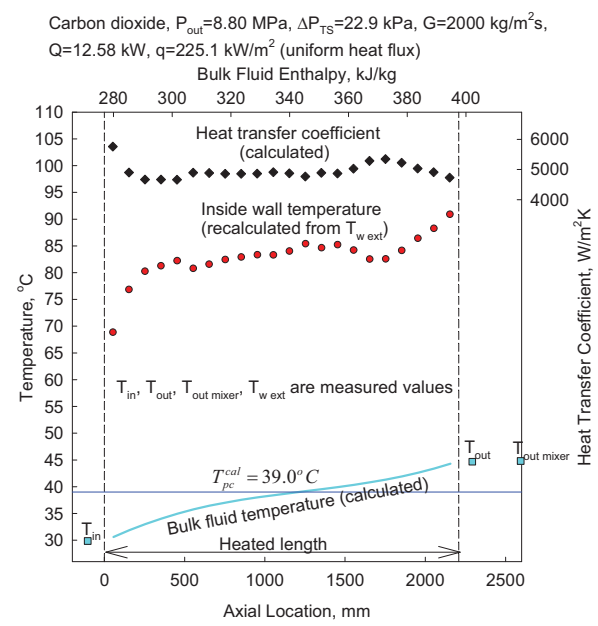


**Figure A.13d. Temperature Variations along Test Section at  $P_{out}=8.80 \text{ MPa}$  and  $G=2000 \text{ kg/m}^2\text{s}$ .**

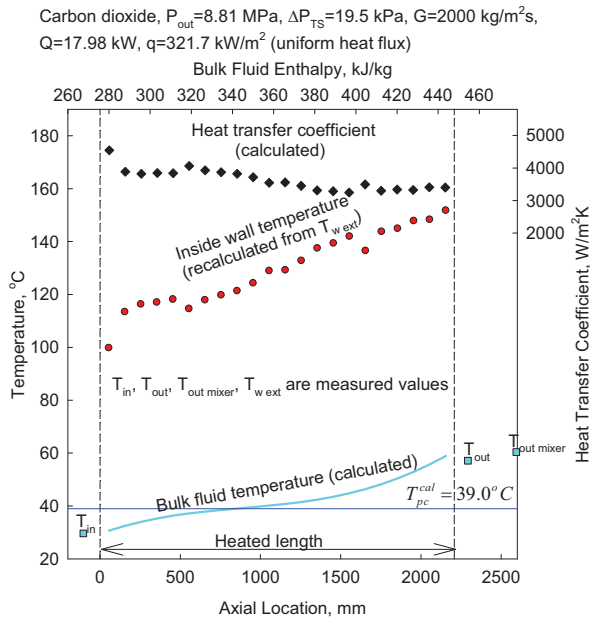


**Figure A.13e. Temperature Variations along Test Section at  $P_{out}=8.81 \text{ MPa}$  and  $G=2000 \text{ kg/m}^2\text{s}$ .**

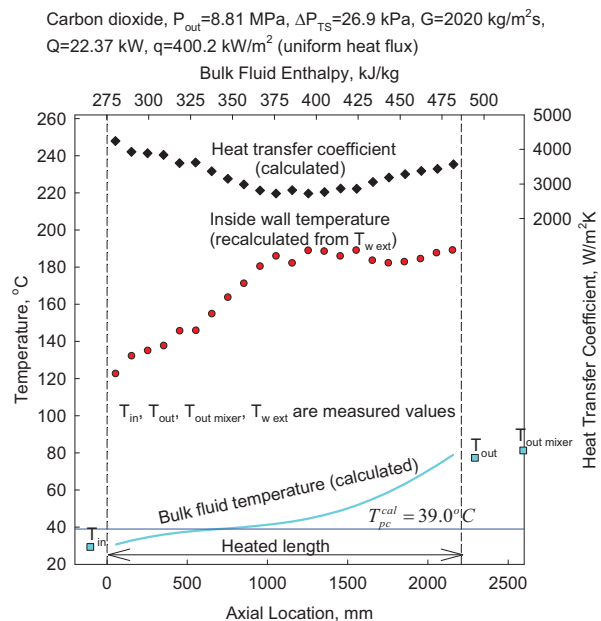


**Figure A.13f. Temperature Variations along Test Section at  $P_{out}=8.81 \text{ MPa}$  and  $G=2020 \text{ kg/m}^2\text{s}$ .**

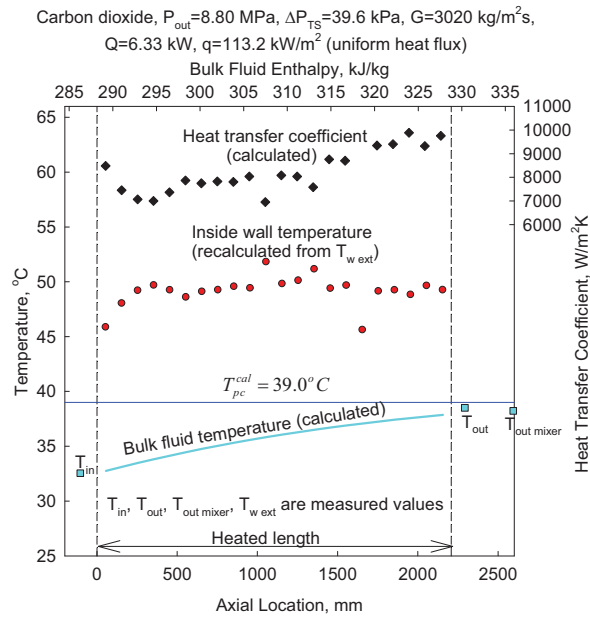


**Figure A.14a. Temperature Variations along Test Section at  $P_{out}=8.80 \text{ MPa}$  and  $G=3020 \text{ kg/m}^2\text{s}$ .**

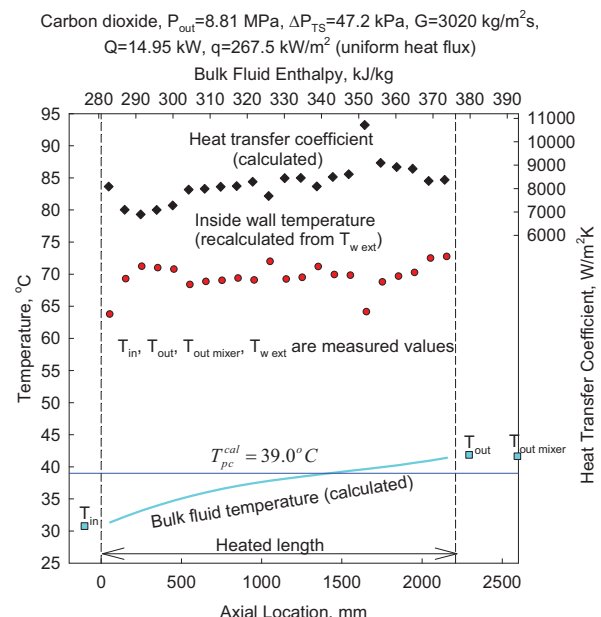


**Figure A.14b. Temperature Variations along Test Section at  $P_{out}=8.81 \text{ MPa}$  and  $G=3020 \text{ kg/m}^2\text{s}$ .**

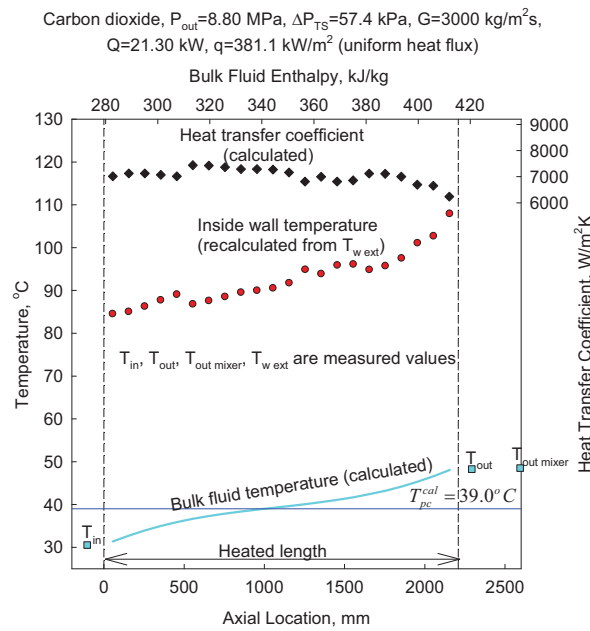


**Figure A.14c. Temperature Variations along Test Section at  $P_{out}=8.80 \text{ MPa}$  and  $G=3000 \text{ kg/m}^2\text{s}$ .**

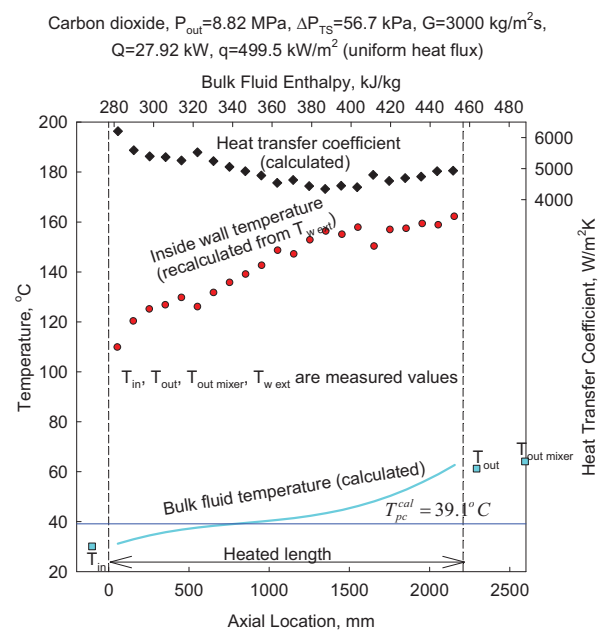


**Figure A.14d. Temperature Variations along Test Section at  $P_{out}=8.82 \text{ MPa}$  and  $G=3000 \text{ kg/m}^2\text{s}$ .**

## APPENDIX B

### Other Datasets Graph Comparisons

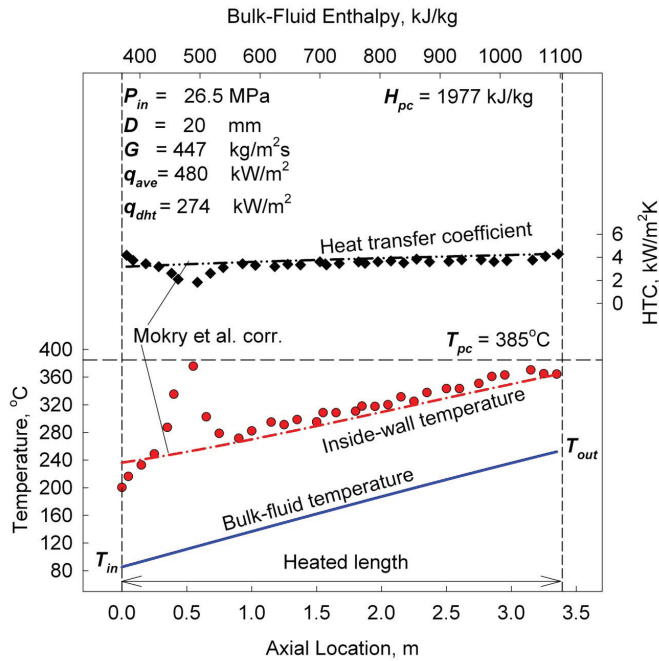


**Figure B.1. Temperature and Heat Transfer Coefficient Variations along a Circular Tube at Various Heat Fluxes: Nominal Operating Conditions –  $P_{in} = 26.5 \text{ MPa}$ ,  $G = 447 \text{ kg/m}^2\text{s}$  (Alferov et al., 1976).**

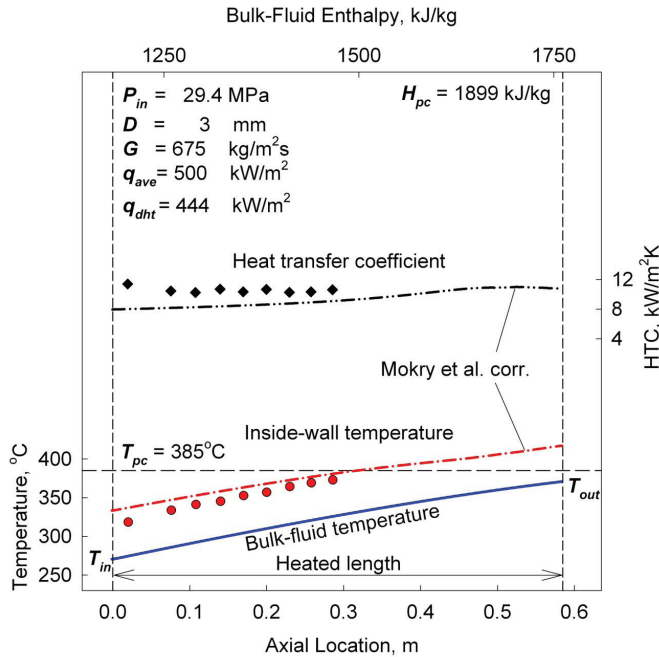


**Figure B.2. Temperature and Heat Transfer Coefficient Variations along a Circular Tube at Various Heat Fluxes: Nominal Operating Conditions –  $P_{in} = 29.4 \text{ MPa}$ ,  $G = 500 \text{ kg/m}^2\text{s}$  (Petukhov, B.S. and Polyakov, A.F., 1988).**

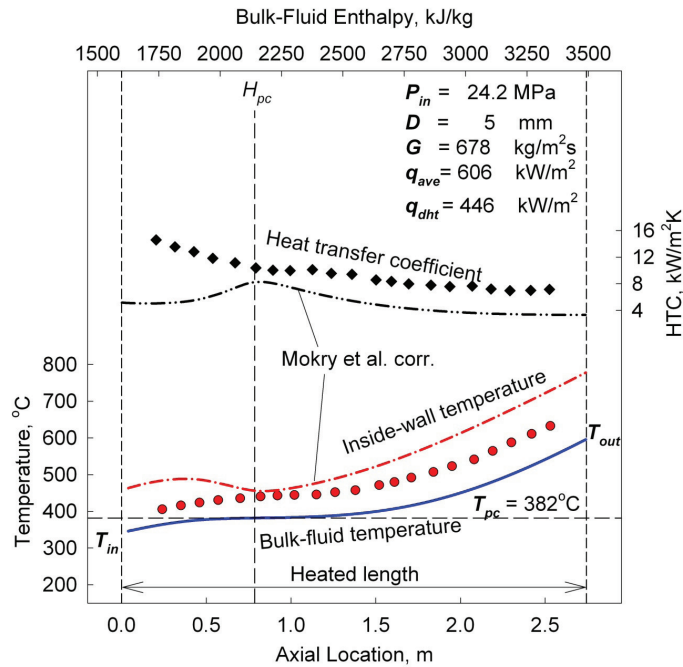


**Figure B.3. Temperature and Heat Transfer Coefficient Variations along a Circular Tube at Various Heat Fluxes: Nominal Operating Conditions –  $P_{in} = 24.2 \text{ MPa}$ ,  $G = 678 \text{ kg/m}^2\text{s}$  (Bishop et al., 1964).**

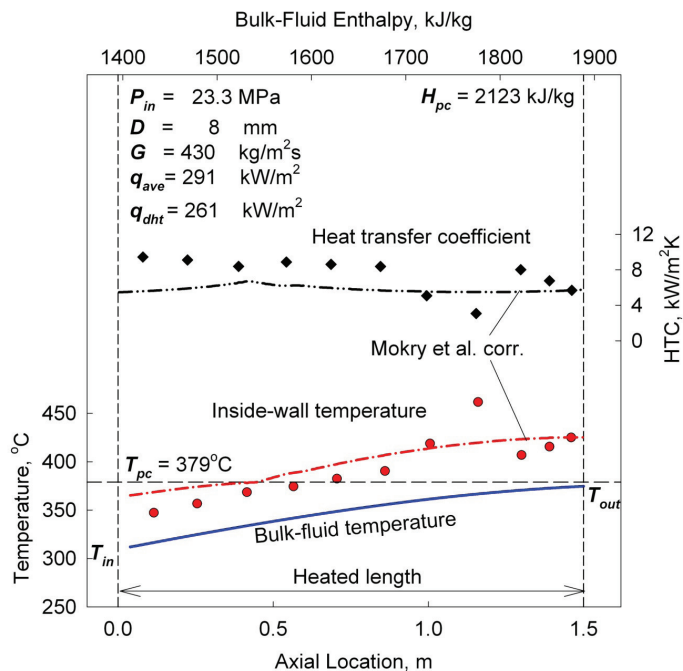
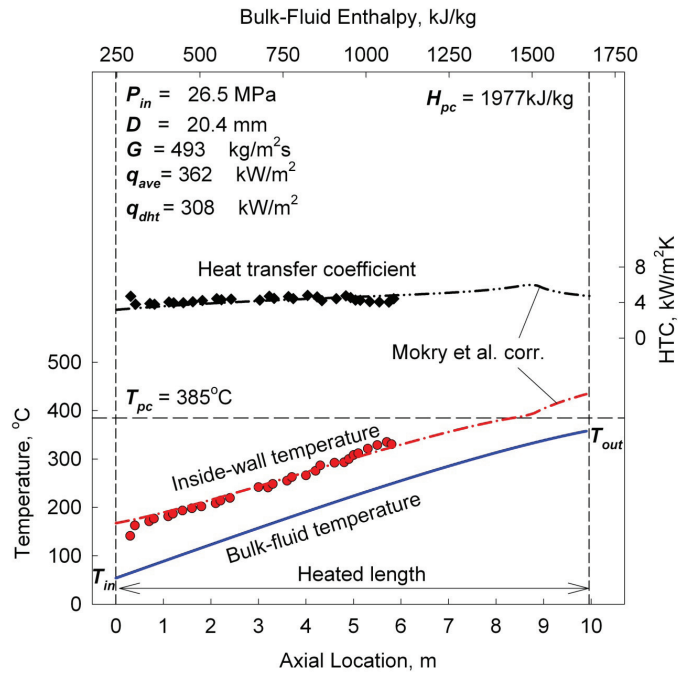
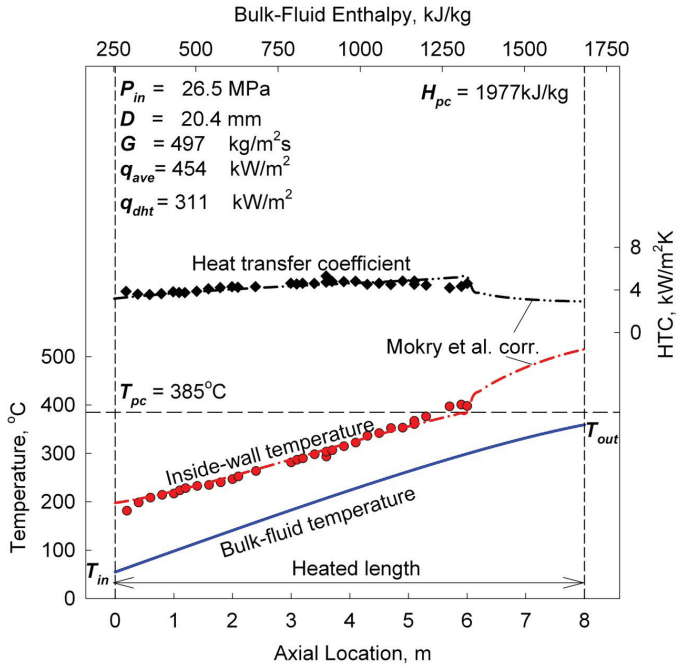


**Figure B.4. Temperature and Heat Transfer Coefficient Variations along a Circular Tube at Various Heat Fluxes: Nominal Operating Conditions –  $P_{in} = 23.3 \text{ MPa}$ ,  $G = 430 \text{ kg/m}^2\text{s}$  (Shitsman, 1963).**

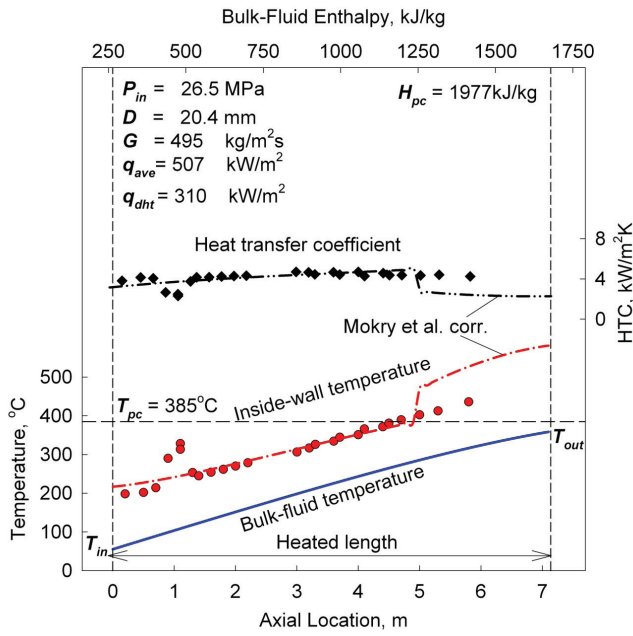


(a)



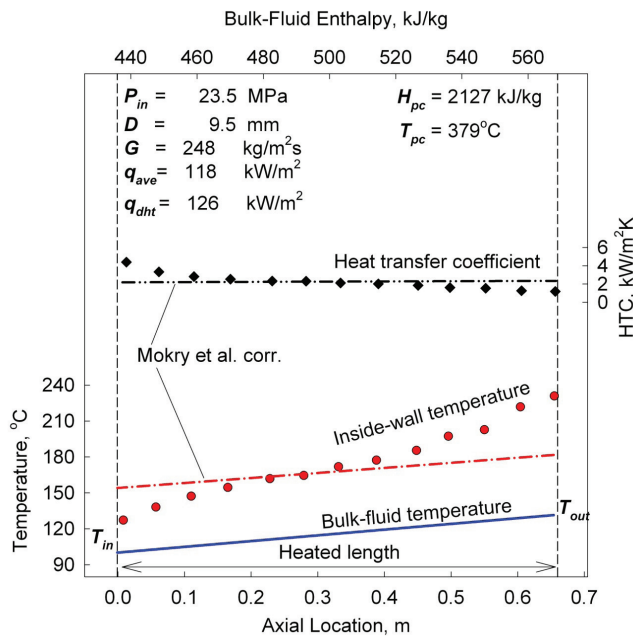
(b)

**Figure B.5 (a-b). Temperature and Heat Transfer Coefficient Variations along a Circular Tube at Various Heat Fluxes: Nominal Operating Conditions –  $P_{in} = 26.5 \text{ MPa}$ , (a)  $G = 493 \text{ kg/m}^2\text{s}$ ; (b)  $G = 497 \text{ kg/m}^2\text{s}$  (Vikhrev et al. 1967).**



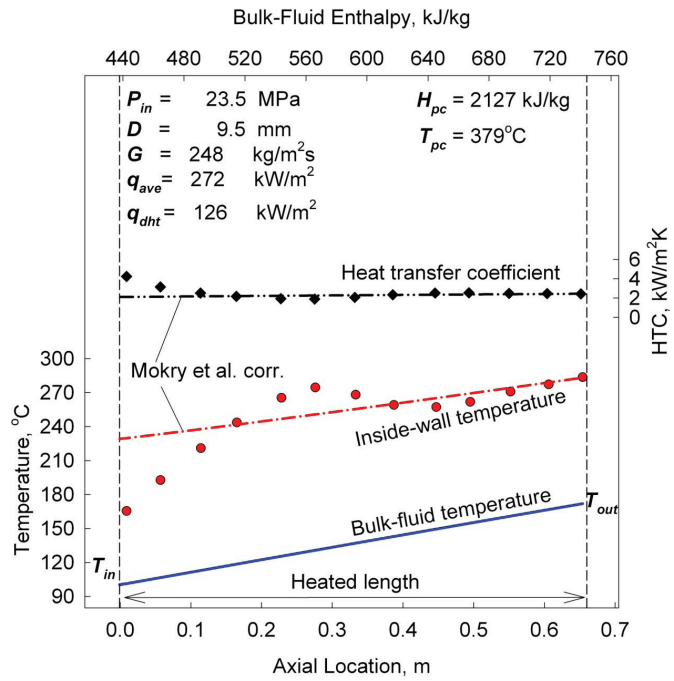
(c)

**Figure B.5 (c).** Temperature and Heat Transfer Coefficient Variations along a Circular Tube at Various Heat Fluxes: Nominal Operating Conditions –  $P_{in} = 26.5 \text{ MPa}$ ,  $G = 495 \text{ kg/m}^2\text{s}$  (Vikhrev et al. 1967).

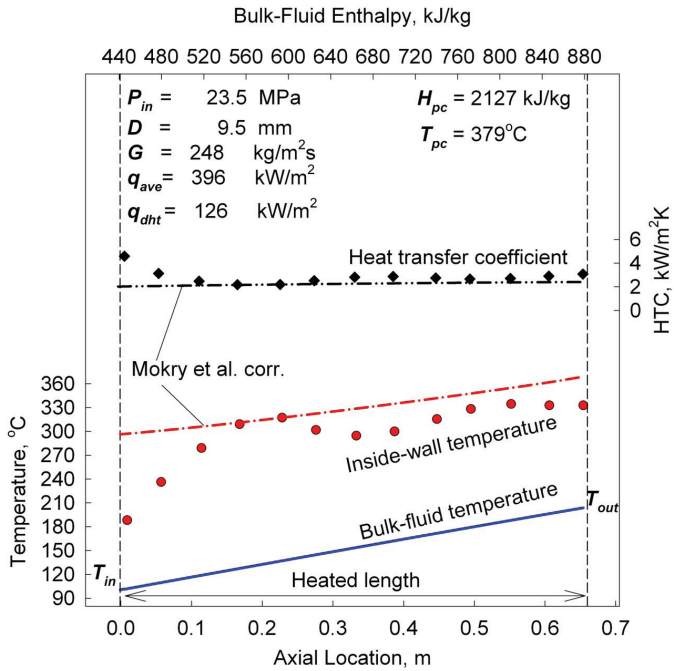


(a)

**Figure B.6 (a).** Temperature and Heat Transfer Coefficient Variations along a Circular Tube at Various Heat Fluxes: Nominal Operating Conditions –  $P_{in} = 23.5 \text{ MPa}$ ,  $G = 248 \text{ kg/m}^2\text{s}$  (Pis'mennyy et al. 2005).

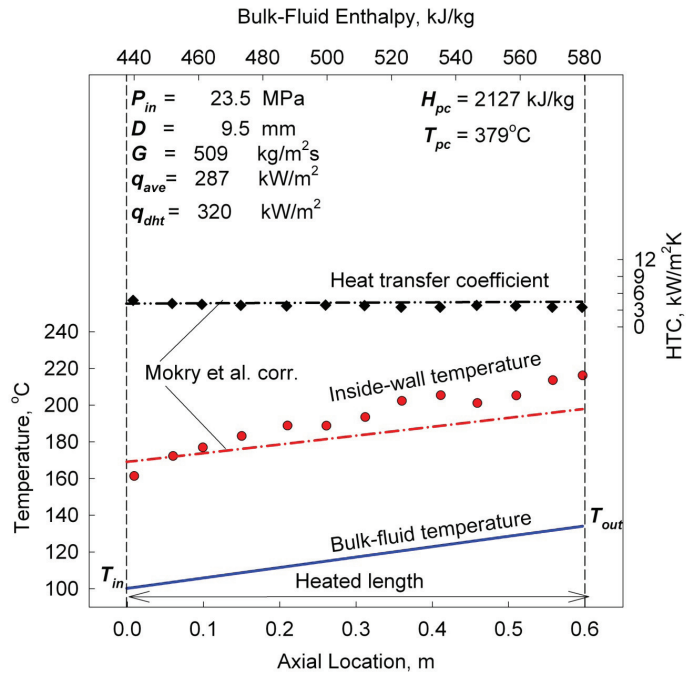


(b)

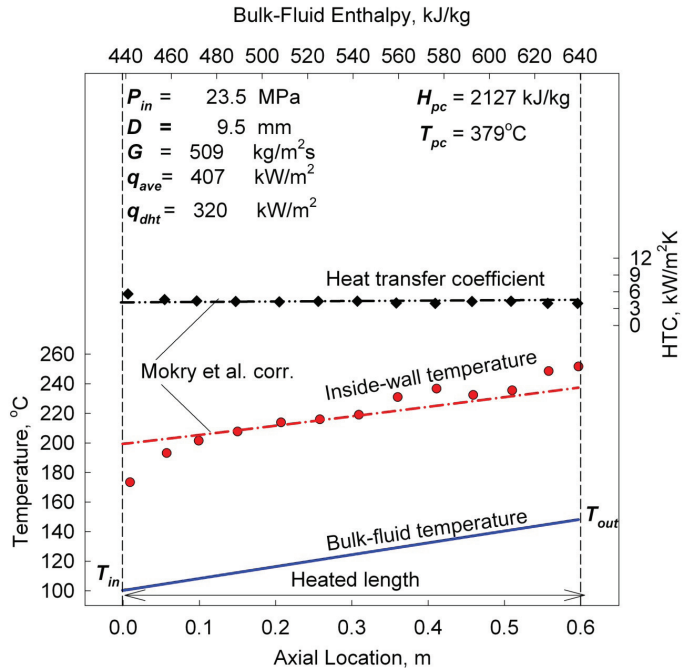


(c)

**Figure B.6 (b-c). Temperature and Heat Transfer Coefficient Variations along a Circular Tube at Various Heat Fluxes: Nominal Operating Conditions –  $P_{in} = 23.5 \text{ MPa}$ ,  $G = 248 \text{ kg/m}^2\text{s}$  (Pis'menny et al. 2005).**



(d)



(e)

**Figure B.6 (d-e). Temperature and Heat Transfer Coefficient Variations along a Circular Tube at Various Heat Fluxes: Nominal Operating Conditions –  $P_{in} = 23.5 \text{ MPa}$ ,  $G = 509 \text{ kg/m}^2\text{s}$  (Pis'menny et al. 2005).**

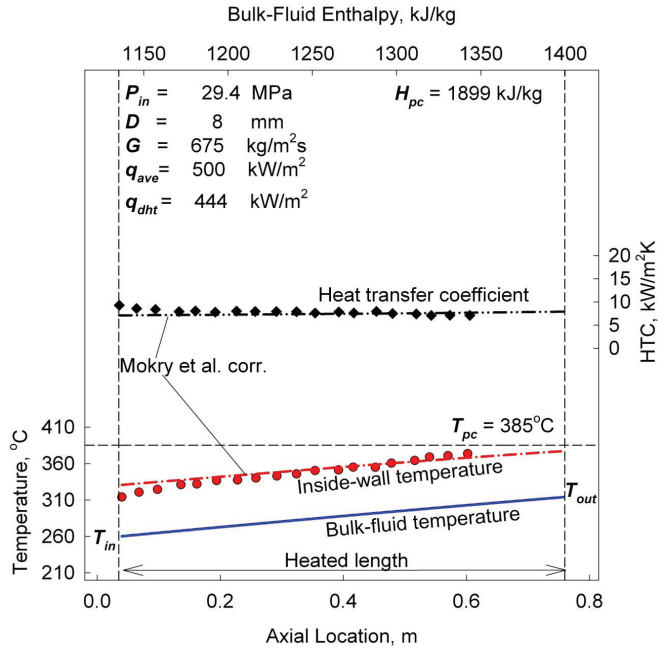
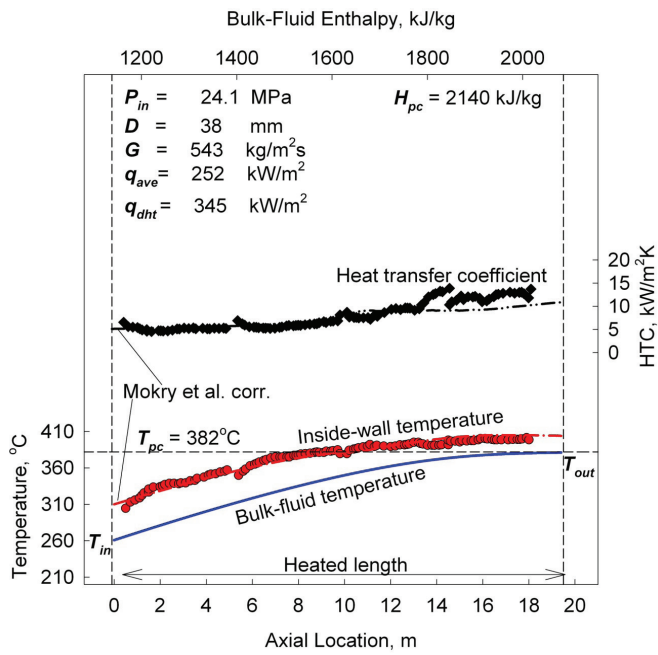
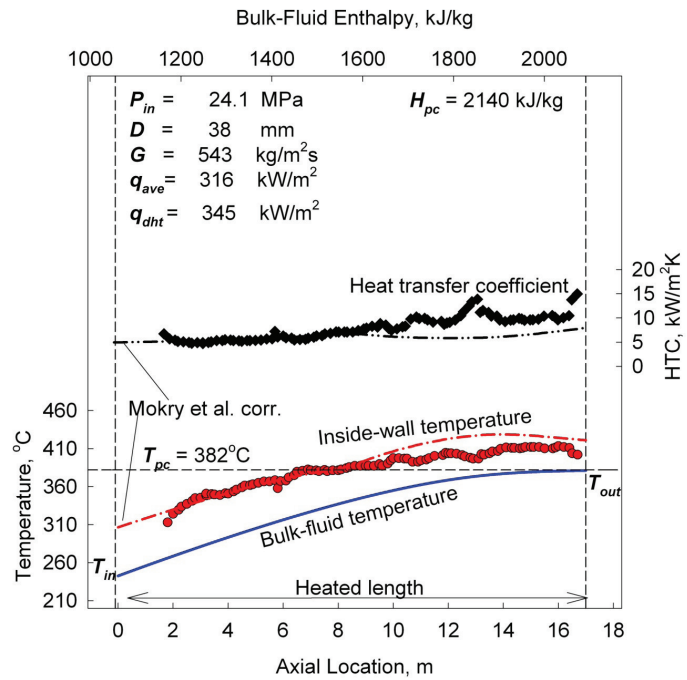


**Figure B.7. Temperature and Heat Transfer Coefficient Variations along a Circular Tube at Various Heat Fluxes: Nominal Operating Conditions –  $P_{in} = 29.4 \text{ MPa}$ ,  $G = 675 \text{ kg/m}^2\text{s}$  (Polyakov, 1975).**

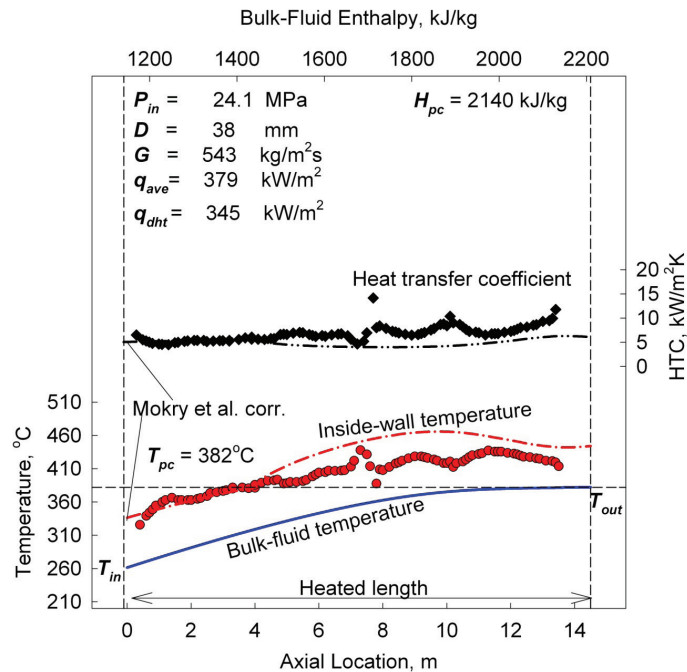


(a)

**Figure B.8 (a). Temperature and Heat Transfer Coefficient Variations along a Circular Tube at Various Heat Fluxes: Nominal Operating Conditions –  $P_{in} = 24.1 \text{ MPa}$ ,  $G = 543 \text{ kg/m}^2\text{s}$  (Lee and Haller, 1974).**



(b)



(c)

**Figure B.8 (b-c). Temperature and Heat Transfer Coefficient Variations along a Circular Tube at Various Heat Fluxes: Nominal Operating Conditions –  $P_{in} = 24.1 \text{ MPa}$ ,  $G = 543 \text{ kg/m}^2\text{s}$  (Lee and Haller, 1974).**

## APPENDIX C

### Conferences Attended, Papers Presented and Awards Received

#### Nuclear Energy for New Europe 2009 International Conference

- Mokry, S., Farah, A., King, K., Gupta, S., Pioro, I. and Kirillov, P., 2009. ***Development of Supercritical Water Heat-Transfer Correlation for Vertical Bare Tubes***, Presented at the Nuclear Energy for New Europe 2009 International Conference, Bled, Slovenia, September 14 – 17, 2009.

#### 17<sup>th</sup> International Conference on Nuclear Engineering (ICON17)

- Mokry, S., Gospodinov, Ye., Pioro, I. and Kirillov, P., 2009. ***Supercritical Water Heat-Transfer Correlation for Vertical Bare Tubes***, Presented at the 17<sup>th</sup> International Conference on Nuclear Engineering, Brussels, Belgium, July 12 – 16, 2009.
- Kuznetsov, Yu.N., Smolin, V.N., Pioro, I.L., Mokry, S. and Gospodinov Ye., 2009. ***Experimental Study on Heat Transfer to Supercritical Water Flowing in 6-m Long Vertical Circular Tube***, Presented at the 17<sup>th</sup> International Conference on Nuclear Engineering, Brussels, Belgium, July 12 – 16, 2009.
- Razumovskiy, V.G., Pis'Menny, Eu.N., Koloskov, A.Eu. and Pioro, I., 2009. ***Heat Transfer to Supercritical Water in Vertical Circular Channel and 3-Rod Bundle***, Presented at the 17<sup>th</sup> International Conference on Nuclear Engineering, Brussels, Belgium, July 12 – 16, 2009.

#### SCCO<sub>2</sub> Power Cycle Symposium 2009

- Mokry, S., Pioro, I. and Duffey, R., 2009. ***Experimental Heat Transfer to Supercritical CO<sub>2</sub> Flowing Upward in a Bare Vertical Tube***, Presented at the SCCO<sub>2</sub> Power Cycle Symposium 2009, Rensselaer Polytechnic Institute, Troy, New York, USA, April 29 – 30, 2009.

## 5<sup>th</sup> Annual Student Research Day

- Mokry, S., Gospodinov, Ye., Kirillov, P. and Pioro, I., 2008. ***Supercritical Water Heat Transfer in a Vertical Bare Tube***, Presented at the 5<sup>th</sup> Annual Student Research Day, University of Ontario Institute of Technology, Oshawa, Ontario, Canada, August 22<sup>nd</sup>, 2008.
- Mokry, S., Naidin, M., Baig, F., Gospodinov, Ye., Zirn, U., Bakan, K., Pioro, I. and Naterer, G., 2008. ***Conceptual Thermal-Design Options for Pressure-Tube SCWRs with Thermochemical Co-Generation of Hydrogen***, Presented at the 5<sup>th</sup> Annual Student Research Day, University of Ontario Institute of Technology, Oshawa, Ontario, Canada, August 22<sup>nd</sup>, 2008.

## 16<sup>th</sup> International Conference on Nuclear Engineering (ICON 16)

- Mokry, S., Naidin, M., Baig, F., Gospodinov, Ye., Zirn, U., Bakan, K., Pioro, I. and Naterer, G., 2008. ***Conceptual Thermal-Design Options for Pressure-Tube SCWRs with Thermochemical Co-Generation of Hydrogen***, Presented at the 16<sup>th</sup> International Conference on Nuclear Engineering, Orlando, Florida, USA, May 11 – 15, 2008.

## 4<sup>th</sup> Annual Student Research Day

- Mokry, S., Gospodinov, Ye. and Pioro, I., 2007. ***Supercritical Water Heat Transfer Correlation for 6-m Long Vertical Bare Tube***, Presented at the 4<sup>th</sup> Annual Student Research Day, University of Ontario Institute of Technology, Oshawa, Ontario, Canada, August 13<sup>th</sup>, 2007.

## Awards

- **ICON 17, Akiyama Medal** awarded for the best poster, presentation and paper in the student track. (Mokry, S., Gospodinov, Ye., Pioro, I. and Kirillov, P., 2009. Supercritical Water Heat-Transfer Correlation for Vertical Bare Tubes).

- **ICONE 16**, Awarded Best Paper in the student track from North America. (Mokry, S., Naidin, M., Baig, F., Gospodinov, Ye., Zirn, U., Bakan, K., Pioro, I. and Naterer, G., 2008. Conceptual Thermal-Design Options for Pressure-Tube SCWRs with Thermochemical Co-Generation of Hydrogen).
- **UOIT Student Research Day 2008**, Awarded Poster of the Year. (Mokry, S., Naidin, M., Baig, F., Gospodinov, Ye., Zirn, U., Bakan, K., Pioro, I. and Naterer, G., 2008. Conceptual Thermal-Design Options for Pressure-Tube SCWRs with Thermochemical Co-Generation of Hydrogen).

## APPENDIX D

### Publications of S. Mokry

(In total: 13 technical papers)

#### Refereed Journal Papers

1. Naidin, M., Mokry, S., Baig, F., Gospodinov, Ye., Zirn, U., Pioro, I. and Naterer, G., 2008. *Thermal-Design Options for Pressure-Channel SCWRs with Cogeneration of Hydrogen*, Journal of Engineering for Gas Turbines and Power, ASME, January 2009, Vol. 131, 8 pages.

#### Refereed Conference Proceedings

1. Naidin, M., Pioro, I., Duffey, R., Mokry, S., Grande, L., Villamere, B., Allison, L., Rodriguez-Prado, A., Mikhael S. and Chophla, K., 2009. *SuperCritical Water-Cooled Nuclear Reactors (SCWRs): Thermodynamic Cycle Options and Thermal Aspects of Pressure-Channel Design*, International Conference on Opportunities and Challenges for Water Cooled Reactors in the 21<sup>st</sup> Century, Book of Extended Synopses, Vienna, Austria, October 27 – 30, pp. 134 – 135.
2. Mokry, S., Farah, A., King, K., Gupta, S., Pioro, I. and Kirillov, P., 2009. *Development of Supercritical Water Heat-Transfer Correlation for Vertical Bare Tubes*, Proceedings of the Nuclear Energy for New Europe 2009 International Conference, Bled, Slovenia, September 14 – 17, 2009, Paper #210, 13 pages.
3. Naidin, M., Mokry, S., Pioro, I., Duffey, R. and Zirn, U., 2009. *SCW NPPs: Layouts and Thermodynamic Cycles*, Proceedings of the Nuclear Energy for New Europe 2009 International Conference, Bled, Slovenia, September 14 – 17, 2009, Paper #704, 12 pages.
4. Mokry, S., Gospodinov, Ye., Pioro, I. and Kirillov, P., 2009. *Supercritical Water Heat-Transfer Correlation for Vertical Bare Tubes*, Proceedings of the 17<sup>th</sup> International Conference on Nuclear Engineering, Brussels, Belgium, July 12 – 16, 2009, Paper #76010, 8 pages.
5. Kuznetsov, Yu., Smolin, V., Pioro, I., Mokry, S. and Gospodinov, Ye., 2009. *Heat Transfer to Supercritical Water Flowing in 6-m Long Vertical Circular Tube*, Proceedings of the 17<sup>th</sup> International Conference on Nuclear Engineering, Brussels, Belgium, July 12 – 16, 2009, Paper #75903, 10 pages.

6. Naidin, M., Mokry, S., Monichan, R., Chop; a, K., Pioro, I., Naterer, G. and Gabriel, K., 2009. ***Thermodynamic Analysis of SCW NPP Cycles with Thermo-Chemical Co-Generation of Hydrogen***, Proceedings of the International Conference on Hydrogen Production, May 3 – 6, 2009, UOIT, Oshawa, Ontario, Canada, 15 pages.
7. Mokry, S., Pioro, I. and Duffey, R., 2009. ***Experimental Heat Transfer to Supercritical CO<sub>2</sub> Flowing Upward in a Bare Vertical Tube***, Proceedings of the Supercritical Carbon Dioxide Power Cycle Symposium 2009, Rensselaer Polytechnic Institute, Troy, New York, April 29 – 30, 2009, 15 pages.
8. Naidin, M., Pioro, I., Zirn, U., Mokry, S. and Naterer, G., 2009. ***Supercritical Water-Cooled NPPs with Co-Generation of Hydrogen: General Layout and Thermodynamic-Cycles Options***, Proceedings of the 4<sup>th</sup> International Symposium on Supercritical Water-Cooled Reactors, Heidelberg, Germany, March 8 – 11, 2009, Paper #78, 11 pages.
9. Pioro, I., Zirn, U., Duffey, R., Naidin, M., Mokry, S., Gospodinov, Ye. and Baig, F., 2008. ***Supercritical Water-Cooled Nuclear Reactors: Thermodynamic-Cycles Options***, Proceedings of the 6<sup>th</sup> International Conference on Heat Transfer, Fluid Mechanics and Thermodynamics, Pretoria, South Africa, June 30 – July 2, 2008, Paper #PI1, 9 pages.
10. Pioro, I., Kirillov, P., Mokry, S. and Gospodinov, Ye., 2008. ***Supercritical Water Heat Transfer in a Vertical Bare Tube: Normal, Improved and Deteriorated Regimes***, Proceedings of the International Congress on Advanced Nuclear Power Plants, Anaheim, California, USA, June 8 – 12, 2008, Paper #8333, 10 pages.
11. Gospodinov, Ye., Mokry, S., Pioro, I. and Kirillov, P., 2008. ***Supercritical Water Heat Transfer in a Vertical Bare Tube***, Proceedings of the 16<sup>th</sup> International Conference on Nuclear Engineering, Orlando, Florida, USA, May 11 – 15, 2008, Paper #48546, 11 pages.
12. Mokry, S., Naidin, M., Baig, F., Gospodinov, Ye., Zirn, U., Bakan, K., Pioro, I. and Naterer, G., 2008. ***Conceptual Thermal-Design Options for Pressure-Tube SCWRs with Thermochemical Co-Generation of Hydrogen***, Proceedings of the 16<sup>th</sup> International Conference on Nuclear Engineering, Orlando, Florida, USA, May 11 – 15, 2008, Paper #48313, 13 pages.

## Papers Prepared for Publications

Farah, A., King, K., Gupta, S., Mokry, S. and Pioro, I., 2010. **Comparison of Existing Heat-Transfer Correlations for Supercritical Water in Vertical Bare Tubes**, Abstract accepted to the 2<sup>nd</sup> Canada-China Joint Workshop on Supercritical Water-Cooled Reactors (CCSC-2010), Toronto, Ontario, April 25 – 28.

Mokry, S., Farah, A., Gupta, S., King, K. and Pioro, I., 2010. **Comparative Study and Advancement of Supercritical Water Heat-Transfer Correlation for Vertical Bare Tubes**, Abstract accepted to the 2<sup>nd</sup> Canada-China Joint Workshop on Supercritical Water-Cooled Reactors (CCSC-2010), Toronto, Ontario, April 25 – 28.

Mokry, S., Farah, A., King, K., Gupta, S. and Pioro, I., 2010. **Updated Heat-Transfer Correlation for Supercritical Water in Vertical Bare Tubes**, Abstract accepted to the 7<sup>th</sup> International Conference on Heat Transfer, Fluid Mechanics and Thermodynamics, Antalya, Turkey, July 19 – 21.

Mokry, S., Farah, A., King, K., Gupta, S., Chophla, K., Pioro, I. and Kirillov, P., 2010. **Development of a Heat-Transfer Correlation for Supercritical Water Flowing in a Vertical Bare Tube**, Abstract accepted to the 2010 International Heat Transfer Conference (IHTC 2010), Washington D.C., USA, August 8 – 13.

Mokry, S., Pioro, I., Kirillov, P. and Gospodinov, Ye., 2010. **Supercritical-Water Heat-Transfer in a Vertical Bare Tube**, to be published in Nuclear Engineering and Design, 9 pages.

Pioro, I., Duffey, R., Naidin, M., Mokry, S., Grande, L., Villamere, B., Peiman, W., Saltanov, Eu., Allison, L., Rodriguez-Prado, A., and Mikhael, S., 2010. **Supercritical Water-Cooled Nuclear Reactors: NPP Layouts and Thermal Design Options of Pressure Channels**, Abstract accepted to the 17<sup>th</sup> Pacific Basin Nuclear Conference, Cancun, Mexico, October 24 – 30.

Pioro, I.L., Kirillov, P.L., Mokry, S.J. and Gospodinov, Y.K., 2010. **Supercritical Water Heat Transfer in a Vertical Bare Tube: Normal, Improved and Deteriorated Regimes**, to be published in Nuclear Technology, 31 pages.